OPTICAL FREQUENCY REFERENCES IN ACETYLENE-FILLED HOLLOW-CORE
OPTICAL FIBER AND PHOTONIC MICROCELLS

by

CHENCHEN WANG

B.S., University of Science and Technology of China, 2008

AN ABSTRACT OF A DISSERTATION

Submitted in partial fulfillment of the requirements for the degree

DOCTOR OF PHILOSOPHY

Department of Physics
College of Arts and Sciences

KANSAS STATE UNIVERSITY
Manhattan, Kansas

2015

Abstract

Optical frequency references have been widely used in applications such as navigation, remote sensing, and telecommunication industry. For stable frequency references in the near-infrared (NIR), lasers can be locked to narrow absorption features in gases such as acetylene. Currently, most Near NIR references are realized in free space setups. In this thesis, a low-loss hollow-core optical fiber with a diameter of sub millimeters is integrated into the reference setup to provide long interaction lengths between the filling gas and the laser field, also facilitate the optical interaction with low power levels. To make portable NIR reference, gas can be sealed inside the hollow-core fiber, by creating a photonic microcell. This work has demonstrated all-fiber optical frequency references in the Near IR by fabricating and integrating gas sealed photonic microcells in the reference setup. Also, a thoughtful study regarding the lineshape of the fiber-based reference has been accomplished. According the proper modeling of a shift due to lineshape, a correction was applied to our previous absolute frequency measurement of an NIR optical frequency reference. Furthermore, effects of the hollow-core fibers, including mode-dependence frequency shift related to surface modes are explored. In addition, angle splicing techniques, which will improve the performance of the fiber-based frequency reference have been created. Low transmission and return loss angle splices of photonic bandgap fiber, single mode PCF, and large core kagome to SMF-28 are developed and those fibers are demonstrated to be promising for photonic microcell based optical frequency references. Finally, a potentially portable optical metrology system is demonstrated by stabilizing a fiber-laser based frequency comb to an acetylene-filled optical fiber frequency reference. Further work is necessary to fabricate an all-fiber portable optical metrology system with high optical transmission and low molecular contamination.

OPTICAL FREQUENCY REFERENCES IN ACETYLENE-FILLED HOLLOW-CORE

OPTICAL FIBER AND PHOTONIC MICROCELLS

by

CHENCHEN WANG

B.S., University of Science and Technology of China, 2008

A DISSERTATION

submitted in partial fulfillment of the requirements for the degree

DOCTOR OF PHILOSOPHY

Department of Physics

College of Art and Sciences

KANSAS STATE UNIVERSITY

Manhattan, Kansas

2015

Approved by:

Major Professor

Kristan L. Corwin

Copyright

Chenchen Wang

2015

Abstract

Optical frequency references have been widely used in applications such as navigation, remote sensing, and telecommunication industry. For stable frequency references in the near-infrared (NIR), lasers can be locked to narrow absorption features in gases such as acetylene. Currently, most Near NIR references are realized in free space setups. In this thesis, a low-loss hollow-core optical fiber with a diameter of sub millimeters is integrated into the reference setup to provide long interaction lengths between the filling gas and the laser field, also facilitate the optical interaction with low power levels. To make portable NIR reference, gas can be sealed inside the hollow-core fiber, by creating a photonic microcell. This work has demonstrated all-fiber optical frequency references in the Near IR by fabricating and integrating gas sealed photonic microcells in the reference setup. Also, a thoughtful study regarding the lineshape of the fiber-based reference has been accomplished. According the proper modeling of a shift due to lineshape, a correction was applied to our previous absolute frequency measurement of an NIR optical frequency reference. Furthermore, effects of the hollow-core fibers, including mode-dependence frequency shift related to surface modes are explored. In addition, angle splicing techniques, which will improve the performance of the fiber-based frequency reference have been created. Low transmission and return loss angle splices of photonic bandgap fiber, single mode PCF, and large core kagome to SMF-28 are developed and those fibers are demonstrated to be promising for photonic microcell based optical frequency references. Finally, a potentially portable optical metrology system is demonstrated by stabilizing a fiber-laser based frequency comb to an acetylene-filled optical fiber frequency reference. Further work is necessary to fabricate an all-fiber portable optical metrology system with high optical transmission and low molecular contamination.

Table of Contents

List of Figures

xv

xvi

List of Tables

Acknowledgements

I would like to thank my major advisor Dr. Kristan Corwin for all of her enormous support and mentoring at my Ph.D study in such an excellent research project. I would like to thank Dr. Brian Washburn for his valuable help and guidance. I feel truly lucky have worked with them in the past seven years.

I also would like to thank all my rest committee: Dr. Andrew Rys, Dr. Vinod Kumarappan, Dr. Carlos Trallero, and Dr. Asad Esmaeily for serving as my committee members. I would like to thank Dr. LarryWeaver for helpful discussion on FM modeling spectroscopy, and the James R. Macdonald Laboratory staff, especially Mike Wells for customize the vacuum chambers.

I would like to thank Dr. Fetah Benabid, head of the Gas-Phase Photonics Materials group at the XLIM Institute, France for providing the hollow-core photonic crystal fibers that are central to this work, and his generous support while working at the XLIM Institute. Additionally, I would like to thank Dr. Tom Bradley and Dr. GEROME Frédéric for useful discussion and great support in the lab during the initial investigation optical fiber splicing techniques.

I would like to thank Dr. Jeffrey Nicholson, a distinguished member of technical staff at OFS Laboratories for providing the newly-developed, single mode fiber that are vital to this work.

In the end, I would like to thank my lab mates. It's a great pleasure to know and have worked with your all: Dr. Kevin Knabe, Dr. Karl Tillman, Dr. Shun Wu, Dr. Jinkang Lim, Dr. William Hageman, Dr. Rajesh Kadel, Xiaohong Hu, Neda Dadashzadeh, Mattithyah Tillotson, Ryan Luder, and Kushan Weerasinghe.

Chapter 1.   Introduction and Motivation

Nowadays, most high precision professional equipment and timekeeping apparatus require stable and accurate external frequency references. The performance of optical frequency references is characterized by two basic parameters: stability and accuracy. The stability of the frequency reference tells how much the frequency changes over time and accuracy measures how well the frequency reference gives the correct frequency. Throughout the history, a lot of work have been done to make the frequency references more stable and accurate. One of the most commonly used frequency references is a quartz crystal oscillator [1]. With a stability of 10^{-8} at 1s and an accuracy of 10^{-5}, the quartz crystal oscillator has been widely used in integrated circuits (IC) devices and timekeeping apparatus such as watches since 1920 [2, 3]. Another commonly used frequency reference is Global Positioning System (GPS) disciplined oscillator which receives signals from the precise clocks aboard satellites [4]. Except for navigation proposes, GPS disciplined oscillator can also be used as a frequency/time transfer for synchronizing equipment in scientific laboratories. The GPS disciplined oscillator has a stability of 10^{-11} at 1s and an accuracy of 10^{-13}, which is almost the most stable and accurate radio frequency (RF) reference. To obtain better stability and higher accuracy, people work towards optical frequency references.

1.1.   Introduction of optical frequency references

An optical frequency reference [5] is a stable frequency device realized in a quantum transition in an atom, ion or molecule. It widely used for frequency calibration or as a frequency standard for precision professional equipment [5-7]. Optical frequency references are the most accurate time

and frequency standards known, promising at least two significant advantages over radio frequency references, such as a GPS disciplined Rb Oscillator. The first practical cesium atom clock was carried out in 1955 at the National Physical Laboratory (NPL) in the UK [8]. A stability of 10^{-10} at 1s was reached by the transition between two hyperfine structure ground states of cesium-133 atoms. Improvements of the cesium-133 clock were accomplished at National Institute of Standards and Technology (NIST) in the US for the following 50 years and a stability of 10^{-15} at 1s has been achieved [9]. Currently, the most accurate optical frequency reference is strontium lattice clock which uses a design of lattice-confined neutral atoms for clock operation at NIST [10]. The strontium lattice clock has a stability of 10^{-16} at 1s and an accuracy of 10^{-18}. However, for these high precision optical frequency references such as cesium and strontium clocks mentioned above, the experimental systems are always complex and require stable laboratory environment for calibrations. Thus, high precision portable frequency references will be useful for practical measurements without requiring stable laboratory environment. This thesis goal is to develop all-fiber optical frequency references which combine both features of accuracy and portability.

In a simple configuration, one realization uses molecular absorption lines as reference frequencies, and a laser is stabilized to an appropriate molecular absorption line. In the near infrared wavelength region from 1300 to 1550 nm, gases such as acetylene, carbon monoxide, methylene chloride and hydrogen cyanide have been widely used as optical frequency references [11-18], as shown in (Figure 1-1). Optical frequency references using some of these gasses have been fabricated by National Institute of Standards and Technology (NIST), summarized in Table 1-1 [13-15].
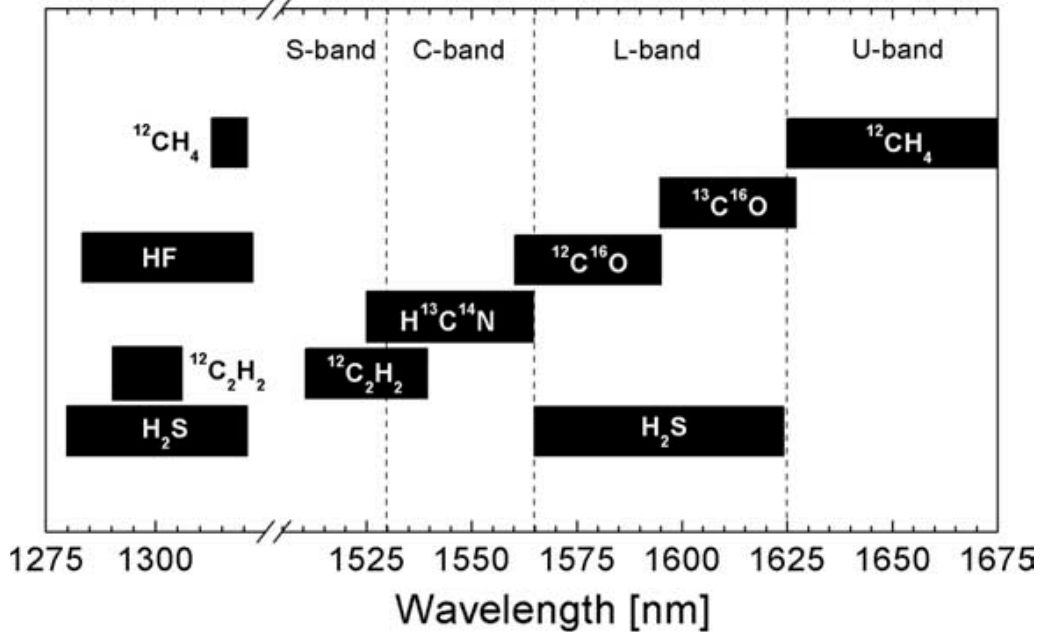
Figure 1-1: Reproduced from Ref. [11]. Most common gases for optical frequency references in the near infrared wavelength range [11-18].

Table 1-1: NIST wavelength calibration references in the near infrared wavelength range [13-15].

Gas	SRM #	Wavelength (nm)
$^{12}C_2H_2$	2517	1510 - 1540
$H^{13}C^{14}N$	2519	1530 - 1560
$^{12}C^{16}O$	2514	1560 - 1595
$^{13}C^{16}O$	2515	1595 - 1630

In this work, saturated absorption spectroscopy (SAS) is selected to obtain a narrow spectral feature of $^{12}C_2H_2$ for the stabilization of the laser frequency. The traditional frequency references realized in free-space and cavity configurations usually require bulky containers and complex free space alignments to fulfill the required interaction lengths and high saturation intensities [19-23]. Moreover, the best accuracy free-space and cavity configurations that have been achieved for acetylene optical frequency references in free-space and cavity configurations is ~2 kHz [21, 22]. We utilize low-loss hollow core fibers with a diameter from 10 ~ 100 μm to

3

integrate into the SAS setup to provide long interaction lengths between the filling gas and the laser field, and also to facilitate the optical interaction with low power levels. Our previous group member Kevin Knabe has been demonstrated a 10 kHz acetylene frequency reference inside a ~70 μm hollow-core fiber between two vacuum chambers [24]. Details of the kagome frequency reference will be discussed in Chapter 2. Furthermore, hollow optical fibers can be spliced to solid core fibers to produce hermetically sealed photonic microcells [25-28], allowing the creation of a portable, robust and user-friendly all-fiber device that requires limited maintenance or alignment.

As for the commercially available acetylene frequency references, there are portable optical references made by NIST with an accuracy at 5×10^{-7} [29] and more expensive (> $ 100k) commercial acetylene stabilized diode lasers (Neoark Model:C2H2LDS-1540) with a higher accuracy at 1×10^{-10} [30]. A comparsion of fractional instabilities and accuracies between the commerical acytlene frequency refrences and the poentential fractional instability and accuracy of this work are shown in Table 1-2.

Table 1-2 Fractional instabilities and accuracies of the commercial acetylene frequency references and the potential fractional instability and accuracy of this work [29, 30].

Optical frequency references	Fractional instability at 1s	accuracy	Description
Neoark acetylene stabilized diode laser	1×10^{-11}	1×10^{-10}	Free-space, fragile
NIST Vapor cell (commercial)	5×10^{-7}	5×10^{-7}	Portable, robust, not very accurate
Gas-filled hollow fiber (this work)	1×10^{-12}	5×10^{-11}	All fiber

As mentioned in the table above, the work of all-fiber based optical frequency reference towards realizing a portable optical frequency with 4 orders of magnitude improvement in fractional stability and accuracy over the commercial references of comparable cost, and with an

accuracy comparable to references of much higher cost.

The optical frequency reference not only offers ultrahigh frequency stability (at least 10^6 times higher than microwaves) and the most accurate frequency standard known, but also can measure frequencies up to hundreds of THz directly. In the last decade, the performance of optical frequency references has been improved by almost four orders of magnitude, and a Nobel Prize in Physics was awarded to J. Hall and T. Hänsch for their contributions to laser-based precision spectroscopy [31]. This gas-filled hollow-core fiber microcell optical reference may take the place of a radio frequency reference, and serve as an optical reference for a portable phase-stabilized carbon nanotube fiber laser comb. The combination of optical frequency reference technique and optical frequency comb technique allows the creation of an all-fiber metrology system. The all-fiber metrology system holds great potential for a multitude of applications from laboratory usage to industrial communications.

1.2. Thesis outline

The purpose of this dissertation research is to create and optimize the optical frequency reference based on sealed photonic microcells with low pressure (10^{-6} atm) acetylene inside. In the experiment, we fully characterized and improved the performance of the acetylene frequency reference system. We also developed a theoretical model for a systematic study of the optical reference and solved previously unanticipated problems. In addition to the design of the hollow-core fiber-based optical frequency references, we created an all-fiber optical metrology system by stabilizing an all-fiber optical frequency comb to the fiber-based acetylene frequency references.

Chapter 2 briefly reviewed the acetylene frequency references inside hollow-core photonic

crystal fibers (HC-PCFs), including the experimental setup and the realization of dispersion-shaped error signals. Then this chapter is followed by the calibration of acetylene optical frequency references. Both the instability and the accuracy are studied through the Allan deviation calculation of the beatnote measurement with an optical frequency comb and the absolute frequency calculation based on the recorded beatnote frequencies. In addition, chapter 2 talks about the unresolved issues of the acetylene frequency references at the beginning of this project.

Chapter 3 discusses the possible solutions to those issues mentioned in chapter 2. Techniques such as slow molecular selection and molecular temperature reduction are studied to reduce transition linewidth. Also, a three-cornered hat measurement is designed and taken to find the individual instability of our best acetylene frequency reference. Furthermore, investigation reveals distorted lineshape due to the frequency difference introduced by an AOM between the pump and probe beam. Then an additional shift at the kHz level that is created by this lineshape distortion was applied to our previous absolute frequency measurement of the P(13) acetylene transition line.

Chapter 4 focuses on the finding of suitable HC-PCFs for portable frequency references. A second vacuum chamber acetylene frequency reference is built to study additional HC-PCFs, which includes 10 μm non-PM and PM photonic bandgap fiber (PBGF), 20 μm PBGF, and a novel single mode HC-PCF. We repeat what we have done in Chapter 2 to calibrate the instabilities and accuracy of the acetylene frequency references using those fibers. From the investigation, we find the 20 μm PBGF and the novel single mode HC-PCF would be more suitable for making portable acetylene frequency references.

Chapter 5 investigates the splicing techniques between different types of HC-PCF to standard single mode fiber (SMF). Those splice techniques are critical to making portable photonic

6

microcells which can be utilized in all-fiber based optical frequency references. For illustration, in this chapter, we also introduce the ordinary optical fiber splicing procedures and talk about the characterization of splicing parameters, such as insertion loss, return loss, and splicing strength.

Chapter 6 introduces the concept of photonic microcells, describes methods of fabrication, and explains their benefits to the applications such as fiber-based optical frequency references. Measurement and calibration are applied to two photonic microcells over the period of two years. In addition to the instability and accuracy of photonic microcells, we also study how the outside experiment alteration such as changing of beam power, beam polarization, and environment conditions will alter the quality of the frequency calibration.

Chapter 7 shows our work of using the gas-filled hollow-core photonic crystal fiber (HC-PCF) optical reference as an optical reference for a portable fiber laser frequency comb. A particular locking circuit is designed to stabilize the repetition frequency of the optical frequency comb to the optical reference since the optical frequency comb does not have an intracavity EOM for high-speed control. We also measure how well the stability of the acetylene optical reference is transferred from the locked comb tooth to other teeth using a 2nd optical frequency reference a few nm away from the frequency reference we used for comb tooth stabilization.

Chapter 8 provides a summary of this thesis work and discusses the future directions toward all-fiber based optical frequency metrology system.

Chapter 2. Review of Acetylene Frequency Reference inside Hollow-core Photonic Crystal Fiber (HC-PCF)

Accurate acetylene frequency references near 1.5 μm are very useful for optical telecommunication, gas sensing, metrology, and many other applications. Using the technique of saturated absorption spectroscopy (SAS) inside a power build-up cavity [23, 32] and vapor cell [22], frequency references with an accuracy of 2 kHz have been created. However, those acetylene frequency references are realized in free space configurations [22, 33] and require long interaction lengths and high saturation intensities. Furthermore, since the optical fibers are intrinsically flexible and small, the all-fiber based optical frequency reference provides the possibility to transform a laboratory instrument into a commercial system. Also, the low-loss optical guidance hollow-core photonic crystal fibers (HC-PCFs) provide us the ability to fill the core with any desirable medium in gaseous form. Optical frequency references inside HC-PCF have the potential for robustness and portability. To demonstrate this, our previous group member Kevin Knabe's thesis work on an acetylene frequency reference inside a hollow-core fiber between two vacuum chambers proved a 10 kHz frequency reference [24]. The result represents a factor 100 improvement over previously reported results in fiber [34].

2.1. Saturated absorption spectroscopy

When a laser beam passes through a molecular gas vapor (i.e. acetylene), the absorption of light by the molecule depends on the frequency of the incident laser beam. Without any specific technique in the experiment probing the maximum of absorption of a molecular gas, due to the

Doppler broadening, the uncertainty of the measurement is limited and the natural linewidth of molecular resonance is not detectable. Nonlinear techniques are useful for overcoming the problem of Doppler broadening at room temperature. One such technique is Doppler-free SAS and was developed in 1966 by the research group of Arthur L. Schawlow. SAS provides the possibility to observe linewidth limits below the Doppler limit in molecular gas and has been widely used in applications such as optical frequency references.

The theory of saturated absorption spectroscopy has been well studied in Ref [35]. In the SAS experimental setup, a pump-probe scheme is used. Even when both beams are at the same frequency, they will address different molecular velocities unless both are on resonance. When the two beams address the same molecules which have zero velocities along the direction of laser propagation, the strong pump beam will excite many of the molecules from the lower-level state to an upper state. When a photon from the probe beam passes through the molecules, there is a high chance the molecule in the upper state will undergo stimulated emission. Thereby, we can observe a small dip in the absorption feature when we sweep the laser frequency through the resonance frequency (Figure 2-1). There are many techiniques can be used to obtain the nature linewidth of the transition line.
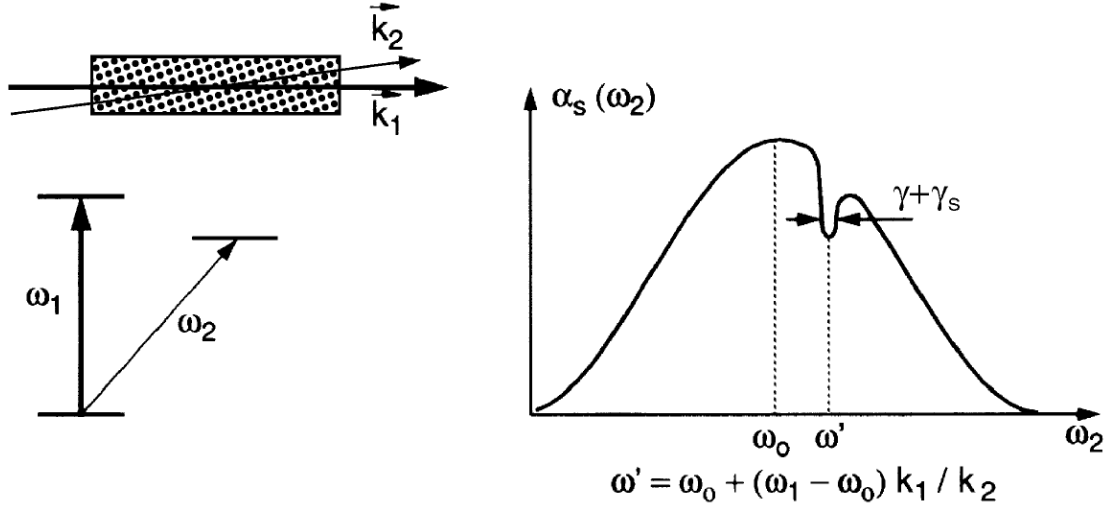
Figure 2-1: Reproduced from Ref.[35]. Dip in the Doppler-broadened absorption profile burned by a strong pump beam ω_1 at ω_0 and detected by a weak probe beam ω_2 at ω'. $\vec{k_1}$ and $\vec{k_2}$ are the wave vectors of the pump beams and probe beams.

Using the theory in Ref. [35], when probe beam propagates collinearly or anticollinearly with the pump beam, the effective absorption coefficient α of the probe beam in terms of laser frequency ω can be expressed as:

$$\alpha = A_g \exp\left[-\frac{\left(\omega - \omega_0 \pm \Delta\omega\right)^2}{0.36\omega_D^2}\right]\left[1 - \frac{A_l\left(\omega_l / 2\right)^2}{\left(\omega - \omega_0\right)^2 + \left(\omega_l / 2\right)^2}\right] \tag{2.1}$$

where ω_0 is the resonant frequency of molecule; A_g is the amplitude of the Doppler absorption; ω_D is the Doppler linewidth; $\Delta\omega$ is the frequency difference between probe beam and pump beam, the $+$ sign holds for collinear and the $-$ sign for anticollinear propagation of probe and pump beams; A_l is the amplitude of sub-Doppler absorption; and ω_l is the sub-Doppler linewidth.

2.1.1 Optical setup of gas-filled hollow core fiber frequency references

In our 10 kHz fiber-based optical frequency reference setup relying on molecular absorption

10

(Figure 2-2), a 19-cell kagome HC-PCF, with a core diameter of 68 μm and a length of 4.1 m, lies

between two vacuum chambers. Loss at 1.5 μm of this particular fiber is around 1 dB/m. This fiber

is fabricated by our collaborators Fetah Benabid's group at XLIM Institute in France (formerly at

the University of Bath, U.K.), and greater details of this fiber will be discussed in later chapters.

The vacuum chambers are evacuated down to 1 mtorr with a turbo vacuum pump and then filled

to the desired pressure with $^{12}C_2H_2$ (5 - 200 mtorr). The windows of the vacuum chambers are

wedge-cut windows with infrared anti-reflective coatings to guarantee that the free space laser

beams can be coupled into the ends of the fibers with minimal reflection.
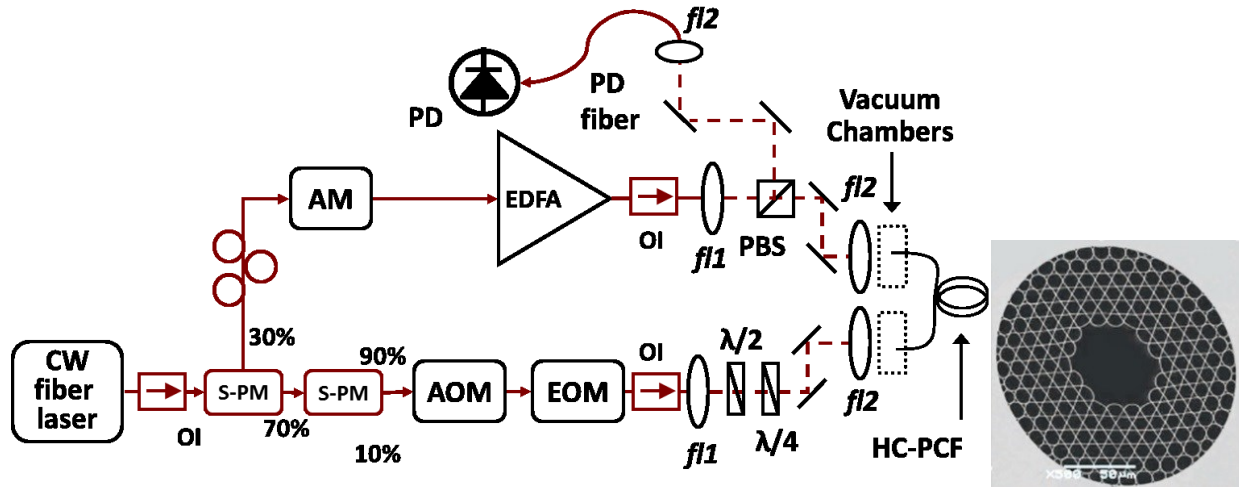
Figure 2-2: Adapted from Ref. [36]. Optical schematic of gas-filled hollow-core fiber frequency references based on vacuum chambers. The probe beam is split before the pump beam is amplified to allow for fixing the amount the probe power. Shown are amplitude modulator (AM), acousto-optic modulator (AOM), electro-optic modulator (EOM), polarizing beam splitter (PBS), optical isolator (OI), half wave plate (λ/2), quarter wave plate (λ/4), f = 60 mm N-BK7 Plano-convex lenses($fl1$), f = 15 mm Geltech aspheric lenses ($fl2$), optical circulator (C), and photo-detectors (PD). Inset: cross section of 19-cell kagome HC-PCF used in the setup.

A narrow linewidth continuous-wave (CW) fiber laser (Orbits Lightwave, Inc.) is utilized

in this experiment to observe the P(13) v_1+v_3 overtone transition in $^{12}C_2H_2$. The output of the fiber

laser is split into a probe beam and a pump beam. The pump beam is amplified by an erbium-doped fiber amplifier (EDFA) up to 200 mW to saturate the molecules. The probe beam goes through an acousto-optic modulator (AOM) so that the interference between the probe and the reflected pump occurs at the AOM modulation frequency ($f_{AOM} = \sim -60$ MHz). Then an electro-optic modulator (EOM) (General Photonics) is used to create sidebands spaced at the EOM modulation frequency ($f_{EOM} = 22$ MHz) for frequency modulation (FM) spectroscopy [37]. The probe and pump beams couple to free space through $f = 15$ mm Geltech aspheric lenses and are then coupled to the kagome fiber through $f = 60$ mm N-BK7 plano-convex lens. Those lenses are chosen based on the beam size and the numerical aperture (NA) of the fibers. The probe exiting the kagome fiber is separated from the pump by a polarizing beam splitter, coupled to a multi-mode fiber (MMF), and detected by a 125 MHz photodetector (New Focus 1811-FC). The pump beam is amplitude modulated (AM) at 900 kHz for background noise rejection. By applying a ramp voltage to the piezoelectric transducer (PZT) of the fiber laser, a sub-Doppler saturated absorption signal and antisymmetric error signal were observed as shown in Figure 2-3. The linewidth of P(13) overtone transition line in $^{12}C_2H_2$ is about 10 MHz. The 10 MHz is broader than the 1 MHz transition line observed in the vapor cell and power build-up cavity setups [21, 38]. The broader linewidth in our experiment is dominated by the transit time broadening; due to the small HC-PCF's core confinement, some gas molecules collide with inner core walls before they interact with the laser field.
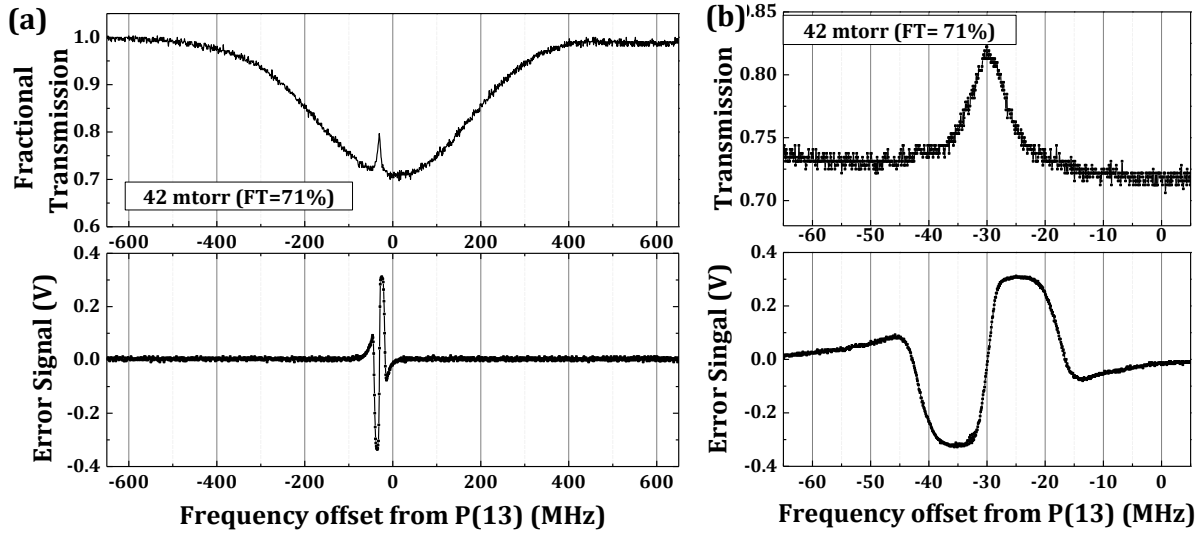
Figure 2-3: Adapted from Ref. [36]. (a) Top: Fractional transmission of a 4.1 m long kagome HC-PCF with a $^{12}C_2H_2$ pressure of 42 mtorr, and a pump power of 25 mW exiting the fiber; bottom: error signal of sub-Doppler vs. scanned frequency around the P(13) transition. The laser frequency was scanned at 1.2 GHz/sec. (b) same as (a), but zoomed in on the sub-Doppler absorption feature.

2.1.2 Electrical schematic for error signal generation

The electrical schematic used to generate Doppler-free error signals is shown in Figure 2-4. Connector type electrical components from Mini-Circuits are employed in this setup. The probe signal which contains the FM and AM information is detected by a photodetector (PD). This PD signal is split by a Bias Tee (ZFBT-6G+) to a DC portion for probe signal detection and an RF portion for error signal generation. The RF portion of the PD signal is filtered through two bandpass filters (BBP-21.4+) for noise reduction, then amplified (ZFL-1000LN+), and mixed (ZAD-6+) at f_{FM} (22 MHz) for FM demodulation. A Doppler-free error signal (FM error) is observed. The synthesizer (SRS DS345) at the LO input of the mixer shares the time base with the synthesizer which is used to drive the EOM. Via adjusting the relative phase delay between the two synthesizers, we selectively observe the FM dispersion error signal of the SAS of acetylene.

13

The FM error is further filtered (BLP-2.5+), amplified (ZFL-1000LN+), and mixed (ZAD-6+) at f_{AM} (900 kHz) for AM demodulation. The AM demodulation is used to reduce offsets due to the Doppler-broadened background and to acquire an AM error signal (Figure 2-3) with a higher signal to noise (S/N) ratio.
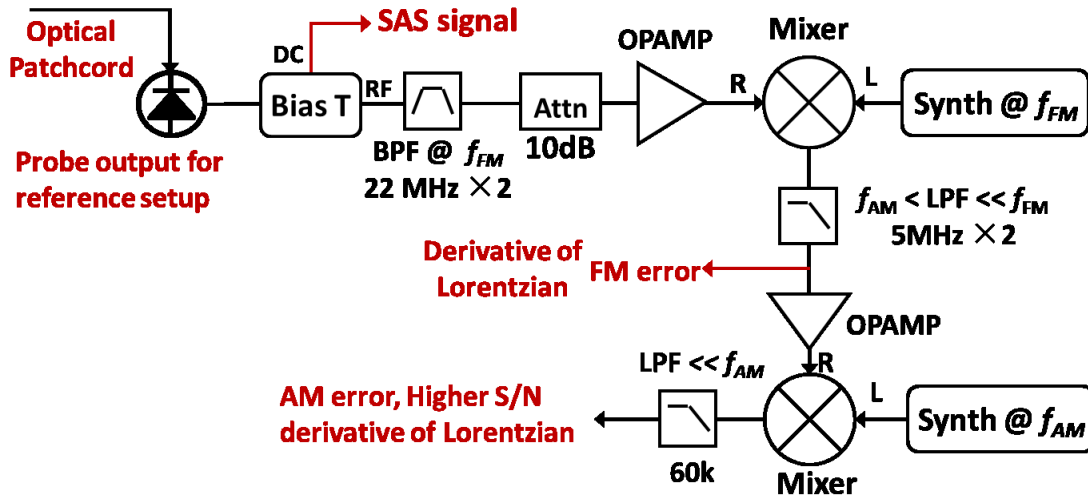
Figure 2-4: Electrical schematic for FM and AM error signal generation. Bias T: Bias Tee; FM: Frequency modulation; AM: Amplitude modulation; BPF: Band pass filter; LPF: Low pass filter; Attn: Attenuator; OPAMP: Operational Amplifier; Synth: SRS DS345 synthesizer. Frequency demodulation schematic contains a BPF, an OPAMP, a mixer driven at the modulation frequency, and an LPF.

2.1.3 Frequency stabilization

The schematic of the feedback control loop of the CW fiber laser frequency is shown in Figure 2-5. The antisymmetric error signal (AM error) is used as the input signal to the locking electronics which feeds back to the CW fiber laser's PZT for frequency stabilization near the P(13) overtone transition in $^{12}C_2H_2$. By comparing the desired voltage (0 V) and the measured voltage from the AM dispersive error signal, the locking electronics stabilize the AM dispersion error signal at zero voltage. Correspondingly, the frequency of the CW fiber laser is stabilized at the frequency of the

14

P(13) zero velocity class. In this way, we obtained a stabilized CW frequency reference.
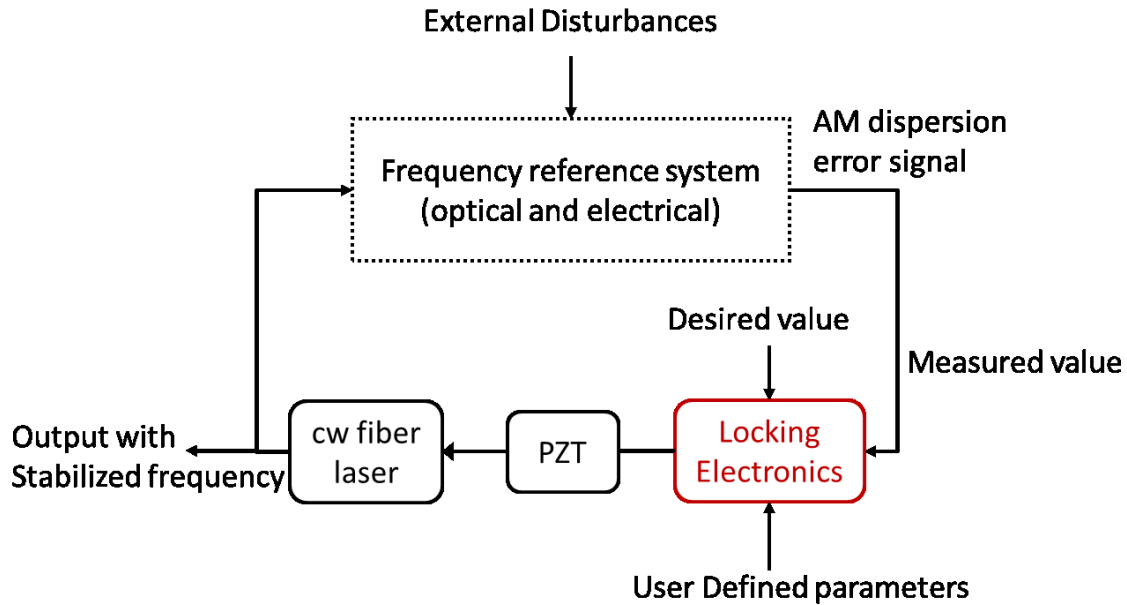
Figure 2-5 Block diagram for feedback control loop of CW fiber laser frequency. PZT: piezoelectric ceramic transducer; Locking Electronics: Precision Photonics locking servo LB1005.The antisymmetric error signal (AM error) is used as the input signal to the locking electronics which feeds back to the CW fiber laser's PZT for frequency stabilization near the P(13) overtone transition in $^{12}C_2H_2$.

Precision Photonics high-speed servo controller LB1005 is used in the feedback control loop of CW laser frequency. The frequency response of the high-speed servo controller profile with low-frequency gain limit (LFGL) is measured (Figure 2-6), and agrees with the proportional-integral filter gain shown on the datasheet.
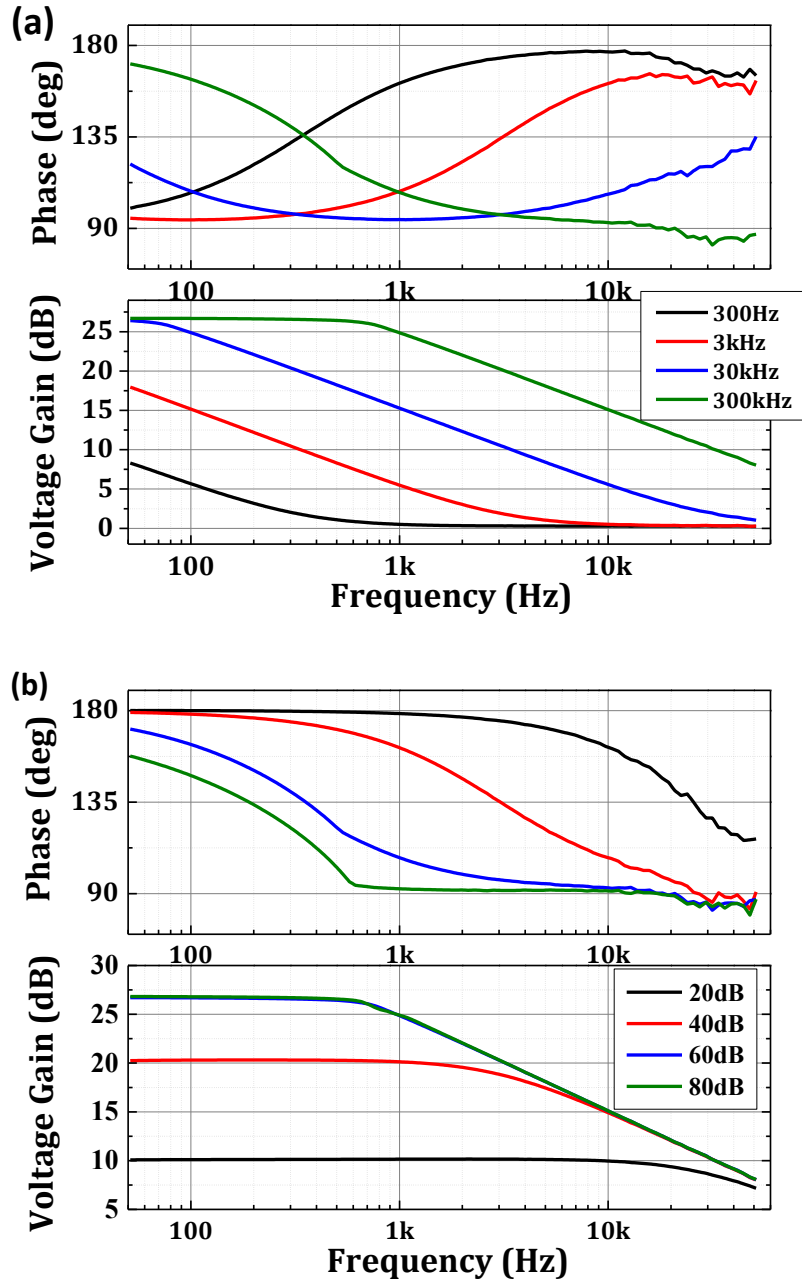
Figure 2-6: Frequency response (top: phase shift; bottom: amplitude) of the LB1005 high-speed servo controller with low-frequency gain limit. (a) Fix the LFGL at 60dB, and measure the frequency response when the PI corner frequency at 300 Hz, 3 kHz, 30 kHz, and 300 kHz; (b) Fix the PI corner frequency at 300 kHz, and measure the frequency response when the LFGL at 20 dB, 40 dB, 60 dB, and 80 dB.

Following is the standard locking procedure we used for laser frequency stabilization, and

Figure 2-7 shows the error signal before and after it is locked:

16

1. Stop scanning the laser, and use the DC offset to the PZT to center the detected SAS transmission signal on the Lorentzian feature, change the DC voltage slowly to make sure the level traces in the feature;

2. Turn lock switch to "LFGL";

3. Increase the proportional gain and LFGL (up to 90 dB) slowly, until the response oscillates, and then back down to stop the oscillations;

4. Turn switch to "Lock" to give a gain at DC.
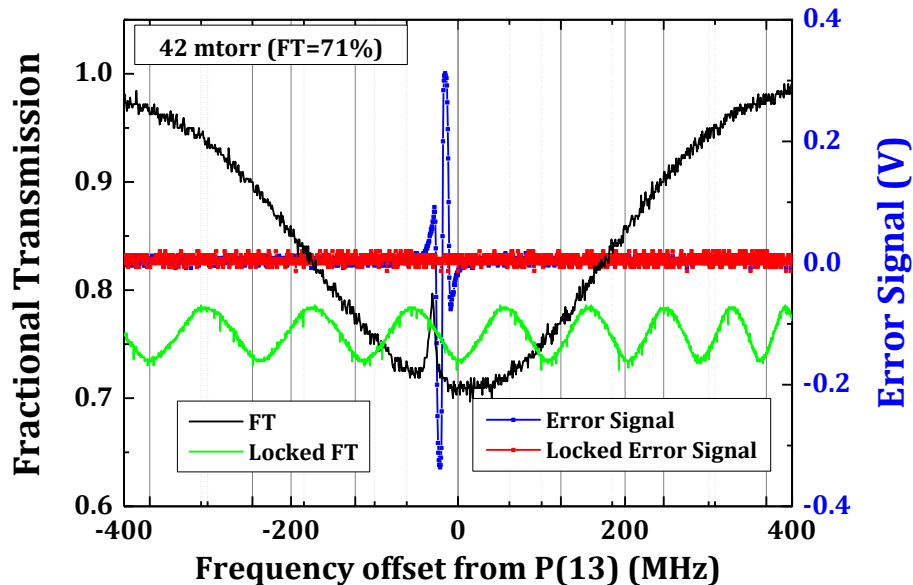
Figure 2-7: Fractional transmission and dispersion error signal before (plotted versus frequency) and after (plotted versus time) the laser being locked. The fractional transmission (black), and the dispersion error signal (blue) are observed when scanning the laser frequency. When the scanning is stopped, and the laser is locked, the error signal (blue) becomes the red, and the fractional transmission (black) becomes the green. The oscillation in the locked transmission signal (FT) is due to the 900 kHz AM frequency. If the green deviates a lot (goes to the top of the screen), the laser is out of lock.

To check if the laser frequency is correctly locked to the Lorentzian feature, there are normally two methods of verification. The first method is to reduce the proportional gain and flip

the switch back to "Lock off". The transmission signal should be close to the center of the Lorentzian feature. The other method is to monitor the DC level of the transmission signal after the laser is locked. Since the locking occurs near the bottom of the fractional transmission curve, the DC level should be much different when the laser is locked correctly than when the laser is not correctly locked.

2.2.   Stability and accuracy

Once the CW laser is stabilized to the acetylene frequency reference, it will have a very narrow frequency range near the resonant frequency of $^{12}C_2H_2$ overtone transition. When it comes to characterizing the performance of a frequency reference, frequency stability and accuracy are critical values. Our experiment focuses on the time-domain characterization of frequency references. The stability determines the frequency reference's consistency over time, while the accuracy tells the difference between the measured value or average value and the actual or published value. In our system, the frequency instability and absolute frequency uncertainty of the time-domain measurements may be from the temperature fluctuation around the fiber, environment vibration and the long-term aging of the gas-filled fiber cell.

For calibration, one method to directly measure the frequency variations of a frequency reference is the heterodyne frequency measurement. This frequency variation is converted down by a phase stabilized carbon nanotube fiber laser (CNFL) frequency comb [39] (Figure 2-8). Then the down-converted frequency is filtered, amplified, and fed into a frequency counter. Then we can calibrate the stability and accuracy of the frequency reference using the recorded converted down frequencies.

18

Specifically, the CNFL comb has a typical ring configuration where the carbon nanotubes act as a saturable absorber inside the cavity. The carbon nanotubes are placed on the end of an optical connector and a PZT fiber stretcher is used to control the cavity length. The laser is followed by a parabolic pulsed fiber amplifier, and then a supercontinuum is generated in the highly nonlinear fiber. By using different Fiber Bragg gratings (FBGs), we can select different portions of the supercontinuum to work at various wavelengths, from 1μm to 2μm (Figure 2-9) for this particular CNFL comb. The repetition frequency (f_{rep}) of the comb is detected using a portion of the light from the laser output, and it is stabilized by feedback to control the cavity PZT. The carrier-envelope offset (CEO) frequency (f_0) of the comb is obtained from an f-to-$2f$ self-referenced method [39]. The CEO frequency (f_0) is further controlled by the current of the pump laser diode. Both the f_{rep} (~ 167 MHz) and f_0 (~60 MHz) are detected and stabilized to a GPS disciplined Rb oscillator (Rb/GPS) (model GPS10RB).
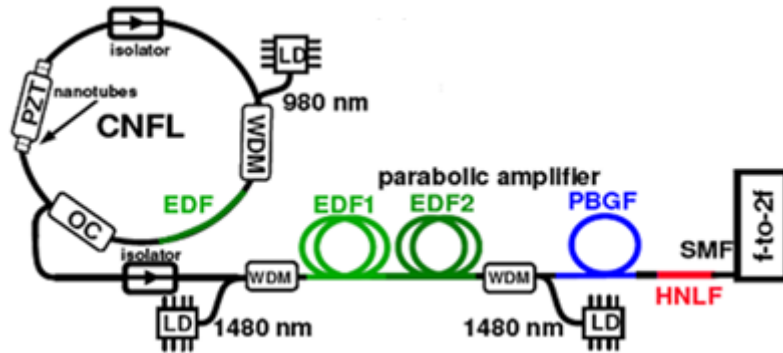
Figure 2-8: Reproduced from Ref. [39]. Schematic of the CNFL frequency comb. LD: laser diode; OC: output coupler; WDM: wavelength division multiplexer; PZT: piezoelectric transducer; EDF: erbium-doped fiber; PBGF: photonic bandgap fiber; SMF: single mode fiber; HNLF: highly nonlinear fiber.
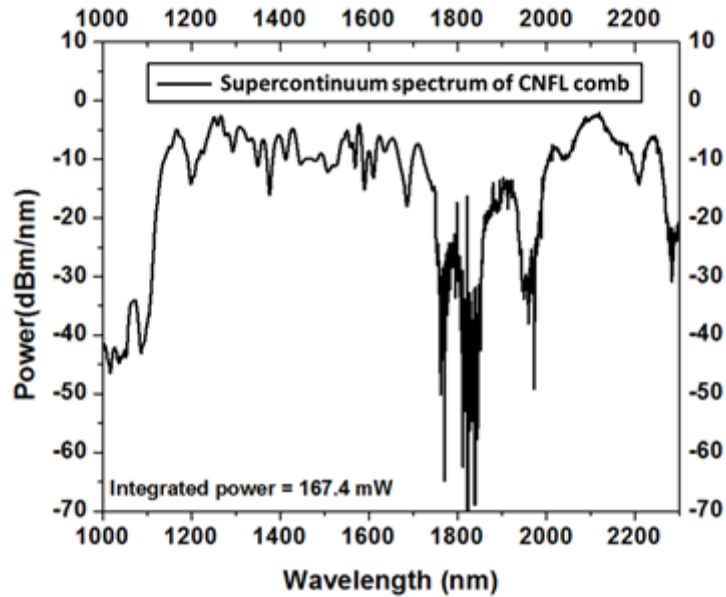
Figure 2-9: Reproduced from Ref. [39]. Supercontinuum spectrum of the CNFL frequency comb after the HNLF.

When a CW laser is locked to the acetylene frequency reference, one portion of the light split from the CW laser heterodyne beats with a tooth of the comb supercontinuum spectrum (Figure 2-10a). In this way, the frequency variations from the acetylene frequency reference is converted down to the beatnote frequency. As shown in Figure 2-10b, a 0.2 nm bandwidth reflecting FBG is used to filter out the unwanted supercontinuum of the CNFL comb. The center wavelength of the FBG is close to the wavelength of the stabilized frequency reference. Then, the filtered spectrum of the comb beats with the stabilized CW laser in order to obtain a beat frequency which is in the RF domain. Thus, this beat frequency can be filtered, amplified by electronics, and recorded by a frequency counter (HP53132A). The frequency counter also refers to the GPS/Rb signal for calibration purposes. The recorded frequency varies time of one of our measurements is plotting in Figure 2-10c, showing a 10 kHz frequency variance over a time period of about 90 mins. This measured results exhibits an oscillation with a period of ~15 minutes, and this

oscillation is correlated to air-conditioner cooling cycles in the lab.
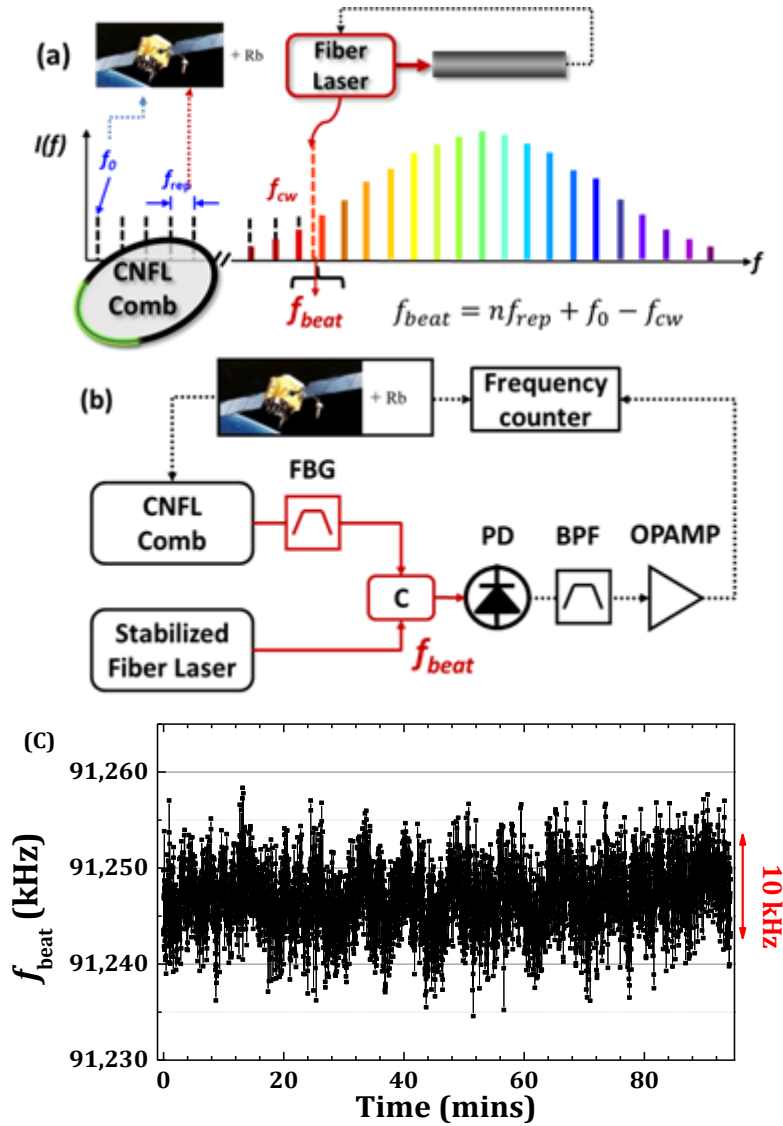
Figure 2-10: (a) Spectrum of the CNFL comb phase stabilized to the GPS-disciplined Rb oscillator and a CW laser stabilized to $^{12}C_2H_2$ inside kagome HC-PCF; the RF beat frequency can be obtained from the heterodyne of a comb tooth and the CW reference (fiber laser). (b) Optical and electrical schematic for the heterodyne beat frequency measurement. Solid lines are optical fiber connections, and dotted lines are electrical connections. The frequency counter (HP53132A) is used to record the various RF signals. FBG: fiber Brag grating. (c) Adapted from Ref.[24], recorded beat frequencies between CW reference and GPS-referenced frequency comb vs. time, recorded at a 1 s gate time using a counter. Oscillations with a period of ~15 minutes correlate to air-conditioner cooling cycles.

2.2.1. Allan deviation

Allan deviation is a two-sample variance (Eq.(2.2)) to measure the frequency stability of clocks, oscillators, and amplifier [40]. Unlike the standard deviation, which only indicates deviation information from a mean value, the Allan deviation indicates frequency variations from sample to sample. Furthermore, the Allan deviation was invented to characterize both systematic and random noise [41].

$$\sigma_y(\tau) = \sqrt{\frac{1}{2(M-1)}\sum_{i=1}^{M-1}(y_{i+1}-y_i)^2} \tag{2.2}$$

where M is the number of samples, y_n is the nth frequency measurement which is recorded or averaged for a time τ. And in some cases, y_n is the nth non-unit relative frequency measurement and gives the Allan deviation in a format of fractional instability, which we are going to use in this thesis.

Figure 2-11 is an example showing how the measured frequency and its corresponding Allan deviation are related. Three measurements are compared here, clearly shown in Figure 2-11. The pink triangle data represents a frequency that is not accurate nor stable, the green square shows an accurate but not stable frequency, and the orange star data is an accurate and stable frequency measurement. Generally speaking, a smaller Allan deviation means a better stability of the measured frequency at a given sample period.
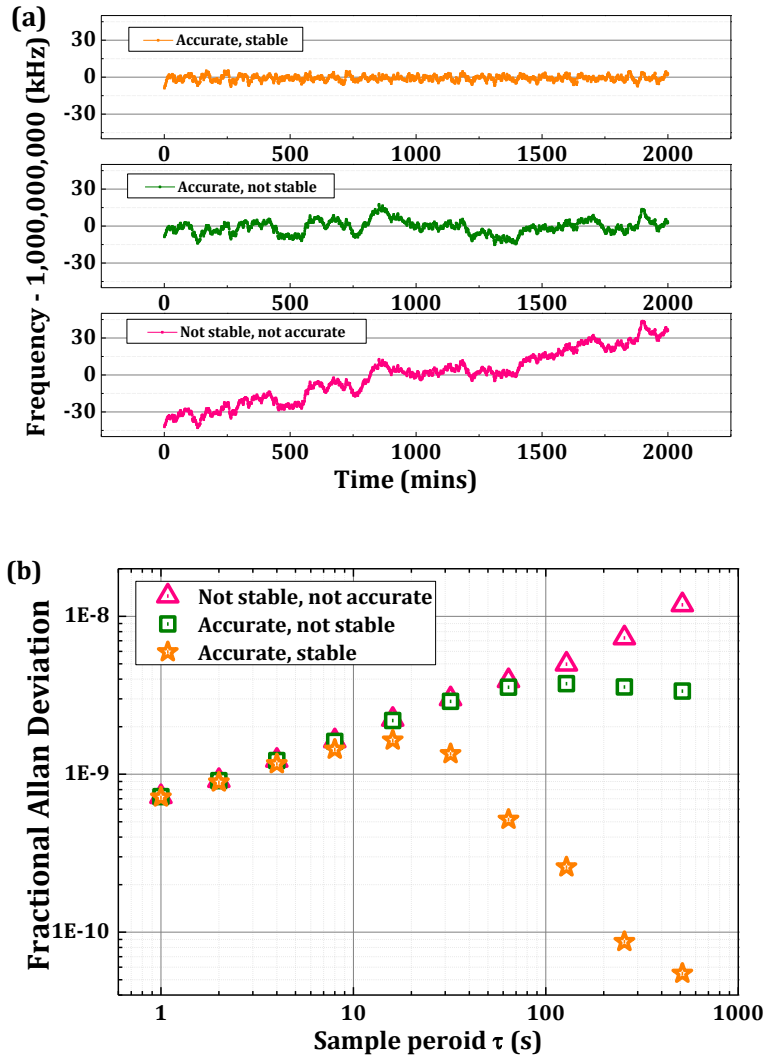
Figure 2-11: (a) Examples of the different measurements of a 1 GHz frequency and (b) the corresponding Allan deviations. Three cases are given out: pink triangle: the measured frequency is not accurate nor stable; green square: the measured frequency is accurate but not stable; orange star: the measured frequency is accurate and stable.

The stability of our acetylene frequency reference can be calibrated using Allan deviation from the RF beat frequency, shown in Figure 2-12, and a stability of 1.2×10^{-11} at 1s sample period time was obtained in our previous measurement [24]. The RF beat frequency between our optical references and frequency comb is shown in Figure 2-12 and also its calculated Allan deviation.
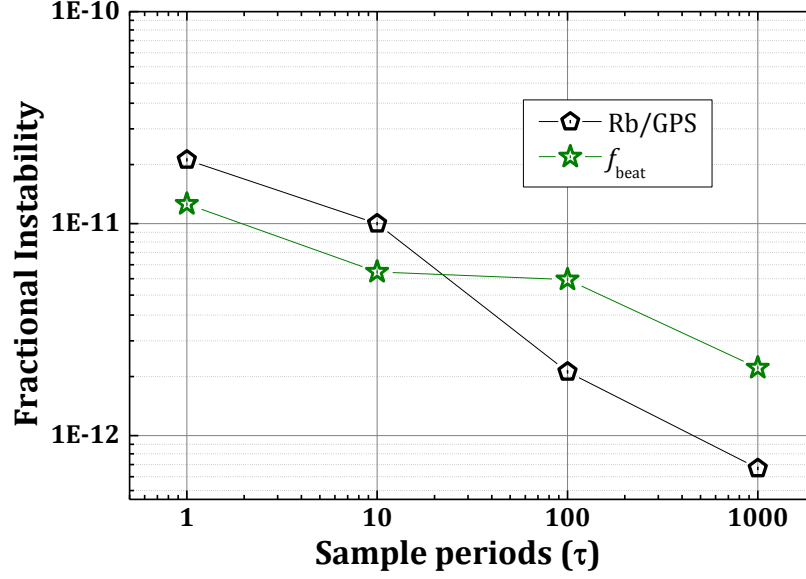
Figure 2-12: Adapted from Ref.[24]. (a) Frequency of the beat between the HC-PCF acetylene-stabilized laser and the CNFL frequency comb vs. time recorded at a 1 s gate time using a frequency counter. Oscillations with a period of ~10 minutes correlate to air-conditioner cooling cycles. (c) Optical fractional frequency instability vs. sample period for f_{beat} (filled squares) and the GPS disciplined Rb oscillator (open pentagons).

2.2.2. Absolute frequency measurement

Besides the stability calculated from the Allan deviation to fully characterize this CW optical frequency reference, the accuracy of its absolute frequency is also an important parameter [24]. The relationship between the measured optical reference's frequency (f_x) and the frequency of the nearest comb tooth (f_n) are given by the equations:

$$f_x + \frac{1}{2} f_{AOM} \pm \left| f_{beat} \right| = f_n = n \cdot f_{rep} \pm \left| f_0 \right| \tag{2.3}$$

where f_x is the frequency of the $^{12}C_2H_2$ P(13) ro-vibrational transition measured in the experiment, f_{AOM} is the frequency of the probe beam's AOM, f_n is the nearest comb tooth frequency, and 'n' is the nearest tooth mode number. The signs of f_{beat} and f_0 are ambiguous due to the mixing process, and are determined by changing the frequency lock point of both f_{rep} and f_0 while

24

observing f_{beat}.

To calculate the stabilized optical reference's frequency (f_x), we need to know the comb mode number 'n'. This can either be directly measured, or deduced from earlier measurements.

To directly determine the mode number 'n' without previous knowledge of the reference frequency, we can beat the reference frequency with two or more comb teeth by changing the repetition frequency of the locked comb [42]. After an initial heterodyne measurement between the optical frequency reference and the frequency comb, we change the repetition frequency of the comb to beat the frequency reference with at least a second comb tooth. The initial heterodyne measurement is between the reference and a comb tooth with model number 'n', and the second heterodyne measurement the comb tooth which beat with reference has a model number 'n + m'. The model number variance 'm' is directly observed in the experiment. Similar to Eq.(2.3), we could determine both the model number 'n' and its uncertainty δn using the following equation:

$$f_x + \frac{1}{2} f_{AOM} \pm |f_{beat1}| = f_n = n \cdot f_{rep1} \pm |f_{01}|$$
$$f_x + \frac{1}{2} f_{AOM} \pm |f_{beat2}| = f_{n+m} = (n+m) \cdot f_{rep2} \pm |f_{02}|$$
(2.4)

The signs of f_{beat} and f_0 are determined by changing the frequency lock point of both f_{rep} and f_0 while observing f_{beat}.

However, due to the limited tuning range of the repetition frequency of the comb[43], we are not using this method is our experiment. Instead, we used an alternative method to calibrate the absolute frequency of the frequency reference, which is to determine the model number 'n' with previous knowledge of the reference frequency. That is, we used an approximate absolute frequency beforehand (accurate to hundreds MHz) but not the exact value to calibrate model number 'n' of the nearest comb tooth that beats against the frequency reference. Then we obtain

25

the absolute frequency of the acetylene frequency reference using Eq.(2.3).

Due to the linear pressure shift of acetylene $^{12}C_2H_2$ v_1+v_3 rotational vibrational combination band [44], in our previous calibration of the gas-filled fiber optical frequency reference [24], a series of measurements were made under different acetylene pressures. Then a linear fitting was applied to the calculated acetylene line in order to find out the absolute frequency of the measured acetylene under vacuum. The beat frequency between the stabilized CW laser and the CNFL frequency comb was measured over 30 mins at 1 s gate time. Figure 2-12 plots the frequency of the reference with the AOM shift removed (f_x) versus acetylene pressure inside the acetylene-filled kagome fiber, and every measurement has an independent realignment of the SAS setup.
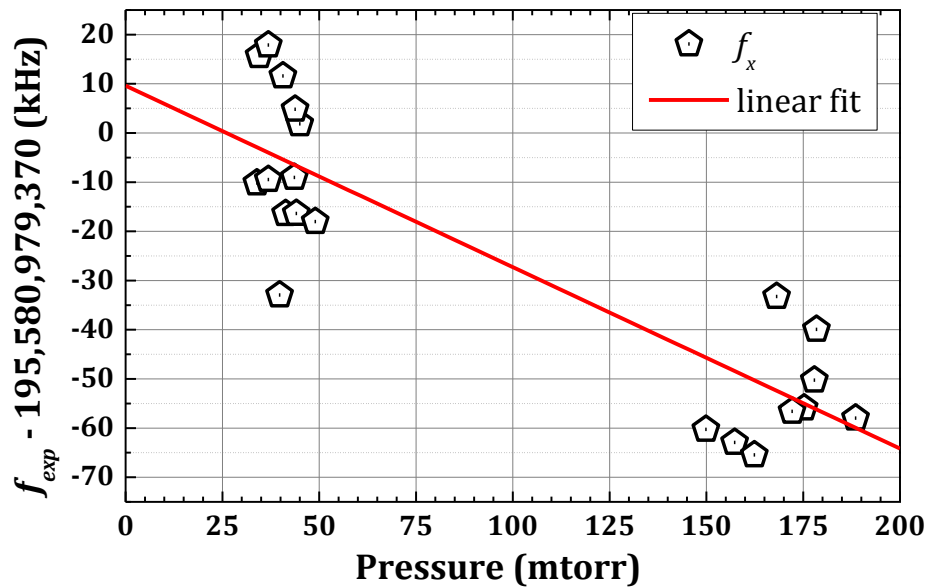
Figure 2-13: Reproduced from Ref.[24]. Absolute frequency measurement of the stabilized-laser to the acetylene P(13) line versus acetylene pressure. The kagome fiber length is 4.1 m, and a linear fitting is applied for the correction of pressure-induced frequency shift. Every measurement has an independent alignment to get rid of the frequency drifts due to free-space coupling into the kagome fiber. The linear fit gives a zero-pressure intercept of (195,580,979,378.0 ± 9.3) kHz.

After the correction for power shift is made, a linear fit to these data gives a zero-pressure

intercept of $(195,580,979,378.0 \pm 9.3)$ kHz with a slope of (-369 ± 48) kHz/torr. This measurement agrees within the uncertainty of other published values of the P(13) line measured in power build-up cavities and vapor cells, which have much narrower linewidths in the sub-Doppler features (FWHM ~ 1 MHz) [21, 45], shown in Table 2-1. We demonstrated a 10 kHz accuracy frequency reference on the $^{12}C_2H_2$ transition P(13) inside a hollow-core fiber between two vacuum chambers.

Table 2-1: Adapted from Ref.[36]. Mean $^{12}C_2H_2$ $v_1 + v_3$ P(13) frequency and uncertainty for this work [24], and for other published work [21, 45].

	Mean P(13) value (kHz)	Uncertainty (kHz)
This work	195,580,979,378.0	9.3
Ref. **[45]**	195,580,979,370.4	3.7
Ref. **[21]**	195,580,979,371.1	10.2

2.3. Remaining issues of acetylene frequency reference

The above calibration of the stability and accuracy of the acetylene frequency reference inside HC-PCF proves that the gas-filled kagome fiber is a suitable medium for portable precision spectroscopy. However, during our measurements, we observed there are several remaining issues of the acetylene frequency reference, which may degrade the frequency reference's performance.

2.3.1. Short-term stability

Short-term stability of a frequency device is usually measured over periods less than 10 s and resembles unpredictable noises. As mentioned in section 2.2, the direct fractional frequency instability of the acetylene frequency reference was calibrated from the in-loop heterodyne frequency measurement between the acetylene reference and the frequency comb. Therefore, the

direct fractional instability of the heterodyne frequencies includes the instability of both the frequency reference and the frequency comb, and is determined by the less stable one of the two. As Figure 2-12 shows, the measured short-term stability of our acetylene reference was limited by the GPS-disciplined Rb oscillator. The GPS is used to lock the comb. To better characterize the short-term stability, we locked a second laser to a duplicate acetylene-filled fiber frequency reference and compared them. Because of equipment availability, one lock was not as robust as the other, and consequently we used a well know three-cornered hat method [46] to extract the stabilities of each reference. The three-cornered hat measurement also used two frequency references and further included a frequency comb. We will explain the three-cornered hat method in greater detail in section 3.2.

2.3.2. Mode-dependent frequency shift

The kagome HC-PCFs used in our setup are typically multi-mode and therefore suffer from mode-dependent frequency shift [47]. This shift was observed as a sensitivity of the reference lock point to optical alignment of the free-space pump and probe beams into the fiber. Such modal frequency dependence may arise from sensitivity of sub-Doppler spectroscopy to wavefront curvature, and makes the portable frequency reference subject to environmental stresses such as thermal fluctuation and vibration, which cause modal interference within the fiber.

In our experiment, a frequency shift up to 100 kHz is observed when we change the pump and probe beam alignment (Pump x, Pump y, Probe x, Probe y of Figure 2-14) into the kagome fiber such that the power through the fiber was reduced by half. To ensure this frequency shift is not completely caused by the power reduction, we compared with the frequency shift when the

power was reduced to half but alignment was preserved (Pump power, Probe power of Figure 2-14). From the comparison result shown in Table 2-2, the frequency shift is not completely due to the power reduction through the fiber, but may also be caused by coupling to different modal content of the fiber when we change the pump and probe beam alignment.

Furthermore, we observed a similar behavior when we changed the alignment into the PD fiber (MMF x, MMF y of Figure 2-14), an 80 kHz frequency shift is detected. What is more important here is that the frequency shift is centered on the alignment when the power throughput the fiber is optimized (maximized). When the system's peak power was optimized through the kagome fiber and fiber connected to the photodetector, the frequency of the lock point was repeatable to ± 10 kHz.
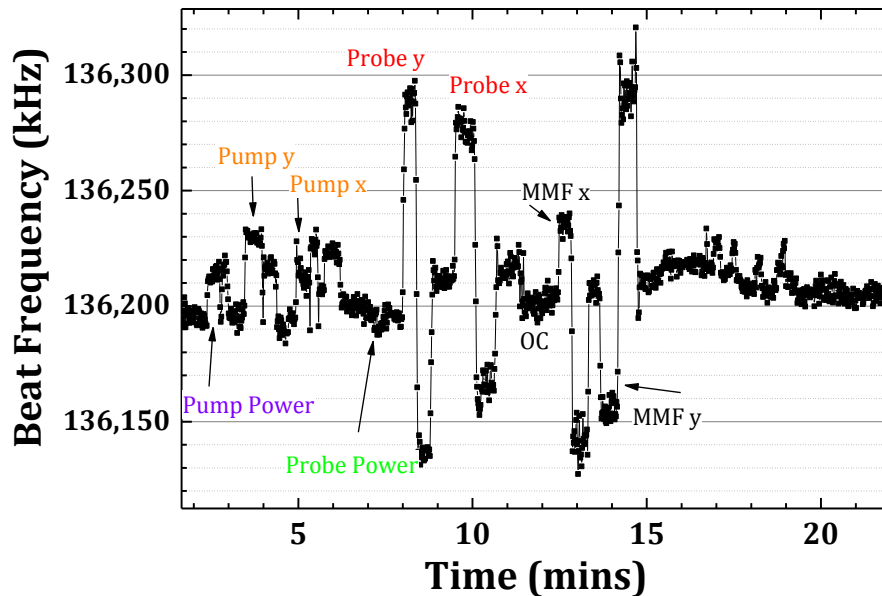
Figure 2-14: Adapted from Ref. [43]. Frequency shifts of the CW reference due to the misalignment of probe beam and pump beam. The beat frequency between the CNFL frequency comb and the CW reference is plotted vs. time. The text on the graph shows what parameters of the CW reference were changed to result in a change of the beat note frequency. x: horizontal mirror position; y: vertical mirror position; MMF: multimode fiber connected to the photodetector; OC: original coupling.

Table 2-2: Comparison of the frequency shifts of the CW reference when the power through the fiber is reduced to half of the original amount by changing different parameters of the reference.

Parameters	Pump x, y	Probe x, y	Pump power	Probe pump	MMF x, y
Frequency shift (kHz)	50	150	35	20	80

To reduce the frequency shift problem from the alignment sensitivity of the kagome fiber, a novel HC-PCF that is optimized for single mode operation [48] would be useful in our acetylene SAS setup. More details will be discussed later.

2.3.3. *Polarization sensitivity*

Besides the mode-dependent frequency shift of the acetylene frequency reference we discussed above, there is an additional frequency sensitivity of the reference lock point to the angle between the polarizations of the probe and pump beams coupled into the fiber in the SAS setup. When the probe polarization was changed by 30°, a shift of ~ 40 kHz (Figure 2-15) was detected in the beat frequency of the acetylene reference and the CNFL comb.

One thing to be noticed here is that the beat frequency is centered when there is an orthogonal polarization between the probe and pump beams. And when the probe polarization is adjusted by 30°, the power of the portion of probe beam which is still orthogonal to the pump beam is reduced by a factor of 2 ($\cos^2 30° = 1/2$). From the results in section 2.3.2 that a 20 kHz frequency shift was observed when the probe power was reduced by a factor of 2, we may conclude that the reference lock point is sensitive to the polarization between the probe and pump beams.

One possible solution to this sensitivity is to use polarization maintaining HC-PCF to make a frequency reference, which will further be discussed in a later chapter.
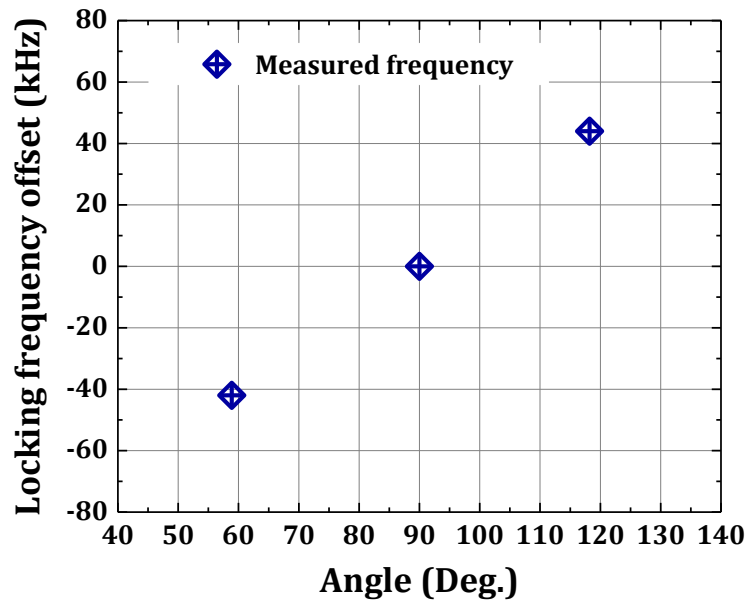
Figure 2-15: Adapted from Ref.[49]. Frequency shifts of the acetylene frequency reference due to the angle between the probe and pump polarization. The beat frequency between the CNFL comb and the reference is plotted vs. angle between the probe polarization and pump polarization.

Chapter 3. Improvement of Frequency Stabilization and Characterization

As we discussed in the last section, saturated absorption spectroscopy (SAS) inside hollow-core photonic crystal fibers (HC-PCFs) allows us to build a robust and portable frequency reference. More importantly, the fiber geometry can give long interaction lengths between the filling gas and the laser field, and the low-loss of HC-PCF facilitates the optical interactions with low power levels. Although the small core size limits the linewidth of saturated absorption features, fiber-based spectroscopy can still provide high accuracy frequency measurements[24]. A 10 kHz accuracy frequency reference is demonstrated in a $^{12}C_2H_2$ transition inside a hollow-core fiber between two vacuum chambers [24].

The linewidth broadening of the gas-filled fiber frequency references sets an inherent limit on its performance, affecting the stability and accuracy of the frequency references. Therefore, approaches are investigated to narrow the linewidth of the molecular transition with an aim towards improving the stability of gas-filled fiber frequency references. Besides the techniques for linewidth narrowing, we improved the short-term stability measurement of the P(13) $\nu_1 + \nu_3$ transition in $^{12}C_2H_2$ by constructing a second vacuum-chamber-based fiber reference and making a three-cornered hat measurement. In addition, for a better characterization of the absolute frequency measurements, a small correction ($< 1\sigma$) to the absolute frequency is calculated and applied to the previous results [24], based on careful modeling of an asymmetric error signal [37]. In the end, a single mode HC-PCF is used to improve the mode-dependent frequency shift we observed in the multi-mode kagome based frequency references.

3.1. Linewidth reduction

The linewidth and signal-to-noise (S/N) ratio of the molecular transition can determine the optimum stability (σ) of a frequency standard at different sample period [5] by:

$$\sigma(\tau) = \frac{\Gamma}{f_{C_2H_2} \cdot (S/N) \cdot (BW) \cdot \tau^{1/2}} \tag{3.1}$$

where Γ is the linewidth of the measured absorption line, $f_{C_2H_2}$ is the frequency of the absorption line, S/N is the signal to noise ratio, BW is the bandwidth of the low-pass filter right before the servo electronics, and τ is the sample period of the frequency requisition. In order to experimentally narrow the linewidth and increase S/N ratio of the molecular transition, techniques such as slow molecule selection and temperature reduction have been explored in this section.

3.1.1 Slow molecule selection

The $^{12}C_2H_2$ transition linewidth (Γ) inside HC-PCF is broadened by different physical mechanisms in different pressure ($p_{^{12}C_2H_2}$) and pump power (P) ranges [34, 50]. We use two dimensionless parameters in Eq.(3.2) for illustrating the mechanisms, summarized in Table 3-1.

$$\eta = \frac{p_{^{12}C_2H_2}}{p_0}, \quad \theta = \sqrt{\frac{P}{P_{sat}}} \tag{3.2}$$

Where $p_0 = 2.2$ torr, $P_{sat} = 23$mW is the saturation power of $^{12}C_2H_2$ spectroscopy inside 10μm HC-PCF [51].

Table 3-1: $^{12}C_2H_2$ transition linewidth determination mechanism

Regime	Parameters	Linewidth determined by
1	$\theta \leq \eta \leq 1$	pressure
2	$\eta \leq \theta \leq 1$	pump power
3	$\eta \leq 1 \leq \theta$	fiber core size
4	$1 \leq \eta$	intermolecular collisions

The gas-filled HC-PCF provides long interaction lengths for use with weak molecular transitions. However, a small inner core size of the fiber limits the linewidth (transit-time limit) of the saturated absorption feature (regime 3), thereby limiting the stability and accuracy of the reference. In order to narrow the transition linewidth (Γ) inside HC-PCF, we use the technique of slow molecule selection provided by Hald et. al. [34]. A commercially available 7-cell HC-PCF [52] with a core size of 10 μm was used in Hald's experiment. Sub-Doppler linewidths on the order of 40 MHz were observed at high pump power ($\geq$ saturation power of 23 mW, regime 3). By reducing the pump power (switch to regime 2 from regime 3), only the "slow" molecules with smaller radial velocities have enough time to interact with the field, and longer interaction times between the field and molecules lead to a narrower linewidth. In the meantime, the slow molecules can provide a similar S/N ratio due to a higher degree of saturation. In Hald's paper, the linewidth was reduced to 15 MHz when the pump power was reduced below the saturation power.

For a more accurate measurement of the acetylene linewidth at low pressure and low power, we repeated Hald's measurement in our 19-cell kagome system (Figure 2-2). The probe power of our experiment is normally around 0.2 mW unless the pump power is smaller than 0.2 mW. When the pump power is below 0.2 mW, we reduce the probe power to make it equal to the pump power. The linewidth, S/N ratio of the error signal, and calculated ratio of S/N to Γ (Figure 3-1) are observed and calculated.
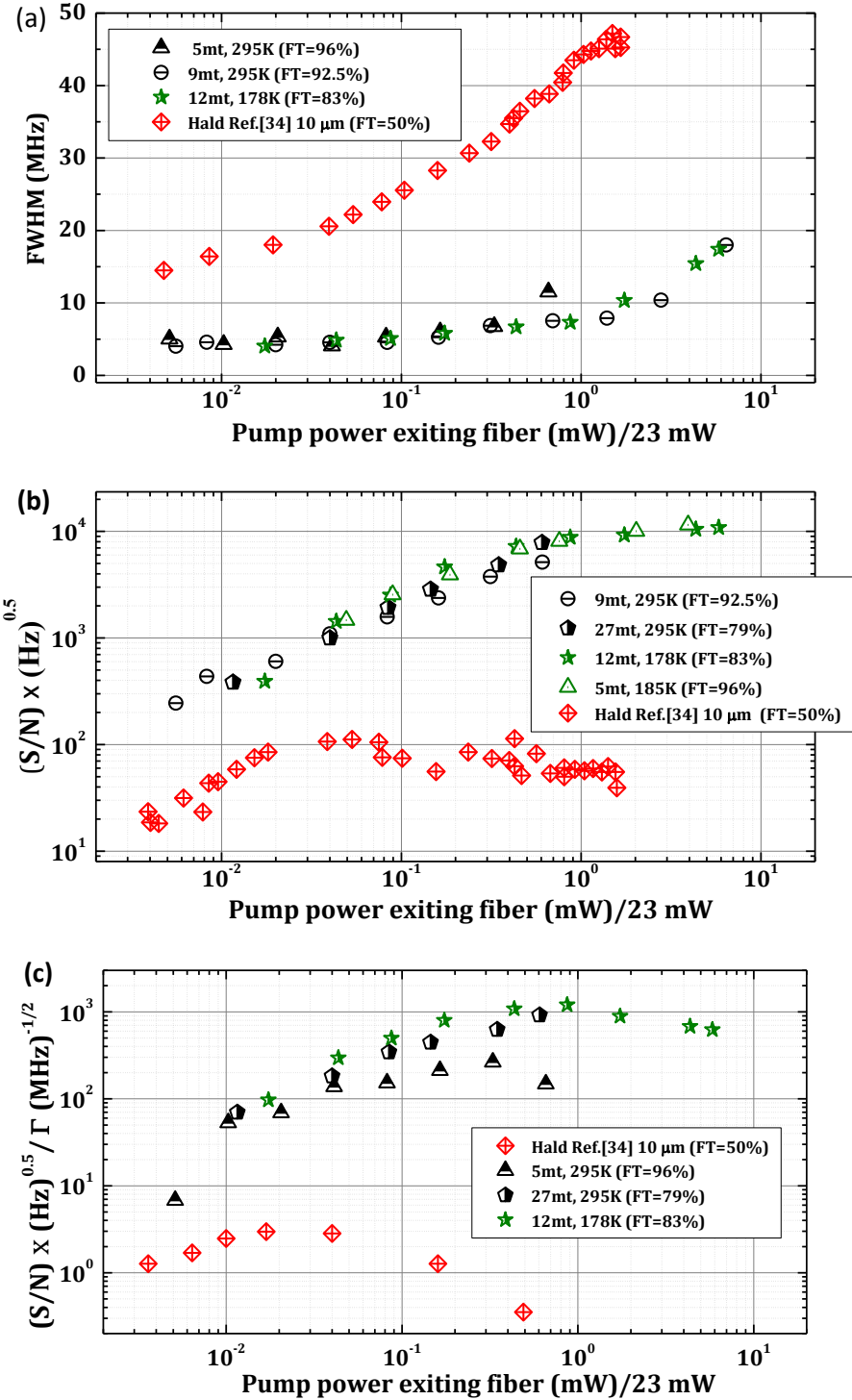
Figure 3-1: (a) FWHM, (b) S/N ratio and (c) S/N ratio to Γ of error signal vs. normalized pump power of the P(13) ν₁+ν₃ transition in $^{12}C_2H_2$ inside 4.1 m length of large-core (70 μm) kagome fiber. Data is measured at both room temperature (~295 K) (black) and cold temperature (~180 K) (green) using the experiment setup shown Figure 2-2, and compared with Hald's observation (red) in 10 μm HC-PCF Ref [34].

In our gas-filled kagome fiber, we observed a factor of two reductions in linewidth (from 10 MHz down to 5 MHz) by reducing the pump power (Figure 3-1a), although the starting linewidth is much narrower than that shown in Ref [34]. However, the S/N ratio of the SAS error is also reduced (Figure 3-1b), limiting the utility of the narrowing. The large core size fiber in our reference, which results in a small linewidth, requires a much lower acetylene pressure than Ref. [34] for wall collisions dominating over molecule-on-molecule collisions. So background pressure is more likely to limit our results than those of Ref. [34], and our measurement is more sensitive to the background pressure (we more easily fall into regime 1 than regime 2 when we keep reducing pump power).

3.1.2 *Molecule temperature reduction*

In order to reduce the effect of background pressure ($P \propto T$) on our reference and the average velocities of molecules ($v \propto \sqrt{T}$), we reduced the temperature of the acetylene-filled kagome fiber. We expect an increase in the S/N ratio and a decrease in the linewidth under a lower background pressure and a slower average velocity.

Experimentally, we used liquid N_2 and a heating plate with a temperature servo to control the temperature of the acetylene-filled kagome fiber (Figure 3-2). In the experiment, we did not observe any absorption at temperatures below $\sim$ 165 K. Acetylene may dissolve in acetone at temperature below $\sim$ 165 K, and the dissolved acetylene caused the absorption to disappear. We added more liquid N_2 to the temperature bath reservoir and fixed the current ($\sim$ 2A) through the resistors on the heating plate. We tracked the temperature of HC-PCF, when the temperature is close to 150 K, we turned on the temperature servo system (Figure 3-3a).

36

By carefully choosing the set point and other parameters of the temperature proportional-integral-derivative (PID) controller (Omega CN 7500), the PID controller automatically converts the measured temperature to an input signal parameter for the PID controller. Then the output signal from the PID controller is sent to the locking electronics, and the locking electronics send an output voltage to the resistors mounted on the heating plate. The locking electronics here are working as a proportional servo for increasing the control bandwidth. An output current is flowing through the resistors, and the heating plate is heated up. The PID control schematic is shown Figure 3-3b. When the input of the PID controller is lower than the set point, the PID controller will increase the output current, and when the input is higher than the set point, the PID controller will decrease the output current. Correspondingly, the temperature control unit will heat up and cool down. We successfully stabilized the temperature of kagome fiber to ~ 178 K for 37 mins.
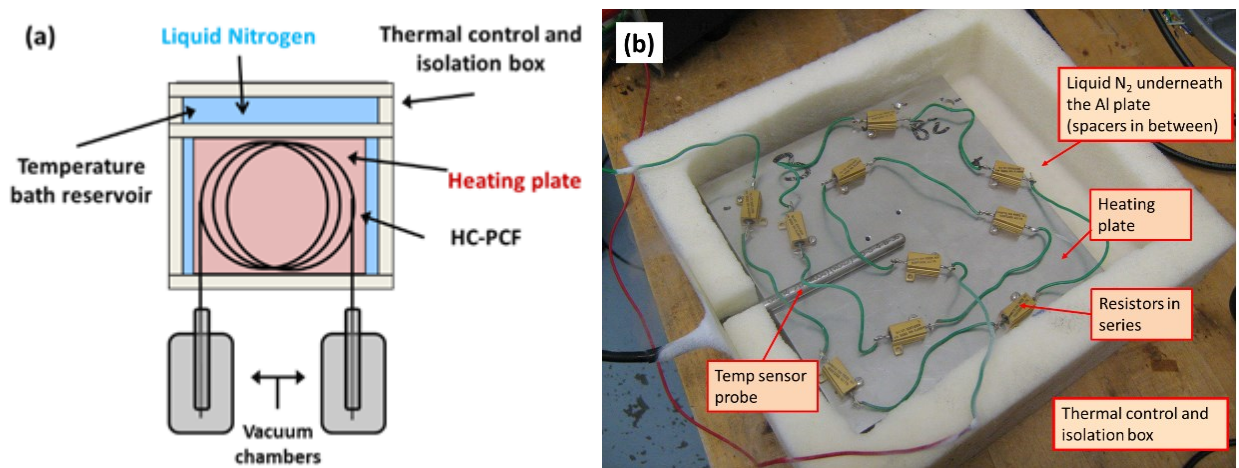
Figure 3-2: (a) Physical layout (top view) of the temperature control of gas-filled HC-PCF. The thermal box has a separate reservoir (with holes drilled to connect to the reservoir) so that a temperature bath can be loaded without directly pouring it on the HC-PCF. (b) Actual construction layout of the temperature control of gas-filled HC-PCF, the HC-PCF (not shown) is attached to another thin layer Aluminate plate and set on the top of the heating plate. The liquid N₂ is underneath the heating plate.
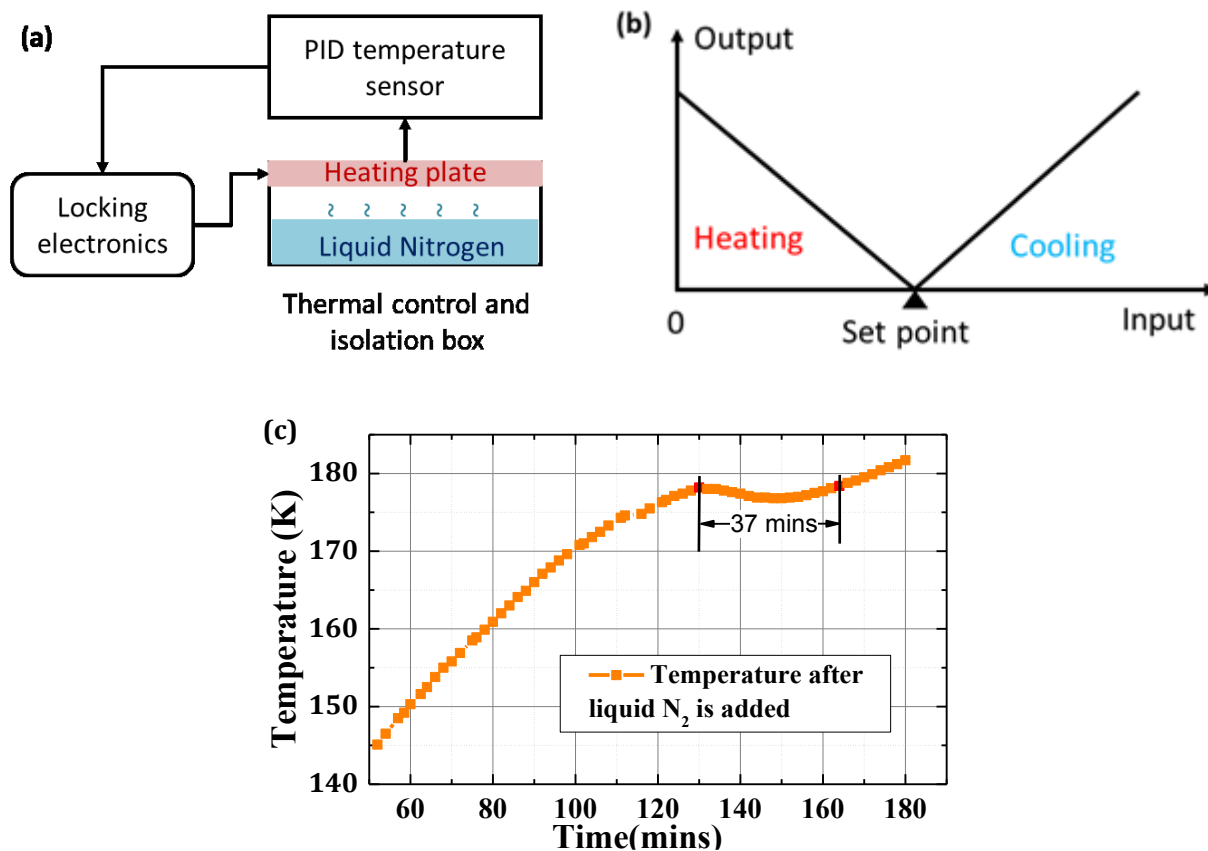
Figure 3-3: (a) Schematic for temperature feedback control of gas-filled HC-PCF. PID temperature sensor: Omega Autotune PID Temperature controller CN7500. Locking Electronics: Precision Photonics locking servo LB1005. (b) PID control by Omega CN 7500. (c) Temperature of the gas-filled HC-PCF versus time after loading liquid nitrogen. Temperature was stabilized at ~ 178 K for 37 mins.

We repeated the measurement of acetylene SAS at ~ 178 K using the setup in Figure 2-2. The linewidth, S/N ratio of the error signal, and calculated ratio of S/N to linewidth were measured and plotted in Figure 3-1 (green data points). Unfortunately, we did not observe any essential changes in linewidth and only a small improvement in S/N ratio may due to the background contaminations in the fiber. In the experiment, a lower background pressure may be required to observe the slow molecule selection mechanism in the acetylene-filled kagome fiber reference setup. It can be realized by improving the tightness of the vacuum chambers. Even so, the stability

of our frequency standard is still two orders better than Ref. [34] (Figure 3-1c), which may due to smaller core size, and also higher-speed modulation (Table 3-2).

Table 3-2: Experiment parameters for acetylene saturation absorption spectroscopy

	Fiber core size	AM modulation frequency
Hald Ref [34]	10 μm	1.3 kHz
This work	70 μm	900 kHz

3.2. Three-cornered hat measurement

In general, the frequency stability (Allan deviation) of a frequency reference is measured only by the heterodyne measurement with another frequency reference, which has superior frequency stability. The direct frequency instability from the heterodyne measurement can be used as the instability of the frequency device under test. However for the case in which the other frequency device does not have a superior stability to the device under test, a standard procedure is to use three or more frequency devices and to compare these devices two by two [46].

3.2.1. Comparison of three frequency devices with fractional instability

In this case, three frequency devices A, B, and C are compared two by two as shown in Figure 3-4. The fractional instability (Allan deviation) of the heterodyne frequencies between two of the devices are respectively σ_{AB}, σ_{AC}, σ_{BC}, and directly related to the fractional instability of the each frequency device σ_A, σ_B, σ_C.

$$\sigma_{AB}^2(\tau) = \sigma_A^2(\tau) + \sigma_B^2(\tau)$$
$$\sigma_{AC}^2(\tau) = \sigma_A^2(\tau) + \sigma_C^2(\tau) \qquad (3.3)$$
$$\sigma_{BC}^2(\tau) = \sigma_B^2(\tau) + \sigma_C^2(\tau)$$

Where τ is the sample period for the fractional instability calculation.
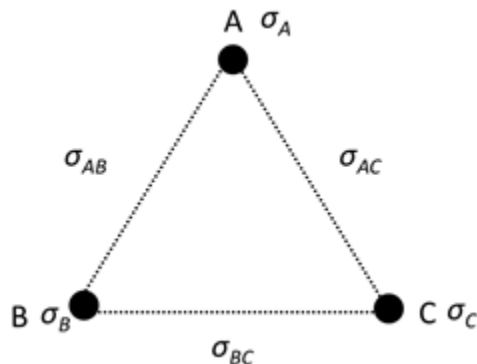
Figure 3-4: Three-cornered hat measurement by comparing frequency devices two by two. σ_{AB}, σ_{AC}, **and** σ_{BC} **is the fractional instability of the heterodyne frequencies between two of the devices while** σ_A, σ_B, **and** σ_C **are the fractional instabilities of each frequency device.**

To obtain the fractional instability of an individual frequency device such as A, under the assumed uncorrelated frequency instability, we have:

$$\sigma_A(\tau) = \sqrt{\frac{1}{2}\left(\sigma_{AB}^2(\tau) + \sigma_{AC}^2(\tau) - \sigma_{BC}^2(\tau)\right)} \tag{3.4}$$

Notably, the revisited three-cornered hat measurement [53] can be used to obtain a better estimation of fraction instability σ_A of each frequency device. When N frequency devices are included in one system, N(N-1)/2 different sets of frequencies devices are formed for each set. For simplification, in our experiment, we only use three frequency devices and assume they are uncorrelated.

3.2.2. Individual frequency reference stability acquisition

For a better characterization of the short-term stability, we locked a second laser to a duplicate gas-filled fiber and compared them. As we mentioned in the last chapter, we introduced the three-cornered hat method [46] to extract the stabilities of each reference.

To obtain our best reference stability, we measured the beat frequencies among the CNFL comb and two stabilized fiber lasers (Figure 3-5a). The fiber lasers are independently locked to the $^{12}C_2H_2$ P(13) transition in two separate kagome-structured HC-PCFs between vacuum chambers in Figure 2-2. Under the assumption that the CNFL comb and two stabilized fiber lasers are uncorrelated, we calculated the fractional instability of each individual laser (laser 1 and 2), and compared with the individual fractional instability of other groups' acetylene stabilized lasers realized in free-space gas cells [22, 54]. In Refs. [22, 54], only the fractional instability between two identical stabilized lasers was measured and calculated. For comparison, we divide the fractional instability between two identical stabilized lasers by $\sqrt{2}$ and use the divided fractional instability as the fractional instability of each individual laser.

Even though our acetylene linewidth is a factor of 10 broader than the gas cell setup [22, 54], the stability of our fiber-based reference is still comparable to their results, as shown in Fig. 3b. Furthermore, the stability of 2×10^{-12} at 0.1 s of our fiber-based acetylene frequency reference is obtained. To our knowledge, this performance is comparable to the best stability achieved in acetylene frequency references [54].
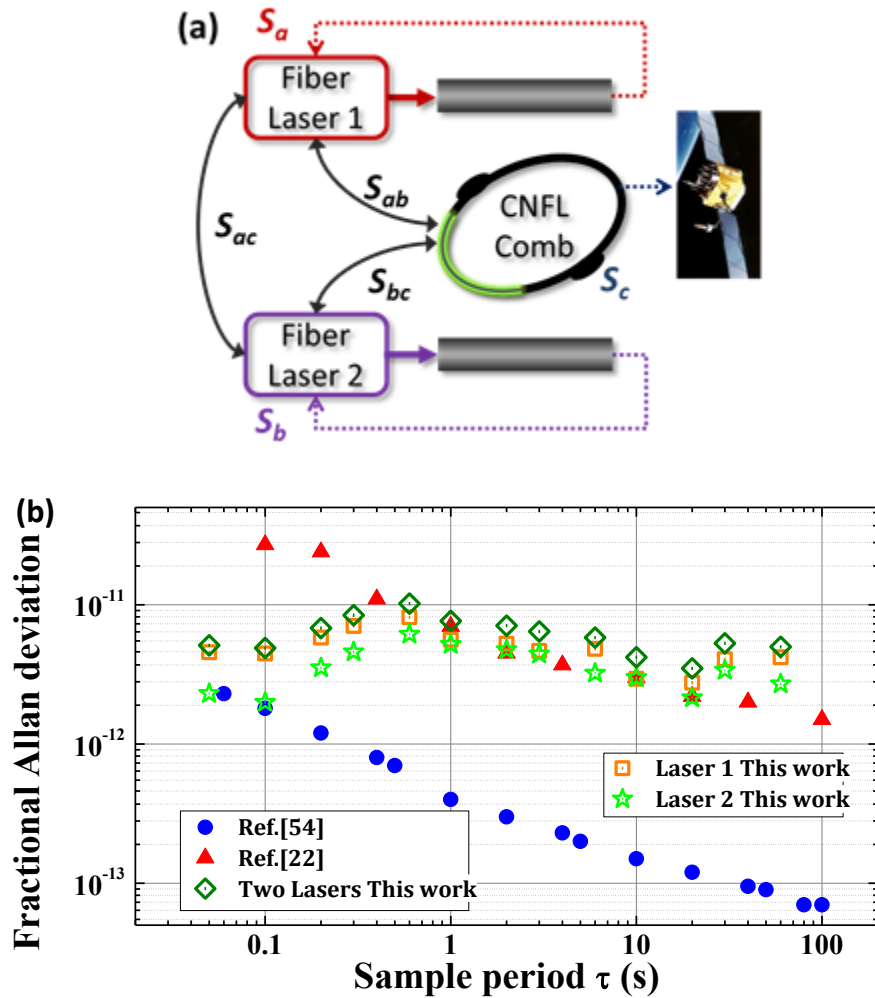
Figure 3-5: Adapted from Ref. [36, 55]. (a) Schematic of the three-cornered hat measurement between two acetylene-stabilized fiber lasers and a phase stabilized CNFL comb. (b) Fractional Allan deviation of acetylene-stabilized fiber laser 1 and laser 2 from the three-cornered hat measurement compared to modified data from Ref. [54] and Ref. [22].

3.3. Frequency modulation modeling

While our previous absolute frequency measurement of the P(13) acetylene transition line agreed with other published values within 1σ [21, 45], further investigation reveals distorted lineshape due to the frequency difference introduced by an AOM between the pump and probe beam. This distortion creates an additional shift at the kHz level which can be calculated by extending the frequency modulation (FM) modeling describe in Ref.[37].

42

3.3.1. Basic theory

In Ref. [37], a theoretical analysis of the lineshapes of FM spectroscopy is carried out under various experimental conditions. Similar to Ref. [37], an experiment arrangement for FM spectroscopy is used especially in saturation absorption spectroscopy (SAS) is shown in Figure 3-6.
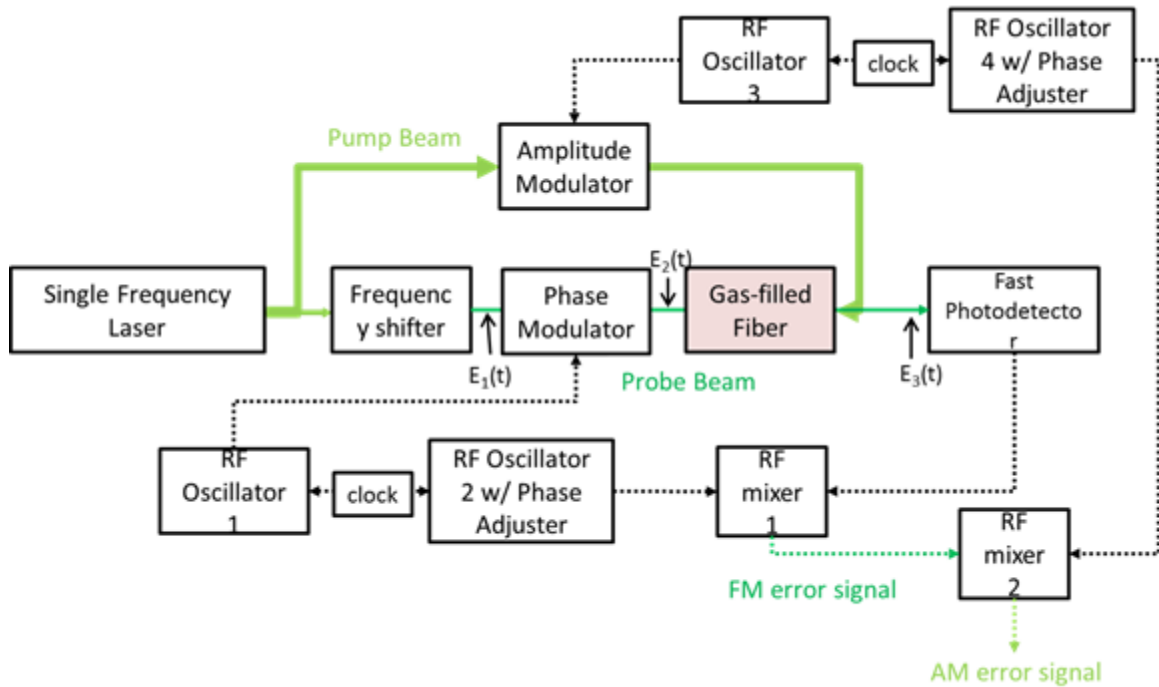
Figure 3-6: Block diagram of FM spectroscopy. The experimental arrangement also includes an amplitude modulation for background noise rejection. Solid lines are optical fiber connections, and dotted lines are electrical connections. $E_1(t)$, $E_2(t)$, and $E_3(t)$ are respectively the probe electric field after the frequency shifter, after the FM phase modulator, and after the sample gas.

In general, the electric field $E_1(t)$ after the frequency shifter is described by:

$$E_1(t) = \frac{1}{2} E_1(t) + c.c. \tag{3.5}$$

where

$$E_1(t) = E_0 \cdot \exp(i\omega_c t) \tag{3.6}$$

43

E_0 is the electric field amplitude of the original laser beam after the frequency shifter, and ω_c is the carrier frequency of the electric field $E_1(t)$. We use a normalized E_0 ($E_0 = 1$) in following derivation.

When FM modulation index M is small ($M \ll 1$), the FM modulated electric field $E_2(t)$ is described by:

$$E_2(t) = \frac{1}{2}E_2(t) + c.c. \tag{3.7}$$

where

$$E_2(t) = -\frac{M}{2}\exp[i(\omega_c - \omega_m)t] + \exp(i\omega_c t) + \frac{M}{2}\exp[i(\omega_c + \omega_m)t] \tag{3.8}$$

ω_m is the FM modulation frequency, and $\omega_c - \omega_m$, $\omega_c + \omega_m$ are the frequencies of two sidebands.

The FM modulated electric field $E_2(t)$ then passes through the sample gas containing the spectral feature, and the transmitted electric field through the sample gas is:

$$E_3(t) = \frac{1}{2}E_3(t) + c.c. \tag{3.9}$$

where

$$E_3(t) = -T_{-1}\frac{M}{2}\exp[i(\omega_c - \omega_m)t] + T_0\exp(i\omega_c t) + T_1\frac{M}{2}\exp[i(\omega_c + \omega_m)t] \tag{3.10}$$

$$T_j = \exp(-\delta_j - i\varphi_j), \quad j = -1, 0, 1 \tag{3.11}$$

$T_j (j = -1, 0, 1)$ represents the amplitude transmission at $\omega_c - \omega_m$, ω_c, and $\omega_c + \omega_m$ respectively. δ_j describes the attenuation, and φ_j describes the optical phase shift of each frequency component. The attenuation (δ) can be obtained from the theoretical line profiles and the measured absorption curve, and the optical phase shift (φ) can be derived from the attenuation (δ) by using the Kramers–Kronig relations (Eq.(3.12)).

44

$$\varphi(\omega) = -\frac{1}{\pi} p \int_{-\infty}^{\infty} \frac{\delta(\omega')}{\omega' - \omega} d\omega' \tag{3.12}$$

Furthermore, the intensity envelope $I_3(t)$ (Eq.(3.13)) of the transmitted beam that goes to the photodetector is proportional to $|E_3(t)|^2$. Ignoring terms of order M^2 and assuming the attenuation and phase shift difference between the sidebands and the carrier are small ($\ll 1$),

$$I_3(t) \propto |E_3(t)|^2 = \exp(-2\delta_0)[1 + (\delta_{-1} - \delta_1)M\cos(\omega_m t) + (\varphi_{-1} + \varphi_1 - 2\varphi_0)M\sin(\omega_m t)] \tag{3.13}$$

Then the fractional transmission of the transmitted beam is:

$$FT = \exp(-2\delta_0) \tag{3.14}$$

The FM absorption error signal can be derived from:

$$S_1(\omega) \propto \frac{1}{T} \int_0^T I_3(t)\cos(\omega_m t)dt \tag{3.15}$$

The FM dispersion error signal is:

$$S_2(\omega) \propto \frac{1}{T} \int_0^T I_3(t)\sin(\omega_m t)dt \tag{3.16}$$

From above, the FM spectroscopy of the sample gas depends on the complete information of the amplitude and phase shift of the carrier and two modulated sidebands. In addition, an amplitude modulation (AM) is further added for background noise rejection. By subtracting the error signal with pump on from the error signal with pump off, a background noise-free residual error signal after the pump beam AM can be obtained.

3.3.2. *Theoretical FM spectroscopy of acetylene*

A mathematical computing code (Appendix A) was written for the FM modeling of acetylene SAS. As stated in the last section, the amplitude information (δ) and the phase information (φ) from the Doppler and sub-Doppler features are required for computing the FM absorption error, FM dispersion error, and AM error.

In the measurement of acetylene FM spectroscopy, when there is only a probe beam, the attenuation δ of the Doppler absorption is given as [35]:

$$\delta_D(\omega) = \frac{1}{2} \cdot A_g \cdot Exp\left[-\frac{(\omega + 2\pi \cdot 0.5 f_{AOM})^2}{0.36\ \omega_D^2}\right] \tag{3.17}$$

where A_g is the amplitude of the Doppler absorption, ω_D is the Doppler linewidth, and f_{AOM} is the frequency shift of the probe beam from the laser frequency.

In the presence of the pump, the attenuation coefficient is given by Eq. (2) multiplied by a Lorentzian, resulting in

$$\delta_S(\omega) = \delta_D(\omega) \cdot \left(1 - \frac{A_l}{R^2[\omega] + 1}\right) \tag{3.18}$$

where R[ω] is a normalized frequency given by the expression

$$R[\omega] = \frac{\omega}{2\pi f_l / 2} \tag{3.19}$$

Here, A_l is the amplitude of sub-Doppler absorption, and f_l is the sub-Doppler linewidth of the P(13) transition of $^{12}C_2H_2$.

In Equations (3.17) and (3.18) above, ω_D = 470 MHz is calculated from the Doppler-broadened width of the P(13) line of $^{12}C_2H_2$, f_l is the linewidth of the sub-Doppler (Lorentzian) feature, and the parameters A_g and A_l are related to the fractional transmission and pump power

measured in the spectroscopy. The typical values of $A_g = 0.69$, $A_l = 0.3$, and $f_l = 10$ MHz are for a signal with a 50% fractional transmission (FT), and with 32 mW of pump power exiting the fiber.

Following the derivation in section 3.3.1 with the optical frequency modulation frequency occuring a frequency of 22 MHz, the attenuation δ, fractional transmission phase shift φ, FM absorption error signal, and FM dispersion error signal of SAS are calculated with and without the presence of the pump beam (pump-on and pump-off). Figure 3-7 and Figure 3-8 show the plots of those calculations versus a varying frequency (≫ FM modulation frequency) near the carrier frequency. The amplitudes of error signals are multiplied by a factor of 326 in order to normalize the AM dispersion signal in a later calculation.
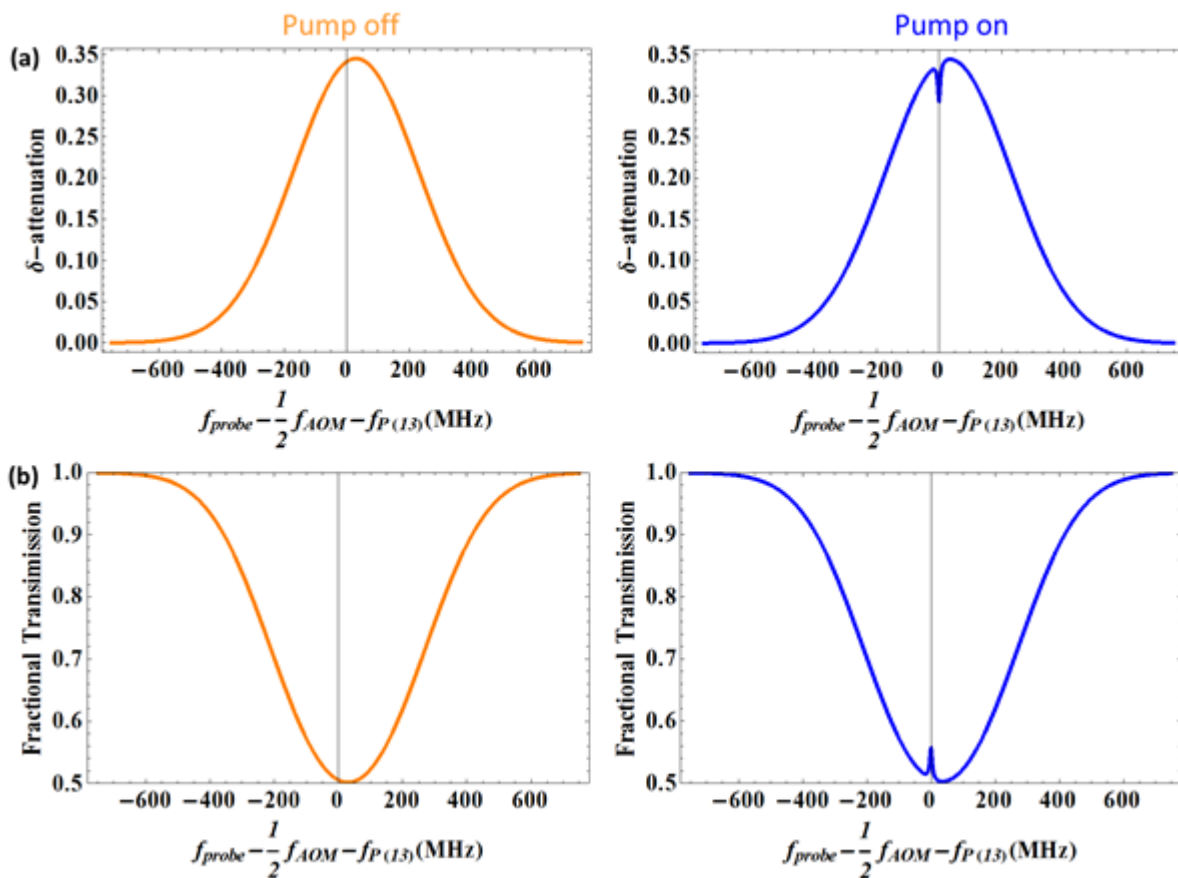
Figure 3-7: Theoretical calculations (left: pump-off; right: pump-on) of SAS of P(13) line of $^{12}C_2H_2$, with an FT of 50%, exiting fiber pump power of 32 mW, and FM frequency at 22 MHz. (a) The attenuation δ; (b) the fractional transmission.
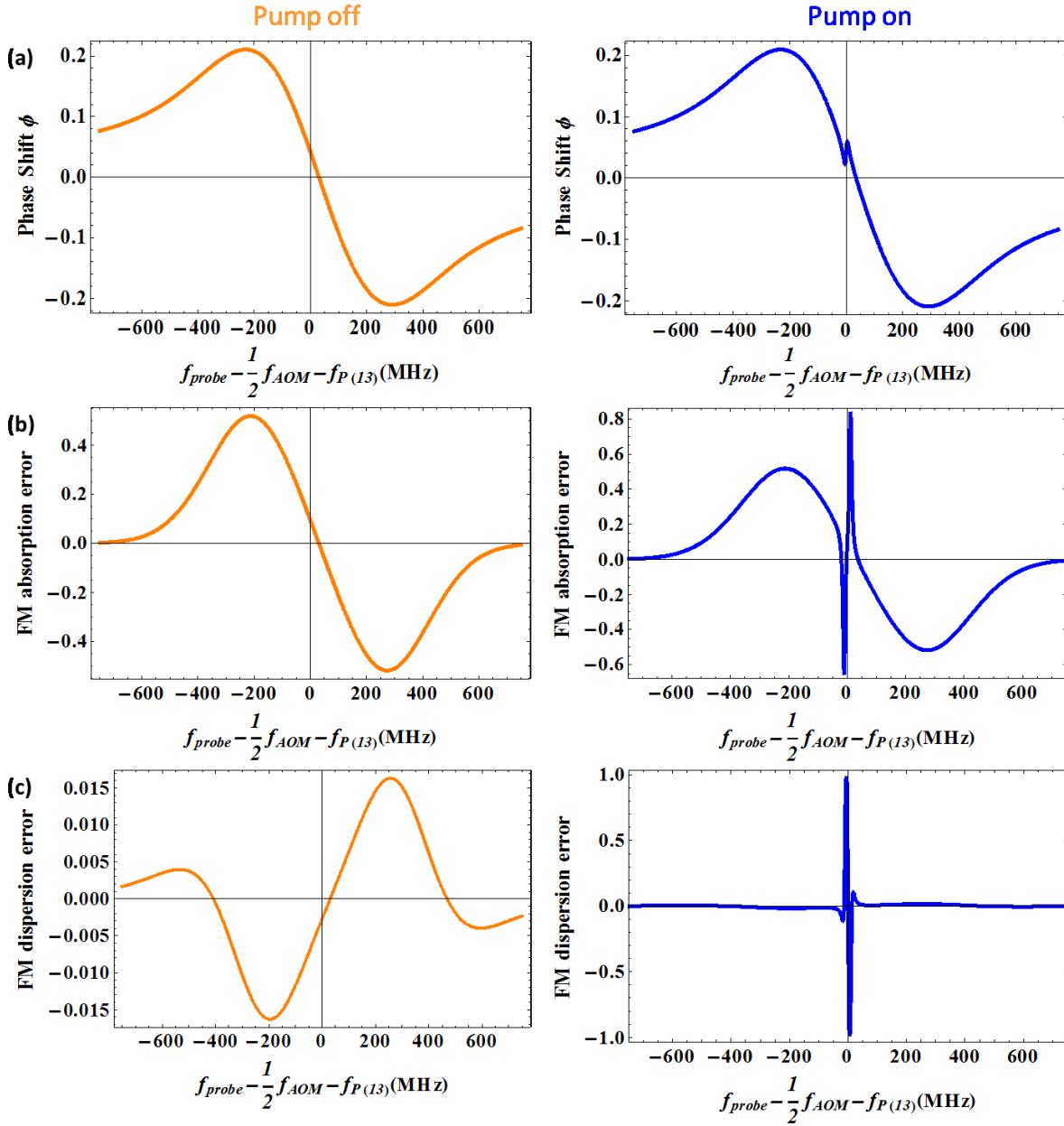
Figure 3-8: Theoretical calculations (left: pump-off; right: pump-on) of SAS of P(13) line of $^{12}C_2H_2$, with an FT of 50%, exiting fiber pump power of 32 mW, and FM frequency at 22 MHz. (a) The optical phase shift φ; (b) the FM absorption error signal; and (c) FM dispersion error signal. The amplitude of error signals is multiplied by a scale factor of 326 for the normalization of AM dispersion error signal from this calculation.

For verification of this FM modeling, we compared the calculated FM absorption error signal and FM dispersion error signal with what we measured in the experiment in the presence of

both the probe beam and the pump beam (Figure 3-9). The calculated error signal is proportional to what is observed in the experiment. For further verification, we change the phase shift difference between each sideband and the carrier and calculate the FM dispersion error signal, and compare to what we observe in the experiment. In the experiment, this is done by changing the relative phase between RF oscillators for frequency modulation (RF oscillator 1 and 2 in Figure 3-6). The theoretical lineshapes agree well with the measured lineshapes observed in the experiment.
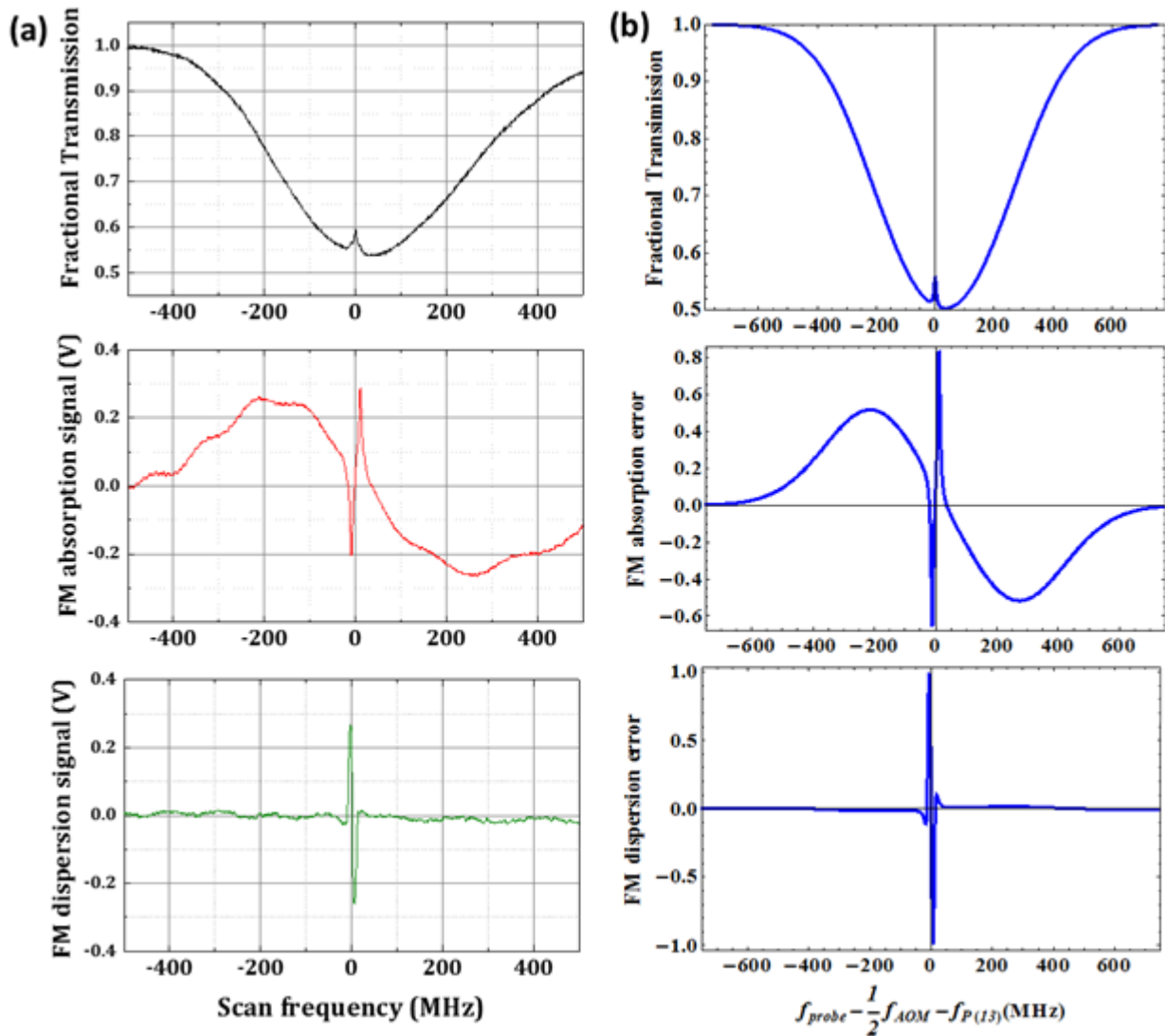
Figure 3-9: Saturated absorption fractional transmission, FM absorption signal, and FM dispersion error signal comparison between (a) experimental measurement and (b) FM modeling calculation.

In addition, we can calculate a residual error signal by subtracting the FM error signal with pump-off from the error signal with pump-on to get rid of background noise. In the experiment, an amplitude modulation (AM) is added to the pump beam for this purpose. Figure 3-11 shows the calculated AM absorption error signal and AM dispersion error signal. The calculated error signal is proportional to what is detected by the PD. In our experiment, we use the AM dispersion error signal to stabilize the laser frequency.
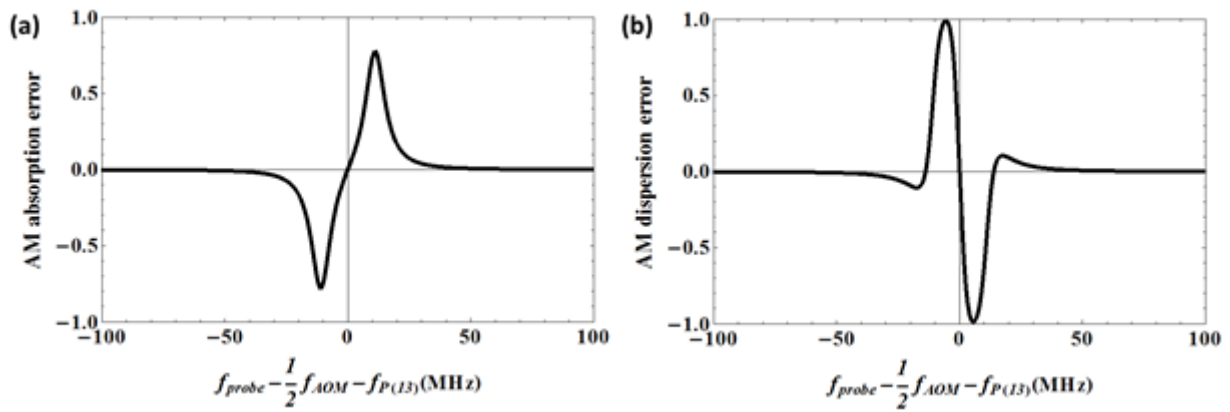
Figure 3-10: AM error signal calculated by subtracting the FM error signal with pump off from the error signal with pump on. (a) AM absorption error signal and (b) AM dispersion error signal.

3.3.3. *Absolute frequency correction*

In the experiment, we stabilized a CW laser to the zero-crossing of the AM error signal. In Figure 3-11b, clearly the error signal crosses zero at a point shifted by $\Delta f = 9$ kHz from the zero of the x-axis. This shift is due to the asymmetry of the sub-Doppler feature, which is caused by the frequency difference between the pump and probe beam arising because the probe frequency is shifted by the AOM.
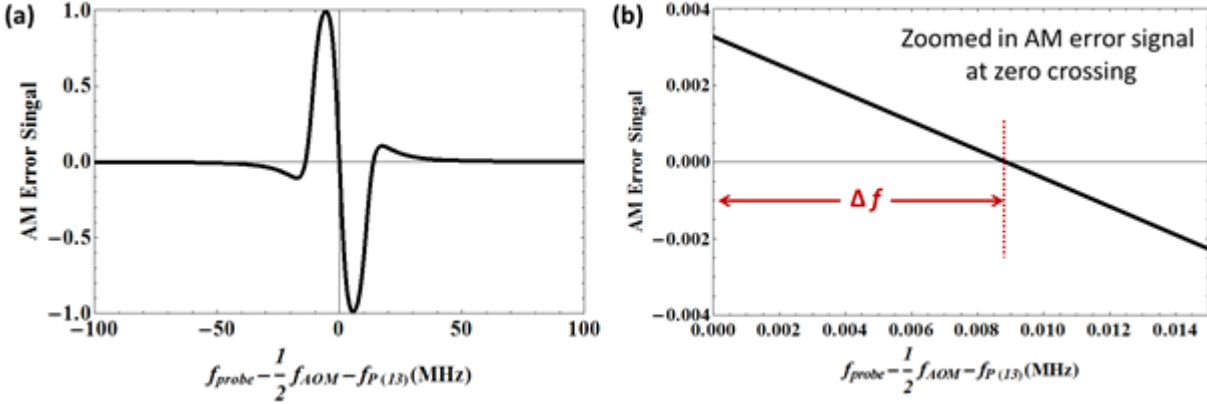
Figure 3-11: Adapted from Ref. [36]. (a) Normalized residual error signal by subtracting the FM dispersion error signal with pump-off from the error signal with pump-on of SAS of P(13) line of $^{12}C_2H_2$, with an FT of 50%, exiting fiber pump power of 32 mW, and FM frequency at 22 MHz. The calculated error signal is proportional to what is detected by the PD; (b) same as (a) but plotted over a smaller range to show the frequency of the zero-crossing.

To validate this model experimentally, we made two measurements of the same absolute frequencies using two different AOMs; one shifts the probe frequency by ~ − 60 MHz, and the other shifts the probe frequency by ~ 200 MHz. These two measurements were made under the same acetylene pressure, pump power and comb conditions. Figure 3-12 shows the calculated absolute frequency before (Figure 3-12a) and after (Figure 3-12b) applying this shift caused by the frequency difference of probe and pump beam. The measured absolute frequency of the same transitions before correction by Δf differed by 20±5 kHz while after the frequency correction they differ by 5±5 kHz (i.e. they agree).
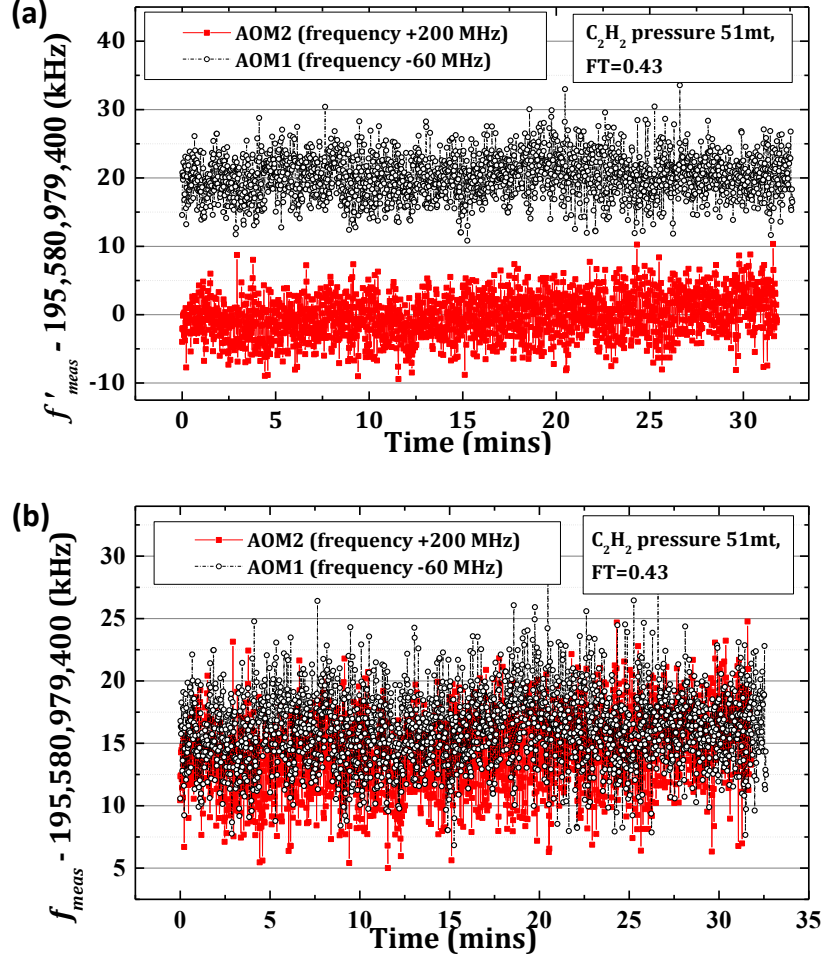
Figure 3-12: Adapted from Ref. [36]. Measured absolute frequency of the $^{12}C_2H_2$-stablized laser vs. time with a $^{12}C_2H_2$ pressure of 51 mtorr inside the 7.9 m-long kagome fiber, recorded at a 1s gate time using a counter: (a) before correcting for the shift caused by frequency difference between probe and pump, (b) after correction. Black open-circle: probe frequency was shifted by ~ − 60 MHz with respect to the pump (AOM1), red solid-square: probe frequency was shifted by ~ + 200 MHz with respect to the pump (AOM2).

In our previously reported absolute frequency measurement in a 4.1 m kagome HC-PCF [24], we took the measured laser frequency(f'_{meas}) to be:

$$f'_{meas} = f_{v0,P} - \frac{1}{2} f_{AOM} \qquad (3.20)$$

where $f_{v0,P}$ is the frequency of the P(13) zero velocity class at the given pressure, and extrapolated to zero pressure to get the frequency of the P(13) line at zero pressure, here called $f'_{P(13)}$, as shown

in Figure 3-13. However, this analysis [24] neglects Δf. The corrected frequency of the P(13) line at zero pressure, called $f_{P(13)}$, is corrected by Eq. (3.21) to each measurement and re-analyzed (Figure 3-13).

$$f_{meas} = f_{v_0,p} - \frac{1}{2} f_{AOM} - \Delta f = f'_{meas} - \Delta f \qquad (3.21)$$
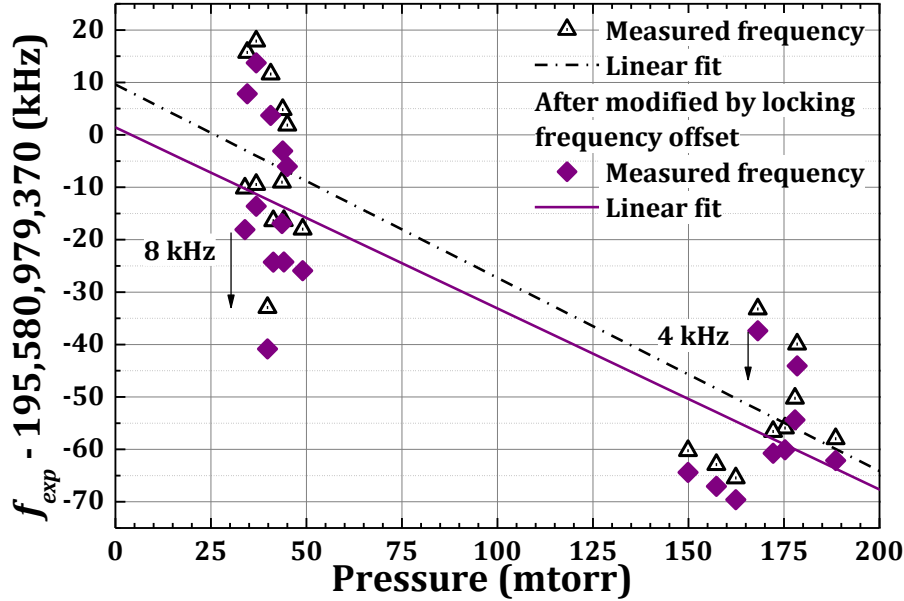
Figure 3-13: Adapted from Ref. [36]. Absolute frequency measurement of the stabilized-laser to the acetylene P(13) line versus acetylene pressure. The kagome fiber length is 4.1 m, and a linear fitting is applied for the correction of pressure-induced frequency shift. Open triangle with solid linear fit line denotes absolute frequency before correction by Δf; Solid diamond with dash-dot linear fit indicates absolute frequency after correction by Δf. Each data point indicates an independent alignment to avoid frequency offsets due to free-space coupling into the kagome fiber. After applying the locking frequency shift, the linear fit gives a zero-pressure intercept of 195,580,979,371.4 ± 9.3 kHz, compared with the previously reported zero-pressure intercept of 195,580,979,379.6 ± 9.3 kHz [24].

In Figure 3-13, data were taken at two different pressure brackets in our absolute frequency measurements and gave us two different sets of parameters of A_g and A_l. So, an 8 kHz shift is applied to those lower pressure measurements, and a 4 kHz shift is applied to the higher pressure measurements. After multiplying the locking frequency shift, the accuracy of the kagome

frequency reference adjusts to 1.4 kHz, showing a better agreement with previous measurements

of the P(13) line [21, 45] (Table 3-3).

Table 3-3 Adapted from Ref. [36]. Mean $^{12}C_2H_2$ $v_1 + v_3$ P(13) frequency and uncertainty for this work (before[24], after considering the frequency shift Δf caused by FM modeling) and for referenced work [21, 45].

	Mean P(13) value (kHz)	Uncertainty (kHz)
This work after mod. Δf Ref. [36]	195,580,979,371.4	9.3
This work before mod. Δf Ref. [24]	195,580,979,378.0	9.3
Ref. [45]	195,580,979,370.4	3.7
Ref. [21]	195,580,979,371.1	10.2

The re-analysis vacuum-chamber-based acetylene frequency reference shows high precision frequency reference can be realized using large-core kagome HC-PCFs. And in order to make the frequency reference system more portable, gas-filled fiber cells are needed to replace vacuum chamber. However, a direct splice between large-core kagome HC-PCF and SMF is difficult because of the different fiber outer diameters. Thus, a further exploration of vacuum-chamber-based acetylene frequency reference using other HC-PCFs with smaller outer diameters is needed, as discussed in the next chapter.

Chapter 4.   Suitable Hollow-core Fibers for Frequency References

Hollow-core photonics crystal fibers (HC-PCFs) guide light in a hollow core. The hollow core is created by removing the center cell and its adjacent cells from the cladding structure during fabrication process [56]. In the category of Hollow-core Photonic Crystal Fibers (HC-PCFs), there are two main different types of HC-PCFs, namely photonic bandgap fibers (PBGFs) and kagome-structured fibers [57]. Figure 4-1 shows the geometry difference between a 19-cell PBGF and a 19-cell kagome-structured fiber. The conventional PBGF has hexagonal cladding cells while the kagome fiber has kagome structured cells. The geometry difference between the two fibers results in a difference in the optical properties of fiber, such as center wavelengths, attenuation, and transmission bandwidth. HC-PCFs have been widely used in applications such as power delivery, sensors, and non-linear optics [58-63]. We use the HC-PCFs in the application of precision spectroscopy of molecular gases.
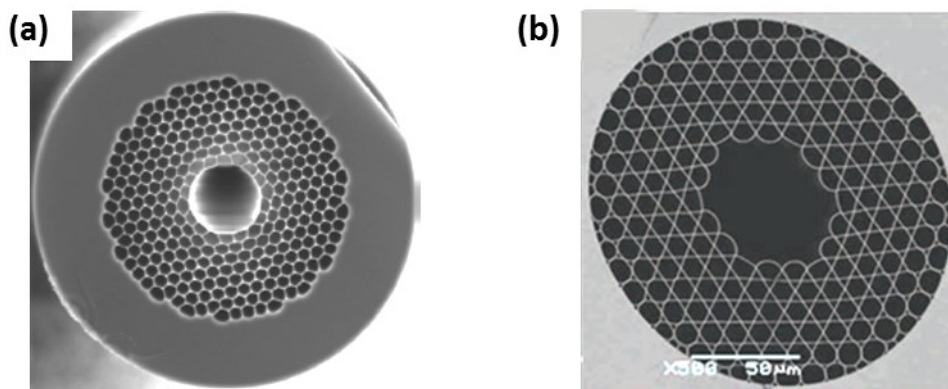
Figure 4-1 Scanning electron microscope (SEM) images of (a) PBGF [64] and (b) kagome-structured fiber. PBGF is commericall avaiable and kagome fiber is fabricated by the Gas-phase photonic and microwave materials group (GPPMM). The hollow core of the fiber is created by leaving the center and the adjacent microstructured cladding cells from the cladding structure during fabrication, leaving a 19-cell defect.

Our previous work [24] establishes the 19-cell kagome photonic crystal fiber (PCF) as a suitable medium for precision spectroscopy of molecular gases. However, that fiber is hard to splice with standard single mode fiber SMF-28 since the outer diameter of the 19 cell kagome PCF (305 μm) is roughly two times bigger than the outer diameter of SMF-28 (125 μm). Thus, the necessary to explore other suitable HC-PCFs for gas-filled frequency references is required for the purpose of easier splicing between HC-PCFs to SMF-28.

While kagome fiber can be tapered and spliced to SMF [28], the best splice loss between the tapered large-core kagome fiber and SMF is around 2 dB, which is higher than the 0.9 dB splice loss for a PBGF. However, the kagome-structured hollow-core fibers are not commercially available yet. Therefore, we investigated three commercially available HC-PCFs for use in the all-fiber photonic microcell (PMC) frequency references. Because of their similar outer diameters of those commercially available HC-PCFs (~120 μm) compared with SMF-28 (125 μm), they have the potential to make acetylene-filled photonic microcells (PMCs). The PMCs will further lead the development of potential portable all-fiber optical frequency references.
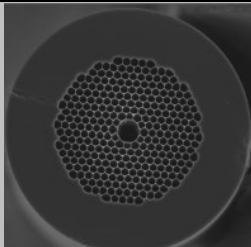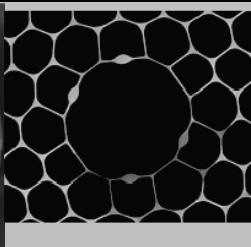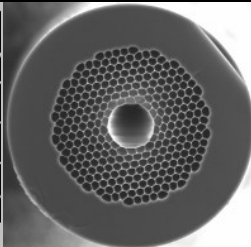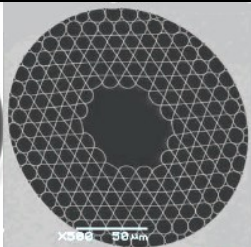
4.1. Different types of HC-PCFs used in acetylene frequency references

In this section, we are going to test those commercially available photonic bandgap fibers (PBGF s) in our gas-filled fiber optical frequency reference based on vacuum chambers. Three fibers being tested: 7-cell PBGF (HC-1550-02), 7-cell polarization maintaining (PM) PBGF (HC-1550-PM-01), and 19-cell PBGF (HC19-1550-01). Both 7-cell PBGFs have a core size of 10 μm, and 19-cell PBGF has a core size of 20 μm. The parameters of those PBGFs are shown in Table 4-1,

compared with the kagome fiber we used in our acetylene frequency reference [24].

To initially test these commercially available fibers, we removed the kagome fiber in the reference setup and replaced with each PBGF. The lengths of each PBGFs are 1 m and the optical pump powers exiting the fibers are 30 mW. The experimental setup is the same as shown in Figure 2-2 except that f = 15 mm Geltech aspheric lenses are used to couple the free space beams to each PBGF. The pressure in this test is about 500 mtorr, which gives us ~ 50% fractional transmission. For both the 10 μm PBGFs (fiber A and B) 40 MHz FWHM error signals were observed, and a 22 MHz FWHM error signal was obtained in the 20 μm PBGF (fiber C).

Table 4-1: Adapted from Ref. [36]. Fiber parameters for the HC-PCFs

#	A	B	C	D
Cross Section				
Fiber Name	7-cell PBG	PM 7-cell PBG	19-cell PBG	19-cell kagome
Part number	HC-1550-02	HC-1550-PM-01	HC19-1550-01	*
Core diameter	11 μm	11 μm	20 μm	70 μm
Outer diameter	120 μm	120 μm	115 μm	315 μm
Attenuation at 1550 nm	< 0.02 dB/m	< 0.02 dB/m	< 0.02 dB/m	~ 1dB/m

*Fabricated by the Gas-phase photonic and microwave materials group (GPPMM).

4.1.1. Linewidth measurement in different HC-PCFs

We compared the linewidth from this experiment on the P(13) transition to our previous acetylene linewidth measurements on the P(11) transition inside 0.9 m fiber A and 0.8 m fiber C (Figure 4-2) [43]. The P(11) and P(13) transitions of acetylene have similar absorption coefficients. The

previous linewidth measurements are plotted at different acetylene pressures and different pump

powers. With an acetylene pressure of 500 mtorr and a pump power exiting the fiber of 30 mW,

the linewidths from the previous measurements on P(11) transition were 24 MHz in fiber A, and

40 MHz in fiber C. The measured linewidths are close to the linewidth of the P(13) transition.

Details are shown in the description of Figure 4-2 [43].
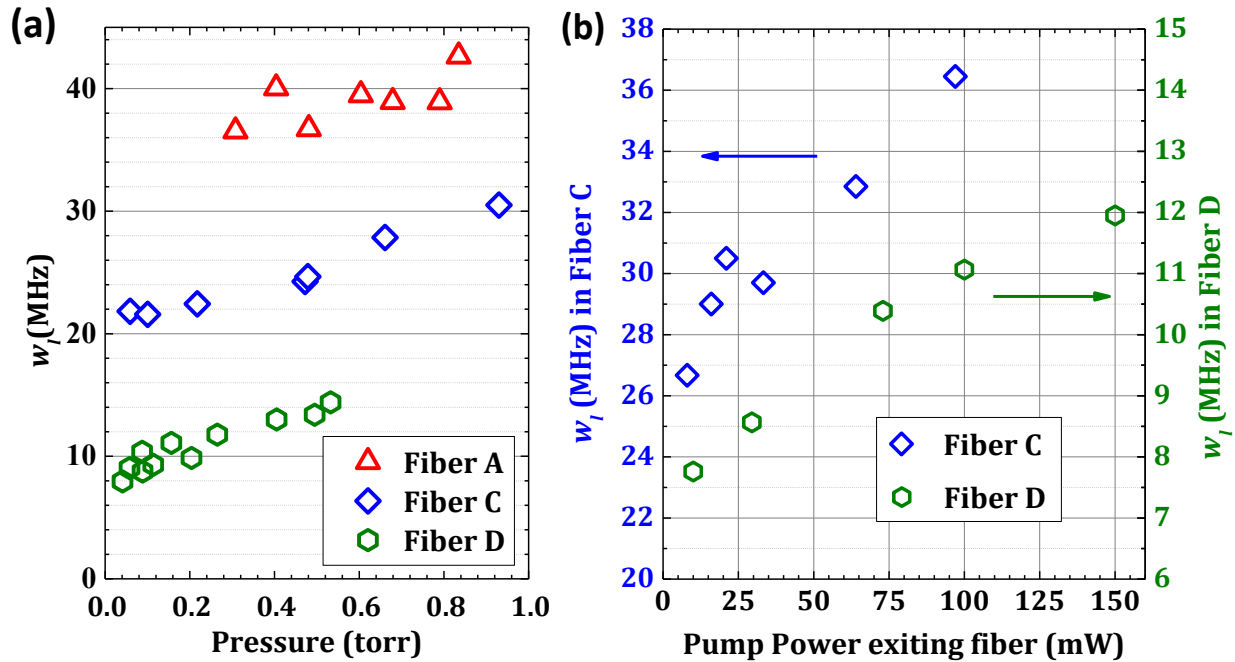
Figure 4-2: Reproduced From Ref. [43]. Sub-Doppler FWHM w_l as a function of acetylene pressure and optical pump power. a) w_l versus acetylene pressure with fit lines extrapolated to zero pressure for three different HC-PCFs. Data taken in the 10 μm (triangles) and 20 μm (diamonds) HC-PCF were taken on the P(11) transition [65], while data in the 70 μm kagome HC-PCF (hexagons) was taken on the P(13) transition [24]. The lengths of each fiber were 0.9 m, 0.8 m, and 4.1 m and the optical pump powers exiting the fibers were 30 mW, 29 mW, and 32 mW for the 10 μm, 20 μm, and 70 μm core fibers, respectively. b) w_l versus optical pump power exiting the 20 μm PBGF (blue diamonds, left axis) and 70 μm kagome HC-PCF (green hexagons, right axis). For the 20 μm PBGF, the fiber length was 0.8 m, and the pressure was 1 torr, corresponding to an FT = 25%. The kagome fiber's length was 1.4 m, and the pressure inside the fiber was near 200 mtorr, corresponding to 60% FT.

4.1.2. Allan deviation in different HC-PCFs

We stabilize a CW laser to the error signals obtain using the fiber mentioned above, then the heterodyne frequencies between the laser and a phase stabilized frequency comb are measured. We calibrate the fractional stability of the laser locked to the acetylene P(13) transition line using the recorded heterodyne frequencies, shown in Figure 4-3.

The 20 μm PBGF (Fiber C) exhibits a factor of 2 worse stability (2.2×10^{-11}) than our previous kagome reference (Fiber D) 1at 1s sample period, which is due to the smaller core size of the PBGF and therefore larger linewidth (due to transit time broadening). The measured stability agrees with the predicted value of 2.4×10^{-11} using Eq. (3.1) and 10 MHz linewidth measured in the kagome fiber. As for the 10 μm PBGF (Fiber A and D), we predicted a stability of 4.5×10^{-11} shown as solid triangles in Figure 4-3 by scaling the stability offered at 1 s in large-core kagome to the smaller signal to noise (S/N) ratio and larger linewidth. Even so, the 10 μm PBGF observed in the measured fractional Allan deviation (3×10^{-10}) is a factor of 6 worse than the expected value. A possible explanation of why the measured fractional Allan Deviation is much larger than the expected value will be discussed in the next section.

The results shown in Figure 4-3 tells us that the stability of the PBGF based acetylene frequency reference is worse than that of the kagome fiber, but the PBGF might still be a good candidate for making portable acetylene frequency reference. The linewidth reduction techniques discussed in section 3.1 can be applied to the PBGF based acetylene frequency references to obtain better performances of the references.
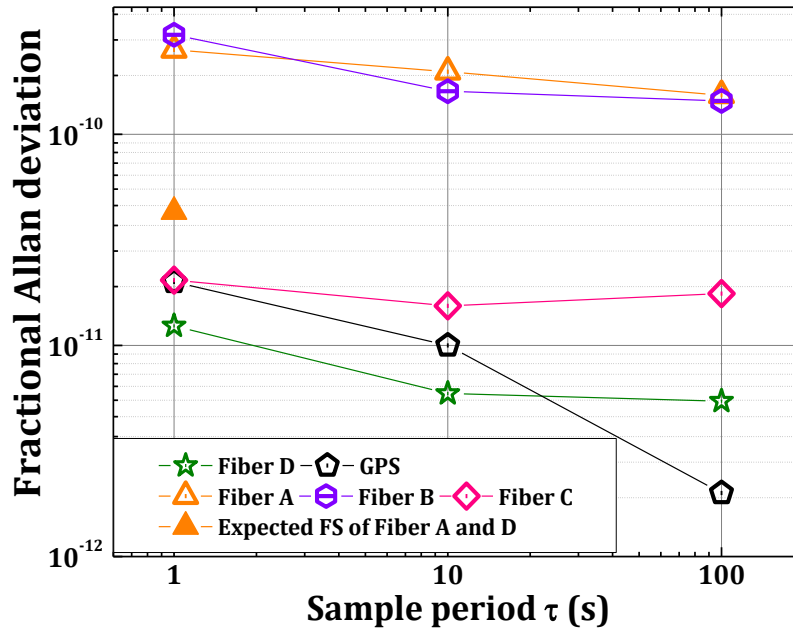
Figure 4-3: Adapted from Ref. [36]. Fractional instability of the beat between the frequency comb and the fiber-based acetylene reference made with different HC-PCFs shown in Table 4-1 (Fiber A-D). GPS stability is shown here for comparison.

4.2. Surface modes on HC-PCFs

To explain this degraded S/N ratio, we observed that the 10 μm PBGF (Fiber A, B) exhibits large surface mode effects. Surface modes refer to a collection of modes guided in the glass region between the core and cladding [47], *i.e.* the core surround. These modes have higher loss and wavelength-dependent coupling to the core modes. High coupling to these can result in wavelength-dependent loss in the fibers as shown in Ref. [65]. The frequency instability may be higher than expected due to these surface modes, which contribute a 40% variation (Figure 4-4) in off-resonant transmitted power in the 10 μm PBGF (Fiber A and B) offered here. By comparison, the variation in the 20 μm core fiber (Fiber C) is only 5%, while that in large-core kagome is less than 1%.

60
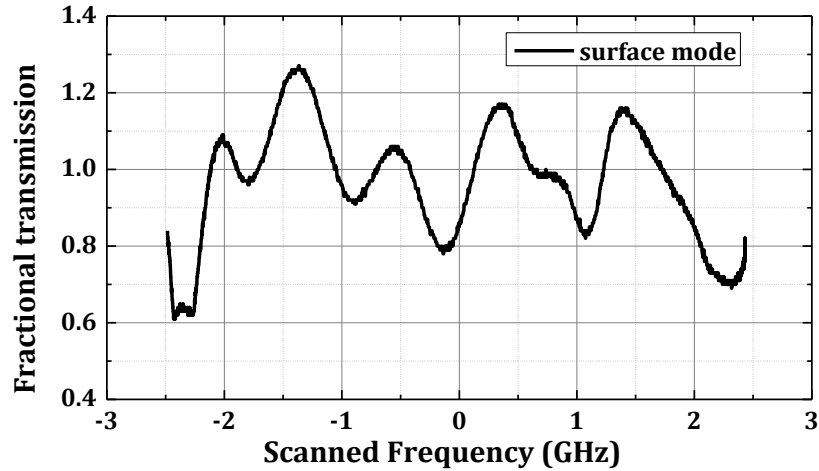
Figure 4-4: Fractional transmitted signal in the 10 μm PBGF (Fiber-A) vs. frequency under vacuum. The oscillations in this fiber are due to coupling between the hollow-core mode and "surface modes" in the silica cladding.

4.2.1. *Surface mode comparison between kagome fiber and PBGF*

These surface modes may not only contribute an oscillating background [65] but may also corrupt a quantitative analysis of the lineshape [51]. For example, in Figure 4-5, the PBG fiber exhibits a much greater surface mode than the kagome fiber, the strong coupling between the core mode and the surface mode causes a highly asymmetric error signal (i.e. lineshape distortion) in our acetylene frequency reference based on the PBG fiber.
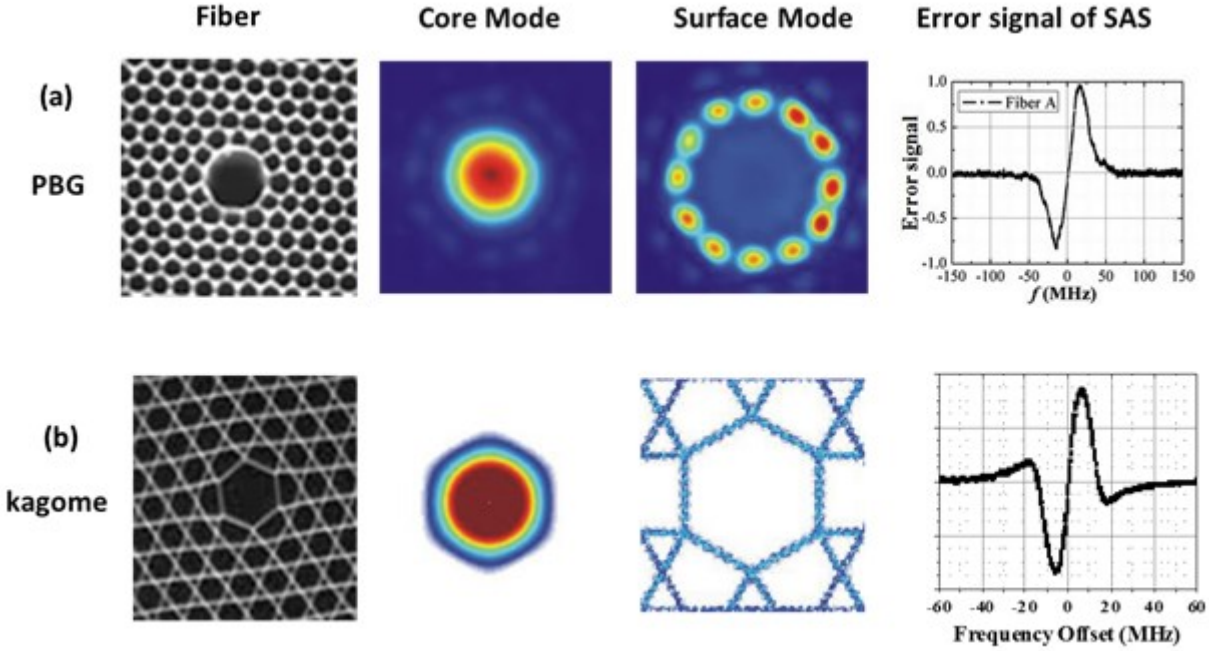
Figure 4-5: (a) The lineshape distortion of acetylene P(13) transition caused by the surface modes in PBG fiber, (b) the asymmetric lineshape inside a surface mode free kagome fiber for comparison. Coupling between core modes (2nd column) and surface modes (3rd column) in PBG causes a lineshape distortion (4th row). The core mode and surface mode of PBG and kagome fiber are taken from Ref. [66] and Ref. [67].

4.2.2. *Analysis of surface modes in PBGF*

In fibers with strong wavelength-dependent transmission, we also observe an intensity dependent frequency shift of around 500 kHz in the error signal along with a highly asymmetric trace, which is obtained by Pound-Drever-Hall style modulation as described above. Pump amplitude modulation should reject such background. Thus, the "survival" of the off-resonant transmission modulation to the error signal is at first surprising. The asymmetry (A) of the error signal is defined as

$$A = \frac{V_1 - V_2}{(V_1 + V_2)/2} \qquad (4.1)$$

62

where V_1 and V_2 are the absolute value of the maximum and minimum voltages of the error signal.

To investigate the effect of the coupling between a core mode and surface modes, we consider the simple case where the coupling occurs only between a single core mode and a single surface mode [36]. In this case the probe signal at the photoreceiver can be written in the following manner

$$V_{PD} = V_{core} + V_{SM} + 2\sqrt{V_{core}V_{SM}}\,\cos\left(\Delta\Phi + \Delta\Phi_{NL}\right) \tag{4.2}$$

where

$$\Delta\Phi = \Delta\beta L_{fiber} \tag{4.3}$$

is the phase due to the mode beating between the core mode and surface mode, $\Delta\beta$ is the difference in the propagation constant between the two modes and L_{fiber} is the effective length of the fiber. $\Delta\Phi_{NL}$ is an additional phase that depends on the pump intensity and is caused by the Kerr effect. Ignoring the Kerr effect in the hollow core, the associated propagation constant difference that gives rise to this phase shift is

$$\Delta\beta_{NL} = n_2^{SM} I_{SM} \left(2\pi / \lambda\right) \tag{4.4}$$

Here the n_2^{SM} is the nonlinear refractive index of the silica core-surround and I_{SM} is the intensity of the surface mode which can be written as

$$I_{SM} = 0.4 P_{pump} / A_{eff} \tag{4.5}$$

If one estimates the surface mode effective area A_{eff} to be on the order of $3 \times 10^{-11} \text{cm}^2$, which is an experiential value for a similar fiber taking into account the glass thickness of the fiber core and the near field intensity profile, and $n_2^{SM} = 3 \times 10^{-16} \text{cm}^2/\text{W}$, the induced frequency shift due to this nonlinear optical coupling is ~ 500 kHz. This 500 kHz agrees with the intensity dependent frequency shift in the error signal along with a highly asymmetric trace, calculated by adding a

63

sinusoidal term to Eq. (3.17) to simulate the surface mode in the calculation (Appendix B).

First we consider the same surface mode to be present when the pump is off and on. The attenuation δ_{SD} of the Doppler absorption is expressed in Eq.(4.6), and the period of the sinusoidal term is obtained by measuring the transmission signal of PBGF while scanning the input laser frequency.

$$\delta_{SD}(\omega) = \delta_D(\omega) + \delta_{SM}(\omega) = \delta_D(\omega) - \frac{1}{2}A_s \sin\left(\frac{f}{f_s}\right) + C_s$$

(4.6)

where δ_D is the same in Eq.(3.17), A_s is the amplitude of the sinusoidal term, f_s is the period of the sinusoidal term, and C_s is the amplitude offset of the sinusoidal term.

We repeated the FM modulation by using Eq.(4.6). The simulation results are shown in Figure 4-6 and Figure 4-7. When a 40% contrast surface mode with 500 kHz period is present, f_s = 500 kHz, A_s = 0.025, and C_s = 0.015. However, the asymmetry A of the theoretical signal that is calculated by applying Eq. (4.1) to the theoretical error signal does not agree with the highly asymmetric trace observed in the experiment. We further consider a dynamic effect to solve this problem.
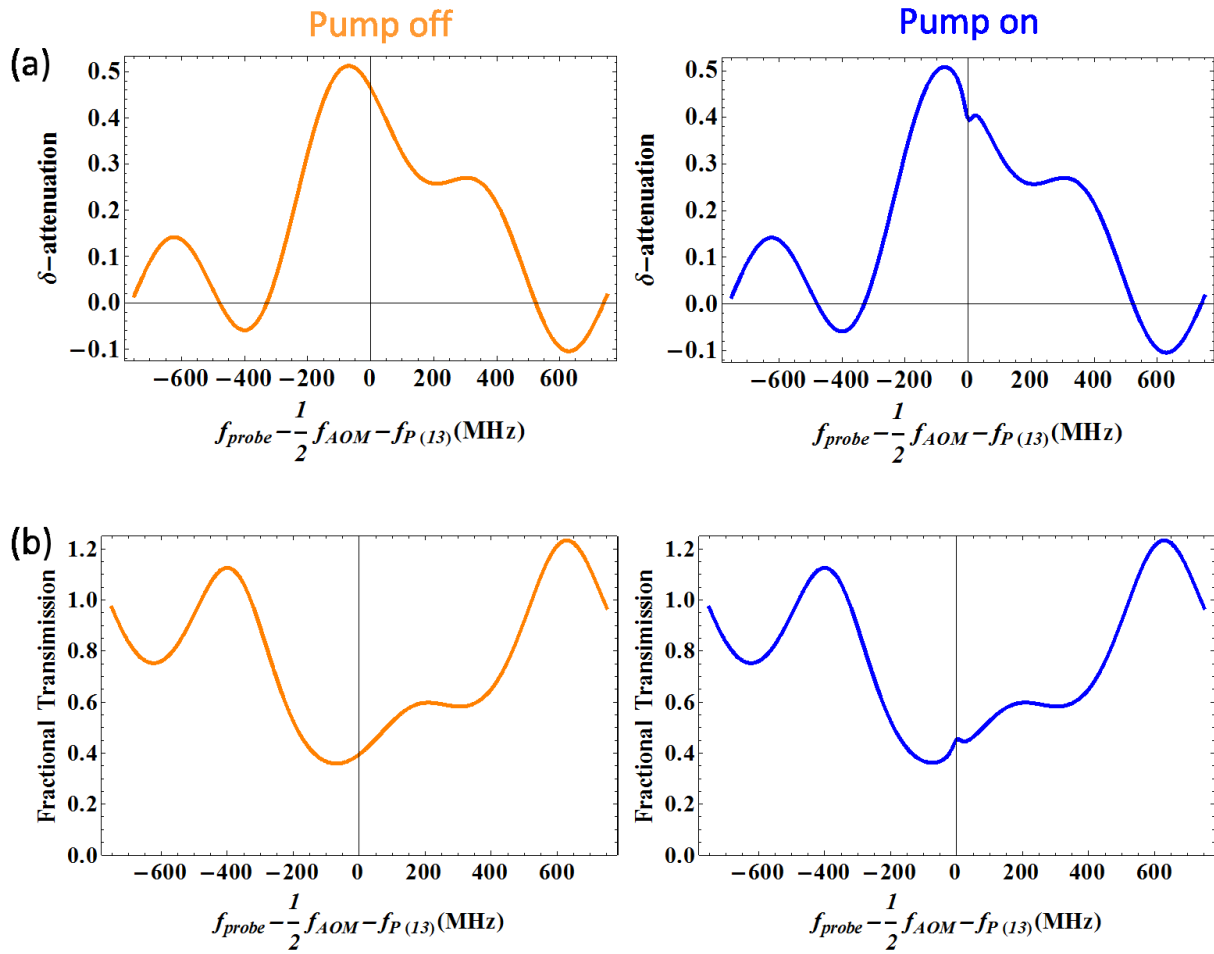
Figure 4-6: Theoretical calculations (left: pump-off; right: pump-on) of SAS of P(13) line of $^{12}C_2H_2$ inside a 10 μm PBGF in the presence of surface modes. The FT is 50%, exiting fiber pump power is 32 mW, and FM frequency is at 22 MHz. (a) The attenuation δ; (b) the fractional transmission.
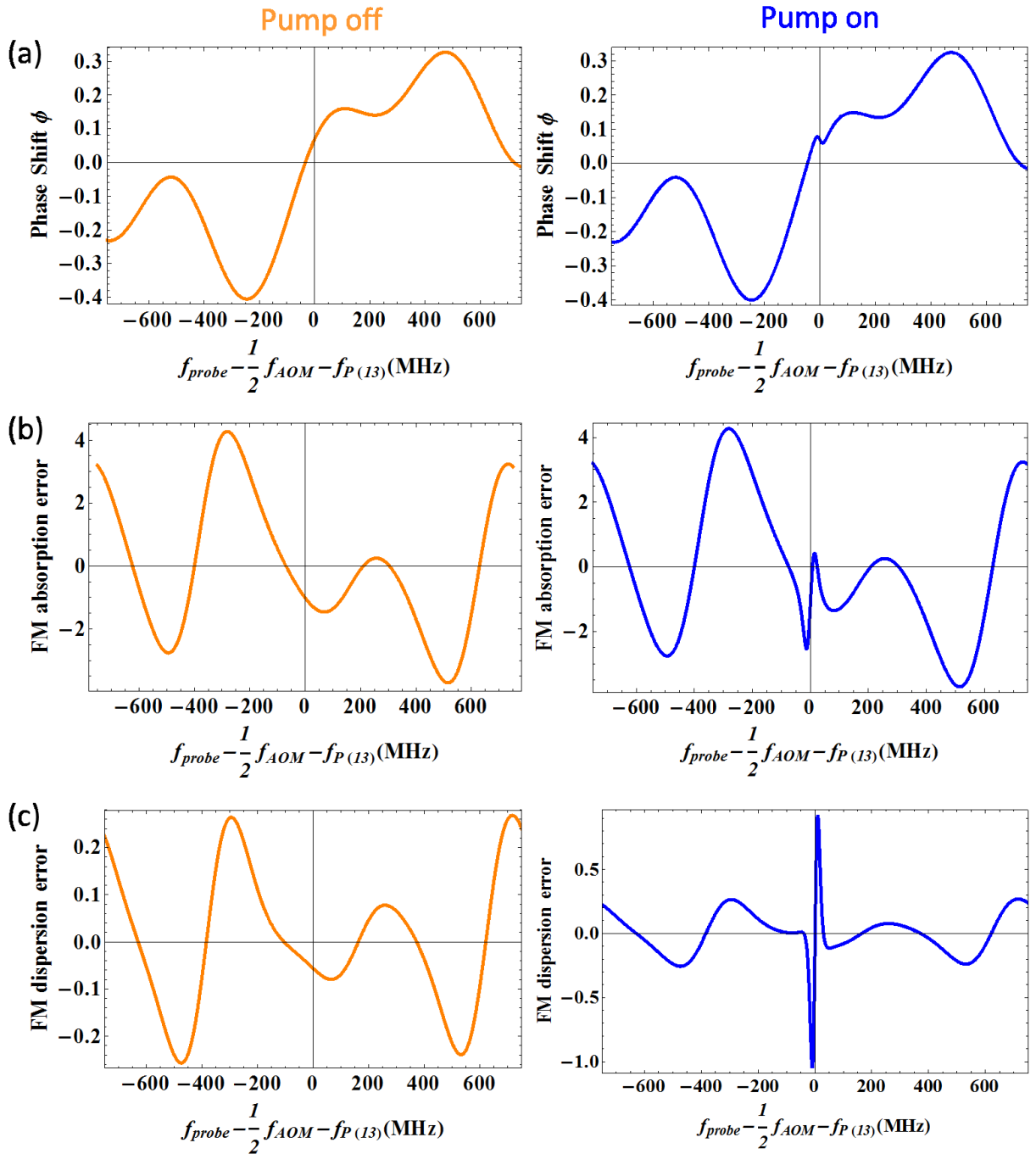
Figure 4-7: Theoretical calculations (left: pump off; right: pump-on) of SAS of P(13) line of $^{12}C_2H_2$ inside a 10 μm PBGF in the presence of surface modes. The FT is 50%, exiting fiber pump power is 32 mW, and FM frequency is at 22 MHz. (a) the optical phase shift φ; (b) the FM absorption error signal; and (c) FM dispersion error signal. The amplitude of error signals is multiplied by a scale factor of 953 for the normalization of the AM dispersion error signal from this calculation.
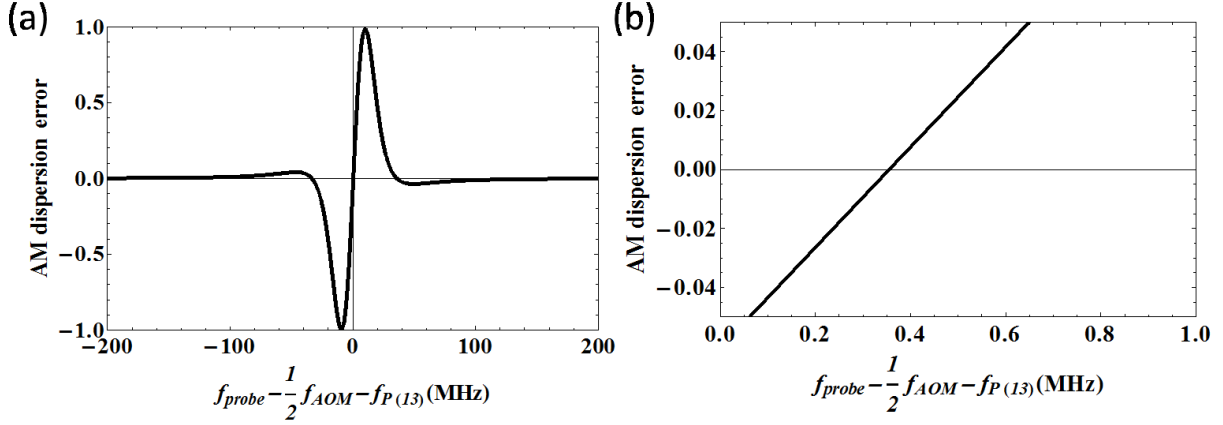
Figure 4-8: Adapted from Ref. [36]. (a) Normalized residual error signal by subtracting the FM dispersion error signal with pump off from the error signal with pump on of SAS of P(13) line of $^{12}C_2H_2$ inside a 10 μm PBGF with the presence of surface mode. The FT is 50%, exiting fiber pump power is 32 mW, and FM frequency is at 22 MHz. The calculated error signal is proportional to what is detected by the PD; (b) same as (a) but plotted over smaller range to show the frequency of the zero-crossing.

As mentioned above, in addition to the frequency shift, a dynamic effect (Kerr effect) might cause the highly asymmetric trace. The Kerr effect induces an intensity dependent coupling strength between the core mode and the surface mode, which renders the error signal asymmetry (A) dependent on the pump intensity. Figure 4-10 illustrates this through considering the error signal shape evolution when the coupling of the core mode with the surface modes. When a shape evolution is taken into account, the attenuation coefficient with the presence of the pump will be different in Eq. (3.18). In the 10 μm fiber we calculated above, an additional phase shift is introduced in the sinusoidal term.

$$\delta'_{SD}(\omega) = \delta_D(\omega) + \delta'_{SM}(\omega) = \delta_D(\omega) - \frac{1}{2} A_s \sin\left(\frac{f}{f_s} + \Delta\varphi\right) + C_s \tag{4.7}$$

where δ_D is the same in Eq.(3.17), A_s is the amplitude of the sinusoidal term, f_s is the period of the sinusoidal term, C_s is the amplitude offset of the sinusoidal term, and $\Delta\varphi$ is the additional phase

67

shift caused by the Kerr effect comparable to 2π.

Both theoretical and experimental curves are calculated by applying Eq. (4.1) to the plotted error signal (Figure 4-10). The calculated error signal exhibits very little asymmetry when the surface mode is neglected or when only $\Delta\Phi$ is considered. However, when $\Delta\Phi_{NL}$ is included, the experimentally observed (Figure 4-10b) asymmetry of 20% is obtained theoretically (Figure 4-10a). This arises because the pump beam intensity changes the surface mode as it is modulated, so that pump amplitude modulation does not reject the signal due to the surface mode.

Even without taking into account the change of $\Delta\Phi_{NL}$ caused by the pump modulation, a slow thermal drift in $\Delta\Phi$ will introduce a frequency shift of up to 373 kHz when a 40% contrast surface mode is present (Figure 4-8b and Figure 4-10c). Therefore it is clear that very small changes in the surface mode will lead to changes in the lock point, causing frequency instability (Figure 4-3) and inaccuracy.
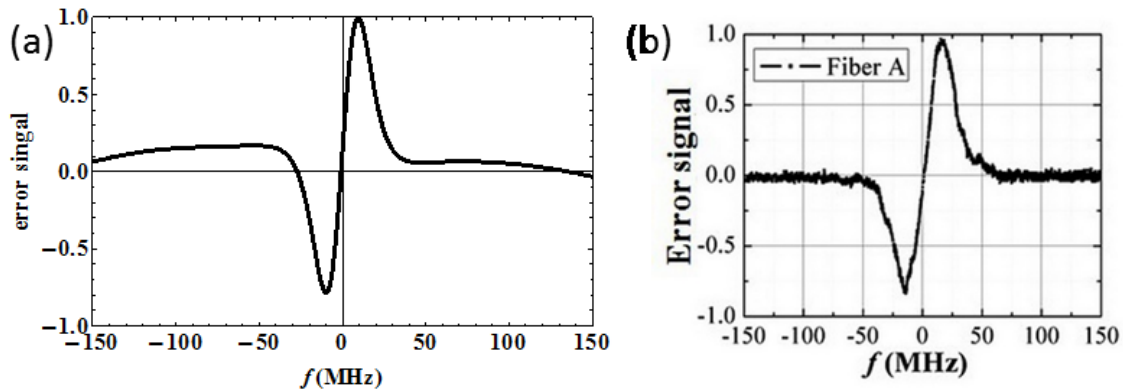
Figure 4-9: Adapted from Ref. [36]. (a) Calculated error signal in acetylene-filled 10 μm PBGF with the nonlinear effect caused by pump power modulation. (b)Experimental error signal.
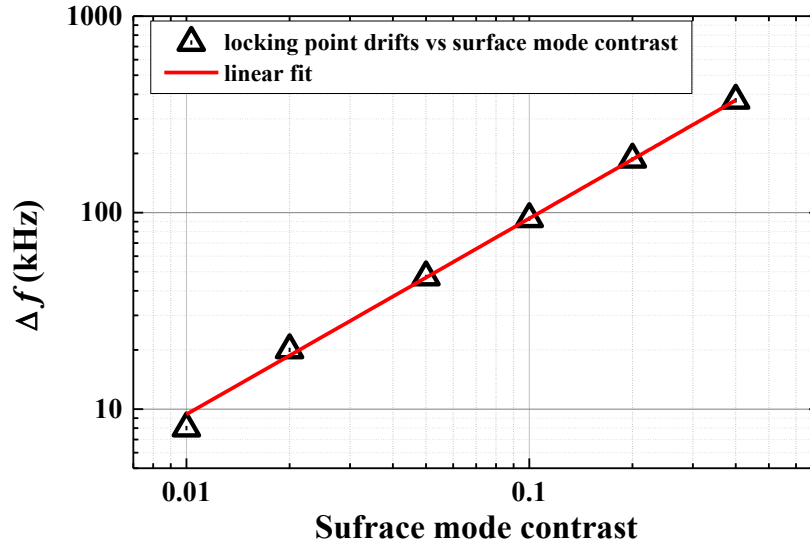
Figure 4-10: Adapted from Ref. [36]. In acetylene-filled 10 µm PBGF calculated maximum locking frequency change verse different surface mode contrast when varying only ΔΦ (not ΔΦ $_{NL}$) by π to mimic slow thermal drift.

4.3. Polarization maintaining HC-PCFs

Polarization maintaining fiber was also explored to improve the reference, which is motivated by the observation of a 40 kHz shift (Figure 2-15) when the probe polarization is changed by 30^0. This shift is considerable compared with the 10 kHz accuracy obtained in the kagome reference, and polarization may limit the accuracy of a gas-filled photonic microcell reference. One possible solution is to use polarization maintaining (PM) HC-PCF to make gas-filled microcell references. The commercially available 7-cell PM HC-PCF (Fiber B in Table 4-1) from NKT Photonics was tested, and a stability of 3.0×10^{-10} at 1 s sample period has been achieved (Figure 4-3).

4.3.1. Contrast ratio of PM HC-PCF

In the experiment, a linear film polarizer was placed before the vacuum chamber on the probe arm to guarantee a linearly polarized probe beam, and a half-wave plate was placed after the polarized

beam to adjust the polarization of the probe beam coupled into the fiber. We measured the extinction ratios of the probe beam exiting the fiber (Figure 4-11) at different probe polarization angles in order to find the polarization maintaining axis of the PM fiber. A polarization beam splitter (PBS) cube in the probe arm guarantees that linear light is coupled into the PM fiber. A half-wave plate is placed after the PBS cube to change the polarization of the light coupled into the PM fiber. At each angle of the half-wave plate, the contrast ratio of the PM fiber output (C) is found from the maximum transmission (p_{max}) and minimum transmission (p_{min}) by rotating the linear polarizer (Eq.(4.8)). The half-wave plate is rotated every 5 degrees for the contrast ratio measurement and the results are shown in Figure 4-12.

$$C = \frac{p_{max} - p_{min}}{p_{max}} \qquad (4.8)$$
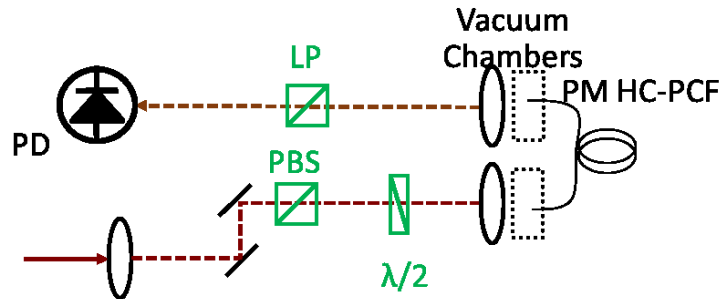
Figure 4-11: Experimental setup for finding the polarization maintaining axis of the PM fiber with 1m length. PBS: polarization beam splitter cube to guarantee linear light coupled to PM fiber, λ/2: half-wave plate to change the polarization of the light coupled into the PM fiber, LP: linear polarizer to find the contrast ratio of the output beam at each angle of the half-wave plate.

The maximum contrast ratio indicates that the probe beam is coupled to either the fast or slow axis of the PM fiber, and thus polarization is preserved when the beam is traveling through the fiber.
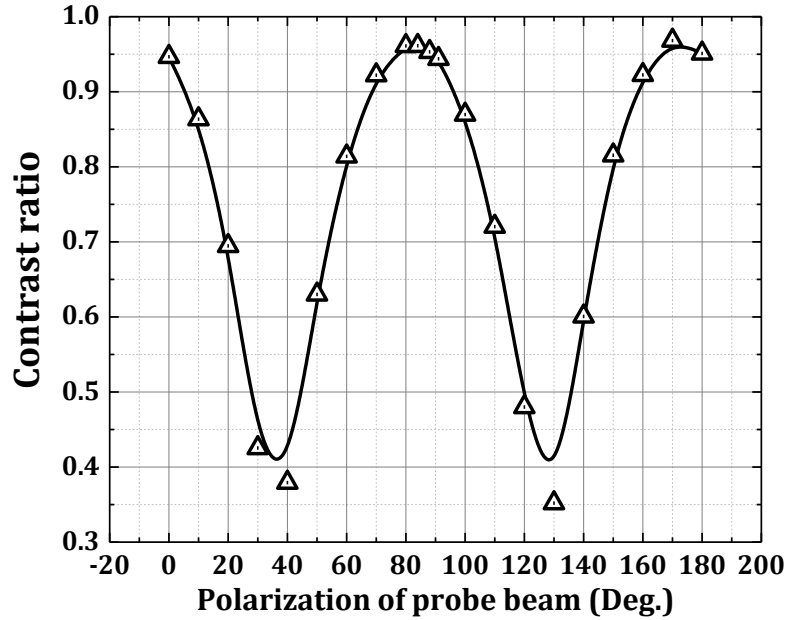
Figure 4-12: Adapted from Ref. [36]. Contrast ratio of probe power exiting the fiber versus the angle of probe polarization in vacuum; solid line, fitting curve of measured data. The maximum contrast ratio indicates that the probe beam is coupled to either the fast or slow axis of the PM fiber.

4.3.2. Fast axis of PM HC-PCF

Beat frequencies against a frequency comb are also measured when the probe beam is coupled to each axis. The acetylene pressure is 500 mtorr, and the PM fiber length is 1m. When the light is coupled to the 178^0 axis, the beat frequency is centered at 69,600 kHz with a drift of $\pm$ 400 kHz. And when the light is coupled to the 88^0 axis, the beat frequency is centered at 68,510 kHz with a drift $\pm$ 30 kHz. There is a $\sim$ 1 MHz shift in the average values of beat frequencies. A possible explanation is this PM fiber has a different wavelength-dependent transmission near the fast and slow axis or the surface mode exhibits polarization dependence. Since the drift is a factor of 10 smaller in the 88^0 axis than the 178^0 axis, in our following measurement, we couple the probe beam to the 88^0 axis.

71
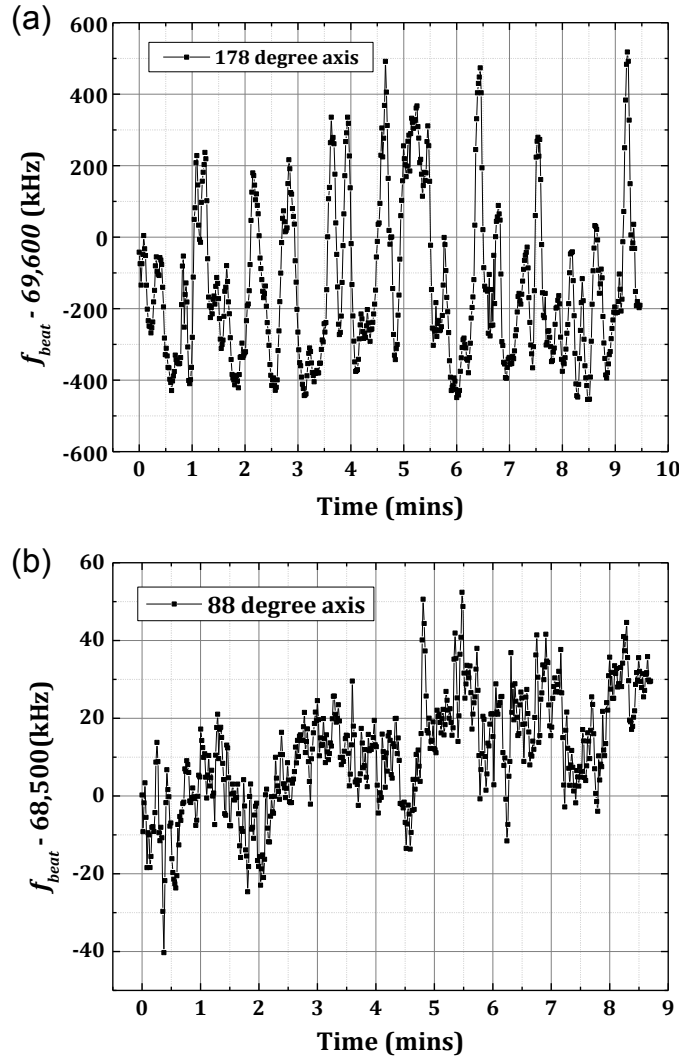
Figure 4-13: Beat frequencies against a frequency comb are also measured when the probe beam was coupled into each axis (a) 178^0 axis and (b) 88^0 axis. About 1 MHz shift in the average values of beat frequencies is observed when light is coupled to the 88^0 and 178^0 axis.

4.3.3. *Absolute frequency measurement*

By coupling the probe to the 88^0 axis, which is the fast or slow axis (Fig. 9a), the absolute frequency measurements (Figure 4-14) are investigated at three different pressure ranges. The results gave us ~ 1 MHz uncertainty in each frequency range. The beatnote frequency excursions on the 15 minutes time scale (*i.e.* "beatnote noise") of up to 0.5 MHz were detected (the error bar

on Figure 4-14). Linear fitting is applied to the data and gives the absolute frequency after accounting for power shift and pressure shift. The uncertainty reflected in the gas-filled PM fiber reference is thought to be due to the effect of surface modes we discussed above, and the results in a frequency reference with only 1 MHz accuracy at best.
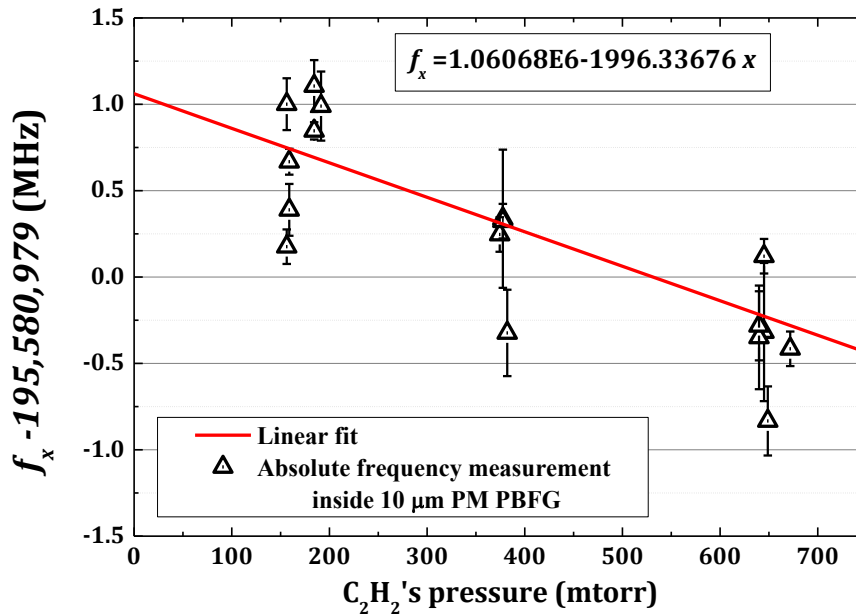
Figure 4-14: Absolute frequency measurement of $^{12}C_2H_2$ P(13) line inside the 1m PM PBGF (fiber B in Table 4-1) with a linear fit line. Each data point indicates an independent alignment to avoid frequency offsets due to free-space coupling into the PM fiber. Zero frequency corresponds to the published value [21]. The linear fit gives a zero-pressure intercept of (195,580,980.2) kHz.

4.4. Single mode HC-PCF

As we mentioned in section 2.3.2, the highest S/N ratio sub-Doppler signals are achieved in the largest core sizes (up to ~100 μm). However, these kagome PCFs are typically multi-mode and therefore suffer from mode-dependent frequency shift [36, 43]. Here, these problems are reduced by using a novel hollow-core fiber that is optimized for single mode operation known as Perturbed Resonance for Improved Single Modedness (PRISM) fiber [48]. The SEM image of the PRISM

fiber and its diameters are shown in Figure 4-15 [48]. The saturated absorption spectroscopy (SAS) signal is expected to be devoid of unwanted surface mode effects, and reduced dependence of the reference on optical alignment is inferred from preliminary locking data.
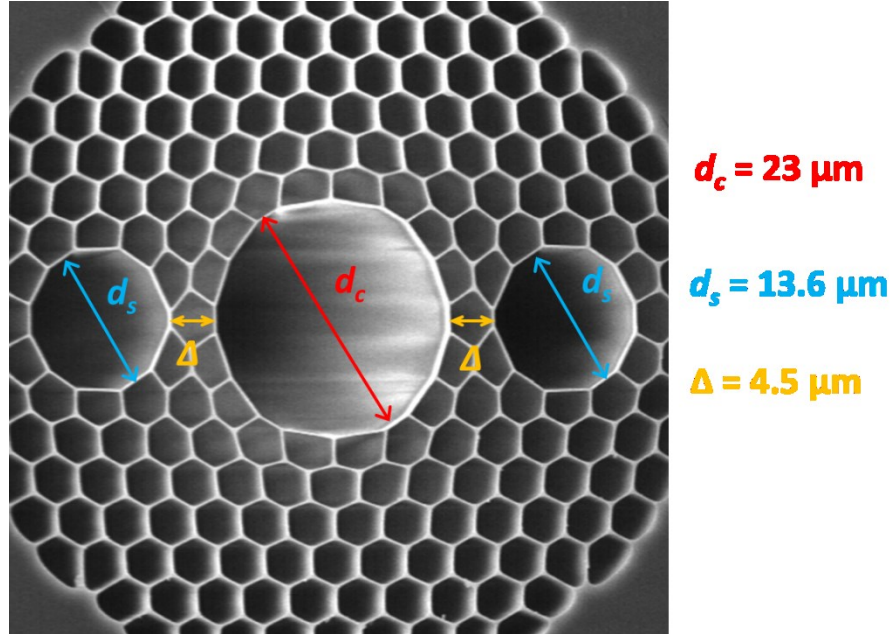
Figure 4-15: Adapted from Ref. [48]. SEM image of the PRISM fiber, the fiber has a 19 cell defect core with a diameter at 23 µm (d_c), and two 7 cell defect shunt cores, with a diameter of 13.6 µm (d_s). The space (Δ) between the center core and the two shunt cores is 4.5 µm.

To initially test this PRISM fiber, we used it for vacuum chamber references as in Ref.[24]. A 10 m fiber with the loss of approximately 15 dB/km is coiled to 5 cm diameter to produce single mode operation, and loaded with acetylene to a pressure of 50 mtorr. A narrow SAS signal (< 10 MHz FWHM), as shown in Figure 4-16a, is obtained with frequency and pump amplitude modulation. No surface mode effects were observed. The SNR of 30 is smaller than that in the kagome reference (~150) [24] due in part to larger transit-time linewidth, residual background pressure, and reduced pump power. To explore the sensitivity of the frequency lock point to optical alignment, we stabilize a CW laser to the absorption feature, and beat it against a phase stabilized frequency comb.
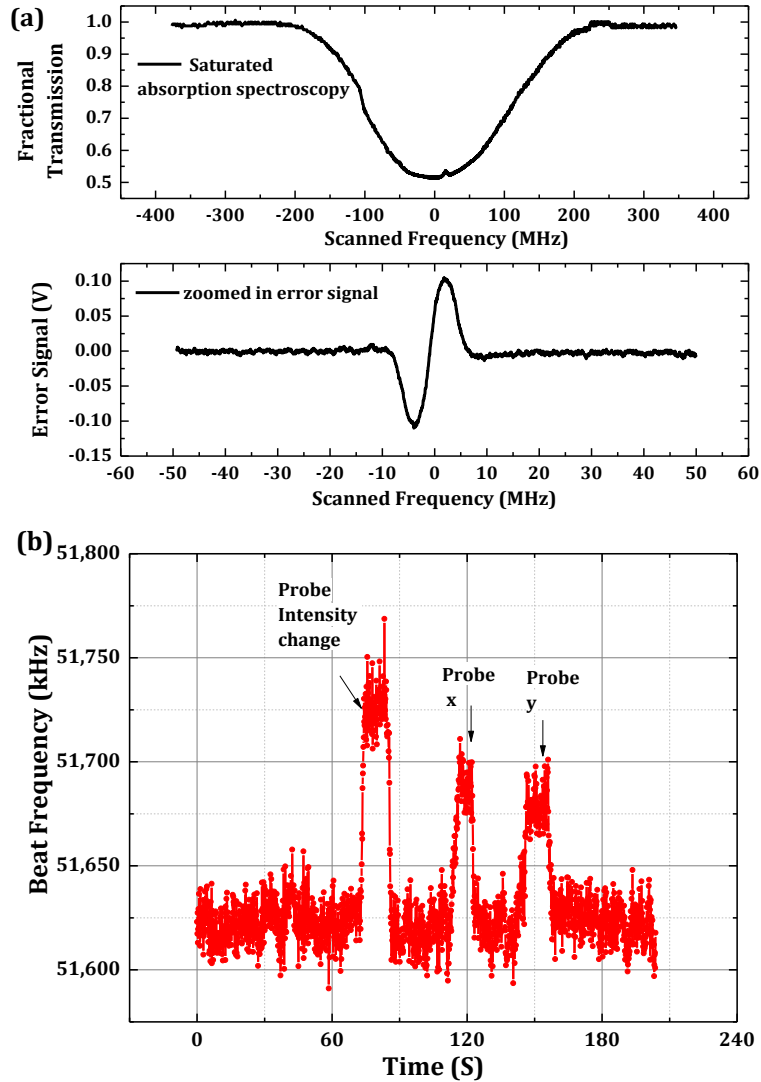
Figure 4-16: Adapted from Ref. [68]. (a) Fractional transmission of P(13) inside PRISM fiber vs. scanned frequency; bottom: zoomed in dispersion error signal of sub-Doppler vs. scanned frequency away from the P(13) transition. (b) Frequency shifts of the CW reference due to probe misalignment. The beat frequency between the frequency comb and the CW reference is plotted vs. time, x: horizontal mirror position; y: vertical mirror position.

Previously [8], the frequency lock point changed by ~20 kHz when the probe power was reduced by a factor of two using an attenuator, but by 100 kHz when the fiber coupling was altered enough to reduce the probe power by a factor of two (Figure 2-14). Here, in a similar test (Figure 4-16b) the shift due to probe power alone is ~ 100 kHz, while the shift due to alignment is only 50

kHz. The factor of five higher sensitivity to the probe power may result from the five times smaller SNR. However, the comparable sensitivity of the reference frequency to probe power and probe alignment may indicate a common cause, namely the change in probe power, rather than frequency dependence on fiber mode. This test will be more conclusive when the SNR ratio in the PRISM fiber is increased.

This PRISM fiber is proved to be suitable for a portable acetylene-filled frequency reference in a 10 m length. We demonstrated a robust conventional splice of PRISM fiber to SMF-28, which is achieved with a typical 2 dB splice loss using a Vytran-2000 fusion splicer (a) [68]. With both ends spliced to SMF-28, the transmission loss through 20 m PRISM fiber coiled to a 5cm diameter is about 7.8 dB. To reduce the 4% Fresnel reflection that degrades the performance of the PMC-based frequency reference, both fibers are cleaved at an 8° angle before splicing; the splice loss increases to 3 dB but the return loss is reduced to -56 dB (b). With one end conventionally spliced and the other angle spliced to SMF-28, the transmission loss through the 20 m fiber is about 10 dB [68].
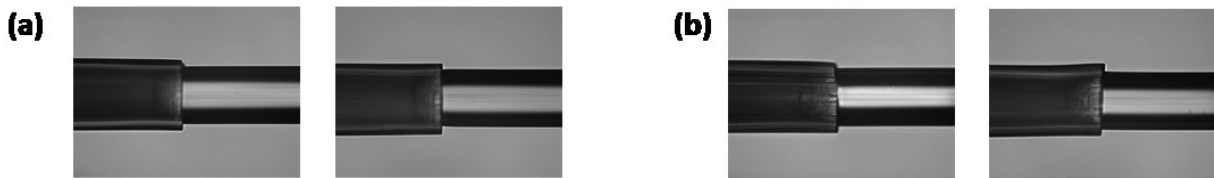
Figure 4-17: Adapted from Ref. [68]. Side-views of (a) a conventional splice and (b) an angle splice of PRISM fiber and SMF-28.

Since the production of the optimal single mode is expected at longer lengths (~10 - 30 m), a more weakly absorbing gas such as ammonia should yield higher SNR because it will be less sensitive to residual background gas pressure.

Chapter 5.   HC-PCF to SMF Splice for Photonic Microcell Fabrication

After the initial estimation and measurement of the performance of vacuum-chamber-based acetylene frequency references using different types of HC-PCFs discussed in the last chapter, we are going to replace the bulky vacuum chambers by creating gas sealed photonic microcells (PMCs) [25, 27, 28]. In this way, we increase the portability of the frequency reference and hope to reduce the sensitivity of the reference to alignment of the fiber in the vacuum setup. To make PMCs and seal the gas inside the PCFs, we need to fusion splice the HC-PCFs and solid core fibers (e.g. SMF-28). In this chapter, we are going to investigate the splices between different types of PCFs and SMFs.

5.1.   Optical fiber splicing process

Splicing is usually used to join two fibers and create a continuous optical path for light transmission. Mechanical splice (butt-coupling) and fusion splice are the two fundamental fiber splicing methods. Figure 5-1a gives out a typical method of making a mechanical splice, which is to align two fibers in a small glass (capillary) tube with a hole just slightly larger than the outside diameter of the fibers. In some cases, index-matching gel is loaded between the fiber ends and the fibers are butted together to obtain a continuous optical path. Mechanical splices are available for both multimode and single mode fibers. Different from the mechanical splices, fusion splices join two optical fibers end-to-end by heat from an electric arc or other types of heat source, shown in Figure 5-1b.
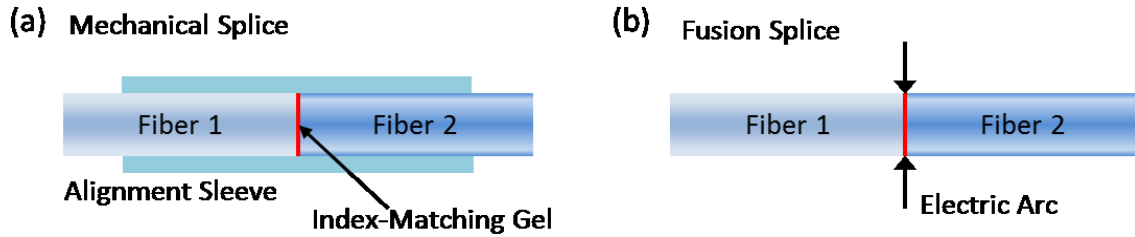
Figure 5-1: Schematic layout of (a) typical mechanical splices and (b) fusion splices. The mechanical splice (a) is aligned in an alignment sleeve and the fibers' ends are butted together with index-matching gel; the fusion splice (b) is aligned on the fiber alignment stage of a fiber fusion splicer and the fibers' ends are joint by electric arc.

Generally speaking, mechanical splices are often used in those applications where the two fibers have a large difference in melting temperatures and fusion splices are employed in those fibers have similar fusion temperatures. Here we focus on joining two fibers' end by fusion splices, because we need create a hermetic joint between PCFs and SMFs. A splicing machine, such as vytran fusion splicer-2000 (Appendix D), is required to achieve a high-quality splice. The splicer first aligns the fibers, then applies a certain amount of heat to melt the fiber ends and push the fibers together.

5.1.1. Four primary fusion splicing steps

The first step is to prepare the fiber by stripping back the external protective coatings and buffer tubes to leave only the bare fibers. Bare fibers need to be clean before the next step, in which we can either wipe the bare fibers using isopropyl alcohol or sonicate the bare fibers to clean out any acrylate coating residue.

The second step is to cleave the fiber. A fiber cleave will first score the fiber and then pull or flex the fiber to break it (Figure 5-2). The cleaving quality largely depends on the cleaver, and a well cleaved fiber end should have a smooth and flat surface. Bad cleaves may end up with chips

and cracks.
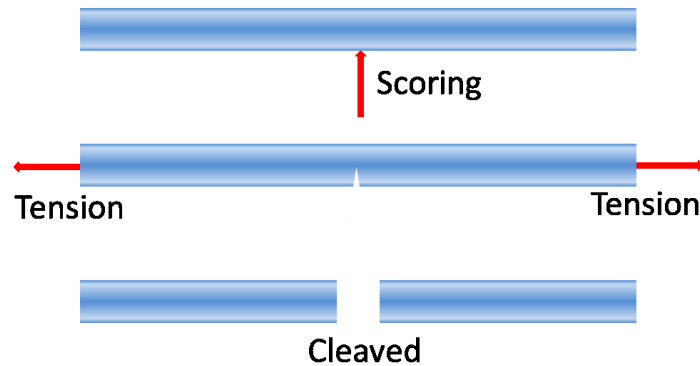
Figure 5-2: Illustration diagram of optical fiber cleaving

The next step is the fusion process. The two cleaved bare fibers from the last step are precisely aligned (Figure 5-3a) for maximum optical light transmission through the fibers. Once the fiber is optimally aligned, an electrical arc or other heating element melts the fiber ends and pushes them together to create a continuous light path through the fiber joint (Figure 5-3b). The fibers in Figure 5-3 used to illustrate this process are Erbium Doped Fiber (LIEKKI™ Er110-4/125) and single mode fiber (Coring SMF-28). Both fibers have a 125 μm outer diameter. More details of fusion splicing can be found in Appendix D . From the splice image captured by the camera on the splicer, a good fusion splice should be free of bubble splices, fiber bending, and dark lines at the splice joint.
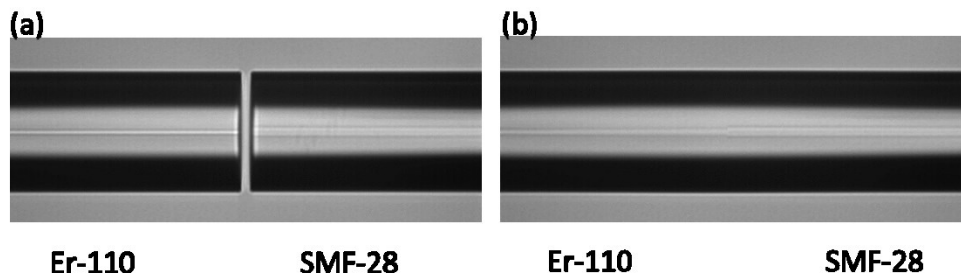
Figure 5-3: Splice image of LIEKKI Er-110 fiber and SMF-28. (a) Fibers are aligned precisely before fusion; (b) Fibers are joined together after fusion.

The last step in the splicing process is to protect the fiber splice joint. The fiber splice joint may break due to the bending and/or pulling forces applied to the fiber during regular fiber handling. Protective tubes such as heat shrink tubing and a mechanical clamp are usually ultilized.

5.2. Splicing parameter characterization

A high-quality splice is important for applications requiring a continuous light path through optical fibers. The main factors affecting the quality of fusion splices are insertion loss at the splice joint, return loss at the splice joint and splice strength. To be noted here, the insertion loss and the return loss of our fiber splice is calibrated by a laser source at 1533 nm. Any transmission and loss number mentioned in the thesis are measured at 1533 nm.

5.2.1. Insertion loss

The insertion loss of the fiber splice can be defined as the loss of optical power at the joint between two fibers (Eq.(5.1)). For the short fiber length, we can ignore the transmission loss of the fiber itself and use the received (P_R) and emitted (P_E) optical power to calibrate the insertion loss of the splice (Figure 5-4).

$$Loss[\text{dB}] = -10\log\left(\frac{P_R}{P_E}\right) \tag{5.1}$$

The emitting power is measured by connecting or coupling a laser source to the emitting fiber (Fiber 1) at the end of the cleaved emitting fiber. Then the receiving fiber (Fiber 2) is spliced to the end of the emitting fiber, the receiving power is then recorded at the end of the receiving fiber. Using Eq.(5.1), the insertion loss of the fusion splice joint can be calculated in dB units. For

two identical fibers, the splice loss using the Vytran-2000 splicer is normally less than 0.05 dB.
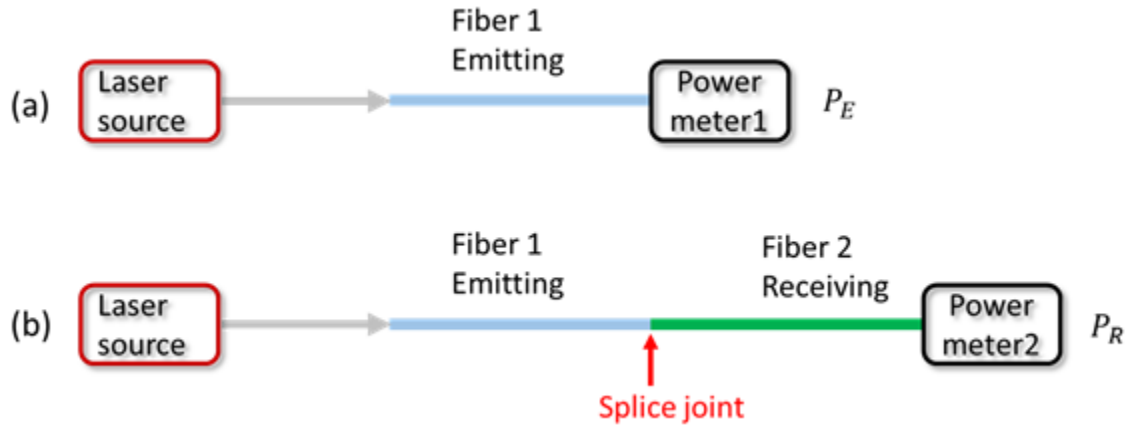
Figure 5-4: Experimental setup for fiber splice insertion loss measurement. (a) The emitting power is measured first when only the emitting fiber (Fiber 1) is connected the laser source. (b) A receiving fiber (Fiber 2) is then spliced to the emitting fiber (Fiber 1) and the receiving power is measured.

Depending on the fibers and the splicer process, there are three basic factors that determine the insertion loss of the fusion splice [69]:

1) Longitudinal offset loss - due to the different fibers parameters, such as core diameter and numerical aperture (NA).

For example, as shown in Figure 5-5, when the receiving fiber (Fiber 2) has a smaller core size than the emitting fiber (Fiber 1), only partial light from the emitting fiber will be transmitted by the receiving fiber. This loss, due to the longitudinal offset, can be estimated using Eq.(5.2).

$$Loss[dB] = -20\log(\frac{r_R}{r_E}); \qquad r_R \leq r_E$$

$$Loss[dB] = -20\log(\frac{NA_R}{NA_E}); \qquad NA_R \leq NA_E$$

(5.2)

where r_E and NA_E are the core size and NA of the emitting fiber; r_R and NA_R are the core size and NA of the receiving fiber.

81
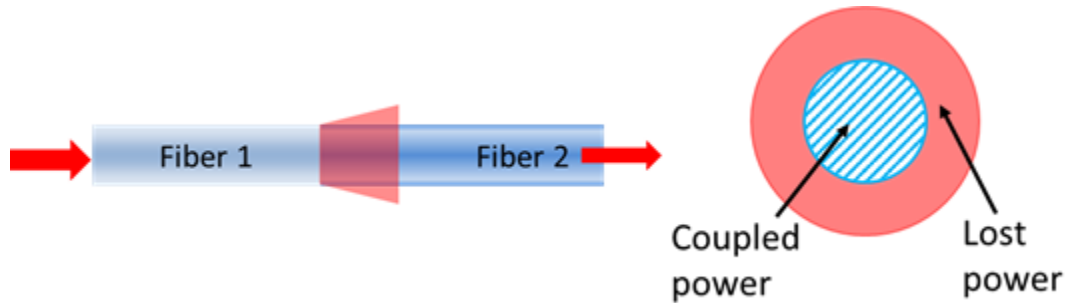
Figure 5-5: The splice insertion loss due to longitudinal offset. The emitting fiber (Fiber 1) has a bigger core size thus a larger numerical aperture (NA) than the receiving fiber (Fiber 2), only partial light is going to be coupled to the receiving fiber.

2) Mechanical loss - due to mechanical misalignment.

As shown in Figure 5-6, the mechanical misalignment between the emitting and receiving fiber may happen during the splicing process. In one case, the two fibers may not be axially aligned well and an offset between fibers is presented. In another case, at least one of the two fibers is bending during the alignment procedure, an angular misalignment may occur. The axial misalignment is the primary causes of the mechanical misalignment loss.
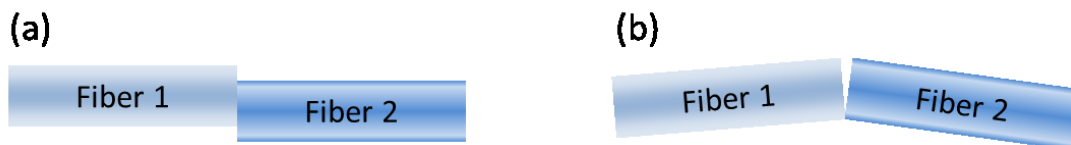
Figure 5-6: The splice insertion loss due to mechanical misalignment. (a) The axial misalignment between the emitting fiber (Fiber 1) and the receiving fiber (Fiber 2); (b) the angular misalignment between the emitting fiber (Fiber 1) and the receiving fiber (Fiber 2).

3) Splice fusion loss - due to the heat of melting fibers.

When the two fibers are spliced together, the transmission through the fiber is typically lower than the transmission when the two fibers are butt coupled. This reduced transmission (increased loss) is called the splice fusion loss; a typical splice fusion loss varies from 0.01 dB to 0.5 dB, due the different fiber types. When the fusion temperature is too high, and/ or the two

fibers are pushed too hard towards each other, the fusion splice loss will be increased.

5.2.2. Return loss

A back reflection (Fresnel reflection) always occurs when there is a change in refractive index at the splice interface between the two fibers (Figure 5-7). For example, when we splice a hollow-core fiber with a solid core fiber, the refractive index is changing from n ~ 1 (the air) to n ~ 1.46 (the fused silica).
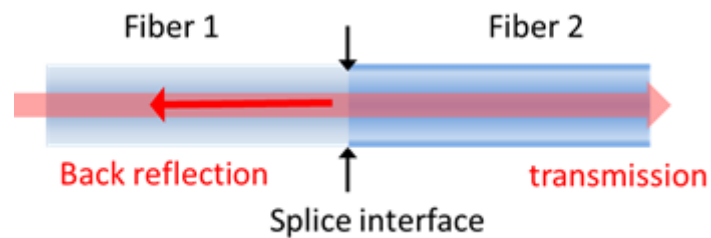
Figure 5-7: Back reflection (Fresnel reflection) occurs at the splice interface of two fibers.

In an optical system, the reflected light may interfere with the transmitted light thus degrading the performance of the optical system. Thus an important splice parameter, optical return loss, is defined by the amount of light that is reflected back to the emitting fiber. To characterize the return loss, we can add an optical circulator to the setup shown in Figure 5-4 to measure the transmission as well as the return loss at the same time (Figure 5-8).
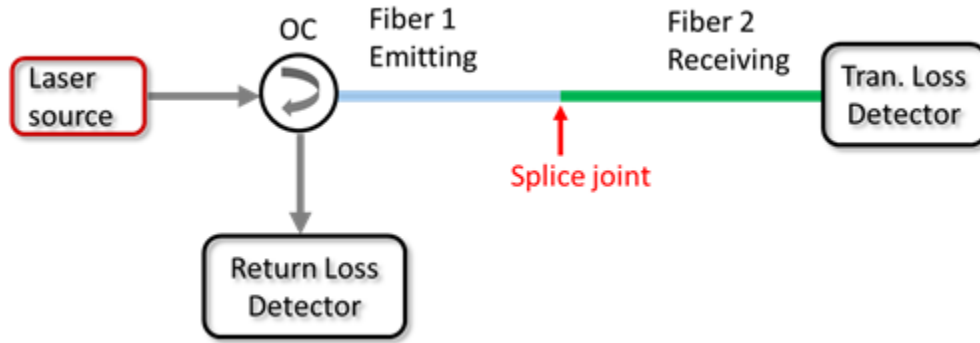
Figure 5-8: Experimental setup for transmission and return loss measurement. OC: optical circulator.

To reduce the return loss between a hollow core fiber and a solid core fiber, we consider to the angle cleave and splice both fibers, since the reflected light will not be reflected back to the path of the transmitted light, the appropriately chosen cleave angle can reduce back reflections to less than -60 dB (Figure 5-9). The typical cleave angle is from 4^0 to 8^0 depending on the types of fibers and applications.
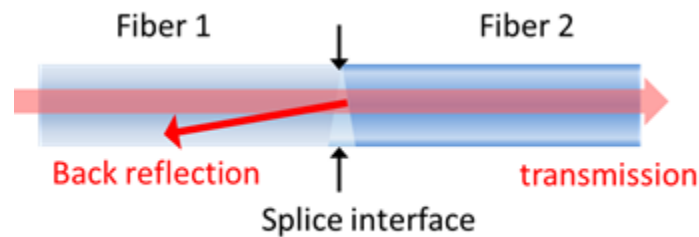
Figure 5-9: Angle cleave and splice to reduce the back reflection (Fresnel reflection) occuring at the splice interface of two fibers.

5.2.3. Fiber strength

An acceptable fiber strength at the splice joint is also a main parameter to determine the splice quality and for practical handling of the fibers. The splice station Vytran-2000 has a built-in fiber strength test for the calibration. Since the splice strength between the hollow-core fiber and solid-

core fiber is not strong enough to pass this test, instead, we pull the fiber holder blocks apart and measure how far we can pull after the splice. If we can pull the two fiber holder blocks apart more than 100 μm without breaking the fiber, the splice is strong enough for the actual application. One example is shown in Figure 5-10. For the splice between 10 μm PBGF (HC-1550-02) and SMF-28, we are able to pull the fiber 160 μm apart before it breaks, telling us the splice strength is good for this particular splice.

Figure 5-10: Splice image before and after the pull test. (a) side-view of a conventional splice of 10 μm PBGF (HC-1550-02) and SMF-28; (b) side-view after pulling test, the two fibers are pulled apart until breaking, the recorded pulling distance is 160 μm. (c) end-view of 10 μm PBGF after pull test; (d) end-view of SMF-28 after pull test.

5.3.   HC-PCFs to SMFs splicing
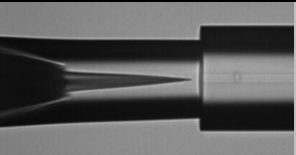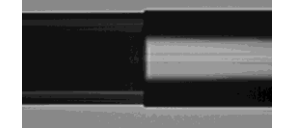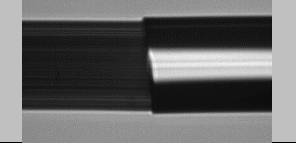
As mentioned in Chapter 4, there are two categories of HC-PCFs, PBGF and kagome PCF, used in our acetylene frequency references. The splices between PBGFs and SMFs, and kagome PCFs to SMFs have been well studies by collaborator, Dr. Benabid at Research institute Xlim, Université de Limoges (France) [25, 27, 59-61].

5.3.1. PBGF to SMF

PBGFs have similar outer diameter to the SMFs, so they are easily spliced together. Splice types such as such the collapsed core PBGF to SMF splice, the conventional splice, and the angle splice have been well done. We have successfully reproduced these splices in our lab. As shown in Table

5-1, the splice images and measured splice parameters at 1.532 nm of splicing between the 7-cell PBGF (Fiber A in Table 4-1) and SMF are summarized.

Table 5-1: Parameters of splice between 7-cell PBGF and SMF

Splice Types	Image	Transmission Loss	Return Loss
Collapsed Core PBGF to SMF		1dB	-16 dB
Conventional Splice		3dB	-60 dB
Angle Splice		> 10 dB	< -60 dB

Collapsed core PBGF to SMF splice is useful for reducing back reflection in the optical system; however, the transmission through this type of splice is always low (< 10%). Vice versa, conventional splicing of the PBGF and SMF can obtain high transmission, but the back reflection will degrade the performance in applications such as pump – probe spectroscopy used in our acetylene frequency references. Interference from the reflected beam and the original beam will decrease the S/N ratio of the sub-Doppler error signal and thus the stability of the frequency references. In this sense, a photonic microcell (PMC) with an angle splice can satisfy both requirements of high transmission and low back reflection.

One factor affecting the quality of the angle splice is the quality of angle cleave of PBGFs; most commercially available angle cleavers could not get very repeatable small angle (6^0 to 8^0) cleaves. Instead of purchasing high cost (> \$ 7k) angled fiber cleaver, we built a rotational fiber holder and use the manual fiber cleaver to achieve the angle cleave. The angle cleave procedure is

shown in Figure 5-11a. Frist we close the holder cover on the cleaver and the clamp on the fiber rotator, then we rotate the fiber by 20^0. In the end, we close the cleaver cover and slide the blade to cleave the fiber. Figure 5-11b exhibits a well cleaved 10 μm PBGF and SMF with a 6^0 cleave angle.
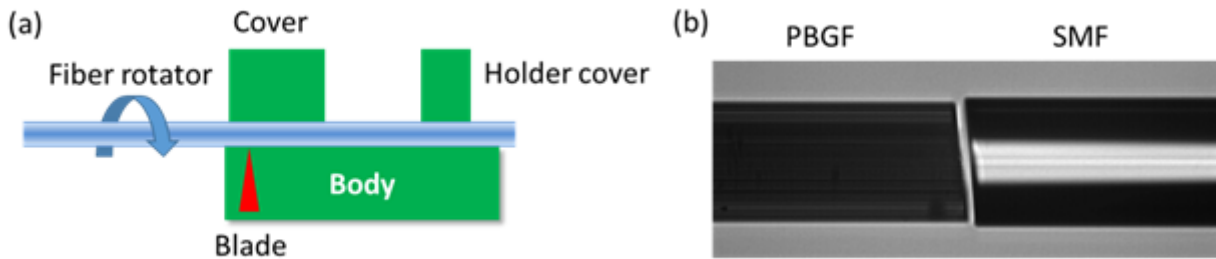
Figure 5-11: (a) Schematic of angle cleaver setup. Fiber rotator is built by adding a fixed height mount to the rotatable fiber clamp (Thorlabs: SM1F1-250) to match the height of the fiber cleaver (DVP Series Fiber Cleaver KL-21); (b) Image of cleaved 10 μm PBGF and SMF. The fiber rotator is rotated 20^0 to achieve a 4^0 cleave angle in both PBGF and SMF.

5.3.2. Kagome PCF to SMF

Kagome PCFs normally have a larger diameter compared with SMF-28 (Figure 5-12); kagome PCFs need to be tapered before being spliced to SMF.
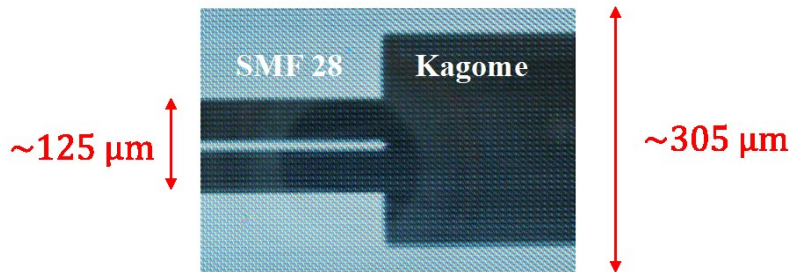
Figure 5-12: Kagome normally exhibits a larger outer diameter than the SMF-28.

For example, a 7-cell kagome PCF has an outer diameter of ~ 305 μm. Its outer diameter need to be tapered down to 125 μm to match the outer diameter of SMF (Figure 5-13) [28, 61, 70]. This tapering can be finished using a Vytran-GPX splicing station with a built-in fiber tapering

function, and a typical tapered length is about 7.5 mm. The microscope images of a 70 μm core kagome PCF before and after tapering are shown in Figure 5-14. The transmission loss of the splice of a large core kagome PCF is ~ 3dB while the return loss is ~ -16 dB.
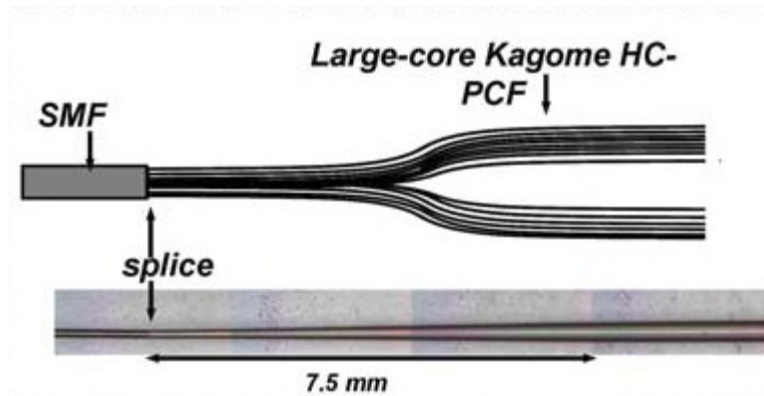
Figure 5-13: Reproduced from Ref. [70]. Schematic of the tapered HC-PCF spliced to the SMF and a photograph of a fabricated kagome HC-PCF tapered and spliced to an SMF.
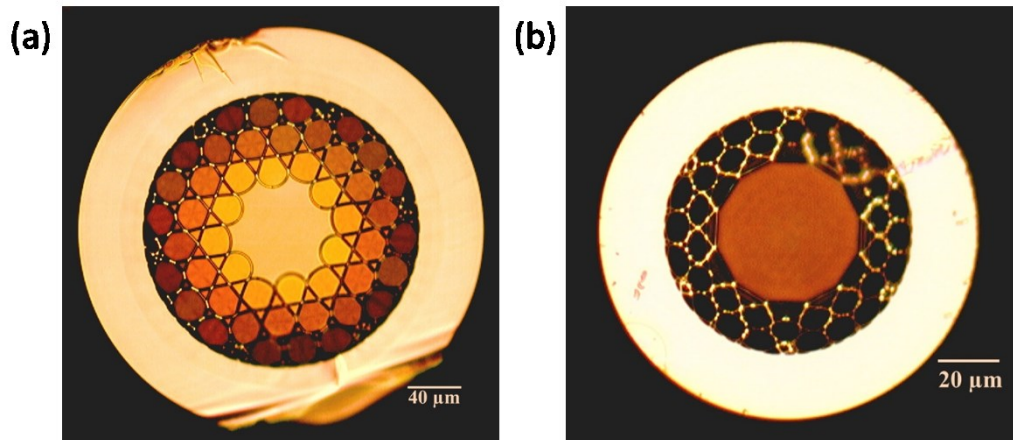
Figure 5-14: Microscope images of a 7-cell kagome PCF (70 μm core size) before and after tapering using a Vytran-GPX splicing station.

Similar to the splice between PBGFs and SMFs, we need to reduce the Fresnel back reflection at the splice interface between the tapered HC-PCF and solid single mode fiber (SMF) using angle cleave and splice. The 4% (-16 dB) reflections at the interface reduce the performance of the PMC-based device, and it is difficult to obtain repeatable 8^0 angle cleaves of the tapered

kagome HC-PCF. Consequently, the angle splice technique used for photonic bandgap fibers is not adequate for the tapered kagome HC-PCF [71]. Two methods have been investigated during my visiting at XLIM (France). One method is that we taper the SMF to match the core size of kagome PCF, then we angle cleave the tapered SMF and insert the tapered SMF into the core of the kagome. At last, we heat the kagome PCF to collapse the core for creating an airtight seal between kagome and SMF (Figure 5-15). While maintaining an acceptable fiber strength and minimal alternation of HC-PCF, the lowest transmission loss being achieved is 7.5 dB. The overlap distance (d) between the tapered SMF (8^0 cleave angle) and the kagome core is ~ 1.6 mm. The return loss is 41 dB.
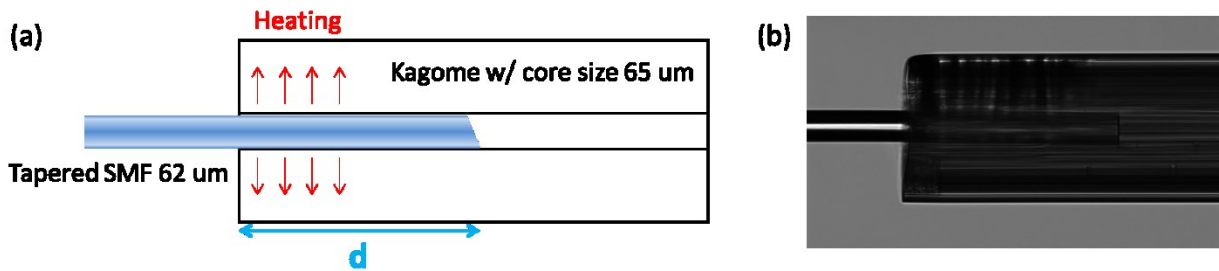
Figure 5-15: (a) Schematic of the splice between tapered SMF and kagome. The SMF is tapered to match the core size of kagome, and inserted into the kagome core. The overlap range of kagome and SMF is heated using a filament fusion splicer to create an air-tight seal. (b) Splice image of tapered SMF and kagome.

The other method for reducing the Fresnel back reflection at the splice interface is that we draw borosilicate capillary sleeves (boro-sleeves) for butt-coupling an angle-cleaved SMF and right-angle cleaved kagome HC-PCF. The boro-silica has a much lower fusion point than the fused silica, thus the boro-sleeve can be heated using a filament fusion splicer without changing the structure of HC-PCF. The boro-sleeve is fused to a lateral side section of the HC-PCF to realize an air-tight seal with minimum physical alteration to the HC-PCF (Figure 5-16). Furthermore, the

borosilicate sleeves are heated 2mm away from the HC-PCF end tip to prevent capillary collapse at the gap between fibers. Two methods are shown here:

1)   a boro-sleeve with a core diameter ID ~ 150 μm, outer diameter OD ~ 300 μm to fit angle-cleaved SMF and tapered kagome HC-PCF (Figure 5-16a);

2)   two boro-sleeves of different sizes to fit both SMF (sleeve ID ~ 150 μm, OD ~ 300 μm) and kagome HC-PCF (sleeve ID ~ 310 μm, OD ~ 620 μm) (Figure 5-16b).
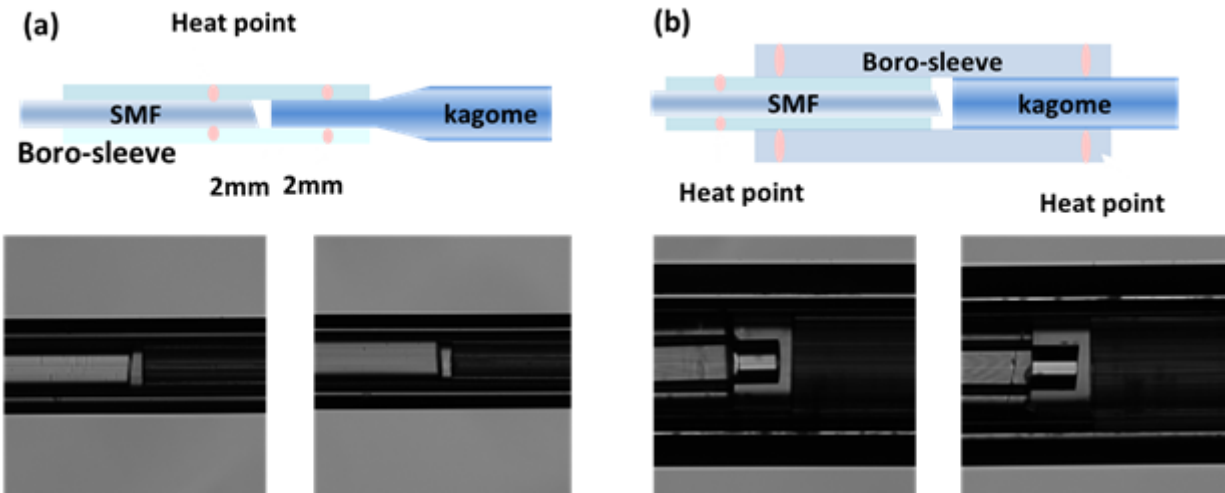
Figure 5-16: Adapted from Ref. [72]. (a) Schematic layout (top) and side-views (bottom) of sleeve splice between angle-cleaved SMF and tapered kagome HC-PCF; (b) sleeve splice between angle-cleaved SMF and un-tapered kagome HC-PCF.

We choose to heat 2 mm away from the HC-PCF end tip based on a careful study of the relation collapsed range of the boro-sleeve with heating time and powers (Figure 5-17).
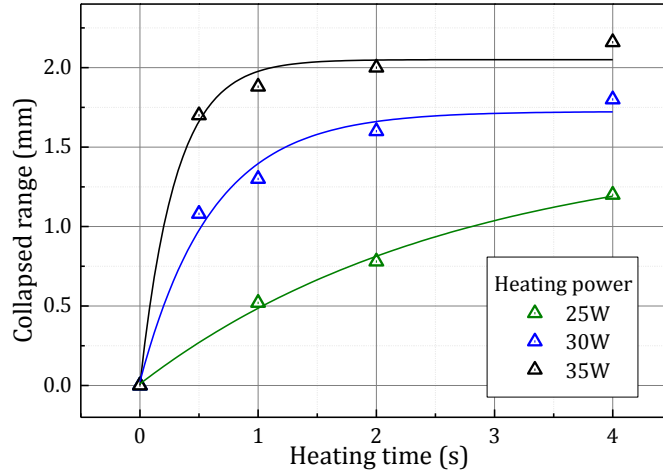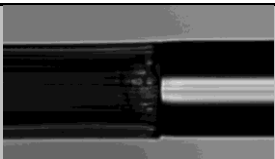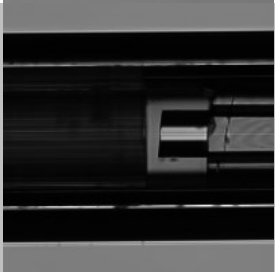
Figure 5-17: Boro-sleeve collapsed range vs. heating time at different heating powers.

The parameters of the boro-sleeve splice are also well calibrated and summarized below with the comparison of the conventional splice between kagome PCFs and SMFs. As shown in Table 5-2, both the sleeve splices between angle-cleaved SMF and un-tapered (or tapered) kagome HC-PCF readily show very strong reduction in optical back reflection while keeping the transmission loss below 3 dB/splice. These splices are suitable for creating low back reflection PMCs. The low Fresnel back-reflection is particularly desirable in the development of a PMC for SAS applications. A PMC that exhibits an angle-splice at one end and a right-angle splice at the other end offers a simple, efficient and all-fiber solution to reproduce the performance obtained in saturation spectroscopy inside acetylene-filled kagome HC-PCF [24].

Table 5-2: Parameters of splice between kagome PCFs and SMF

Splice Types	Image	Transmission Loss	Return Loss
Conventional splice between tapered kagome and SMF		2 dB (1-cell) 3 dB (7-cell)	- 16 dB
Angle splice between tapered kagome and SMF		4.5 dB	- 59 dB
Angle splice between kagome and SMF		2.8 dB	- 43 dB

Chapter 6.   Acetylene Frequency Reference inside PMC

Using the splicing techniques developed in the last chapter, photonic microcells (PMCs) (Figure 6-1) [25, 27, 28] have been created to replace the vacuum chambers. Due to the long interaction lengths of fiber and low insertion loss achieved between HC-PCFs and SMFs, portable, robust, and user-friendly PMC-based devices such as acetylene frequency reference can be developed.
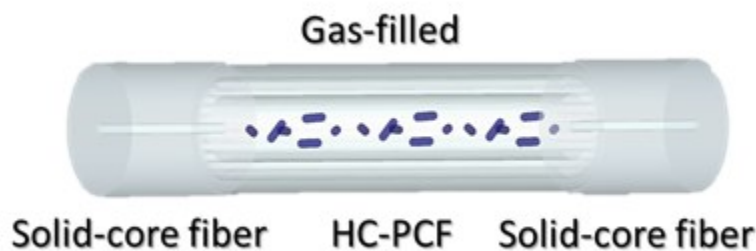
Figure 6-1: Schematic of a photonic microcell. The gas is loaded into the HC-PCF and the end of the HC-PCF is sealed with solid-core fibers.

6.1.   Photonic microcell assembly

Techniques to create PMCs have been demonstrated by Light *et. al*. [27]. One end of the HC-PCF is first spliced to a solid-core fiber. The open end of the HC-PCF is evacuated by a vacuum system, then filled with the desired pressure of acetylene. The HC-PCF is over pressured with helium gas at a pressure exceeding 1 atm. Then the HC-PCF is cleaved and spliced to another solid-core fiber quickly, before the helium is depleted, or the atmosphere enters. After both ends are air tight spliced to solid core fibers, the remaining helium gas inside the microcell will evacuate through a permeation process in the atmosphere, resulting in a gas microcell containing only the initially loaded acetylene.

We use a similar procedure but use a CO_2 laser to melt the end while the helium and

acetylene are inside the fiber (Figure 6-2). By melting the fiber end and trapping the helium and acetylene inside the fiber, we can save some time for preparing the 2nd cleave and splice. We successfully fabricate a photonic microcell using 10 μm PBGF. The transmission loss of this cell is ~ 7dB using an arc splicer. The splices are the conventional splice because the equipment limitation in the lab when this cells is fabricated. By using Vytran splicer and angle splice technique, we would expect a microcell with higher transmission and lower back reflection.
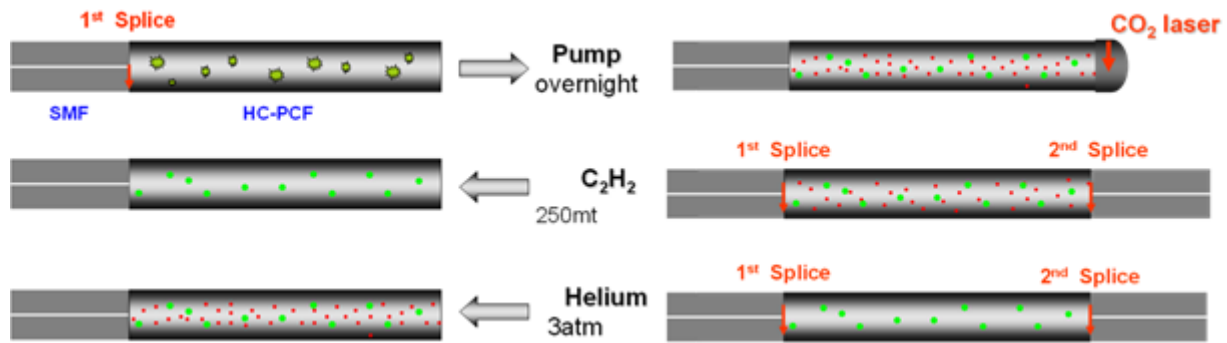
Figure 6-2: Procedure for acetylene microcell assembly. A CO_2 laser is used to melt the fiber end when the acetylene and helium are loaded.

Since we do not have an appropriate fusion splicer and cleaver in the lab for dealing with large core fibers, we are not able to repeat the microcell assembly procedure using large core kagome PCFs at Kansas. My work at XLIM shows that it is not easy to fabricate a larger core (~ 80 μm) kagome PCF microcell due to the limitation of helium diffusion time. The key to making a microcell is the time allowance to finish the 2nd splice without introducing contamination into the fiber. Using the analytical model provided in Ref. [73], we calculate the helium diffusion time inside different core size HC-PCFs (Figure 6-3). The details of this calculation are in Appendix C . The helium diffusion time has a relation to the fiber length (*l*) and core size (*d*) shown in Eq.(6.1) .

$$t \propto \frac{l^2}{d^2} \qquad (6.1)$$

Even with helium pressure at 6 atm, and a fiber length of 12 m, the time to make the 2nd

splice is only 1 min. The short splice time is almost impossible for the actual assembly process

because we need to use the Vytran-GPX splicing station and a regular time to finish a splice using

this splicer is ~ 2 mins.
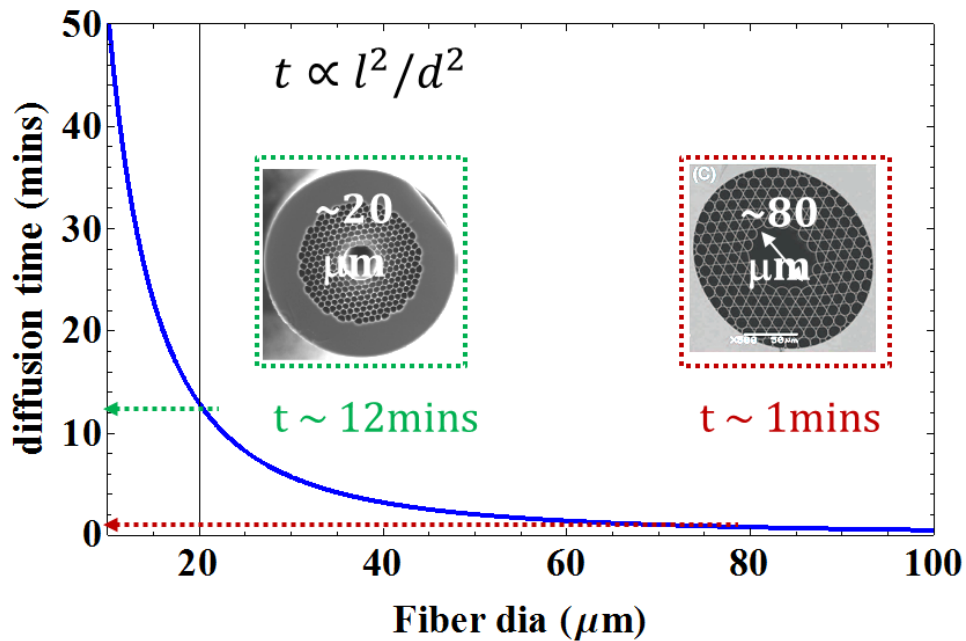
Figure 6-3: Helium diffusion time vs. fiber core diameters. The helium pressure is 6 atm, and the fiber length is 12 m is used in this calculation. The time allowance for the 2nd splice of a 20 μm fiber is ~ 12 mins while only ~ 1m of an 80 μm core fiber.

6.2. Photonic microcell calibration

In the experiment, a narrow linewidth CW laser near 1.5 μm is split by a fiber coupler to generate

a frequency modulated probe beam and an amplitude modulated pump beam. Like what we did in

our vacuum chamber based references, an AOM is used to shift the interference between the probe

and the reflected pump to the AOM frequency and an EOM is used to create sidebands spaced at

the modulation frequency for FM spectroscopy [74]. The pump beam, counter-propagating with

the probe beam, passes through an EDFA to saturate the acetylene molecules. Since the splice loss

is introduced at the two splicing joints, another EDFA is used to increase the probe power coupled

into the PMC. In addition, a fiber circulator is used to separate the probe and pump beams, and the

resulting probe beam is detected by a photoreceiver. The remaining CW light from the laser beats

against a phase stabilized CNFL frequency comb [39] to characterize the stability and accuracy of

the reference. The RF beat frequency is recorded by counters with a 1 s gate time. Two full

photonic microcells and one half photonic microcell with an angle splice are calibrated in our

experiment.
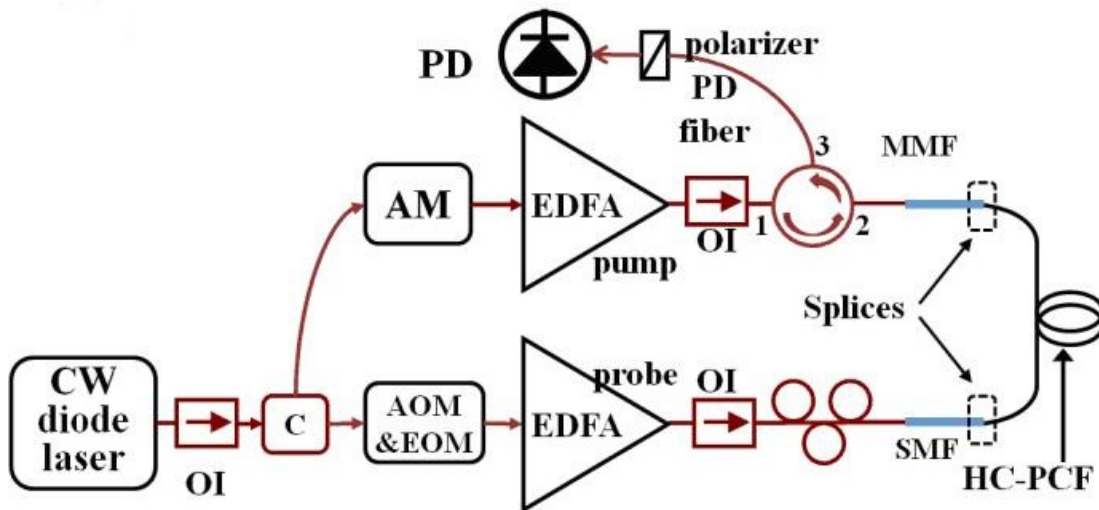
Figure 6-4: Adapted from Ref. [36]. A sealed photonic microcell. Shown are amplitude modulator (AM), acousto-optic modulator (AOM), electro-optic modulator (EOM), polarizing beam splitter (PBS), optical isolator (OI), half wave plate ($\lambda/2$), quarter wave plate ($\lambda/4$), optical circulator (C), and photodetectors (PD).

6.2.1. Full PBGF microcell

One microcell is made of a 10 μm PBGF (Fiber A) microcell, with a length of 4 m and a pressure

of 174 mtorr. 22% transmission on the P(13) line is measured by the CW fiber laser used in the

kagome setup (Figure 2-2). A ramp voltage scans the laser frequency linearly in time to calibrate the linewidth and S/N ratio of the error signal. The typical linewidth is 17 MHz and S/N ratio is 7 with a pump power of 16 mW (Figure 6-5). The broader linewidth and much lower S/N ratio is mainly due to the pump reflection at the splice interface between PBGF and SMF, also the surface mode in the 10 μm PBGF.
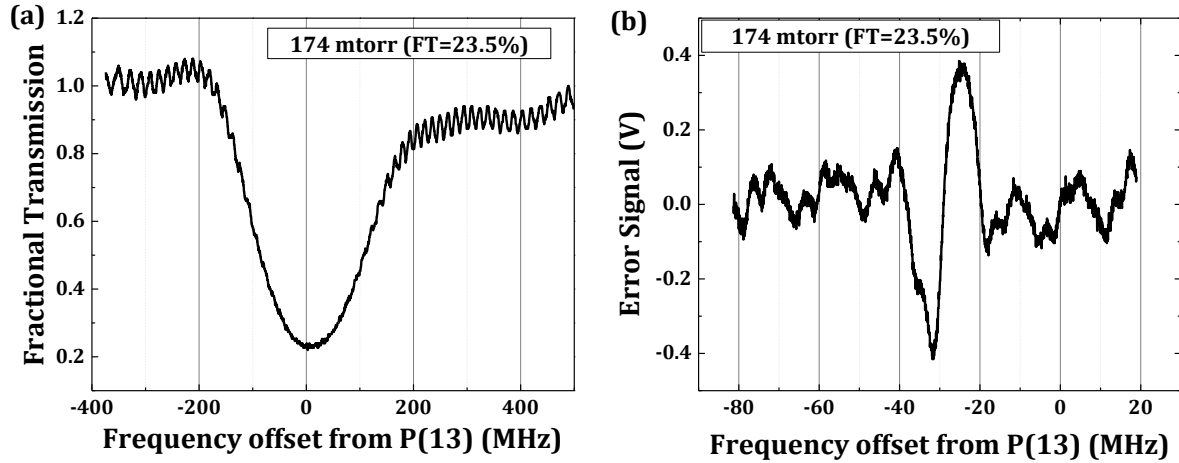
Figure 6-5: (a) Fractional transmission of a 4 m long 7-cell PBGF PMC with a $^{12}C_2H_2$ pressure of 174 mtorr, and a pump power of 16 mW exiting the fiber; (b)error signal of sub-Doppler versus scanned frequency away from the P(13) transition. The laser frequency was scanned at 1.2 GHz/sec.

A 1.5 MHz beatnote noise (Figure 6-6a) is measured on the P(13) v_1+v_3 overtone transition of acetylene inside this 10 μm PBGF microcell. Moreover, the corresponding fractional Allan deviation is in Figure 6-6b. The long-term instability of PBGF PMC-locked lasers may be caused by the drift of the probe polarization mentioned earlier in this paper. The fractional instability at 1s sample period is about 2 orders of magnitude worse than that of our vacuum chamber reference setup [24]. The fractional stability at 1s is dominated by the broadened linewidth, pump reflections, and the surface modes in PBGF.
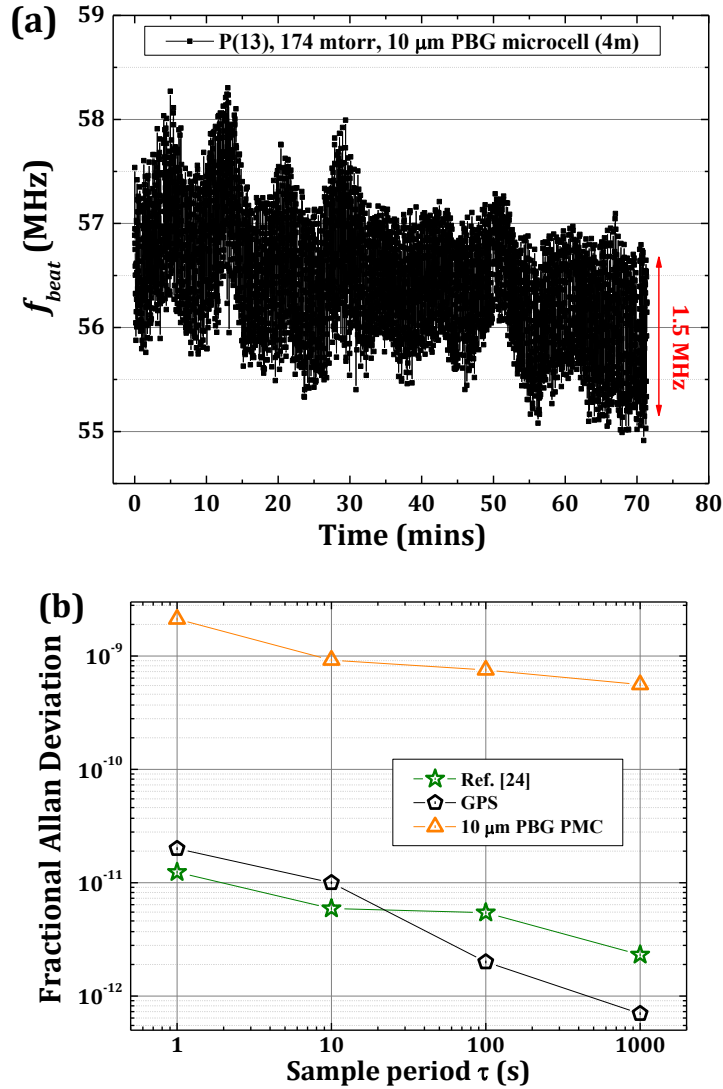
Figure 6-6: Adapted from Ref. [36]. (a) Beat frequency vs. time in $^{12}C_2H_2$-filled 10 μm PBGF PMC for the P(13) line transition; (b) Fractional instability vs. sample period of P(13) line of $^{12}C_2H_2$ PBGF PMC and compaired with the fractional instability taken in acetylene filled large-core kagome HC- PCF in vacuum chamber [24].

6.2.2. *Full kagome microcell*

The other particular microcell, made of a 1-cell kagome (Fiber E), was originally built for an

electromagnetically induced transparency measurement, with a length of 6.5 m and a pressure of

375 mtorr [28]. This kagome microcell leads to a 100% fractional absorption on the P(13) line.

Therefore, a tunable diode laser (Santec TSL-210) is tuned to 1539 nm with 6 mW optical power to measure a weaker line, P(23), which gives a fractional absorption of 76%. An error signal is observed and compared with what is observed in large-core kagome vacuum chamber reference [24]. The linewidth is a factor of 2 worse and the S/N ratio a factor of 10 worse than the error signal obtained in the vacuum chamber reference (Figure 6-7a). A diode laser is stably locked to this 1 cell kagome PMC over 80 minutes and the beatnote frequency excursions ('beatnote noise') is around 50 kHz (Figure 6-7b).
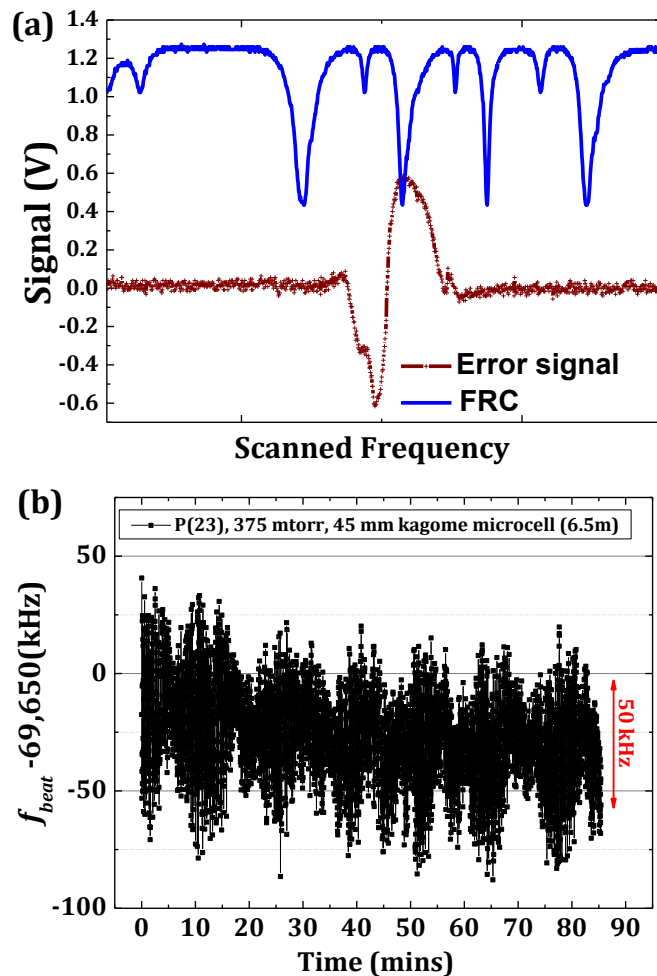
Figure 6-7: Adapted from Ref. [36]. (a) Amplitude of error signal versus frequency offset around the P(23) v_1+v_3 transition in $^{12}C_2H_2$; also shown is the transmission through a fiber ring cavity (FRC) with 39.5 MHz free spectral range, for calibration. (b) Beat frequency versus time in $^{12}C_2H_2$-filled 45 μm kagome PMC for the P(23) line transition.

We also calculated the fractional instabilities of 1-cell kagome microcell beatnote measurements, shown in Figure 6-8. The fractional instability at 1 s sample period time is worse than that of our vacuum chamber reference setup [24]. For the kagome microcell, the fractional stability is mainly caused by broadened linewidth, pump reflections, and the noisier laser.
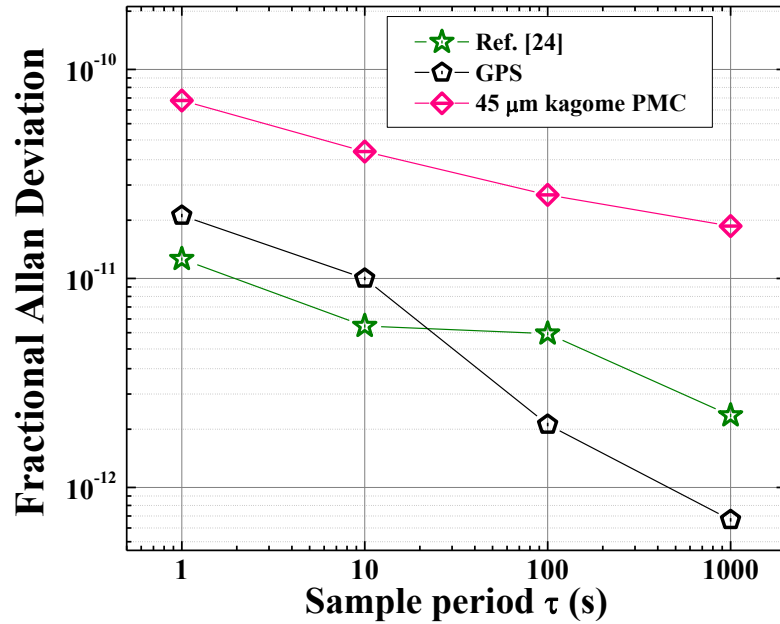
Figure 6-8: Adapted from Ref. [36]. Fractional instability vs. sample period in P(23) line of $^{12}C_2H_2$ kagome PMC and compaired with the fractional instability taken in the acetylene filled large-core kagome HC- PCF in vacuum chamber [24].

We also explored the environmental sensitivity of the kagome PMC-locked laser, as shown in Figure 6-9. In the measurement, the kagome PMC is put in a cardboard box with a lid. Several actions are applied to this particular microcell, such as opening the box, shaking the box, pressing on the PMC, and changing polarizations of the probe and pump beams. A shift of up to 1.2 MHz occurs when we shake the box, and a shift of up to 1 MHz is caused by changing the probe polarization. Fortunately, all those shifts are reversible. The beat frequency returned to its original value (± 0.05 MHz) after all the actions applied on the PMC were set to the beginning states.
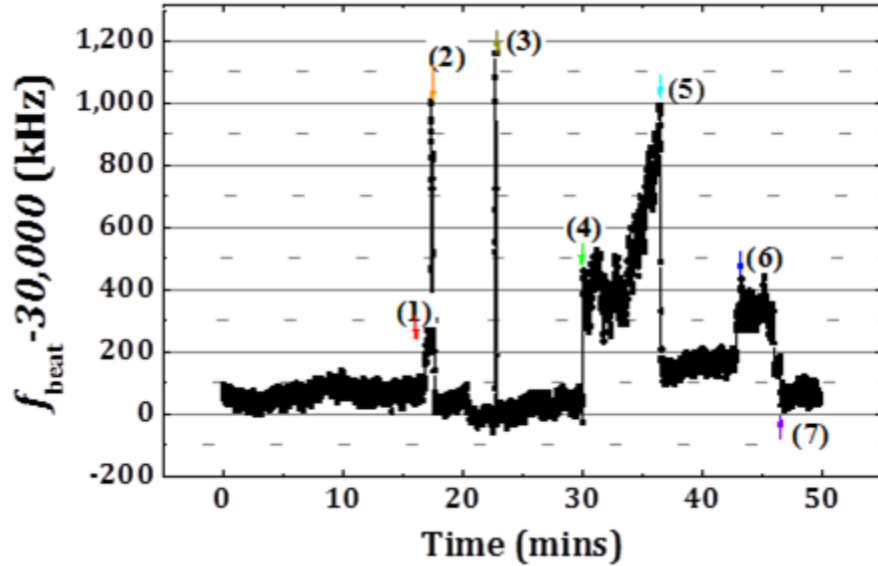
Figure 6-9: Sensitivity measurement in 1-cell kagome PMC, actions: (1) open the lid of carton box, (2) use finger to press on the kagome section of the PMC, (3) shake the box a few seconds, (4) adjust the squeezer on the probe arm to change probe polarization and to reduce probe power by a factor of 2, (5) re-optimize the probe power and bring the probe polarization back to the original state, (6) adjust the squeezer on the pump beam to increase pump reflections by a factor of 3, (7) minimize the pump reflection.

Here, we track the performance of the PMC reference over an extended period. The long-term stability is improved by using a polarization maintaining (PM) erbium-doped fiber amplifier (EDFA) (red triangles) to amplify the probe beam power instead of a non-PM EDFA (yellow squares and cyan hexagons) (Figure 6-10a, b). A stable beat frequency can be measured over 270 mins. We also notice a factor of 2 degradation in the stability after six months compared with our initial data, but no further degradation was observed. The degradation may be caused by outgassing of contaminants in the PMC. We also found deterioration in the PBGF PMC after a delay of a year. Longer evacuation time and heating the HC-PCF before use may help to reduce any impurities in the inner core of the fiber.
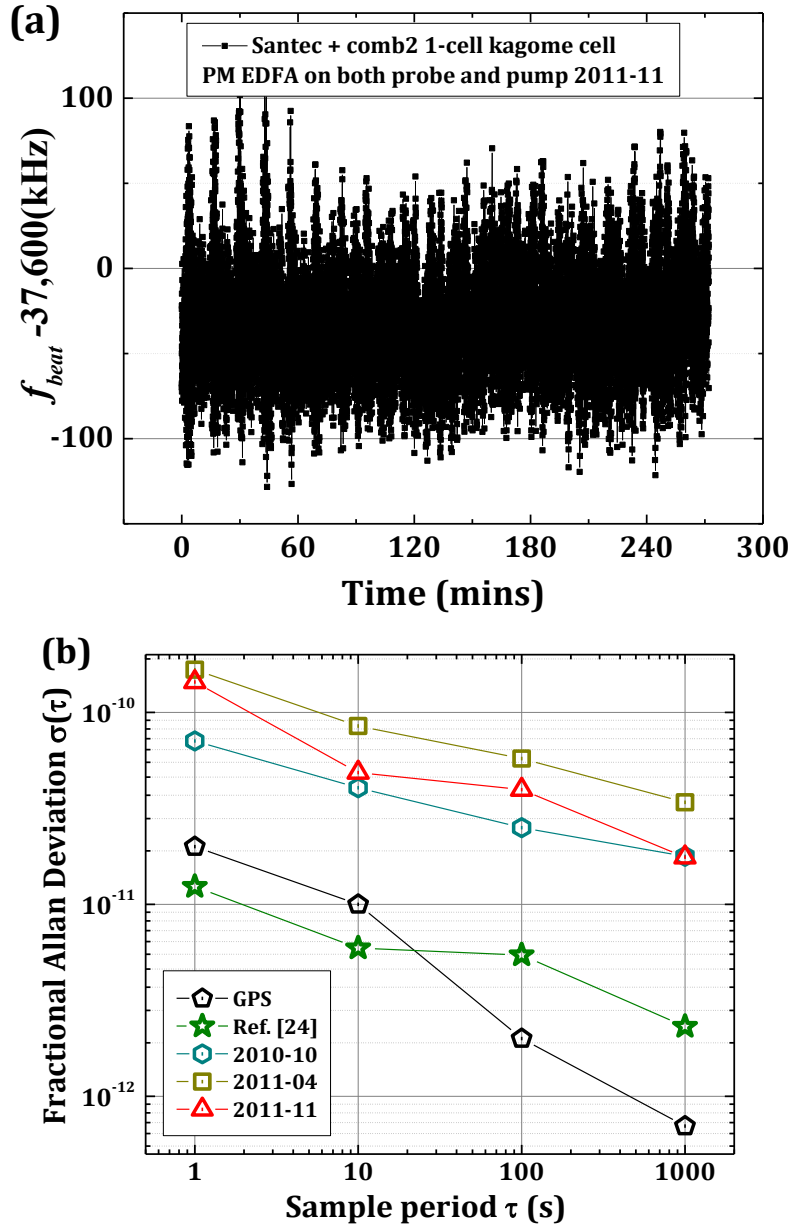
Figure 6-10: Adapted from Ref. [36]. (a) Beatnote between the fiber-based acetylene stabilized laser and the CNFL comb of the P(23) v_1+v_3 transition in $^{12}C_2H_2$ using the PM EDFA to amplify the probe. (b) Fractional Allan Deviation of the beatnote between the fiber-based acetylene stabilized laser and the CNFL comb: cyan hexagons, yellow squares, red triangles: P(23) line in sealed PMC at different dates; green star: P(13) line of acetylene filled large-core kagome HC- PCF in vacuum chamber; black pentagons: GPS-disciplined Rb oscillator.

Even so, our PMC-stabilized acetylene frequency reference shows a reproducibility of ±

170 kHz on the P(23) line of $^{12}C_2H_2$ over one year (Figure 6-11). The P(23) line is measured to be 194,742,536,524 ± 86kHz. Systematic shifts and uncertainties in this absolute frequency measurement arise due to pump power, residual gas pressure and temperature drifts. After the correction due to the pressure shift of - 0.393 MHz/torr [44], our measured P(23) frequency is 194,742,536,671 ± 86 kHz (1σ) (Figure 6-11b), which agrees with previous measurements in a power built-up cavity of 194,742,536,722.9 ± 1.8 kHz [21] within uncertainty.
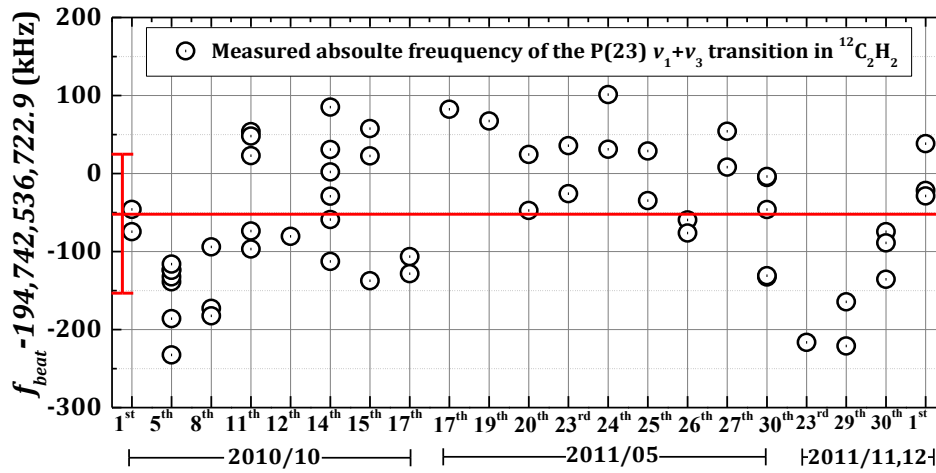
Figure 6-11: Adapted from Ref. [36]. Experimentally measured repeatability of the absolute frequency in the kagome PMC of the P(23) ν₁+ν₃ transition in $^{12}C_2H_2$ at a different date and time; red line: average value of measured absolute frequencies.

6.2.3. Half kagome microcell with an angle splice

A half kagome microcell with one end tapered and angle spliced to SMF is also measured. The setup (Figure 6-12) is similar to that reported in Ref. [24]. The acetylene is loaded through the open end of the kagome half-cell using a vacuum chamber. Figure 6-13 shows the observed absorption signal and the sub-Doppler error signal when 78 mtorr acetylene is loaded to the 14 m kagome half-cell. This low-loss (30 dB/km) single-mode-like kagome HC-PCF is capable of a clear detection of SAS without forming an interface pattern and mode beating. The Fresnel back

103

reflection is significantly reduced by using the angle splice technique we reported in section 5.3.2.

We observed an error signal with 15 MHz FWHM, which is a little boarder compared with the

error signal obtained in the free space setup (Figure 2-2). The boarder lindwidth maybe due to the

contamination introduced during the gas loading and equilibrium process (~ 6 hrs).
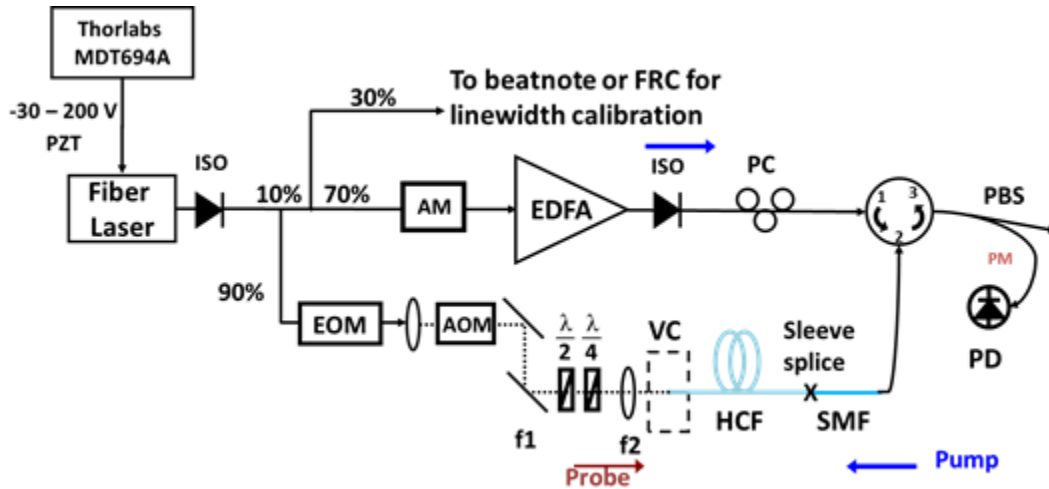
Figure 6-12: Experimental setup for saturated absorption spectroscopy using a reflected pump beam from an angle spliced kagome PCF /SMF half-cell. VC: vacuum chamber used to evacuate and fill the kagome HC-PCF with acetylene gas. EOM: electro-optic modulator; AOM: acousto-optic modulator; AM: amplitude modulator; PC: polarization controller; PD: photodetector; ISO: isolator.
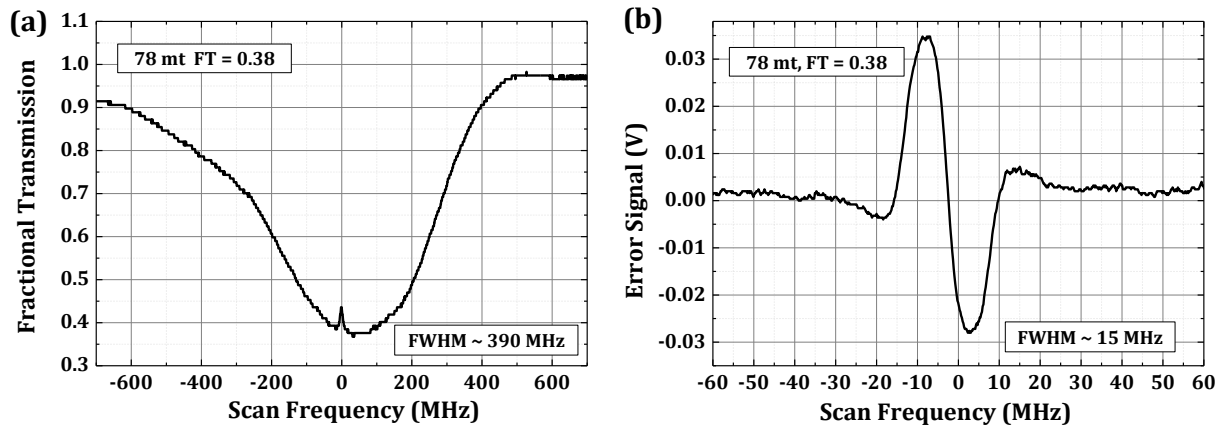
Figure 6-13: Adapted from Ref. [72]. (a) Fractional transmission of a 14 m long 7-cell kagome angle spliced half-cell with a $^{12}C_2H_2$ pressure of 78 mtorr, and a pump power of 18 mW exiting the fiber; (b)error signal of sub-Doppler versus scanned frequency away from the P(13) transition. The laser frequency was scanned at 1.2 GHz/sec.

Similar to the calibration of the full PMC, we stabilize a fiber laser to this half-cell reference and beat against another fiber laser which is stabilized to the free space reference. A stable beatnote was recorded for 25 mins (Figure 6-14). Then the fractional instability of the beatnote is calculated and compared with the fractional instability of the beatnote between two fiber lasers when both are stabilized to free-space references on the P(13) transition of $^{12}C_2H_2$. (Figure 6-15). The fractional instability is a factor of 2 worse than, but shows a similar trend to the instability of the beatnote between two vacuum chamber references [36], which is mainly due to the introduction of contamination during gas loading and equilibrium process. This angle splice technique is useful for PMC-based devices and will improve portable frequency references performance.
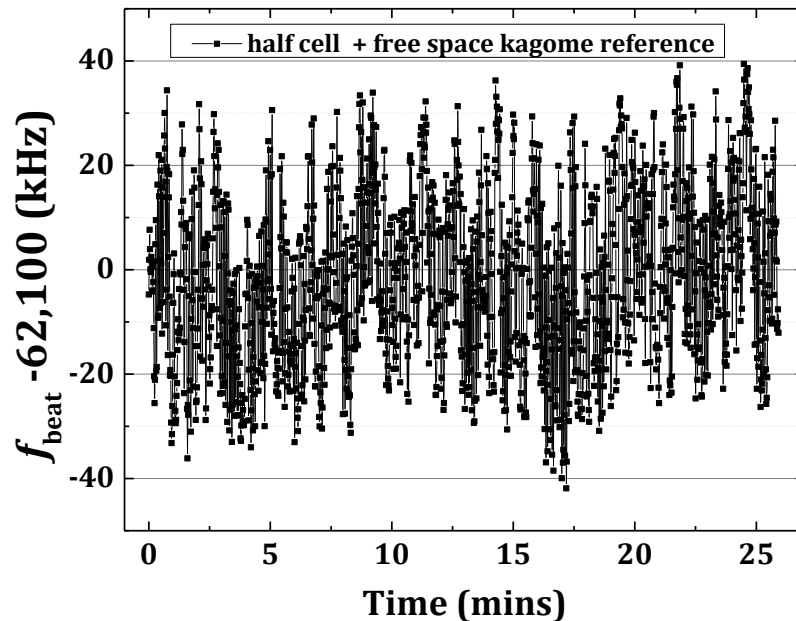
Figure 6-14: Beatnote between the half-cell kagome based acetylene-stabilized laser and the free space kagome based acetylene-stabilized laser of the P(13) $\nu_1+\nu_3$ transition in $^{12}C_2H_2$.
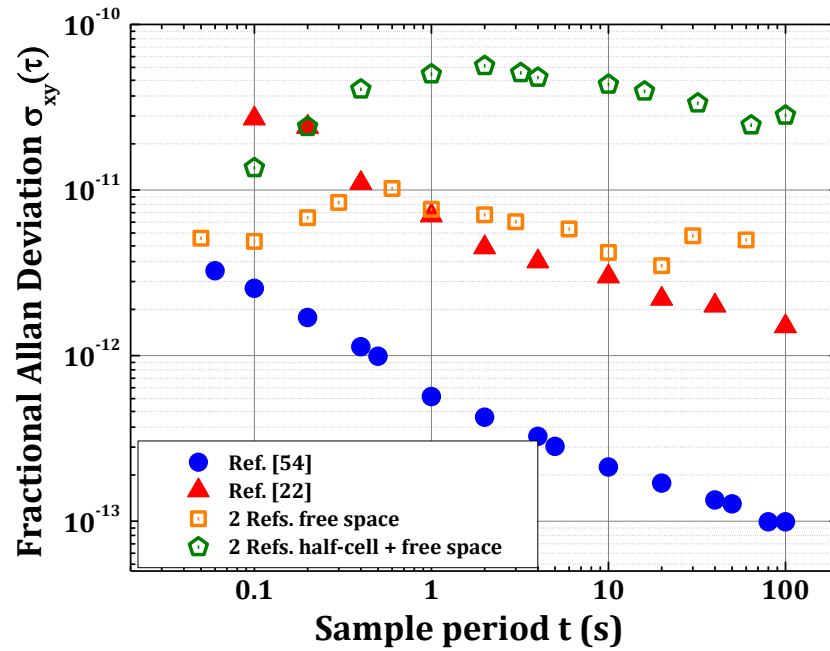
Figure 6-15: Fractional instability of half-cell acetylene-stabilized fiber laser and free space acetylene-stabilized laser compared to two free space acetylene-stabilized lasers and data from Ref. [54] and Ref. [22].

Chapter 7. Stabilized Frequency Comb to Frequency Reference

The frequency comb serves as a direct link from a radio frequency reference to optical frequencies, which is useful for applications such as optical metrology, stable rf frequency generation, and high precision spectroscopy. Optical standards such as atomic clocks are used to stabilize frequency comb parameters [75, 76] including the repetition frequency and carrier-envelop offset (CEO) frequency. Thereby, the accuracy of an optical standard can be transferred to the frequency comb. In this chapter, we use the gas-filled hollow-core photonic crystal fiber (HC-PCF) optical reference [24] as an optical reference for a portable fiber laser frequency comb.

7.1. Comb mode controlling

In this experiment, the comb mode is controlled by the beat frequency between a reference stabilized CW laser and the comb. In many similar systems, an EOM is integrated into the laser cavity for a large locking bandwidth (up to 1 MHz) to achieve a low residual phase noise [76, 77]. However, our NPR comb, which does not have an intracavity EOM, can be stably locked to the acetylene reference using a frequency to voltage (f to v) converter circuit with large tracking frequency range (~ 10 MHz) (Figure 7-1).
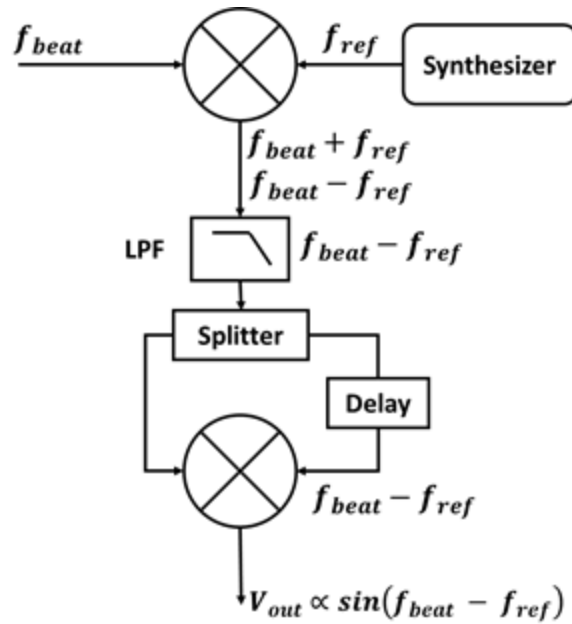
Figure 7-1: Adapted from Ref. [78]. Block diagram of the frequency to voltage (f to v) converter circuit. The DC voltage signal is proportional to the frequency difference between the beat frequency and the reference frequency set by the synthesizer.

The f to v converter converts the beat frequency to a DC voltage error signal used to servo control the PZT in the mode-locked fiber laser cavity. In this way, the beat frequency can be stabilized to the reference frequency set by the synthesizer. Then the comb is stabilized to our acetylene frequency reference in the optical part of the comb spectrum (Figure 7-2).

$$f_{beat1533} = nf_{rep} + f_0 - f_{cw}$$
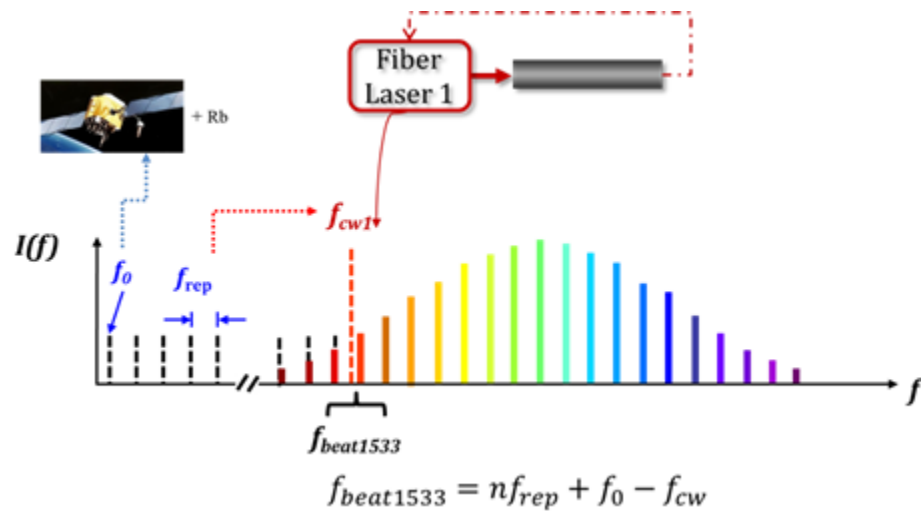
Figure 7-2: Adapted from Ref. [79]. Schematic of fiber-based optical metrology system. The CEO frequency of a comb produced by a mode-locked erbium-doped fiber laser (NPR comb) is stabilized to an rf signal of the Rb-GPS, and its repetition frequency is locked to the acetylene frequency reference at 1532.8 nm.

In the experiment, saturated absorption spectroscopy is used to produce a narrow linewidth (< 10 MHz) sub-Doppler feature, which in turn provides a high signal-to-noise ratio (> 100) error signal for frequency stabilization. A narrow linewidth CW fiber laser is stabilized to an acetylene-filled kagome fiber frequency reference at 1532.8 nm (P(13) overtone transition line) [36], and serves as an optical frequency reference to control the repetition frequency of the fiber laser frequency comb. The frequency comb in this experiment is a mode-locked 89 MHz erbium-doped fiber ring oscillator using the nonlinear polarization rotation (NPR) technique [80]. The total 3.8 mW output power with a 30 nm linewidth from the comb cavity is split into three portions. One portion (90%) goes through an f-to-2f interferometer for CEO frequency detection and stabilization. The CEO frequency is stabilized to a GPS-disciplined Rb oscillator within a few Hz and can be replaced by a quartz oscillator for a more portable system. A small tap from the comb output power is used for repetition frequency detection. The last portion (~ 10%) passes through a fiber Bragg grating and beats against a CW fiber laser which is stabilized to our acetylene frequency reference at the wavelength of 1532.8 nm [36], the P(13) overtone transition of acetylene. The beat frequency is stabilized and fed back to control the repetition frequency of the frequency comb. The stabilized beat frequency and the comb repetition frequency are shown in Figure 7-3.
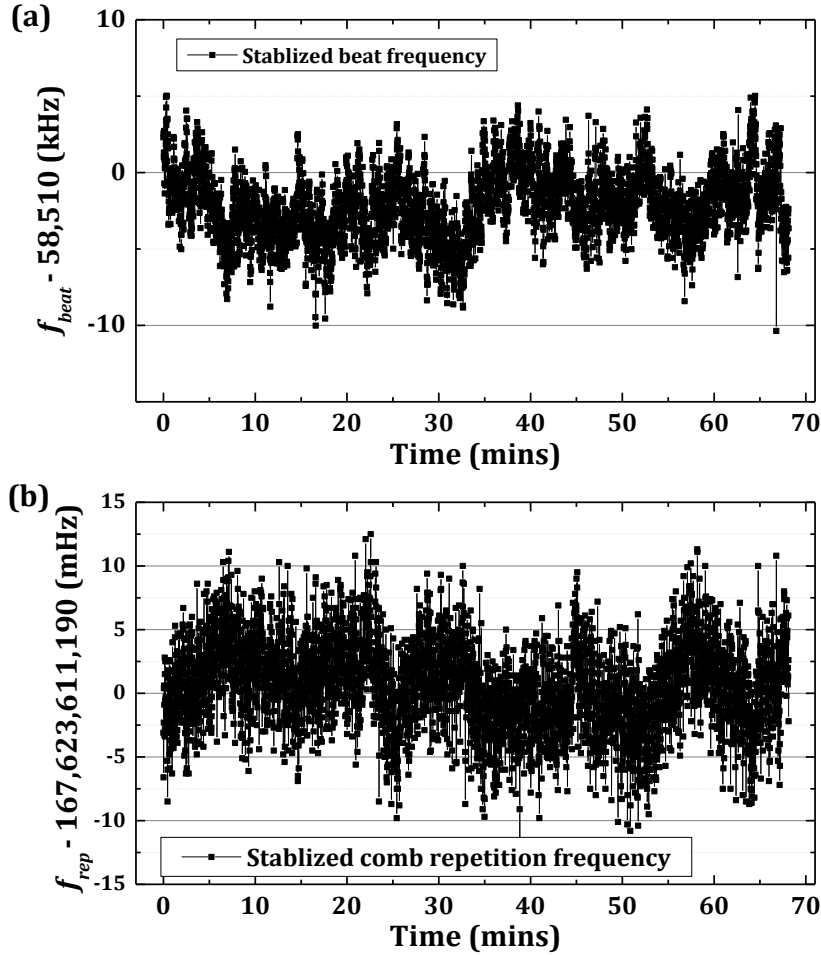
Figure 7-3: (a) Stabilized beat frequency between acetylene frequency on P(13) line and frequency comb and (b) comb repetition frequency using the frequency to voltage (f to V) converter circuit.

7.2. Comb stabilization

We quantified how well the comb is stabilized to the acetylene frequency reference by measuring the comb tooth stability a few nm away. This measurement tells us how the stability of the stabilized comb tooth is transferred to other comb teeth. A noisier tunable diode laser is stabilized to the P(23) overtone transition line at 1539.4 nm using the similar experimental setup in order to test the comb tooth stability 7 nm away from the locking tooth. Once the comb's repetition frequency is stabilized to the acetylene reference (Figure 7-4a: fiber laser 1), we record the locked

beat frequency and calculate its fractional instability.

(a)

$f_{beat1} = |mf_{rep} + f_0 - f_{cw1}|$

$f_{beat2} = |nf_{rep} + f_0 - f_{cw2}|$

(b)
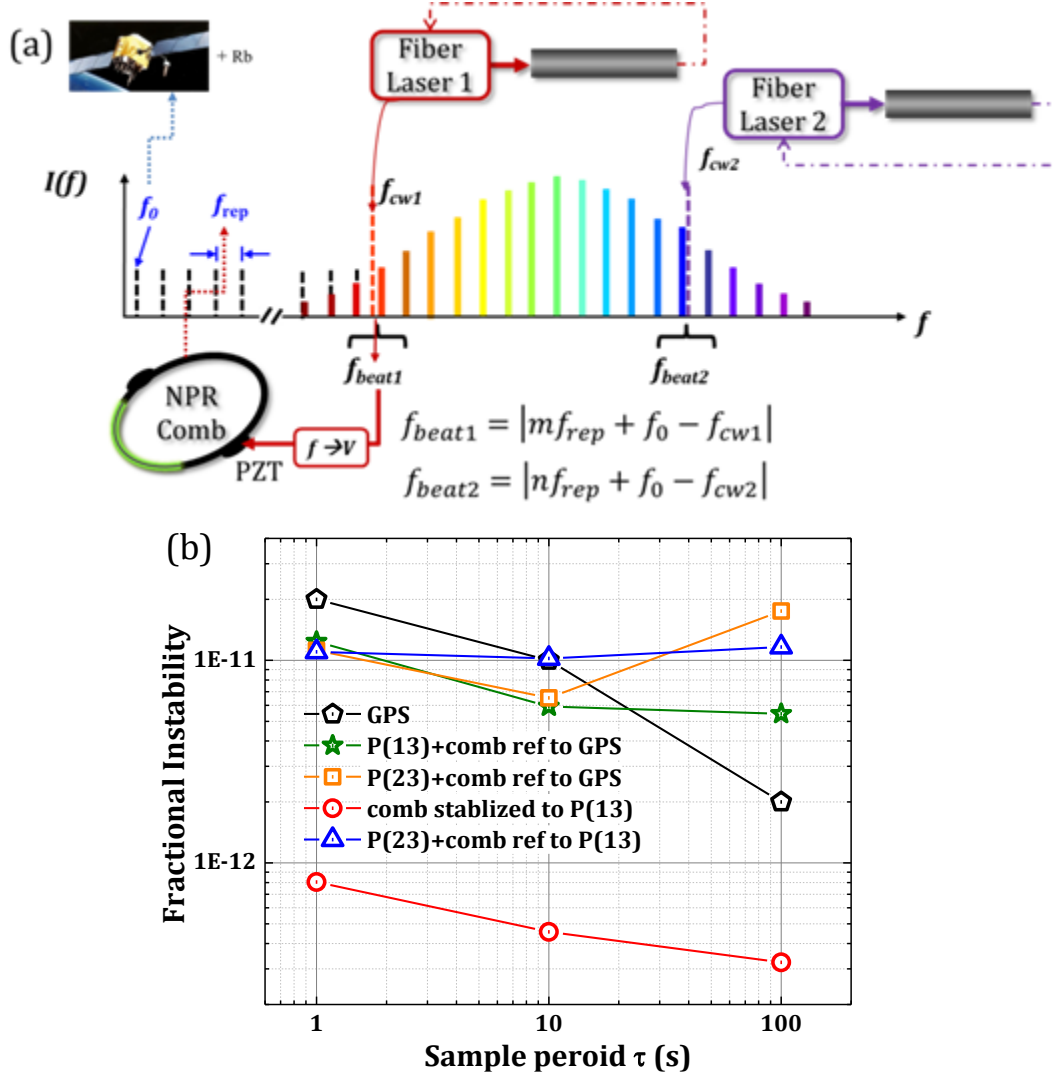
Figure 7-4: Adapted from Ref. [79]. (a) Schematic of fiber-based optical metrology system. The CEO frequency of a comb produced by a mode-locked erbium-doped fiber laser (NPR comb) is stabilized to an rf signal of the Rb-GPS, and its repetition frequency is locked to the acetylene frequency reference at 1532.8 nm. A second acetylene frequency reference at 1539.4 nm measures the stability of the comb tooth 7 nm away from the locking tooth. (b) Fractional instability of the P(13)-referenced comb beat against the P(23) reference (blue triangle) and against the P(13) reference (red circle) [in-loop signal]; the fractional instability of the beat frequency between a GPS-referenced comb and acetylene references at P(13) (green star) and P(23) (orange square).

The measurement shows that an 8×10^{-13} (Figure 7-4b red circle) stability at 1 s is obtained,

which is one order of magnitude improvement compared with the stability of the rf reference (a

GPS-disciplined Rb oscillator) (Figure 7-4b black pentagon). Then we beat the optically referenced frequency comb with another stabilized acetylene reference (Figure 7-4a: diode laser 2) at 1539.4 nm, 7nm away from the locking frequency of 1532.8 nm. The fractional instability of the beat frequency is shown in Figure 7-4b (blue triangle). For comparison, we also plotted the instabilities between an rf-referenced comb and acetylene frequency references at 1539.4 nm and 1532.8 nm (Figure 7-4b orange square and green star). In the measurement, the stability of the optical reference should be transferred across the comb. However, no improvement of the stability is observed over the rf-referenced comb, perhaps due to the noisy diode laser source used to stabilized the acetylene transition at the P(23) line. This problem can be fixed by replacing the diode laser with a narrow linewidth fiber laser, and the 5×10^{-12} stability at 1 s is expected based on the short-term stability measurement of our acetylene reference [36].

The fiber comb is stabilized to an optical fiber reference with good short-term stability and has shown that nearby teeth are no less stable than those generated by a rf-referenced comb. Improved characterization should demonstrate superior short-term stability for neighboring teeth toward a GPS-independent all-fiber metrology system. Furthermore, a fiber frequency reference based on ammonia, which will have a broader range (over 30 nm) of absorption lines, will be developed and will provide a better estimation of how the comb's stability is transferred to other wavelength regions.

In addition, by locking an all-fiber comb to the all-fiber reference [36], we could create a potentially portable fiber-based optical metrology system.

Chapter 8.   Conclusion and Future Directions

This thesis work focuses on developing all-fiber optical frequency references, which combine both features of accuracy and portability. The optical frequency reference not only offers high precision frequency, but also is useful for measuring frequencies up to hundreds of THz directly. For the development of the all-fiber optical frequency reference, the creation of photonic microcell is critical. This portable optical frequency reference may take the place of an RF reference, and serve as the frequency reference for professional equipment such as fiber laser frequency combs. Furthermore, the combination of optical frequency reference technique and optical frequency comb technique allows the creation of an all-fiber metrology system. The all-fiber metrology system holds great potential for a multitude of applications from laboratory usage to industrial communications.

Fiber-based optical frequency reference was initially tested and calibrated using vacuum chambers for gas loading procedure. A 10 kHz vacuum-chamber-based acetylene frequency reference inside a hollow-core fiber was demonstrated in our previous group membeKnabe's thesis work . In my project, a re-analysis to the vacuum-chamber-based frequency reference was applied. Through a three-cornered -hat measurement, the stability of the fiber-based acetylene frequency reference at 100 ms was proved to be 2×10^{-12}, and this short-term stability is comparable with other published values. As for the absolute frequency measurements of the acetylene frequency reference, an additional shift that is created by the distorted lineshape was applied to the measurements on the P(13) transition line. The corrected absolute frequency measurement is more in line with other published values. In addition, problems such as alignment sensitivity and polarization sensitivity in the fiber-based acetylene frequency references were throughfully

investigated.

Large-core kagome HC-PCFs were demonstrated to be useful for the creation of portable optical frequency reference. However, a direct splice would be difficult due to the different outer diameters of kagome and SMF, so we explored several commercially available HC-PCFs which have similar core sizes to the SMF. The work demonstrated that some HC-PCFs yield reduced accuracy and stability due to increased linewidths as anticipated and also exhibit excess noise due to surface modes. The poor performance of 7-cell photonic bandgap fiber (PBGF) was investigated and led to a deeper understanding of the negative role of surface modes in the reference performance.

To find better candidates for the portable acetylene frequency reference, we collaborated with OFS Fitel, LLC and employed a newly-developed, single mode hollow-core fiber for saturated absorption spectroscopy in a molecular gas. The saturated absorption spectroscopy (SAS) signal was observed to be devoid of unwanted surface mode effects, and reduced dependence on optical alignment of the reference is inferred from preliminary locking data.

Toward portable photonic microcell fabrication, robust splicing of the commercially available PBGFs, the novel single mode hollow-core fiber to SMF-28 with both conventional and angle interfaces have been demonstrated locally. The transmission loss < 3 dB/splice was achieved with a return loss < -50 dB for both PBGFs and single mode hollow-core fiber. Moreover, during my ten month visiting at XLIM Institute, France, the angle splice between large-core (> 100 μm) hollow core fiber, and standard single mode fiber was first realized. The angle splice reduced the back-reflection from -16 dB to -60 dB at the splice interface.

Sealed photonic microcells based on PBGF and kagome fiber were characterized over one year and showed agreement with previously published values within 100 kHz (5×10^{-11}), which

can be improved by better splice techniques. These results have led us to focus our efforts to improve the photonic microcell frequency references on sealing large core kagome fiber with angle splices, which will eliminate the adverse effects of surface modes and reflections and bring photonic microcell performance in line with the superior accuracy and stability already observed in vacuum-chamber-based fiber references.

In the end, a potentially portable optical metrology system is demonstrated by using an acetylene-filled optical fiber frequency reference as an optical reference to a fiber laser based frequency comb without an intracavity EOM. An in-loop stability of 8×10^{-13} at 1 s was obtained for the beat frequency between an acetylene reference and fiber frequency comb. It is improved by one order of magnitude compared with the stability of the rf reference (a GPS-disciplined Rb oscillator).

In the future, as a promising candidate for portable frequency references and other accurate photonic microcell -based devices, gas-filled photonic microcells based on angle-spliced single mode hollow-core fibers and SMF-28 will be investigated for frequency stabilization. We expect an improvement in the stability and accuracy of previously reported acetylene-filled photonic microcell references. Furthermore, the acetylene-filled single mode hollow-core fiber photonic microcell optical reference will serve as an optical reference for a portable fiber laser frequency comb. Optical frequency references at a longer wavelength ~ 1.6 nm will also be developed and employed to calibrate the optically referenced frequency comb.

References

1. Vig, J.R., *Quartz Crystal Resonators and Oscillators*. US Army Communications-Electronics Command, January, 2001.

2. Coombs Jr, C.F., *Basic Electronic Instrument Handbook*. American Journal of Physical Medicine & Rehabilitation, 1974. **53**(2): p. 92.

3. Bond, W.L. and J.A. Kusters. *Making Doubly Rotated Quartz Plates*. in *31st Annual Symposium on Frequency Control. 1977*. 1977. IEEE.

4. Masumoto, Y., *Global Positioning System*. 1993, Google Patents.

5. Hollberg, L., et al., *Optical Frequency/Wavelength References*. Journal of Physics B: Atomic, Molecular and Optical Physics, 2005. **38**(9): p. S469.

6. Campbell, G.K. and W.D. Phillips, *Ultracold Atoms and Precise Time Standards*. Vol. 369. 2011. 4078-4089.

7. Ferre-Pikal, E.S. and F.L. Walls, *Frequency Standards, Characterization*, in *Wiley Encyclopedia of Electrical and Electronics Engineering*. 2001, John Wiley & Sons, Inc.

8. Essen, L. and J.V.L. Parry, *An Atomic Standard of Frequency and Time Interval: A Caesium Resonator*. Nature, 1955. **176**(4476): p. 280-282.

9. Oskay, W., et al., *Single-atom Optical Clock with High Accuracy*. Physical Review Letters, 2006. **97**(2): p. 020801.

10. Ludlow, A., et al., *Sr Lattice Clock at 1×10^{-16} Fractional Uncertainty by Remote Optical Evaluation with a Ca Clock*. Science, 2008. **319**(5871): p. 1805-1808.

11. Tuominen, J., et al., *Gas-filled Photonic Bandgap Fibers as Wavelength References*. Optics Communications, 2005. **255**(4–6): p. 272-277.

12. Kaye, W., *Near-infrared Spectroscopy: I. Spectral Identification and Analytical Applications*. Spectrochimica Acta, 1954. **6**(4): p. 257-E2.

13. Gilbert, S.L. and W.C. Swann, *Acetylene $^{12}C_2H_2$ Absorption Reference for 1510 nm to 1540 nm Wavelength Calibration—SRM 2517a*. NIST Special Publication, 2001. **260**: p. 133.

14. Gilbert, S.L. and W.C. Swann, *Carbon Monoxide Absorption References for 1560 nm to 1630 nm Wavelength Calibration–SRM 2514 ($^{12}C^{16}O$) and SRM 2515 ($^{13}C^{16}O$)*. NIST Special Publication, 2002. **260**: p. 146.

15. Gilbert, S.L., W.C. Swann, and C.M. Wang, *Hydrogen Cyanide $H^{13}C^{14}N$ Absorption Reference for 1530 nm to 1560 nm Wavelength Calibration-SRM 2519a*. NIST Special Publication, 2005. **260**: p. 137.

16. Komada, P. and S. Cieszczyk, *Application of Multiple Line Integrated Spectroscopy on CO Concentration Measurement*. Electronics and Electrical Engineering, 2013. **19**(9): p. 46-49.

17. Lundsbergnielsen, L., F. Hegelund, and F. Nicolaisen, *Analysis of the High-Resolution Spectrum of Ammonia ($^{14}NH_3$) in the Near-Infrared Region, 6400-6900 cm^{-1}*. Journal of molecular spectroscopy, 1993. **162**(1): p. 230-245.

18. Burgess, C. and J. Hammond, *Wavelength Standards for the Near-infrared Spectral Region.* Spectroscopy - Springfield, 2007. **22**(4): p. 40.

19. Carr, A., *Hyperfine Studies of Lithium Vapor using Saturated Absorption Spectroscopy.* University of Arizona, Department of Physics, 2007.

20. Moon, H.S., W.K. Lee, and H.S. Suh, *Absolute-Frequency Measurement of an Acetylene-Stabilized Laser Locked to the P(16) Transition of $^{13}C_2H_2$ Using an Optical Frequency Comb.* Instrumentation and Measurement, IEEE Transactions on, 2007. **56**(2): p. 509-512.

21. Madej, A.A., et al., *Accurate Absolute Reference Frequencies from 1511 to 1545 nm of the v_1+v_3 band of $^{12}C_2H_2$ Determined with Laser Frequency Comb Interval Measurements.* J. Opt. Soc. Am. B, 2006. **23**(10): p. 2200-2208.

22. Balling, P., et al., *Absolute Frequency Measurement of Wavelength Standard at 1542nm: Acetylene Stabilized DFB Laser.* Opt. Express, 2005. **13**(23): p. 9196-9201.

23. Czajkowski, A., A.A. Madej, and P. Dubé, *Development and Study of a 1.5 μm Optical Frequency Standard Referenced to the P(16) Saturated Absorption Line in the (v_1+v_3) Overtone Band of $^{13}C_2H_2$.* Optics Communications, 2004. **234**(1-6): p. 259-268.

24. Knabe, K., et al., *10 kHz Accuracy of an Optical Frequency Reference based on $^{12}C_2H_2$-filled Large-core Kagome Photonic Crystal Fibers.* Optics Express, 2009. **17**(18): p. 16017-16026.

25. Benabid, F., et al., *Compact, Stable and Efficient All-fibre Gas Cells using Hollow-core Photonic Crystal Fibres.* Nature, 2005. **434**(7032): p. 488-491.

26. Couny, F., et al., *Electromagnetically Induced Transparency and Saturable Absorption in All-fiber Devices based on $^{12}C_2H_2$-filled Hollow-core Photonic Crystal Fiber.* Optics Communications, 2006. **263**(1): p. 28-31.

27. Light, P.S., F. Couny, and F. Benabid, *Low Optical Insertion-loss and Vacuum-pressure All-fiber Acetylene Cell based on Hollow-core Photonic Crystal Fiber.* Optics Letters, 2006. **31**(17): p. 2538-2540.

28. Wheeler, N.V., et al., *Large-core Acetylene-filled Photonic Microcells made by Tapering a Hollow-core Photonic Crystal Fiber.* Optics Letters, 2010. **35**(11): p. 1875-1877.

29. Swann, W. and S. Gilbert, *Pressure-induced Shift and Broadening of 1510–1540-nm Acetylene Wavelength Calibration Lines.* JOSA B, 2000. **17**(7): p. 1263-1270.

30. *Acetylene Stabilized Diode Lasers*. Available from: http://www.neoark.co.jp/english/product_laser_light_source01.html.

31. Hall, J.L., *Nobel Lecture: Defining and Measuring Optical Frequencies.* Reviews of Modern Physics, 2006. **78**(4): p. 1279.

32. Han Seb, M., L. Won-Kyu, and S. Ho-Suhng, *Absolute-Frequency Measurement of an Acetylene-Stabilized Laser Locked to the P(16) Transition of $^{13}C_2H_2$ Using an Optical-Frequency Comb.* Instrumentation and Measurement, IEEE Transactions on, 2007. **56**(2): p. 509-512.

33. de Labachelerie, M., K. Nakagawa, and M. Ohtsu, *Ultranarrow $^{13}C_2H_2$ Saturated-absorption Lines at 1.5 μm.* Opt. Lett., 1994. **19**(11): p. 840-842.

34.   Hald, J., J.C. Petersen, and J. Henningsen, *Saturated Optical Absorption by Slow Molecules in Hollow-core Photonic Band-gap Fibers*. Physical Review Letters, 2007. **98**(21): p. 213902.

35.   Demtroder, W., *Laser spectroscopy : Basic Concepts and Instrumentation / Wolfgang Demtroder*, in *Springer series in chemical physics ; v. 5*. 1981, Springer-Verlag: Berlin ; New York.

36.   Wang, C., et al., *Acetylene Frequency References in Gas-filled Hollow Optical Fiber and Photonic Microcells*. Applied Optics, 2013. **52**(22): p. 5430-5439.

37.   Bjorklund, G.C., et al., *Frequency Modulation (FM) Spectroscopy*. Applied Physics B: Lasers and Optics, 1983. **32**(3): p. 145-152.

38.   Han Seb, M., L. Won-Kyu, and S. Ho-Suhng, *Absolute-Frequency Measurement of an Acetylene-Stabilized Laser Locked to the P(16) Transition of $^{13}C_2H_2$ Using an Optical Frequency Comb*. Instrumentation and Measurement, IEEE Transactions on, 2007. **56**(2): p. 509-512.

39.   Lim, J., et al., *A Phase-stabilized Carbon Nanotube Fiber Laser Frequency Comb*. Opt. Express, 2009. **17**(16): p. 14115-14120.

40.   Riley, W.J., *Handbook of Frequency Stability Analysis*. NIST Special Publication 1065, 2008.

41.   Rutman, J., and F. L. Walls, *Characterization of Frequency Stability in Precision Frequency Sources*. Proceedings of the IEEE 79.7 (1991): 952-960, 1991.

42.   Long-Sheng, M., et al., *Frequency Uncertainty for Optically Referenced Femtosecond Laser Frequency Combs*. Quantum Electronics, IEEE Journal of, 2007. **43**(2): p. 139-146.

43.   Knabe, K., *Using Saturated Absorption Spectroscopy on Acetylene-filled Hollow-core Fibers for Absolute Frequency Measurements*, in *Physics*. 2010, Kansas State University.

44.   Swann, W.C. and S.L. Gilbert, *Pressure-induced Shift and Broadening of 1510-1540-nm Acetylene Wavelength Calibration Lines*. J. Opt. Soc. Am. B, 2000. **17**(7): p. 1263-1270.

45.   Edwards, C.S., et al., *High-precision Frequency Measurements of the $v_1 + v_3$ Combination Band of $^{12}C_2H_2$ in the 1.5 μm Region*. Journal of Molecular Spectroscopy, 2005. **234**(1): p. 143-148.

46.   Gray, J.E. and D.W. Allan. *A Method for Estimating the Frequency Stability of an Individual Oscillator*. in *28th Annual Symposium on Frequency Control. 1974*. 1974.

47.   West, J., et al., *Surface Modes in Air-core Photonic Band-gap Fibers*. Opt. Express, 2004. **12**(8): p. 1485-1496.

48.   Fini, J.M., et al., *Low-loss Hollow-core Fibers with Improved Single-modedness*. Optics Express, 2013. **21**(5): p. 6233-6242.

49.   Wang, C., et al. *Portable Acetylene Frequency References inside Sealed Hollow-core Kagome Photonic Crystal Fiber*. in *CLEO:2011 - Laser Applications to Photonic Applications*. 2011. Baltimore, Maryland: Optical Society of America.

50.   Chardonnet, C., et al., *Ultrahigh-resolution saturation spectroscopy using slow molecules in an external cell*. Applied Physics B, 1994. **59**(3): p. 333-343.

51. Henningsen, J., J. Hald, and J.C. Peterson, *Saturated Absorption in Acetylene and Hydrogen Cyanide in Hollow-core Photonic Bandgap Fibers.* Opt. Express, 2005. **13**(26): p. 10475-10482.

52. *NKT Photonics. Available from: http://www.nktphotonics.com/side5334.html.*

53. Premoli, A. and P. Tavella, *A Revisited Three-cornered Hat Method for Estimating Frequency Standard Instability.* Instrumentation and Measurement, IEEE Transactions on, 1993. **42**(1): p. 7-13.

54. Hald, J., et al., *Fiber Laser Optical Frequency Standard at 1.54 µm.* Opt. Express, 2011. **19**(3): p. 2052-2063.

55. Wang, C., et al. *Accurate Fiber-based Acetylene Frequency References.* in *Conference on Lasers and Electro-Optics* 2012. San Jose, CA: Optical Society of America.

56. Cregan, R.F., et al., *Single-mode Photonic Band Gap Guidance of Light in Air.* Science, 1999. **285**(5433): p. 1537-1539.

57. Ralf B. Wehrspohn, H.-S.K., Kurt Busch, *Nanophotonic Materials: Photonic Crystals, Plasmonics, and Metamaterials*. 2008.

58. Pinto, A.M.R. and M. Lopez-Amo, *Photonic Crystal Fibers for Sensing Applications.* Journal of Sensors, 2012. **2012**: p. 21.

59. Benabid, F., et al., *Stimulated Raman Scattering in Hydrogen-filled Hollow-core Photonic Crystal Fibres.* Science, 2002. **298**: p. 399-402.

60. Benabid, F., et al., *Light and Gas Confinement in Hollow-core Photonic Crystal Fibre based Photonic Microcells*. 2009. Vol. 4. 2009.

61. Benabid, F. and P.J. Roberts, *Linear and Nonlinear Optical Properties of Hollow-core Photonic Crystal Fiber.* Journal of Modern Optics, 2011. **58**(2): p. 87-124.

62. Choi, H. and P.T.C. So, *Improving Femtosecond Laser Pulse Delivery Through a Hollow-core Photonic Crystal Fiber for Temporally Focused Two-photon Endomicroscopy.* Sci. Rep., 2014. **4**.

63. Fu L, G.M., *Fibre-optic Nonlinear Optical Mircoscopy and endoscopy.* Journal of microscopy, 2007, 226(3): 195-206, 2007.

64. *NKT Photonics*. Available from: http://www.nktphotonics.com/side5334.html.

65. Thapa, R., et al., *Saturated Absorption Spectroscopy of Acetylene Gas inside Large-core Photonic Bandgap Fiber.* Opt. Lett., 2006. **31**(16): p. 2489-2491.

66. Smith, C.M., et al., *Low-loss Hollow-core Silica/air Photonic Bandgap Fibre.* Nature, 2003. **424**(6949): p. 657-659.

67. Couny, F., et al., *Generation and Photonic Guidance of Multi-octave Optical Frequency Combs.* Science, 2007. **318**(5853): p. 1118-1121.

68. Wang, C., et al. *Single-mode Hollow-core Fiber for Portable Acetylene Sub-Doppler Frequency Reference*. in *CLEO: 2014*. 2014. San Jose, California: Optical Society of America.

69. Keiser, G., *Optical Fiber Communications*. 2010.

70. Benabid, F. *Photonic MircoCells based on Hollow-core PCF*. in *Optical Fiber Communication Conference*. 2011. Optical Society of America.

71. Couny, F., F. Benabid, and P.S. Light, *Reduction of Fresnel Back-reflection at Splice Interface between Hollow Core PCF and Single-mode Fiber*. Photonics Technology Letters, IEEE, 2007. **19**(13): p. 1020-1022.

72. Wang, C., et al. *Angle Splice of Large-core Kagome Hollow-core Photonic Crystal Fiber for Gas-filled Microcells*. in *CLEO: 2013*. 2013. San Jose, California: Optical Society of America.

73. Dicaire, I., J.-C. Beugnot, and L. Thévenaz, *Analytical Modeling of the Gas-filling Dynamics in Photonic Crystal Fibers*. Applied Optics, 2010. **49**(24): p. 4604-4609.

74. Hall, J.L., et al., *Optical Heterodyne Saturation Spectroscopy*. Applied Physics Letters, 1981. **39**(9): p. 680-682.

75. Fortier, T.M., et al., *Generation of Ultrastable Microwaves via Optical Frequency Division*. Nat Photon, 2011. **5**(7): p. 425-429.

76. Swann, W.C., et al., *Microwave generation with low residual phase noise from a femtosecond fiber laser with an intracavity electro-optic modulator*. Optics Express, 2011. **19**(24): p. 24387-24395.

77. Nakajima, Y., et al., *A Multi-branch, Fiber-based Frequency Comb with Millihertz-level Relative Linewidths using an Intra-cavity Electro-optic Modulator*. Optics Express, 2010. **18**(2): p. 1667-1676.

78. Trachy, M.L., *Photoassociative Ionization in Cold Rubidium*, in *Physics*. 2008, Kansas State University.

79. Wang, C., et al. *Toward an All-fiber based Optically Referenced Frequency Comb*. in *CLEO: 2014*. 2014. San Jose, California: Optical Society of America.

80. Wu, S., et al. *Sub-Doppler Intrafiber Spectroscopy of $^{12}C_2H_2$ using Amplified Frequency Comb Lines Directly*. in *CLEO: 2013*. 2013. San Jose, California: Optical Society of America.

Appendix A Frequency Modulation Modeling using Wolfram Mathematica

```
(*Parameters*)
M=0.1 (*modulation index*);
ϵ=0(*Degree of asymmetry in sidebands*);
fl=10(*MHz, Lorentzian FHWM*);
σ=470*2 π(*MHz in rad, Gaussian FHWM*);
fm=11(*MHz, frequency of modulation*);
tm=1/fm (*μs, limit of integration for time averaging*);
ΔΩ=2 π fl;
ωm=2 π fm;
faom=-60;
 R[ω_]:=ω/(ΔΩ/2)(*normalized frequency*);


(*Attenuation*)
Doppler[ω_]:=1/2*0.69*Exp[- ((ω+faom* π)²/(0.36 σ2))](*attenuation
function when pump-off*)
Doppler1[ω_]:=Doppler[ω+ωm];
Doppler2[ω_]:=Doppler[ω-ωm];
Plot[Doppler[2 π x],{x,-
750,750},PlotRange→All,Frame→True,FrameLabel→{"f_probe-1/2f_AOM-f_P
(13)(MHz)","δ-
attenuation"},PlotStyle→{Orange,Thickness[0.008]},LabelStyle→{22,Bold}
]

SDoppler[ω_]:=1/2*0.69*Exp[- ((ω+faom* π)²/(0.36 σ2))](1-
0.14/((R[ω])²+1))(*attenuation function when pump-on*)
SDoppler1[ω_]:=SDoppler[ω+ωm];
SDoppler2[ω_]:=SDoppler[ω-ωm];
Plot[SDoppler[2 π x],{x,-
750,750},PlotRange→All,Frame→True,FrameLabel→{"f_probe-1/2f_AOM-f_P
(13)(MHz)","δ-
attenuation"},PlotStyle→{Blue,Thickness[0.008]},LabelStyle→{22,Bold}]


(*fractional transmission*)
Plot[Exp[-2 Doppler[2 π x]],{x,-
750,750},PlotRange→{All,{0.5,1}},Frame→True,FrameLabel→{"f_probe-1/2f_AOM-
f_P (13)(MHz)","Fractional
Transimission"},PlotStyle→{Orange,Thickness[0.008]},LabelStyle→{22,Bol
d}](*FT when pump-on*)

 Plot[Exp[-2 SDoppler[2 π x]],{x,-
750,750},PlotRange→{All,{0.5,1}},Frame→True,FrameLabel→{"f_probe-1/2f_AOM-
f_P (13)(MHz)","Fractional
Transimission"},PlotStyle→{Blue,Thickness[0.008]},LabelStyle→{22,Bold}
](*FT when pump-on*)
```

```
(*Phase shift, error signal*)
ω0=750*2 π;num=2^11;δω=(2 ω0)/(num-1);Δ=0.1;
ω=Table[(j-1)*δω -ω0,{j,1,num}];
phase=Table[0,{j,1,num}];(*phase shift j=0, pump-off*)
phase1=Table[0,{j,1,num}];(*phase shift j=-1, pump-off*)
phase2=Table[0,{j,1,num}];(*phase shift j=1, pump-off*)
E3=Table[0,{j,1,num}];(*transmitted electric field, pump-off*)
I3=Table[0,{j,1,num}];(*intensity to detector, pump-off*)
S1=Table[0,{j,1,num}];(*FM absorption error signal, pump-off*)
S2=Table[0,{j,1,num}];(*FM dispersion error signal, pump-off*)
Sphase=Table[0,{j,1,num}];(*phase shift j=0, pump-on*)
Sphase1=Table[0,{j,1,num}];(*phase shift j=-1, pump-on*)
Sphase2=Table[0,{j,1,num}];(*phase shift j=1, pump-on*)
SE3=Table[0,{j,1,num}];(*transmitted electric field, pump-on*)
SI3=Table[0,{j,1,num}];(*intensity to detector, pump-on*)
SS1=Table[0,{j,1,num}];(*FM absorption error signal, pump-on*)
SS2=Table[0,{j,1,num}];(*FM dispersion error signal, pump-on*)

For[j=1,j≤num,j++,
 {phase[[j]]=1/π NIntegrate[Doppler[x]/(x-ω[[j]]),{x,-16000, ω[[j]]-
Δ},MaxRecursion→40]+1/π NIntegrate[Doppler[x]/(x-
ω[[j]]),{x,ω[[j]]+Δ,16000},MaxRecursion→20]+1/π  Doppler'[ω[[j]]] 2
Δ;(*phase shift j=0, pump-off*)
  phase1[[j]]=1/π NIntegrate[Doppler1[x]/(x-ω[[j]]),{x,-16000, ω[[j]]-
Δ},MaxRecursion→40]+1/π NIntegrate[Doppler1[x]/(x-
ω[[j]]),{x,ω[[j]]+Δ,16000},MaxRecursion→20]+1/π  Doppler1'[ω[[j]]] 2
Δ;(*phase shift j=-1, pump-off*)
  phase2[[j]]=1/π NIntegrate[Doppler2[x]/(x-ω[[j]]),{x,-16000, ω[[j]]-
Δ},MaxRecursion→40]+1/π NIntegrate[Doppler2[x]/(x-
ω[[j]]),{x,ω[[j]]+Δ,16000},MaxRecursion→20]+1/π  Doppler2'[ω[[j]]] 2
Δ;(*phase shift j=1, pump-off*)

E3[[j]]=-Exp[-Doppler1[ω[[j]]]-ⅈ phase1[[j]]+ⅈ (-ωm)t]M (1-ϵ/2)+Exp[-
Doppler[ω[[j]]]-ⅈ phase[[j]]]+Exp[-Doppler2[ω[[j]]]-ⅈ phase2 [[j]]+ⅈ
ωm t] M (1+ϵ/2);(*transmitted electric field, pump-off*)

I3[[j]]=Simplify[E3[[j]]*Conjugate[E3[[j]]]];(*intensity to detector,
pump-off*)
S1[[j]]=tm^{-1} *∫_0^{tm} I3[[j]] * Cos[ωm t]dt;(*FM absorption error signal, pump-
off*)
S2[[j]]=tm^{-1} *∫_0^{tm} I3[[j]] * Sin[ωm t]dt;(*FM dispersion error signal, pump-
off*)
  Sphase[[j]]=1/π NIntegrate[SDoppler[x]/(x-ω[[j]]),{x,-16000, ω[[j]]-
Δ},PrecisionGoal→12,MaxRecursion→40]+1/π NIntegrate[SDoppler[x]/(x-
ω[[j]]),{x,ω[[j]]+Δ,16000},PrecisionGoal→12,MaxRecursion→40]+1/π
SDoppler'[ω[[j]]] 2 Δ;(*phase shift j=0, pump-on*)
  Sphase1[[j]]=1/π NIntegrate[SDoppler1[x]/(x-ω[[j]]),{x,-16000,
ω[[j]]-Δ},PrecisionGoal→12,MaxRecursion→40]+1/π
NIntegrate[SDoppler1[x]/(x-
```

```
ω[[j]]),{x,ω[[j]]+Δ,16000},PrecisionGoal→12,MaxRecursion→40]+1/π
SDoppler1'[ω[[j]]] 2 Δ;(*phase shift j=-1, pump-on*)
   Sphase2[[j]]=1/π NIntegrate[SDoppler2[x]/(x-ω[[j]]),{x,-16000,
ω[[j]]-Δ},PrecisionGoal→12,MaxRecursion→40]+1/π
NIntegrate[SDoppler2[x]/(x-
ω[[j]]),{x,ω[[j]]+Δ,16000},PrecisionGoal→12,MaxRecursion→40]+1/π
SDoppler2'[ω[[j]]] 2 Δ;(*phase shift j=1, pump-on*)

SE3[[j]]=-Exp[-SDoppler1[ω[[j]]]-ⅈ Sphase1[[j]]+ⅈ (-ωm)t]M (1-
ϵ/2)+Exp[-SDoppler[ω[[j]]]-ⅈ Sphase[[j]]]+Exp[-SDoppler2[ω[[j]]]-ⅈ
Sphase2 [[j]]+ⅈ ωm t] M (1+ϵ/2);(*transmitted electric field, pump-
on*)
   SI3[[j]]=Simplify[SE3[[j]]*Conjugate[SE3[[j]]]];(*intensity to
detector, pump-on*)
```

$SS1[[j]]=tm^{-1} * \int_0^{tm} SI3[[j]] * Cos[\omega_m t] dt;$(*FM absorption error signal, pump-
off*)

$SS2[[j]]=tm^{-1} * \int_0^{tm} SI3[[j]] * Sin[\omega_m t] dt;$(*FM dispersion error signal, pump-
on*)
```
   }]


ListLinePlot[Table[{ω[[j]]/(2
π),phase[[j]]},{j,1,num}],Frame→True,PlotRange→All,FrameLabel→{"fprobe-
1/2fAOM-fP (13)(MHz)","Phase Shift
ϕ"},PlotStyle→{Orange,Thickness[0.008]},LabelStyle→{22,Bold}](*Phase
shift,pump-off*)


ListLinePlot[Table[{ω[[j]]/(2
π),Sphase[[j]]},{j,1,num}],Frame→True,PlotRange→All,FrameLabel→{"fprobe-
1/2fAOM-fP (13)(MHz)","Phase Shift
ϕ"},PlotStyle→{Blue,Thickness[0.008]},LabelStyle→{22,Bold}](*Phase
shift,pump-on*)



scale =326; (*error signal scale factor*)

p11=ListLinePlot[Table[{ω[[j]]/(2
π),scale*S1[[j]]},{j,1,num}],Frame→True,PlotRange→All,FrameLabel→{"fpro
be-1/2fAOM-fP (13)(MHz)","FM absorption
error"},PlotStyle→{Orange,Thickness[0.008]},LabelStyle→{22,Bold}](*FM
absorption error,pump-off*)

p12=ListLinePlot[Table[{ω[[j]]/(2
π),scale*S2[[j]]},{j,1,num}],Frame→True,PlotRange→All,FrameLabel→{"fpro
be-1/2fAOM-fP (13)(MHz)","FM dispersion
error"},PlotStyle→{Orange,Thickness[0.008]},LabelStyle→{22,Bold}](*FM
dispersion error,pump-off*)

p21=ListLinePlot[Table[{ω[[j]]/(2
π),scale*SS1[[j]]},{j,1,num}],Frame→True,PlotRange→{{-
750,750},All},FrameLabel→{"fprobe-1/2fAOM-fP (13)(MHz)","FM absorption
```

```
error"},PlotStyle→{Blue,Thickness[0.008]},LabelStyle→{22,Bold}](*FM
absorption error,pump-on*)

p22=ListLinePlot[Table[{ω[[j]]/(2
π),scale*SS2[[j]]},{j,1,num}],Frame→True,PlotRange→{{-
750,750},All},FrameLabel→{"f_probe-1/2f_AOM-f_P (13)(MHz)","FM dispersion
error"},PlotStyle→{Blue,Thickness[0.008]},LabelStyle→{22,Bold}](*FM
dispersion error,pump-on*)

p31=ListLinePlot[Table[{ω[[j]]/(2 π),scale*(SS1[[j]]-
S1[[j]])},{j,1,num}],Frame→True,PlotRange→{{-100,100},{-
1,1}},FrameLabel→{"f_probe-1/2f_AOM-f_P (13)(MHz)","AM absorption
error"},PlotStyle→{Black,Thickness[0.008]},LabelStyle→{22,Bold}](*AM
absorption error*)

p32=ListLinePlot[Table[{ω[[j]]/(2 π),scale*(SS2[[j]]-
S2[[j]])},{j,1,num}],Frame→True,PlotRange→{{-100,100},{-
1,1}},FrameLabel→{"f_probe-1/2f_AOM-f_P (13)(MHz)","AM dispersion
error"},PlotStyle→{Black,Thickness[0.008]},LabelStyle→{22,Bold}](*AM
dispersion error*)

Show[p32,PlotRange→{{0,0.015},{-0.4*10^-2,0.4*10^-2}}](*AM dispersion
error near zero-crossing*)
```

Appendix B Frequency Modulation Modeling using Wolfram Mathematica

```
(*subtract time averaging error signal of pump on and pump off,
include surface modes*)
 M=0.1 (*modulation index*);
ϵ=0(*Degree of asymmetry in sidebands*);
fl=40(*MHz, Lorentzian FHWM*);
σ=470*2π(*MHz in rad, Gaussian FHWM*);
fm=11(*MHz, frequency of modulation*);
tm=1/fm (*μs, limit of integration for time averaging*);
ΔΩ=2 π fl;
ωm=2 π fm;
 R[ω_]:=ω/(ΔΩ/2)(*normalized frequency*);
Doppler[ω_]:=1/2*0.91*Exp[- ((-30*2 π+ω)²/(0.36 σ2))]-1/2 0.25
Sin[ω/500]+0.015(*attenuation function when there is only probe,
w/surface modes*)
Doppler1[ω_]:=Doppler[ω+ωm];
Doppler2[ω_]:=Doppler[ω-ωm];
Plot[Doppler[2 π x],{x,-
750,750},PlotRange→All,Frame→True,FrameLabel→{"f_probe-1/2f_AOM-f_P
(13)(MHz)","δ-
attenuation"},PlotStyle→{Orange,Thickness[0.008]},LabelStyle→{22,Bold}
]
SDoppler[ω_]:=1/2*0.91*Exp[- ((-30*2 π+ω)²/(0.36 σ2))](1-
0.15/((R[ω])²+1))-1/2 0.25 Sin[ω/500]+0.015(*attenuation function when
there is probe and pump, w/surface modes*)
SDoppler1[ω_]:=SDoppler[ω+ωm];
SDoppler2[ω_]:=SDoppler[ω-ωm];
Plot[SDoppler[2 π x],{x,-
750,750},PlotRange→All,Frame→True,FrameLabel→{"f_probe-1/2f_AOM-f_P
(13)(MHz)","δ-
attenuation"},PlotStyle→{Blue,Thickness[0.008]},LabelStyle→{22,Bold}]


 Plot[Exp[-2 Doppler[2 π x]],{x,-
750,750},PlotRange→{0,1.25},Frame→True,FrameLabel→{"f_probe-1/2f_AOM-f_P
(13)(MHz)","Fractional
Transimission"},PlotStyle→{Orange,Thickness[0.008]},LabelStyle→{22,Bol
d}]
Plot[Exp[-2 SDoppler[2 π x]],{x,-
750,750},PlotRange→{0,1.25},Frame→True,FrameLabel→{"f_probe-1/2f_AOM-f_P
(13)(MHz)","Fractional
Transimission"},PlotStyle→{Blue,Thickness[0.008]},LabelStyle→{22,Bold}
]


 ω0=750*2 π;num=2¹¹;δω=(2 ω0)/(num-1);Δ=0.1;
ω=Table[(j-1)*δω -ω0,{j,1,num}];
phase=Table[0,{j,1,num}];(*phase shift caused by attenuation
function*)
```

```
phase1=Table[0,{j,1,num}];
phase2=Table[0,{j,1,num}];
E3=Table[0,{j,1,num}];
I3=Table[0,{j,1,num}];
S2=Table[0,{j,1,num}];
 Sphase=Table[0,{j,1,num}];(*phase shift caused by attenuation
function*)
Sphase1=Table[0,{j,1,num}];
Sphase2=Table[0,{j,1,num}];
SE3=Table[0,{j,1,num}];
SI3=Table[0,{j,1,num}];
SS2=Table[0,{j,1,num}];
SSS2=Table[0,{j,1,num}];
 For[j=1,j≤num,j++,
 {phase[[j]]=-(1/π)NIntegrate[Doppler[x]/(x-ω[[j]]),{x,-16000, ω[[j]]-
Δ},MaxRecursion→20]-1/π NIntegrate[Doppler[x]/(x-
ω[[j]]),{x,ω[[j]]+Δ,16000},MaxRecursion→20]-1/π  Doppler'[ω[[j]]] 2 Δ;
  phase1[[j]]=-(1/π)NIntegrate[Doppler1[x]/(x-ω[[j]]),{x,-16000,
ω[[j]]-Δ},MaxRecursion→20]-1/π NIntegrate[Doppler1[x]/(x-
ω[[j]]),{x,ω[[j]]+Δ,16000},MaxRecursion→20]-1/π  Doppler1'[ω[[j]]] 2
Δ;
  phase2[[j]]=-(1/π)NIntegrate[Doppler2[x]/(x-ω[[j]]),{x,-16000,
ω[[j]]-Δ},MaxRecursion→20]-1/π NIntegrate[Doppler2[x]/(x-
ω[[j]]),{x,ω[[j]]+Δ,16000},MaxRecursion→20]-1/π  Doppler2'[ω[[j]]] 2
Δ;
  E3[[j]]=-Exp[-Doppler1[ω[[j]]]-ⅈ phase1[[j]]+ⅈ (-ωm)t]M (1-
ε/2)+Exp[-Doppler[ω[[j]]]-ⅈ phase[[j]]]+Exp[-Doppler2[ω[[j]]]-ⅈ phase2
[[j]]+ⅈ ωm t] M (1+ε/2);
  I3[[j]]=Simplify[E3[[j]]*Conjugate[E3[[j]]]];
  S2[[j]]=tm⁻¹ *∫₀ᵗᵐ I3[[j]] * Sin[ωₘt]dt;
  Sphase[[j]]=-(1/π)NIntegrate[SDoppler[x]/(x-ω[[j]]),{x,-16000,
ω[[j]]-Δ},PrecisionGoal→12,MaxRecursion→40]-1/π
NIntegrate[SDoppler[x]/(x-
ω[[j]]),{x,ω[[j]]+Δ,16000},PrecisionGoal→12,MaxRecursion→40]-1/π
SDoppler'[ω[[j]]] 2 Δ;
  Sphase1[[j]]=-(1/π)NIntegrate[SDoppler1[x]/(x-ω[[j]]),{x,-16000,
ω[[j]]-Δ},PrecisionGoal→12,MaxRecursion→40]-1/π
NIntegrate[SDoppler1[x]/(x-
ω[[j]]),{x,ω[[j]]+Δ,16000},PrecisionGoal→12,MaxRecursion→40]-1/π
SDoppler1'[ω[[j]]] 2 Δ;
  Sphase2[[j]]=-(1/π)NIntegrate[SDoppler2[x]/(x-ω[[j]]),{x,-16000,
ω[[j]]-Δ},PrecisionGoal→12,MaxRecursion→40]-1/π
NIntegrate[SDoppler2[x]/(x-
ω[[j]]),{x,ω[[j]]+Δ,16000},PrecisionGoal→12,MaxRecursion→40]-1/π
SDoppler2'[ω[[j]]] 2 Δ;
  SE3[[j]]=-Exp[-SDoppler1[ω[[j]]]-ⅈ Sphase1[[j]]+ⅈ (-ωm)t]M (1-
ε/2)+Exp[-SDoppler[ω[[j]]]-ⅈ Sphase[[j]]]+Exp[-SDoppler2[ω[[j]]]-ⅈ
Sphase2 [[j]]+ⅈ ωm t] M (1+ε/2);
  SI3[[j]]=Simplify[SE3[[j]]*Conjugate[SE3[[j]]]];
  SS2[[j]]=tm⁻¹ *∫₀ᵗᵐ SI3[[j]] * Sin[ωₘt]dt;
```

```
   SSS2[[j]]=tm⁻¹ *∫₀ᵗᵐ(SI3[[j]] − I3[[j]]) * Sin[ωₘt]dt;
   }]
  scale = 953;
  ListLinePlot[Table[{ω[[j]]/(2
π),phase[[j]]},{j,1,num}],Frame→True,PlotRange→{{-
750,750},All},FrameLabel→{"fₚᵣₒᵦₑ-1/2f_AOM-f_P (13)(MHz)","Phase Shift
ϕ"},PlotStyle→{Orange,Thickness[0.008]},LabelStyle→{22,Bold}]

  ListLinePlot[Table[{ω[[j]]/(2
π),Sphase[[j]]},{j,1,num}],Frame→True,PlotRange→{{-
750,750},All},FrameLabel→{"fₚᵣₒᵦₑ-1/2f_AOM-f_P (13)(MHz)","Phase Shift
ϕ"},PlotStyle→{Blue,Thickness[0.008]},LabelStyle→{22,Bold}]

  p1=ListLinePlot[Table[{ω[[j]]/(2
π),scale*S2[[j]]},{j,1,num}],Frame→True,PlotRange→{{-
750,750},All},FrameLabel→{"fₚᵣₒᵦₑ-1/2f_AOM-f_P (13)(MHz)","FM dispersion
error"},PlotStyle→{Orange,Thickness[0.008]},LabelStyle→{22,Bold}]

  p2=ListLinePlot[Table[{ω[[j]]/(2
π),scale*SS2[[j]]},{j,1,num}],Frame→True,PlotRange→{{-
750,750},All},FrameLabel→{"fₚᵣₒᵦₑ-1/2f_AOM-f_P (13)(MHz)","FM dispersion
error"},PlotStyle→{Blue,Thickness[0.008]},LabelStyle→{22,Bold}]

  S1=Table[0,{j,1,num}];(*FM absorption error signal, pump-off*)
SS1=Table[0,{j,1,num}];(*FM absorption error signal, pump-on*)
  For [j=1,j≤num,j++,
  {S1[[j]]=tm⁻¹ *∫₀ᵗᵐ I3[[j]] * Cos[ωₘt]dt;(*FM absorption error signal, pump-
on*)
   SS1[[j]]=tm⁻¹ *∫₀ᵗᵐ SI3[[j]] * Cos[ωₘt]dt;(*FM absorption error signal, pump-
off*)
   }]
  p11=ListLinePlot[Table[{ω[[j]]/(2
π),scale*S1[[j]]},{j,1,num}],Frame→True,PlotRange→All,FrameLabel→{"fₚᵣₒ
ᵦₑ-1/2f_AOM-f_P (13)(MHz)","FM absorption
error"},PlotStyle→{Orange,Thickness[0.008]},LabelStyle→{22,Bold}](*FM
absorption error,pump-off*)

  p21=ListLinePlot[Table[{ω[[j]]/(2
π),scale*SS1[[j]]},{j,1,num}],Frame→True,PlotRange→{{-
750,750},All},FrameLabel→{"fₚᵣₒᵦₑ-1/2f_AOM-f_P (13)(MHz)","FM absorption
error"},PlotStyle→{Blue,Thickness[0.008]},LabelStyle→{22,Bold}](*FM
absorption error,pump-on*)

  p3=ListLinePlot[Table[{ω[[j]]/(2
π),SSS2[[j]]},{j,1,num}],Frame→True,PlotRange→{{-
200,200},All},FrameLabel→{"fₚᵣₒᵦₑ-1/2f_AOM-f_P (13)(MHz)","AM dispersion
error"},PlotStyle→{Black,Thickness[0.008]},LabelStyle→{22,Bold}]

  p4=ListLinePlot[Table[{ω[[j]]/(2
π),scale*SSS2[[j]]},{j,1,num}],Frame→True,PlotRange→{{-200,200},{-
```

```
1,1}},FrameLabel→{"f_probe-1/2f_AOM-f_P (13)(MHz)","AM dispersion
error"},PlotStyle→{Black,Thickness[0.008]},LabelStyle→{22,Bold}]

 Show[p4,PlotRange→{{-100,100},{-1,0.99}}]

 Show[p4,PlotRange→{{0,1},{-0.05,0.05}}]

 p31=ListLinePlot[Table[{ω[[j]]/(2 π),scale/2*(SS1[[j]]-
S1[[j]])},{j,1,num}],Frame→True,PlotRange→{{-200,200},{-
1,1}},FrameLabel→{"f_probe-1/2f_AOM-f_P (13)(MHz)","AM absorption
error"},PlotStyle→{Black,Thickness[0.008]},LabelStyle→{22,Bold}](*AM
absorption error*)
```

Appendix C Analytical modeling of the helium and acetylene diffusion time in photonic crystal fibers

Helium (SI unit)

```
a=5*10⁻⁶;δ=3*10⁻¹⁰;m=4*1.66*10⁻²⁷; T=300; k=1.38*10⁻²³;p0=6 (*bar*);L=12;
```

Mean molecular velocity

$$\text{Vavg}=\sqrt{\frac{8kT}{\pi m}}$$

```
1260.05
```

Mean free pass

$$\lambda=(k\ T)/(\sqrt{2}\pi\ p0*10^5\ \delta 2)$$

```
1.72561×10⁻⁸
```

Knudsen number

$$K=\lambda/a$$

```
0.00345121
```

Viscosity:

$$\eta=(\text{Vavg}*m)/(2\sqrt{2}\pi\ \delta 2)$$

```
0.0000104621
```

Diffusion coefficient:

```
Diff[d_,p_]:=(((d*10^-6/2)² p*10⁵)/(8 η))(*d in μm, p in bar*)
```

```
Plot[Diff[dia,6],{dia,10,100},Frame→True,PlotRange→All,FrameLabel→{"Fi
ber dia (μm)","diffusion
coef(m²/sec)"},PlotStyle→{Black,Thickness[0.004]},LabelStyle→{22,Bold}
]
```
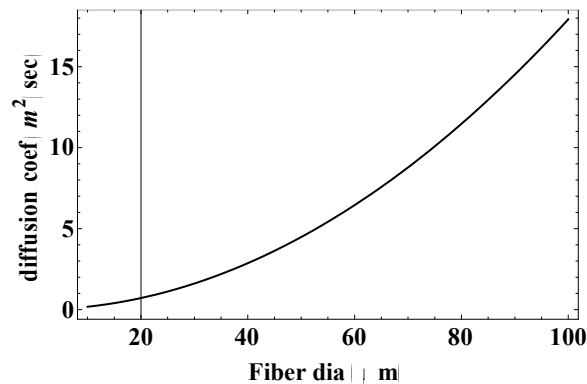


```
LogPlot[{Diff[10,p],Diff[20,p],Diff[40,p],Diff[80,p]},{p,2,8},Frame→Tr
ue,PlotRange→{0.02,20},FrameLabel→{"pressure (bar)","diffusion
coef(m²/sec)"},PlotStyle→{{Blue,Thickness[0.004]},{Orange,Thickness[0.0
04]},{Red,Thickness[0.004]},{Black,Thickness[0.004]}},LabelStyle→{22,B
old}]
```
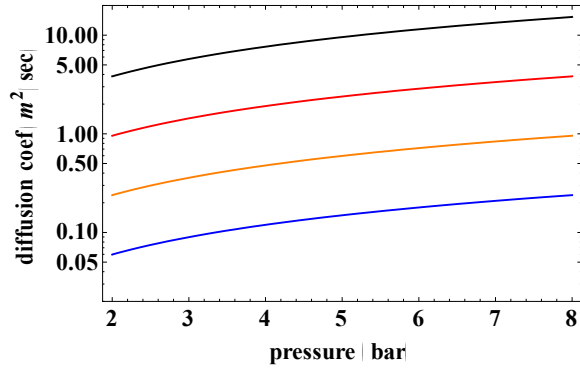
```
Diff[60,6]/Diff[10,6]
36.
```

```
Plot3D[Diff[dia,p],{dia,10,100},{p,2,6},PlotRange→All,AxesLabel→{"p(ba
r)","d(μm)","Diff"},LabelStyle→{22,Bold}]
```
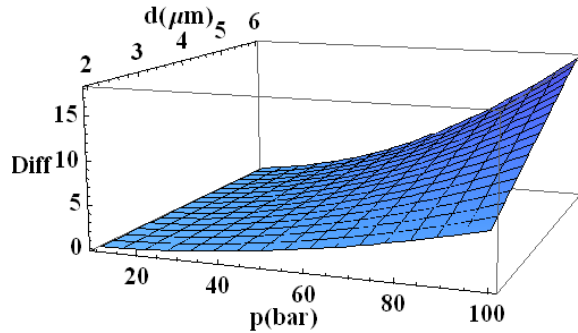

Filling time (mins)
```
tfillHe[d_,p_,pi_]:=(2 L)²/(π2 Diff[d,2pi/3]) Log[π2/8*pi/(pi-p)]/60
```

```
Plot[tfillHe[dia,0.85*6,6],{dia,10,100},Frame→True,PlotRange→All,Frame
Label→{"Fiber dia (μm)","Filling time
(mins)"},PlotStyle→{Blue,Thickness[0.004]},LabelStyle→{22,Bold}]
```
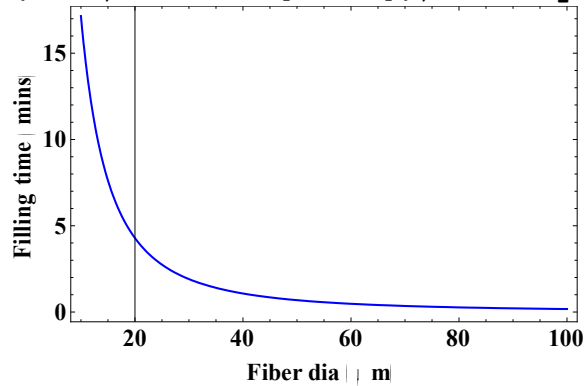


```
Plot[tfillHe[10,p,6],{p,0,0.85*6},Frame→True,PlotRange→All,FrameLabel→
{"pressure (bar)","Filling time
(mins)"},PlotStyle→{Blue,Thickness[0.004]},LabelStyle→{22,Bold}]
```
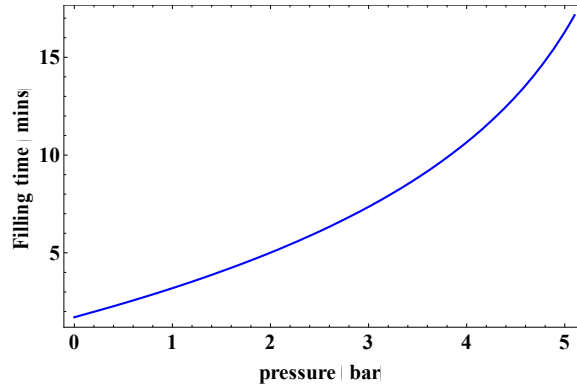
```
LogPlot[{tfillHe[10,p,6],tfillHe[20,p,6],tfillHe[40,p,6],tfillHe[80,p,
6]},{p,0.1,0.85*6},Frame→True,PlotRange→{0.02,20},FrameLabel→{"pressur
e (bar)","Filling time
(mins)"},PlotStyle→{{Blue,Thickness[0.004]},{Orange,Thickness[0.004]},
{Red,Thickness[0.004]},{Black,Thickness[0.004]}},LabelStyle→{22,Bold}]
```
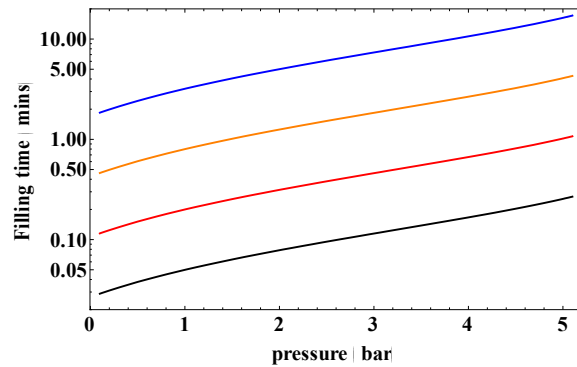


```
 d=60;p0=6;
(0.7)^5*p0
(tfillHe[d,0.85*p0,p0]-
tfillHe[d,0.7*p0,p0])+(tfillHe[d,0.85*0.7*p0,0.7*p0]-
tfillHe[d,(0.7)^2*6,0.7*p0])+(tfillHe[d,0.85*(0.7)^2*p0,(0.7)^2*p0]-
tfillHe[d,(0.7)^3*p0,(0.7)^2*p0])+(tfillHe[d,0.85*(0.7)^3*p0,(0.7)^3*p0]-
tfillHe[d,(0.7)^4*p0,(0.7)^3*p0])+(tfillHe[d,0.85*(0.7)^4*p0,(0.7)^4*p0]-
tfillHe[d,(0.7)^5*p0,(0.7)^4*p0])+(tfillHe[d,0.85*(0.7)^5*p0,(0.7)^5*p0]-
tfillHe[d,(0.7)^6*p0,(0.7)^5*p0])
 1.00842
 2.74303
 d=60;p0=5;
(0.7)^4*p0
(tfillHe[d,0.85*p0,p0]-
tfillHe[d,0.7*p0,p0])+(tfillHe[d,0.85*0.7*p0,0.7*p0]-
tfillHe[d,(0.7)^2*6,0.7*p0])+(tfillHe[d,0.85*(0.7)^2*p0,(0.7)^2*p0]-
tfillHe[d,(0.7)^3*p0,(0.7)^2*p0])+(tfillHe[d,0.85*(0.7)^3*p0,(0.7)^3*p0]-
tfillHe[d,(0.7)^4*p0,(0.7)^3*p0])+(tfillHe[d,0.85*(0.7)^4*p0,(0.7)^4*p0]-
tfillHe[d,(0.7)^5*p0,(0.7)^4*p0])
 1.2005
 1.92879
```

Acetylene (SI unit)

131

```
a=30*10⁻⁶;δ=3*10⁻¹⁰;m=26*1.66*10⁻²⁷; T=300; k=1.38*10⁻²³;Pres=10;L=12;
```

$$Vavg=\sqrt{\frac{8kT}{\pi m}}$$

```
λ=(k T)/(√2π Pres δ2)
K=λ/a
 494.23
 0.00103536
 34.5121
 Diff=2/3 a Vavg
 0.00988461
 x=0.85;
```

```
tfill=(2 L)²/(π2 Diff) Log[π2/8*1/(1-x)]/(60*60)
 3.45584
 Plot[(2 L)²/(π2 2/3 dia/2*10⁻⁶ Vavg) Log[π2/8*1/(1-x)]
/60,{dia,10,100},Frame→True,PlotRange→All,FrameLabel→{"Fiber dia
(μm)","Diffusion time
(mins)"},PlotStyle→{Red,Thickness[0.004]},LabelStyle→{22,Bold}]
```
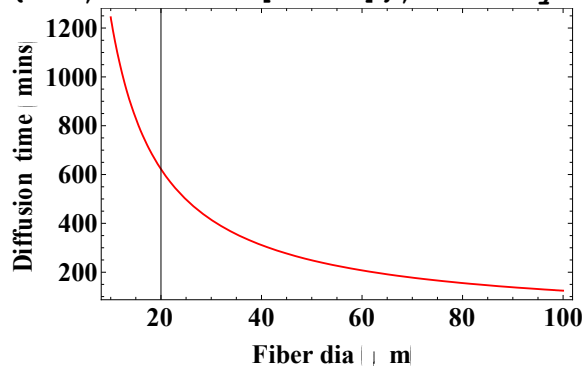


```
 Plot[(L)²/(π2 2/3 dia/2*10⁻⁶ Vavg) Log[π2/8*1/(1-x)]
/60,{dia,10,100},Frame→True,PlotRange→All,FrameLabel→{"Fiber dia
(μm)","Diffusion time
(mins)"},PlotStyle→{Orange,Thickness[0.004]},LabelStyle→{22,Bold}]
```
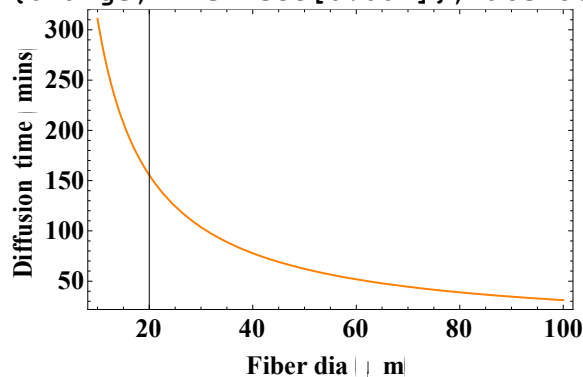


```
 δ=3*10⁻¹⁰;m=26*1.66*10⁻²⁷; T=300; k=1.38*10⁻²³;Pres=10 (*pascal, 0.1mbar,
75mt*);x=0.85;
```

$$Vavg=\sqrt{\frac{8kT}{\pi m}}$$

```
λ=(k T)/(√2π Pres δ2)
Kn[d_]:=(λ/(d/2*10⁻⁶))(*Knudsen number, Fiber dia in μm*)
 494.23
```

```
 0.00103536
 Diff[d_]:=(2/3) ((d*10⁻⁶)/2)* Vavg (*coefficient*)
 tfill1[L_,d_]:=(2L)²/(π2 Diff[d]) Log[π2/8*1/(1-x)]/60 (*Filling time
in mins, one end*)
 tfill2[L_,d_]:=(L)²/(π2 Diff[d]) Log[π2/8*1/(1-x)]/60 (*Filling time
in mins, both ends*)

Plot3D[tfill2[L,dia],{L,1,12},{dia,10,100},PlotRange→All,AxesLabel→{"L
(m)","d(μm)","t(mins)"},LabelStyle→{22,Bold}]
```
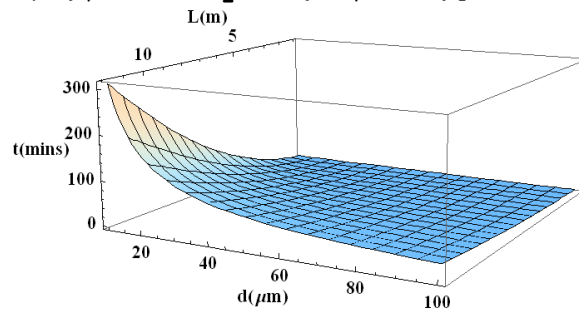


```
 tfill2[4,68] (*Filling time in mins, both ends, 4m 68μm core*)
 5.08212
 tfill2[7.9,85] (*Filling time in mins, both ends, 7.9m 85μm core*)
 15.8588
 tfill1[6,20]/60 (*Filling time in hrs, one end, 6m 20μm core*)
 2.59188
 tfill1[12,60] /60(*Filling time in hrs, one end, 12m 60μm core*)
 3.45584
```

Appendix D Standard Operation Procedure of Vytran FFS-2000 splicer

D.1 Overview of FFS-2000 Workstation Hardware
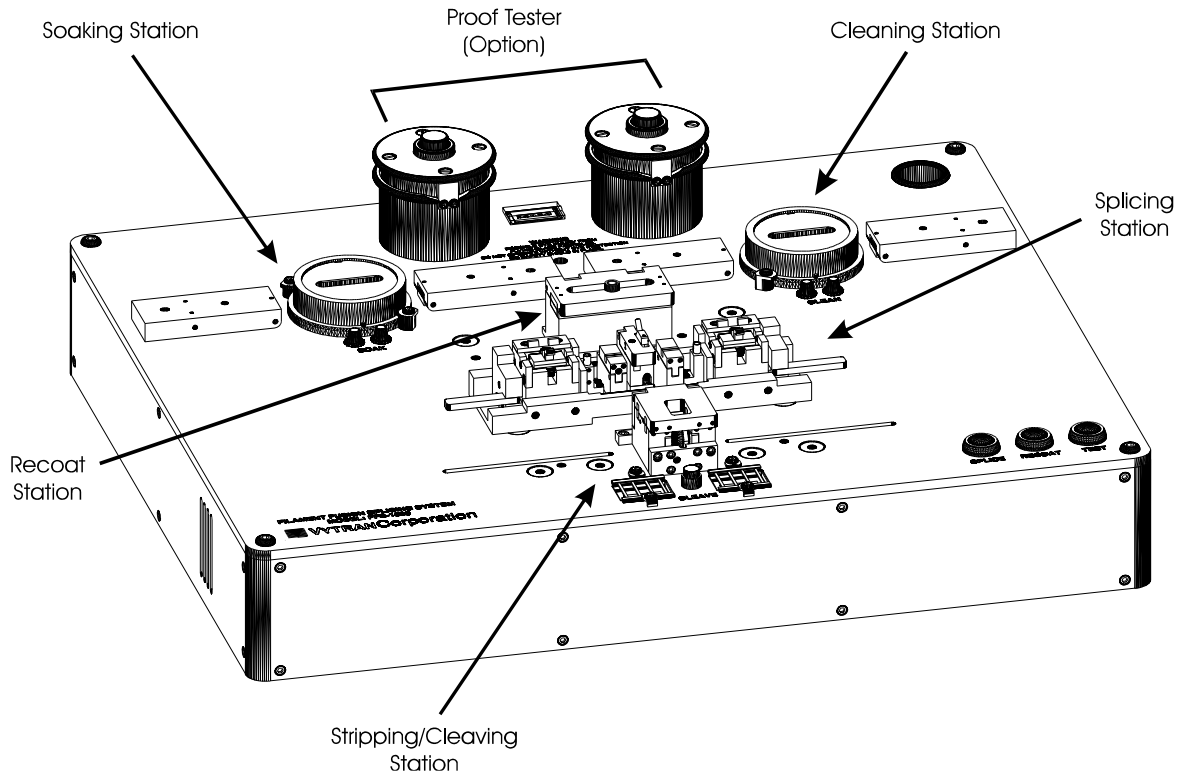
FFS-2000 Workstation Hardware.
Figure from FFS-2000 Fusion Splicing Workstation official manual.

- Transfer Jig. : keep fiber alignment from stage to stage

- Fiber holding blocks (FHB) and Transfer Jig are serialized (# **03464**) to match the splicer.

- If the computer ever fails (already been used for 6-7 years), make sure FireWire card (15 pin LPT connector) is in strapping and can be reinstalled to a new computer.

- Analog inputs for active alignment: feedback system aligns fibers using loss (BNC cable)

- 19 inch screen for computer resolution. Otherwise the image may get distorted.

D.1.1 Stripping and Cleaving station

As shown in below, the top stripper insert is adjustable and can be shifted side to side to align with the bottom insert. The bottom insert is fixed; it inserts into a socket that provides current, and it's insulated and safe to touch. There is a low-temperature level by providing the current through the sensor. When the station is closed, the bottom insert transfer the temperature to the top insert and the stripping blades get heated to a certain temperature. (Thermal – mechanical strippers (TMS))
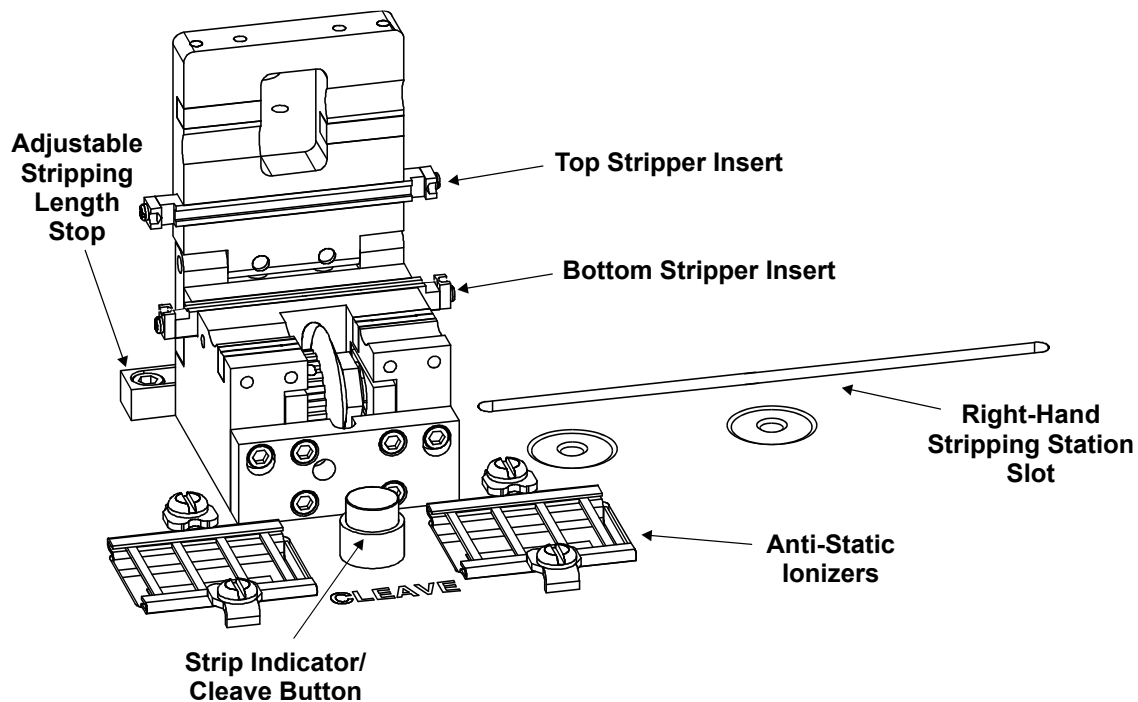
Stripping and Cleaving station of the FFS-2000 splicer
Figure from FFS-2000 Fusion Splicing Workstation official manual.

Striping inserts size (determined by the stripping blade position):

- 125 (glass) -250μm (coating) --- this unit

- 125 - 400μm

- 80 - 180μm (normally a 160μm coating fiber)

Cleave inserts:

- Top: flat (left and right), removable, set by two set screws in the front. We can remove, replace and flip them if needed;

- Bottom: also removable, with a V-groove in it, specific sizes to hold specific size of the glass (need enough surface touch to hold the glass)

Vacuum V-grove in FHB:

- 250μm - this unit, works for SMF, PBG, and EDF.

- 160μm - for HNLF (190μm coating), 135μm V-grove used during training.

Tension on fiber holder block:

- 115- 120 gram for PCF (core size 110μm 19-cell and 115μm 7-cell)

- 210 gram for SMF

- 100 gram for 80μm glass.

Mitutoyo 546-118 Standard Dial Tension Gauge is used to adjust the tension:

Fix one end of the fiber holder, make sure the contact point between FHB and the tension gauge just pass the eyelid on the gauge, and push the block all the way towards the inner wall against the spring tension-pass 200 gram, slowly release the gauge and tap on the top of the fiber holder until seeing small oscillation on the gauge.
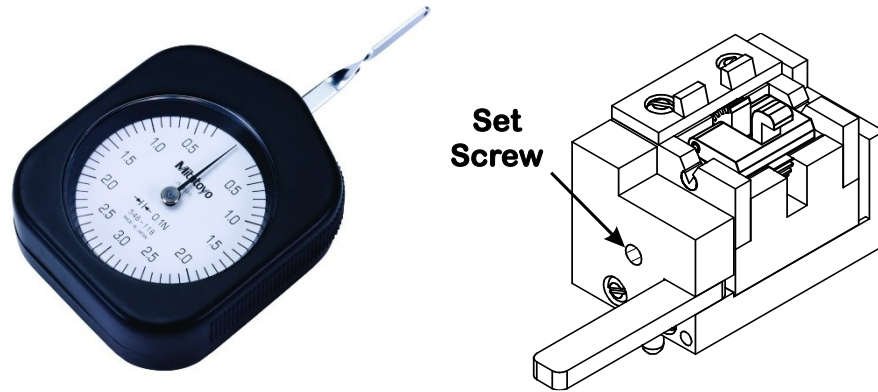
Figure from FFS-2000 Fusion Splicing Workstation official manual.

Reduce tension:

.050" Allen wrench counter-clockwise; increase tension: clockwise (~40 gram/turn).

- Too much tension will cause round surface, high cleave angle, also may break the fiber.

- Less tension would fold the fiber and damage the cleaver blade.

Cleave Wheel:

- Polycrystalline diamond

- Tension- and-scribe cleaving process to score the fiber

- Parameter in software controls how far the blade comes. Blade comes forward X mount

  steps, and starts oscillating, score the glass.

  Pre-cleave in advance (parameter): home to the position starts oscillating;

  Right: 2170, left: 1500-1510.

- Mechanically can be adjusted: rotational angle, sideways, height.

D.1.2 Splicing station
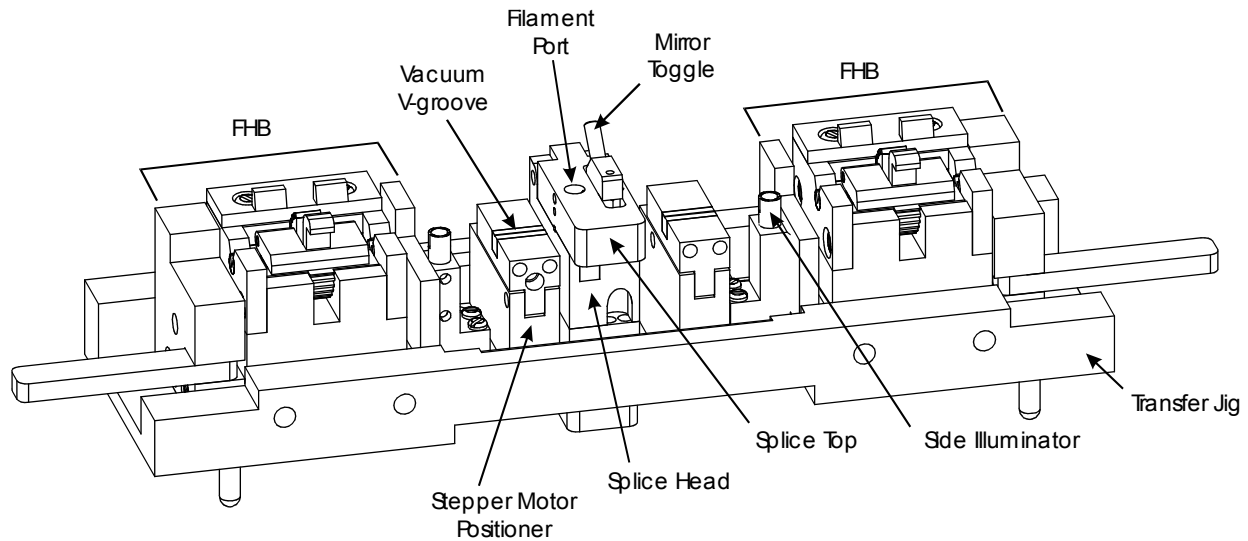
Figure from FFS-2000 Fusion Splicing Workstation official manual.

- Lower the transfer Jig with the FHB and graphite inserts will enable the vacuum. Vacuum pressure depends on the cladding parameter of different fibers. Fibers are only in the graphite inserts and not purpose to touch the side illuminators.

- Splice head has multiple parts for alignment and fusion.

- Illuminate intensity: how much light in the store and how much light in the lens.

- Tungsten filament (in this unit, standard) and iridium filament (lower temperature and quick response – steep ramp, for non-silica soft fibers, 28min file39): SMF 20-21 W splice power, 80μm: 15 W may be still high.

- Filament continues usage lifetime: 40 - 50mins. For SMF, not fire polish: 5 sec/splice, total # ~500 splices. (The lifetime is shown on the bottom status bar - a clock icon)

- Width is also an option, such as 21 W for current filament or 10 W for a wider filament.

- Mirror toggle: ⊔∧⊔ side view mirror ▽ end view mirror.

- Sound to tell if there is a leak of Argon splice cap, it will age the filament. Argon pressure 0.15 lit/min background, splice 0.65 lit/min.

D.1.3 Recoat station
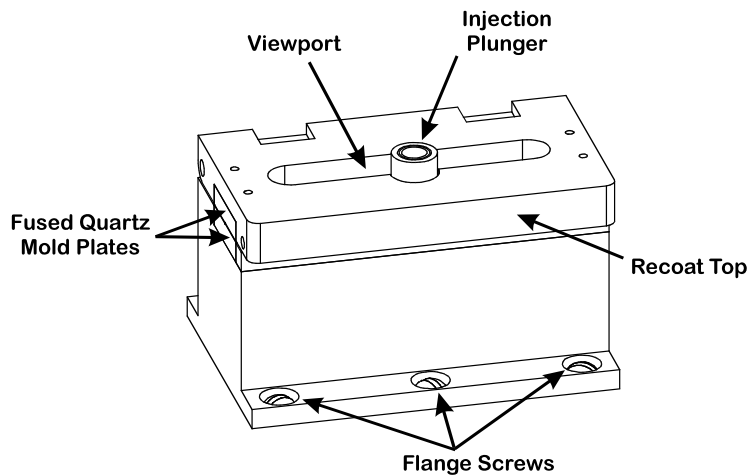
Figure from FFS-2000 Fusion Splicing Workstation official manual.

Recoating size (larger than cladding - stripped interface is protected):

- Mark sure recoat top is flat

- UV Curing, 15 sec.

- 280μm, 430μm - this unit, 600μm

- High index > 1.45 material (SM 9/50)

- KIM wipes between mold plates if not using for a couple of days.

D.1.4 Motors
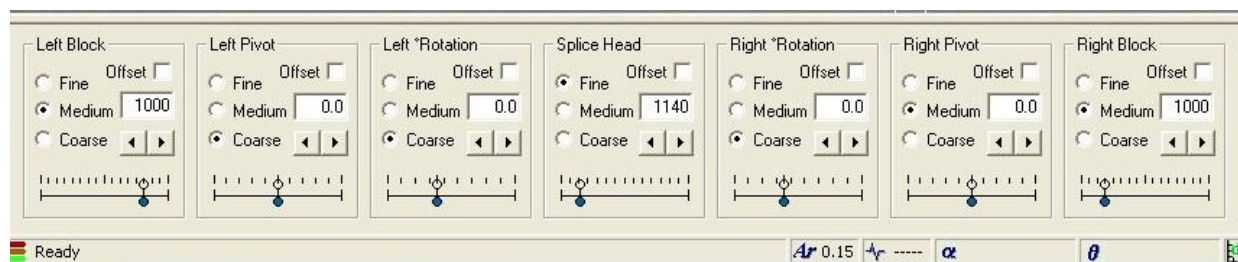
- Motor steps: block (z-direction), Pivot (xy-direction) – no home sensor, set by reference-motor steps (make sure FHBs and transfer Jig. are engaged in the splice station), if motor position and Physical FHB position is not match, reset manually. Pivot can be set to relative home-position (Datum, by command).

- Splice head includes lens, mirror, filament, moves on optical fiber to control offset.

- Filament is on the left, and lens is on the right, so the alignment and splice are not at the same position. Two important terms are used to describe the fiber position:

  1) view-to-splice: Position of fiber used when loading and viewing gap.

  2) view-to-home: Position of fiber during splicing

  Before and after splicing, make sure it's in the view-to-home (in back view). View-to-splice is calibrated.
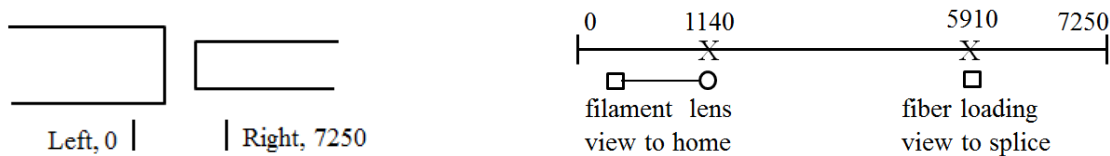
- Motors have physical home sensor:

  1) Rotation lens, 2) focus motor, 3) splice head (lens & filament translation), 4) cleave.

D.1.5 Recovery procedure (ONLY FOR ADVANCED USER)

Use the following procedure if you may believe that FHB are not in the correct positions, either along z or xy. Open the software, all icons are grey..

1. Initialize. Enable traffic viewer (view → comments traffic), for trouble shooting.

2. Make sure FHBs and Transfer Jig are engaged in the splice station, then press Reset button. Reset will do the following actions:

a) Finding home for lens, focus, splice head, cleave blade.

b) Blocks - z, rotation, pivot.

c) Cleaver motion

3. If the blocks are not returning to the same position, reset fails. Possible issues:

   a) Translator (changing rotation motion to linear motion) could be damaged. Fiber may not be centered in the screen.

   b) Splice head is not in where it should be (1140 in our case).

   c) Cleave mechanism: if a lot of sharps drop in cleave station and [Cleave arm] get underneath the cleave arm, the magnetic won't make it to the home sensor. Using vacuum to clean. If the blade is too close to sensor, move cleave blade forward, away from home sensor, then redo the reset.
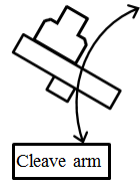
D.1.5.1 *Macro path*

- The macro path is used to send specific line commands to the splicer. Normal operation does not require sending macros. Thus this should be done only by an expert user.

- In the reset process, the sequence is lens, focus, splice head and cleave, and then block position (z)… If it fails right at the cleave, you never see the cleave move, all you hear is a little cracking sound, small steps with low velocity. It mix specific sound, steps away from home sensor, and triggers back away. If it does not, to do that, you could access it using a macro.

- Splice: could use macro path 1 or macro path 2 (execute, use macro).

- Service cleave blade: bring the blade forward to service position away from home sensor, when it reset, it will make sure it finds the home sensor, and then return to the offset position defined.

Some tips:

- In this software, after the 1st reset when the unit turns on, there is a delay (10 - 15s, uploading cleaving parameters) in cleave motor.

- If you are not using the cleave station: do the Reset as normal, then load the fiber manually (make sure there is no buffer in the V-groove section) to the center of the screen, and generally pull the fiber back.

- When manually loading or splicing, make sure motor position in the range 700-1100. To prevent from hitting the limit, before the load, send the motor to 1000 when the FBHs and transfer Jig are engaged. Always use fiber loading button to move the splice head to the right position.

D.1.5.2 Pivot motor (xy)

- No home sensor. When the pivot motor says Zero, but the fiber is not in the center of the screen, maybe fiber is too close to the filament, depends on which fiber is used, too high or too low. Fiber won't align properly.

- The first reason is the motor is jammed, after resetting, step the motor make sure the motor is moving. Second, any debris in the graphite V-groove will change the height of the fiber. Use an eye loop (NRD 1C-400, NY Company) to check the graphite, soft toothbrush or compressed air to clean.

- If, after the cleaning, fiber is still not in the right position, you need datum it.

D.1.5.3 Reset pivot manually

Left pivot (do in back view):

Step left pivot (using medium) the left (negative limit), until hearing small graving sound, then gear stop.

- Case A: if the motor position reaches -125 and the gear not stop. Run out of the software range, send motordatum[1 0] command via the macro path to tell the software that is the Zero position. No matter where the physical position is. Keep step the motor further until hearing the graving sound, and move 1 step back (in medium), use motordatum[1 -9000] command to tell the software that is the left limit, that is the then send Zero on the left pivot.

- Case B: if you have graving sound when motor position does not reach -125, use motordatum[1 -9000] command to tell the software that is the left limit, that is the then send Zero on the left pivot.

Right pivot (do in front view, the same procedure, only motor number is different):

Step right pivot the left (negative limit), until hearing some graving sound (gear stopped).

- Case A: if the motor position reaches -125 and the gear not stop. Run out of the software range, send motordatum[2 0] command to tell the software that is the Zero position. No matter where the physical position is. Keep step the motor further until hearing the graving sound, and move 1 step back (in medium), use motordatum[2 -9000] command to tell the software that is the left limit, that is the then send Zero on the left pivot.

- Case B: if you have graving sound when motor position does not reach -125, use motordatum[2 -9000] command to tell the software that is the left limit, that is the then send Zero on the left pivot.

The ratio of 1 step in software to the motor is 9000:125.

- If the fiber is rising up in the graphite V-groove, the fiber will be seen moving down in back view and up in front view:
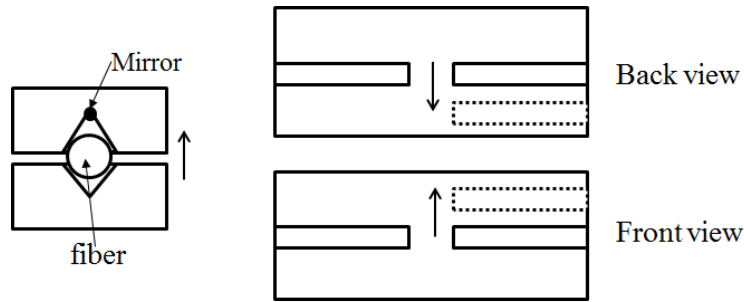
- If the fiber is setting in the bottom of the V-groove, the fiber will too high in the back view, and low in front view. In this case, fiber will be too close to the filament, and the splice power may be too high for splice.
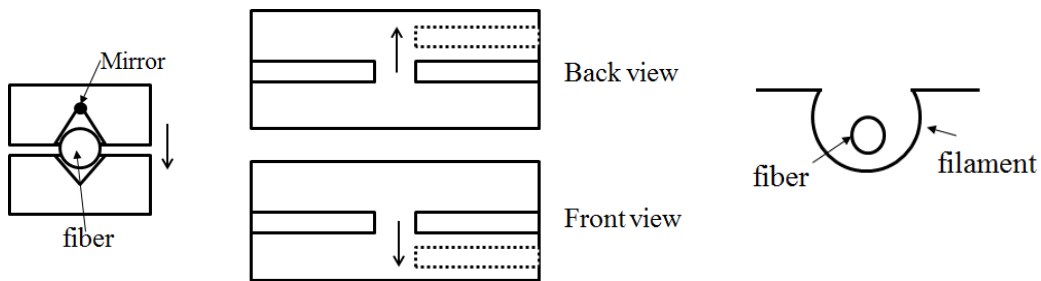
D.1.5.4 Reset translation (z) manually:

This will need to be done if a software command to move the FHB was sent while the FHBs were not engaged in the instrument. If this happens, the mechanical z position and the software z position will not be the same. This needs to be fixed immediately or the blocks may jam at the next software command.

1. Using a screwdriver turn the z position screw (below) all the way to the inner wall (left wall for right FBH), then 3-turns counter-clockwise. This may need to be done to both right and left FHBs.
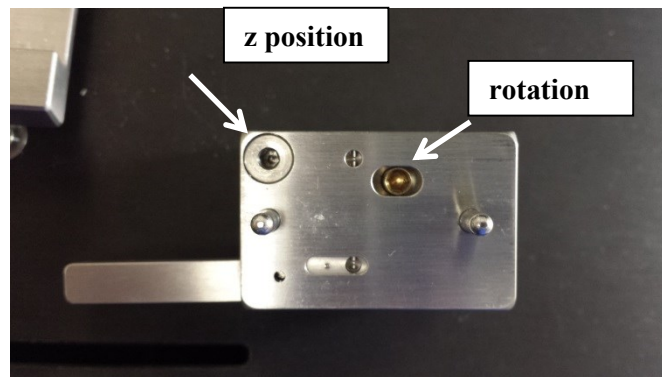
2. Making sure that the FBH is NOT attached to the instrument set the software Block position to 1000. (motor position 700-1100). This may need to be done for right and left Block positions

3. The mechanical and software z positions of the FBGs should be the same.

D.2 Overview of Software Interface

D.2.1 The main screen
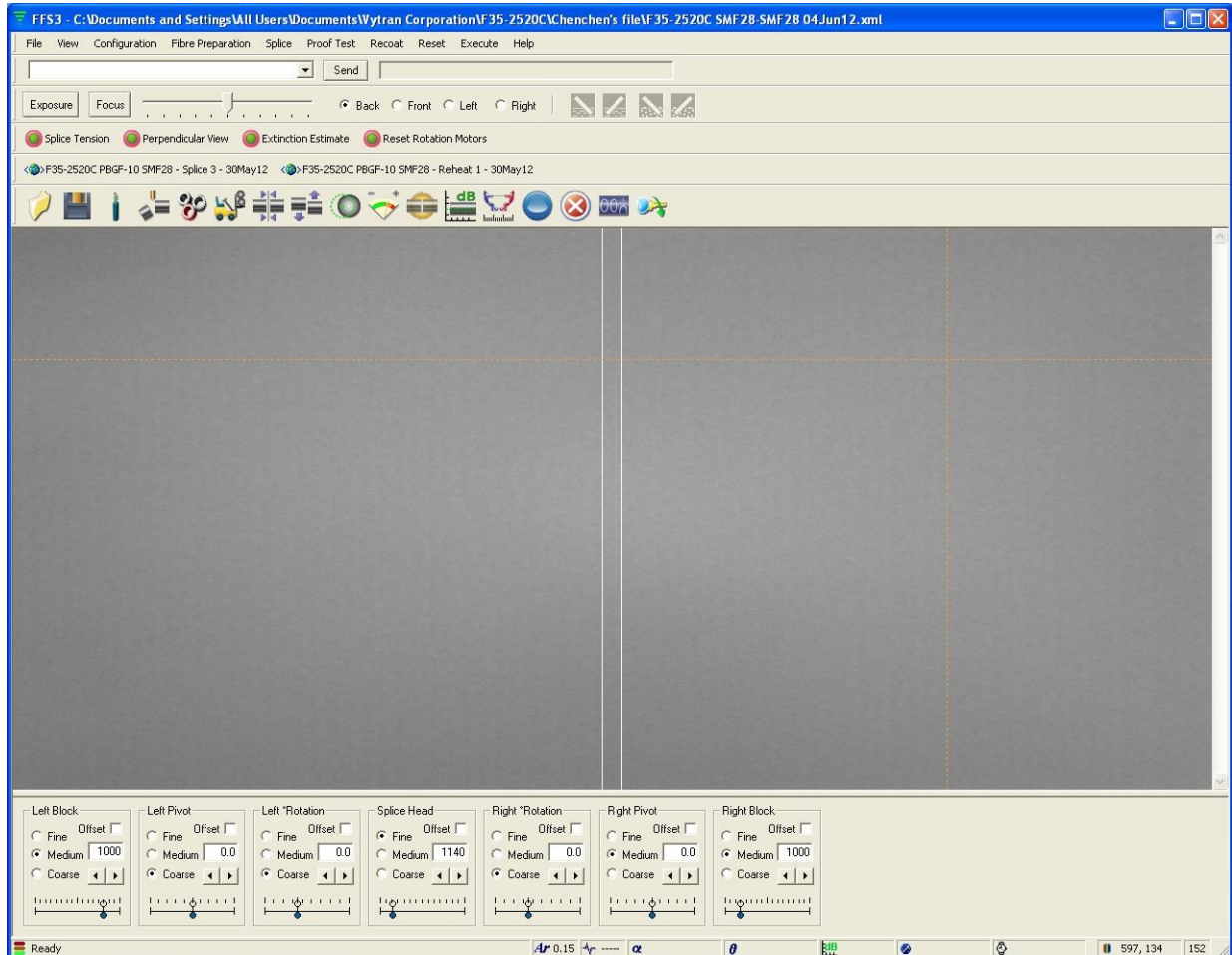
- Camera bar: camera views (Back, front, left, right)

- Cleaning bar: cleaning station, to show cleaning is done;

- Control bar: manual control of each motor on the workstation;

- Status bar: information about current events and to monitor process functions

  Ar: 0.15 (background); filament power; θ: PM rotation angle of PM axis alignment; α:

  fiber cleave angles; ⊙: filament timer, dB: loss estimation, illuminate intensity: 16.2%

(14 - 20%, back and front view may have different numbers, relevant to the alignment to the LED, how close to fiber), grey scale: 140 - 150.

D.2.2 File

File path

C:/Documents and setting/all users/Shared Documents/Vytran

Corporation/F35-2520C

- F35-2520C (filament part number (P/N))

File name

- Filament P/N Fiber types - process - Date

Ex: F35-2520C Er110-SMF28 - Splice 1- 30May12

- All the files are written protected (read-only), if you want to save files, use "Save as". Always use the Administrator account (no guest account or privileged user).

- To save information or image for diagnosis: use "Print Screen", not just "save image". This will tell the information such as motor position, status bar relevant to splice.

- Database option: should never open.
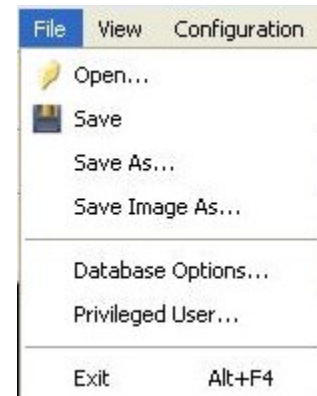
D.2.3 View

Option for enable anything you see on the top menu and logs for troubleshooting proposes.

- Main toolbar

- Process toolbar: link specific processes already invited in the software, such as extinction ratio on PM splice, reset motors.

- Marco toolbar: different macros, such as cleave macro, clean macro.

- Quick open file toolbar

- Process notifications, comms traffic:

  charts and logs to see what's happening during each process. Information can be save as txt file and send to Vytran for diagnosis.

- Guide:

  For the measurement: alignment, cross hair, measurement; "'n' drag enable" is not available in this software.

D.2.4 Configuration

Toolbars

Edit process, macro, and quick open. Or

right click on toolbars to edit them.
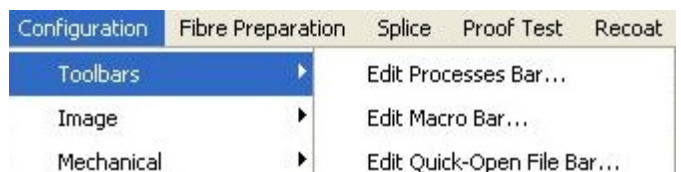
Image
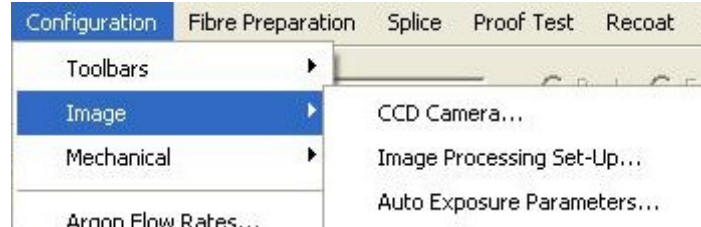
- CCD camera: change types and colors. Never change Camera Properties.

- Side-view LEDs are green LEDs; it mixes green light but based on the frequency we see white light. End-view LEDs are white LEDs.
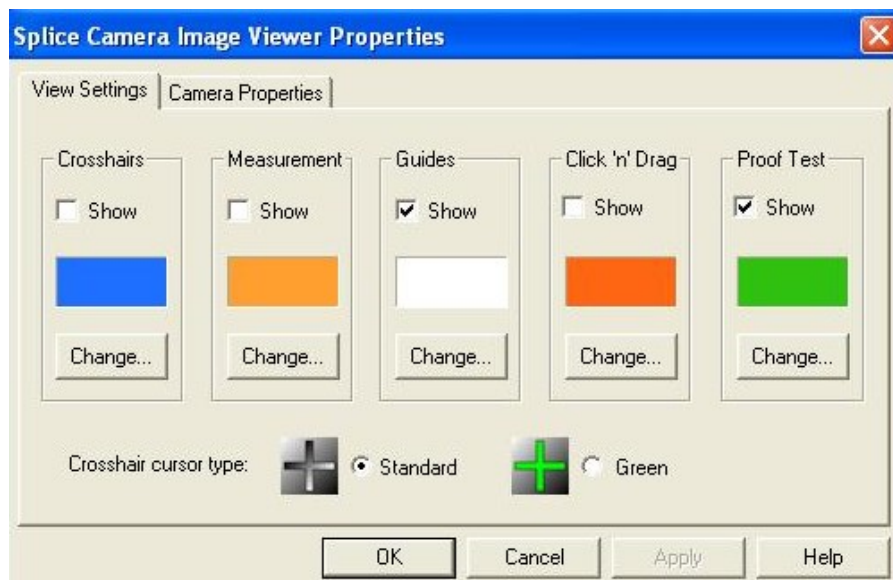
Camera Properties:

- Frame delay 30ms; camera image orientation: Top-down; camera reset period: 250.

- Camera file: C:\program Files\Vytran Corporation\FF3\ccbme37ce.cnf

- Imaging processing setup (never change): they are standard parameters based CCD, pixels resolution, screen size, software organism.

- Edge tolerance (pixels): 0.1; Z-calibration (um/pixel): 0.580; Y-calibration (μm/pixel): 0.625; gap tolerance (pixels): 0.5; aspect ratio (dy/dx): 1; focus offset (steps): -60.

- The focus offset: the only parameter could change here depends on whether you want to see more cladding or more glass.

Mechanical (Don't change, set and optimized)
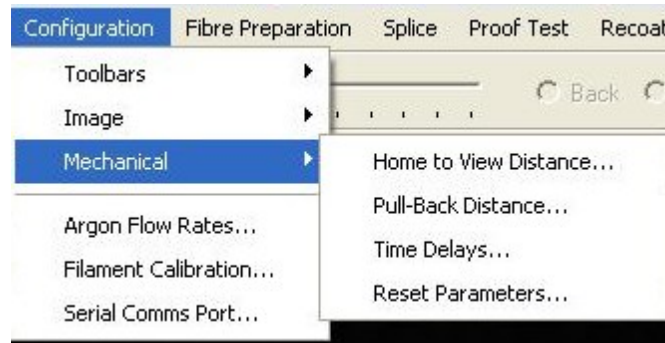
- Home to view distance (1140µm): if you push "Stop" when the splice head is moving, you may lose motor position. This value is critical to process, and you should not change this number randomly.

- If you repeat the "Reset" 3 times, and the fiber is not stopped at the same position, this value is possibly changed. Once this value is changed, you have to do the "Normalization".

- The normalization will change the center filament on the fiber and the power. The "view-to-splice" position is calculated based on home to view distance (normally 4756 µm away from the home to view).

- 4756 is the number shown on the software now, in the training; this number is 4769. Filament is changed.

- Pull back distance (1350µm): when we send the fiber thought side-view (front or back) to end view (left or right), this is the distance move back towards outside, so there is the room to put the mirror between the fibers. If the number is not correct, the mirror may get between the fibers and probably be damaged.

- Time delays (ms): factory settings. Time delay between the execution of command and actual point of motor step. Z: 250; X-Y: 100; rotation: 100; focus: 200; lens: 100; head: 1000.

- Reset parameters: not working in this unit.

Argon flow rates: critical, but you can change it (not every day).

- Purge: 1 (*liter/min*): purge before use splicer once or couple times to clean dust in the filament or other contaminations in the line. This rate changes 1-2 *liter/min* (custom preference).

- Background: 0.15 (*liter/min*), wouldn't affect the splice, constant flow to keep the line from having any contamination. You could change this rate, but this number has to be smaller than 0.65 (splice rate). Otherwise the fiber will move.

- Purge duration: 20-60*s*. If you have not used the splice for a long time, you could purge longer.

The value in the background should be minimized at 0.15 *l/min*, otherwise the unit will collect dust and moisture, and when you turn on the filament, it will turn on the dust on the fiber.

Filament calibration

You could change, but you don't want to. Power offset: -0.65 *W* (based on the Q-tip size), more details in the normalization process. View-to-splice distance: 4756.

Serial Comms port

The serial Comms port can be built in the serial device, but not use in the unit.

D.2.5 Fiber Preparation

Parameters used for stripping, cleaning and cleave.

Soak time

60s (defaults), after 60s, the soak LED (indicator) will turn on. Soak doesn't have ultrasonic.

Strip set-up

- For the TMS (thermal mechanical stripper), there is a background current level 2A, boost level 4A (defaults setting, double current on the boost, not the temperature, 100F in background, and 225F in boost level).

- If you have problems with stripping, possible reasons:

    - Background level is too low, but boost is normal, you may not reach from background to boost within the time period given.

    - Background is normal (2A), boost is low (3A), it won't be hot enough for strip. Graphite element inside the bottom stripper cracks. This will open the circuit, and you will have no heat at all. Before it breaks, it will have the microfracture (graphite pieces), increases the resistance, and the circuit tries to push more current. It might overheat.
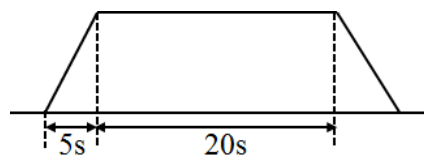
- Warm-up time 5s (ramp time, flashing, from background to boost), boost time 20s (solid).

Clean time

45s (left and right, independent), after 45s, the indicator will turn on, but the can will keep oscillating.

Cleave angle limits

Set out a limit on how big a cleave angle should respond a warning message and prompt a pause

in the process. Those limits could set individually from 1-15^0, depends on difference process.
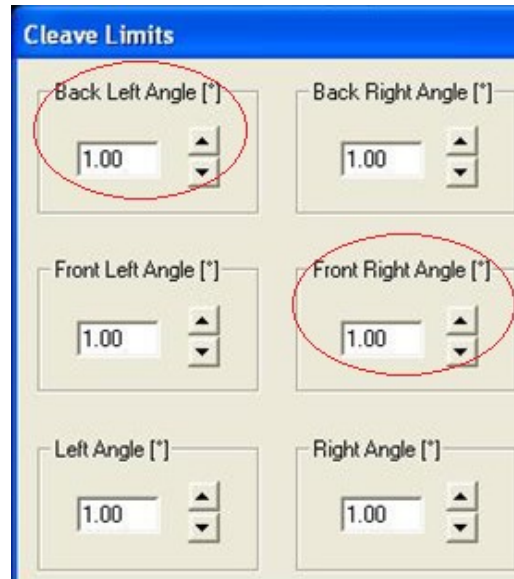
Left fiber is focused in back-view and right fiber in focused in front view. In back-view, it is really

the left angle relevant to us because right fiber isn't focus.

Cleave parameters
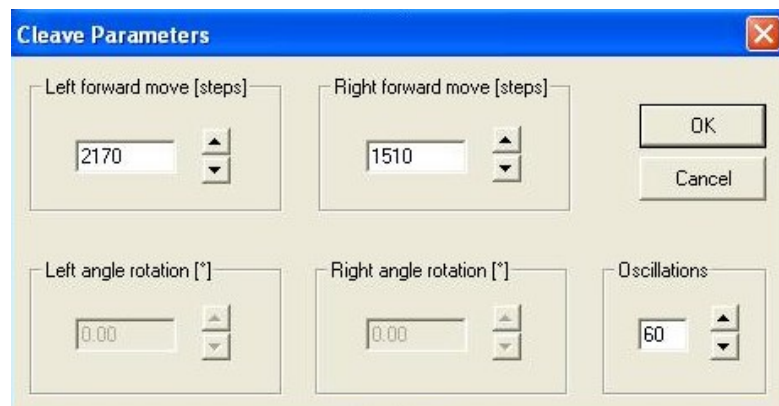
- Pre-cleave advance, steps move before oscillating; it has total 60 oscillations and one more

  motor step for each. The left forward move is 2170 steps, and the right forward move is 1510

steps, based on system alignment, cleave mechanism. Those values are only reason to change if front blade or the outer screws is loose. You have to rise cleave blade or do any kind of mechanism alignment to optimize the cleave process.

- If fiber sharps drop into the gears, that could cause a little back flash and a little drift. Either blade could go too far and hit the fiber before it starts oscillating. Or it will go forward oscillating and never touch the fiber.

- The pre-cleave advance is optimized so that the blade comes forward and oscillating and score the fiber during oscillation period. Ideally, later second half time of the oscillation period. As late as the scribe and touch the fiber, the better cleave, because you don't want to touch the fiber multiple times.

- Tension on the FHB is important to ensure fiber only be scored once.

- Oscillation period 60s is standard; this gives you enough time to visualize and optimize the pre-cleave advance number. You can see the blade oscillation 3-5s, and you will know whether you want to increase or decrease the pre-cleave parameters 5-10 steps to delay the scribe.

- Parameters may change after 5000 cleaves. Possible chip in the blade can make it dull and may not cleave easily. If you scribe the fiber are at the last oscillation, you may have to increase the steps couple of times, or if blade comes loose, you may break the fiber quick, you do not need to reduce the number, but to check mechanically the blade is not loose.

D.2.6 Splice

Splice parameters

Basic parameters save for splice are in this file (SMF28-SMF28). For each splice file, those parameters are unique.
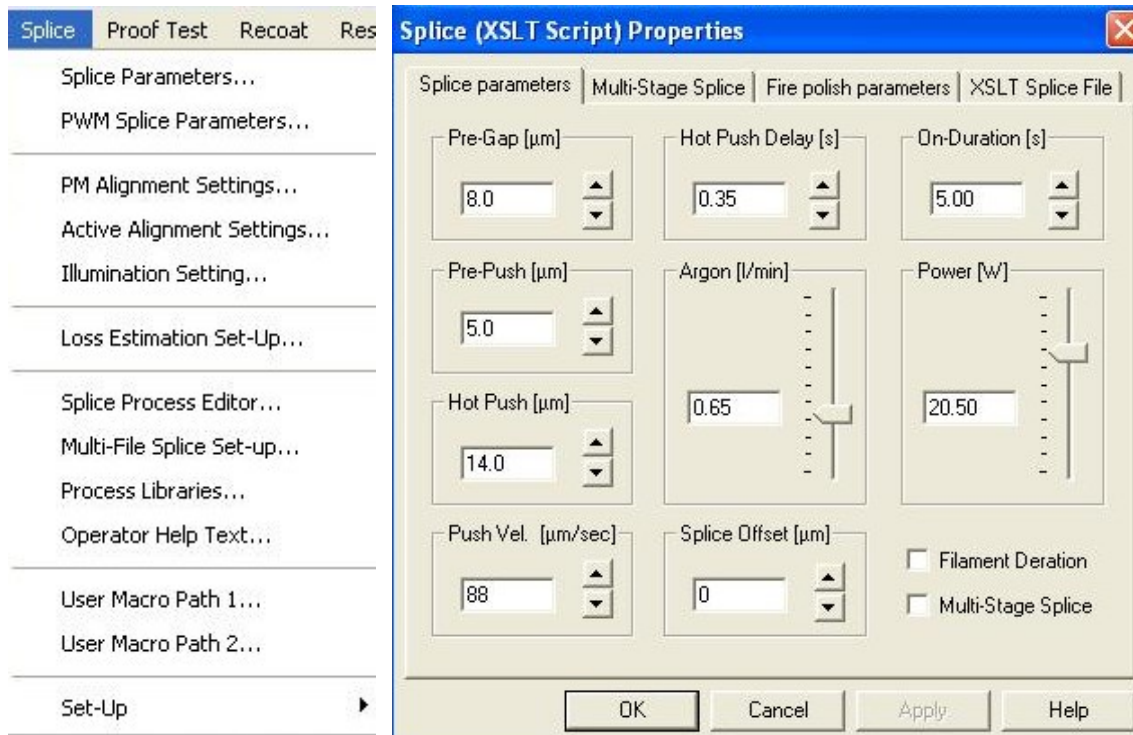
In the sequence of parameters turn on:

- Pre-gap: gap before splice, fibers will be brought to the gap line before the splice starts. Everything else, like how much and how quick it will be pushed, filament power are relevant to the pre-gap value. For bigger fiber, the gap will be larger because you want to keep big fibers away. It is specific for fiber diameter.

- Pre-push: just before the filament turns on, push right fiber towards the left fiber. Left fiber stays on the gap line, and right fiber will push, pass the gap line to touch the left fiber. In normalization file, we only need to tack the fiber, this number is zero.

- Hot-push delay: turn on the filament and wait X (0.35 typically, changing from 0.2-0.4s) amount of time to push the fiber again. Silica starts melting and burns backward. Make sure fiber ends soft enough before push to each other. This number depends on ramp time of

155

filaments, silica melting point, fiber diameter (bigger fiber diameter, more delay), the filament temperature.

- Hot push: push the fiber when the filament is on.

- Push velocity: standard velocity. 88μm/s (700μm/s in the normalization file during training)

- On-duration: ~5.35s, power: ~21W.

- Splice offset

Heat is evenly distributed, equal heat inside and out. It melts the end first and then defuses the core, pushes during temperature is on a certain amount. In standard splice, heat is constant.

Multistage splice (not available now, may be updated later):

- Use all the splice parameters and customize in stages. For special fibers: PCF, dispersion compensation fiber.

- Depends on loss, fiber strength, core alignment, extinction ratio and so on.

- Ex: tack fiber half distance →turn on the filament →move a little bit closer →turn on filament, warm it up →push more →warm up more. (Change argon flow rate, change the power relatively, the pictures below shows an example of splicing PCF to SMF)

- If the multi-stage box checked, it will do multi-stage, otherwise just run normal splice process then fiber polish.
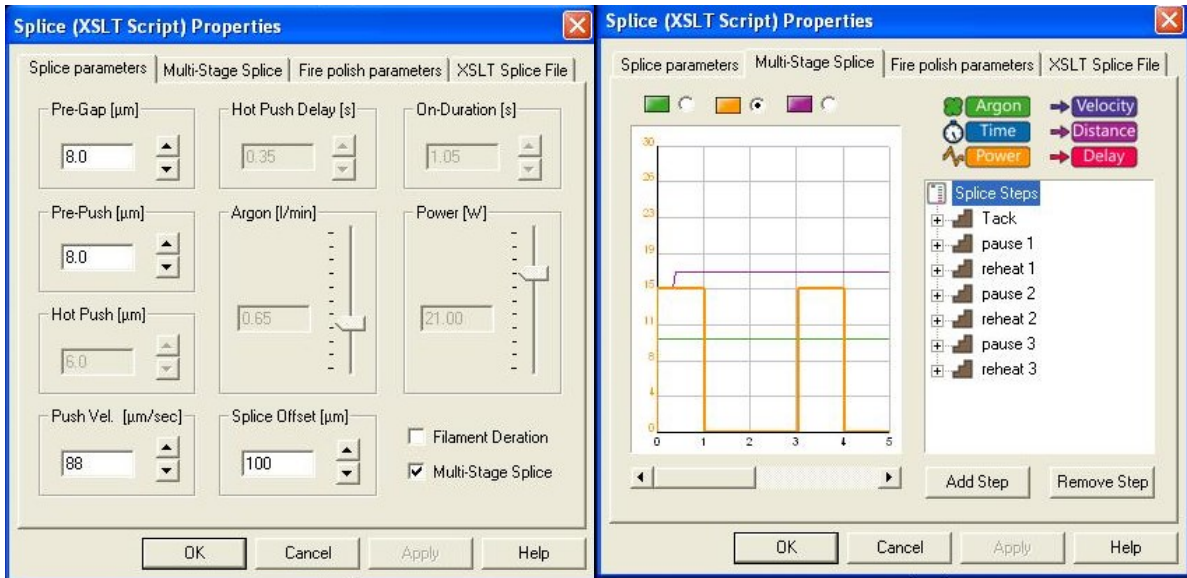
Fire polish:

- No "fire polish" when power is Zero. Normally this power is lower than splice power. In this process, you are scanning the fiber, moving the filament side to side on the sides of the fiber to clean off any debris, do internal expansion.
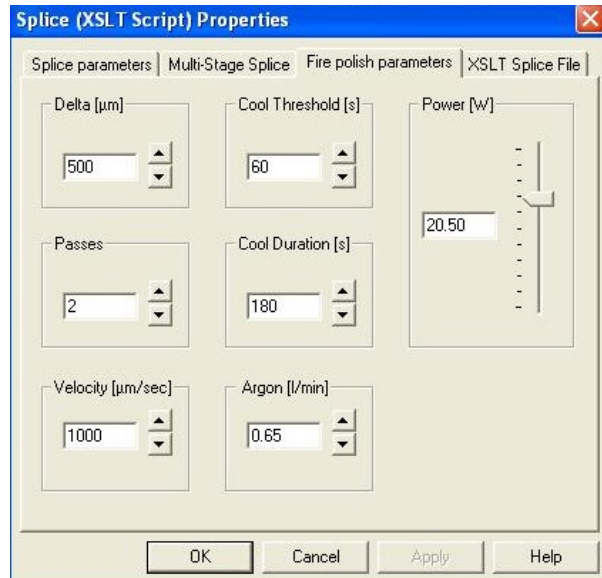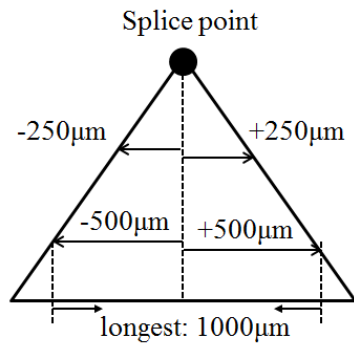
- Filament movement (Delta: 500μm, passes: 2):

  Towards left -250μm →right +250μm (1 pass) →left -500μm →right +500μm (2 passes)

  The longest distance should be less than 1000μm. If you only want 1 pass, the delta is normally

  at 900μm, and for three passes, set delta at 300μm.

- Cool threshold and duration: not sure anymore, filament will be on for 60s, and then turned

  off and cooled for 180s.

XSLT splice file: never change

  It is linked to running splice process, picking parameters.

  "FFS3 splice.xlst" C:\Documents and Settings\Application data\Vytran Corporation

PWM splice parameters

Inside multistage process, it is an alternative way to repeat the same thing. However, it is not going

to change any parameters, only to pause the filament on and off. It's an old way of FFS-2000 to

handle the same process as multistage. Not available in this FF3 version.

PM alignment settings

- These are critical for what's type of PM alignment during the process.

- Pre-defined setting for different standard PM fiber: panda (80μm), tiger, elliptical core, bowtie, and correlation algorithm (more complex, doesn't have to symmetric geometry).

- Select fiber type, and fiber diameter (you could use measurement guide to get this number), it will calculate the P1 (radius of stress rod-panda), P2 (radius of fiber center to the stress rod center).

-

-
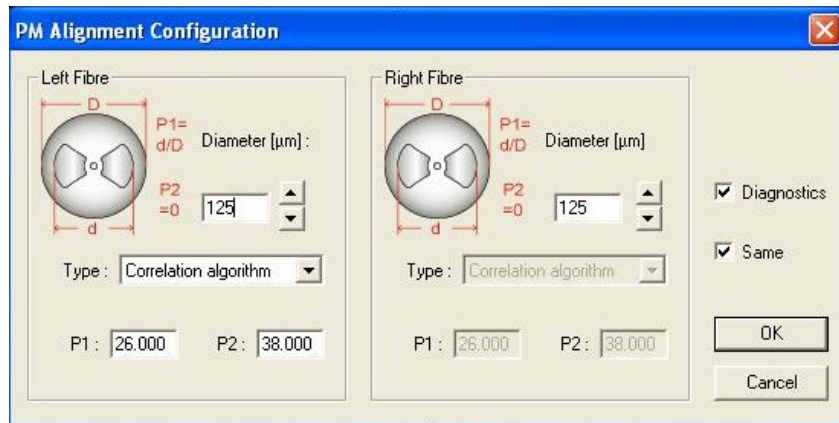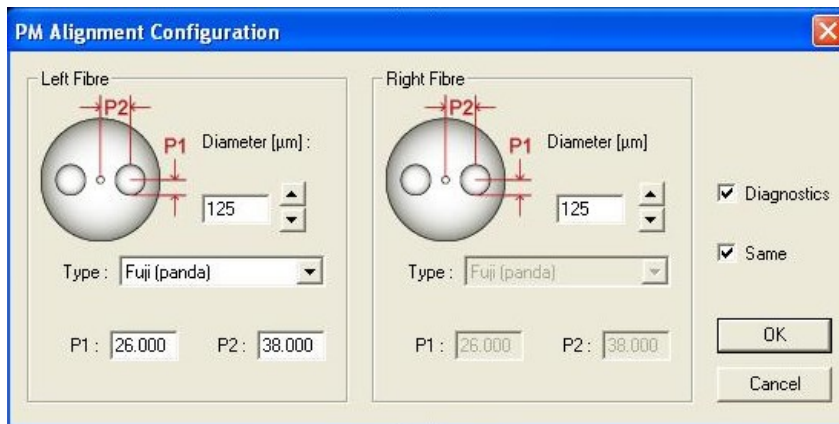
- Ex: If you want to splice a PM HC-PCF to PM panda, select correlation algorithm for left fiber and Fuji (panda) for the right fiber. You can go left view and right view for end alignment, and then edge alignment in back and front view.

Active alignment settings (not active in this unit)

- Analog feedback alignment, if you have a light source on one side, any grating interferes on the other side, feedback from meter (BNC connector to the unit). You can align the fibers based on the lowest loss measurement.

- The fibers will be gaped in back view; left fiber will offset (defined by software +30μm). First it will do edge aligned, and go offset 30μm. Then it will starts stepping down towards back to zero. To each step, pivot is moving, and each step is triggered by feedback from the meter. It records the pivot position and loss value from the analog loss meter. And in the end, it looks at the chart and find out the lowest loss and put the left fiber at that position.

- And in the front view, it will do the same thing. It offsets by 30μm starts stepping down to zero, record pivot position and loss, and return a pivot number.

- Fiber offset setting: where the offset starts with; scan step size (6.3μm): each step shifts X-μm towards zero. Interval: checking single every interval (60000ms).

Illumination setting

Loss estimation setup

- Loss estimation for specific types of fibers. Usually use SMF28 and panda 1550nm, Flex 1060nm is seldom used. Do not change focus offset.

- In the loss estimation setting, there is a calibration setting - an engineering function. It creates an image of the splice and recognizes how linear the splice is, what the detective core pattern is. Based on those, it will generate an update algorithm. Usually, you do this calibration for the change of lens' property, the CCD.

Splice process editor

A popup window will display the selected processes as well as the available processes. The selected processes are stored in the splice file (.ffs). It is important that the operator does not alter the process list as this will adversely affect the performance of the machine. It is intended that only advanced operators create special process lists.

There is the sequence of steps that the splice executes, each of them is macros and processes built in the program (sequence could be changed by drag and pull).
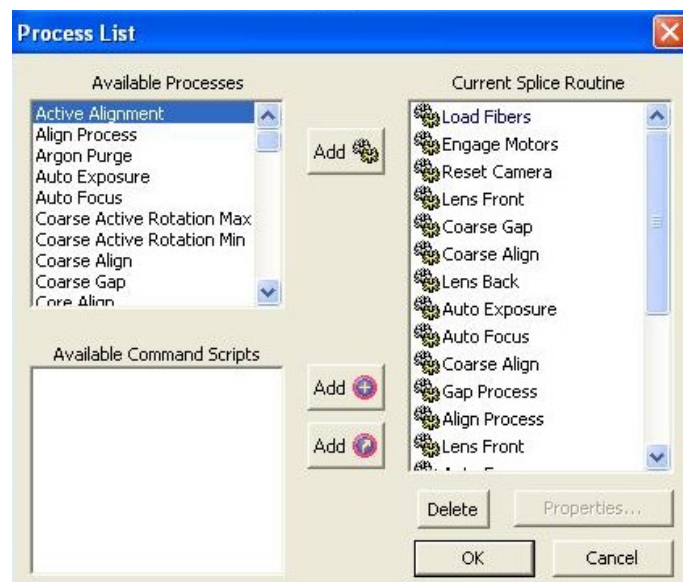
- Load fibers: splice head will move forward to the right because when you load fibers you want to make sure that filament only touch fiber ends, no touch on the sides of the fiber, bare glass.

- Engage motors: pull fiber back to make sure fibers do not overlap. Fibers won't pass the gap line.

- Post-splice tension: tension applied after splice. Auto splice has a tension to step the fiber. Or you can also add tension by moving FHB (1 or 2 medium steps).

- Reset camera: when splice is done, refresh the image and make sure the image is still alive.

- Filament normalization: checking how big is the area of the Q-tip - checking the balance between right Q-tip surface area and left area.

If the Q-tip of the left is bigger than the right one, it means the filament went all the way to the view of splice and stopped shortly, so the left side is too big and right side gets less heat. Based on the area size, it tells change the view-to-splice +10 steps. Next time may be the filament will go a little bit too far right side, and right side may be bigger than the left side, it will try to balance again.

+10 steps   Balance cube-tips and power offset
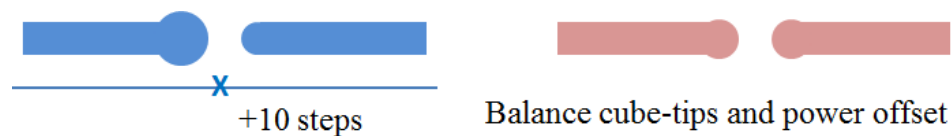
So, it's calculating the view-to-splice, and then at the same time, it's checking Q-tips total size, if it's too big, that means power is too much and it will increase or reduce the filament power offset (this offset will apply to filament power setting). This calculation depends on the age and type of filament. (24:45" - 31:10" File 43)

- You will need to change it when you need to create any new process recipe: save as a new file. Then first, adjust splice parameters, second, adjust splice processes.
- Ex: A "pre-alignment" file: in the back view, focus, align, gap; do the same thing in the front view, focus, align, no gap. You don't need to switch file, after aligning the fibers to the gap line, you could press the splice only button to splice fibers (refer to the edge alignment only recipe).

Multi-file splice setup

Similar to multistage splice, but you could call difference splice files. Link multiple files just like multistage: SMF splice file (change the parameters), after that open second splice file, when you

press the splice button, it will execute those two files. Or you could do pre-alignment first and then add a splice file.

Process libraries

Files are linked, should not be changed. If you are missing the files, you may not able to execute files. When you press the splice button, but nothing happened, this may be a problem. (Don't touch!)

Operator help text

Add custom prompts or operator. In the processes list, you can call for prompt, it will have notice.

Macro path

Two paths to link execute. (45:50" File 43)

Ex: Customize a cleave macro, if you have the rotation option for angle cleave, in this macro (motor 11 is the cleave macro), it is critical to maintain number of forward steps (1670) and return steps (1570). If they have the same number, the blade will go back to the home position. Do not need to use macro unless you need to customize macros.

Spice macro: should not touch.

Blade macro

- Service cleave blade.

Left side of the cleave arm, a small set screw holding the blade and apply pressure on the neck of the blade. Cleave blade has a round mechanism, if you loose enough the set screw, you could shift

the cleave blade sideways by rotating, and the cleave blade can spin to change the alignment of the blade.

If you need to change the blade, loosen the set screw then lift the blade. We use the edge of the cleave arm as a reference for the cleave blade to be straight. This will decide the cleave quality. If the blade is not straight, such as more gap on the top than the bottom from the edge line, you will have high cleave angle and may damage the blade very quickly, more contact on the sideway.

- Cleave home. It moves cleave blade forward and returns back to look for the home sensor.
- All home to shim: for service.

If the reset fails, you could the cleave macro for cleave verify. If the cleave macro works, then you could touch to the all home to shim and execute, you will see the change of lens position, focus, then splice head, to make sure all the three motor are able to home. If not, it will fail this macro as well, and indicate which one fails.

Sequence: lens →focus →splice head (Different from reset: lens →splice head →focus)

Set-up Post-splice tension:

Tension applied after splice. Auto splice has a tension to step the fiber. Or you can also add tension by moving FHB (1 or 2 medium steps).

After splice, post-splice tension, lens back.

D.2.7 Proof test

Setup

Scales: pounds, psi. Timeout (10s): how long it ends before fiber breaks. Then tension reaches a

peak level and holds 10s. Fiber diameter: does not affect the results, just for you knowledge.

Prove test reading

Reading

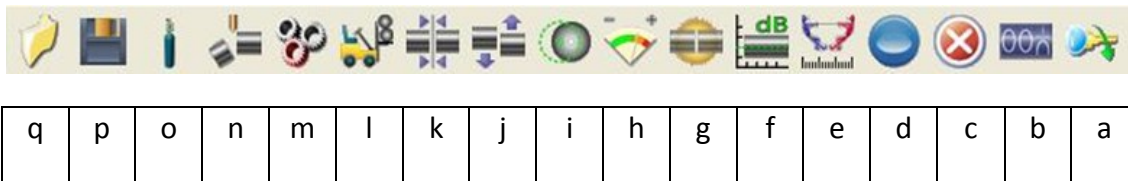Database for qualify the splice.

D.2.8 Recoat

Cure duration: how long the UV is on. SMF splice: 12s. If the lamp degrades, increase the UV

time.

D.2.9 Reset & Execute:

They are the same thing as the process toolbar.

Icons on the process toolbar:

q	p	o	n	m	l	k	j	i	h	g	f	e	d	c	b	a

Left clicking the icons will run the command. Right click will bring up the command's parameters.

a) Initialize: use it when you first time turn on the user interface.

b) Reset: initialization.

c) Stop: stopping any auto process, however try to press it when no motor is moving or least of

amount of motion happens at that moment. It's better to stop during the alignment or gaping

before motors are traveling to splice position. If the motors start moving, just let it go, unless

they are really expensive fiber. After the stop, redo the initialize, reset instead of continuing using.

d) Splice: execute the entire splice process (align →gap →splice), different from splice only (no align and gap).

e)

f) Loss Measurement

g) Splice only (no align and gap)

h)

i) Core alignment: align the core instead of edge alignment.

j) Alignment: edge alignment.

k) Gap: bring fiber to pre-gap position.

l) Load fiber: send splice head to view-to-splice position and back to home. You could use this to make use the splice head comes back.

m) Engage motor: pull back fiber.

n) Cleave: runs cleave macro.

o) Purge: purge for gas.

p) Save: save and overwriting the current file. (1:03:14 File 43)

q) Open file

For tracing what's doing in splice, take screen capture for all information (file name and date).

D.3 Workstation Maintenance

D.3.1 Stripper

1:10:19 File 43

- TMS (thermal-mechanical-stripping) blade, the offset between the top and bottom blades is critical, and it is typically balanced by shifting the top insert sideways. The fiber curls between the blades and strip the coating without too much contact to the glass. If the gap between the blades is less or more, you will have poor stripping. Either will bite the fiber or break the glass. After you close the lid, if it's too less on one side, the other side will be shifted too much and will not strip the fiber at all. This gap has to be balanced.

- Alignment of the blade: from the back of the lid, lid has three holes with set screws (.035" Allan key, only turn 1/2 turn for adjustment). If too loose on the left side, this means the gap is too much, you need to move the top inserts to the right. When you do the alignment, make sure the lid is closed property. To check: put a small piece of thin shim in and close the lid, make sure the lid could grip the shim (on both left and right side). When you tighten those screws, tighten the one in the middle.

Permanent TMS (thermal-mechanical stripping)

Set screws on the back of the lid
(0.035 Allan key, ½ turn for adjustment)

-
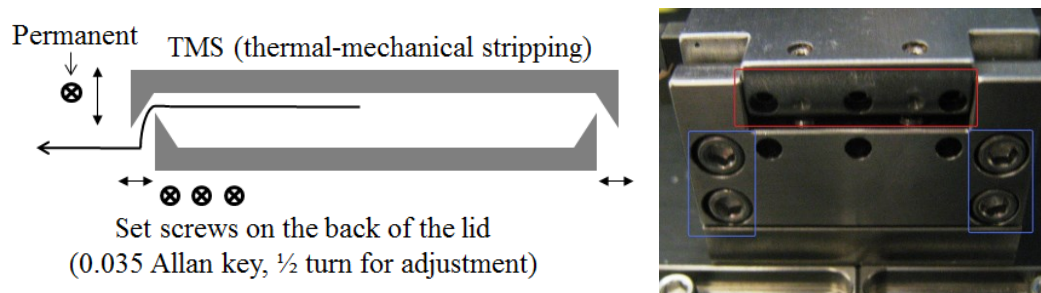
- Never touch the side screw holding the top inserts, this screw is glued in and permanent, determines the height of the blade (vertical, no spin).

- If the lid is not flat, this may affect both stripping and cleave (ex: cleave angle > 0.4). To adjust the flatness of the lid, use 3/32" Allan key to adjust the four set screws behind the lid, those are the screws to hold the lid. When you loose those screws the whole lid will be loose, make sure you do shift the lid sideways. Apply equal pressure front to back, just cracking them to loose, then tighten them and check with the slim again. If there is any debris in the inserts, use acetone and toothbrush to clean (do not touch the cleave blade).

- The magnetic force on the lid will hold the fiber for cleaving. When you turn on the vacuum, there will be vacuum on both TMS inserts and FHBs.

- Fiber stripping: when you put the fiber for stripping, make sure the fiber end in the gap between the blade and the inserts. Close the lid, pull the FHB straight back gentle after 2-3s. If there is any hesitation, the insert will contact the glass, put the fiber back and strip again.

- Tension on FHB: 200-210 gram for SMF-28 (refers to splicer workstation-stripping and cleaving station end at 1:33:50 File 43).

D.3.2 *Argon flow rate*

- Make sure argon is flowing. 0.15*l/min*: pressure set at the tank is 9-12 psi (using 11 psi). Right click on the argon purge icon or select the argon flow rate in the menu to change the flow rate. The output gauge should be never below 9 psi, if there is any leak on the low side -back of the splicer, inside the splicer, when you purge it, the output gauge may drop below 9 psi.

- A needle valve is electronically controlled for X amount of movement for flow rate setting. If the gas is sticky because of contamination from the gas tank, moisture, or poor gas less than research quality (99.995%), it will corrode the needle valve. Every time when try to open it, it will have a fault, basically changing the flow by this needle, as soon as the needle is going

to purge, it pop open too much. And next time when you go from 0.15 to 0.65 for splicing, it may go above 0.65 *l/min*, affects the splice by vibrating the fiber and cooling off the filament.

D.3.3 Replace filament

a) Turn power off

b) Raise the splice head cap.

c) Loosen the set screws on the filament extraction tool using a 0.035" Allen wrench.

d) Locate the slotted end of the extraction tool over the filament in the splice head. Tighten the set screws on the extraction tool.

e) Gently lift the filament out using a front to back rocking motion.

f) Remove the filament from the extraction tool by loosening the set screws.

g) Covering the splice viewport, clean the filament channel using canned air.

h) After replace the filament, use command "setfilamentage[0]" to reset the filament time. It won't be zero until next burning. Use file "burn in (20s, 21W)" to burn the filament after replacement (no fiber, Argon flow rate 0.65 *l/min*), cool for 5-10s and burn one more time.
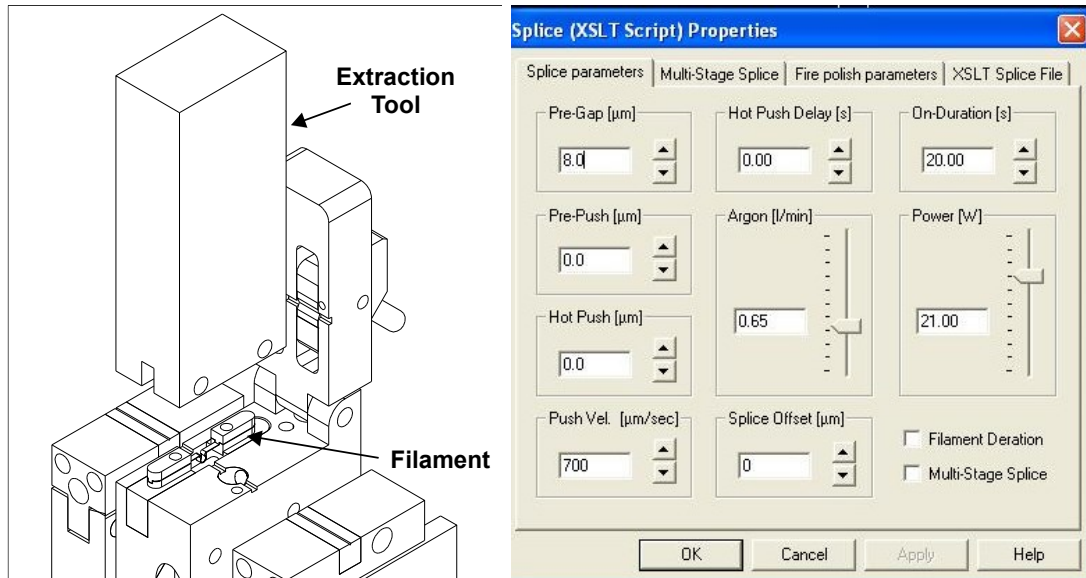
**Figure from FFS-2000 Fusion
Splicing Workstation official manual**

D.3.4 Recoat
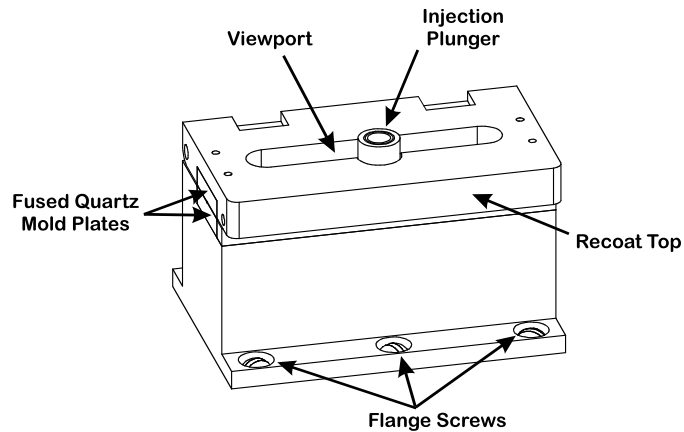
Figure from FFS-2000 Fusion Splicing Workstation official manual.

Refer to the chapter 6 on the splice manual.

- Use acetone and KIM wrap to clean the mold plates, do not use too much. Otherwise acetone

  may go around the edge of the plates, behind, front or underneath. It may shift the blade side

  to side, and tilt the plates. The plates are floated by a little cushion and around by small rubber

  O-rings.

- Unscrew the six flange screws to remove the recoat station and send back for repair if needed. Disconnect the six screws and remove the injection head from the top, and hold the whole mode out.

- Make sure you put gloves on when you are cleaning the lamp.

- When you put the recoat station back, make sure the long side of the post inserts the station.

- The sequence of tightening screws: outer screws →center screws →outer screw... Don't be too tight - all the way down then half-way back, otherwise may damage the mold plate.

- If an air bubble gets trapped within the syringe, turn the syringe upside-down for several minutes to allow the bubble to rise to the tip. Gently push in on the plunger to force out the air bubble.

- Do close the mold plate when the fiber is still loose. The default recoat time is 15s, on panda PM, you can use 20s. When the recoating is done, open the FHB first.

- To determine how good is the recoating, use a microscope and check the eccentricity of the glass.
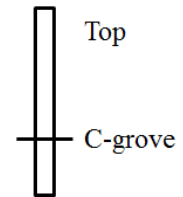
D.4 Standard Operation:

1. Turn-On Procedure

- Open Argon gas valve. Before turn on the unit, make sure argon is flowing - the out gauge of argon regulator is ~11psi. Make sure to open both large and small valve.

- Turn on computer

- Turn on both vacuum pumps (orange pump and the floor cleaning pump)

- Turn on camera light

- Turn on FFS-2000 unit (make sure compute has booted up first)

- Run FFS-2000 software on computer

2. Initialize

Required once a day. First thing to do when you turn on the user interface, use the Initialize button on the process toolbar. **MAKE SURE THE TRANSFER JIG IS IN PLACE WITH THE FIBER HOLDING BLOCKS (FHB) IN THE TRANSFER JIG.** After initiation the positions should be as shown below. This is the standard positions after Initialize and Reset.
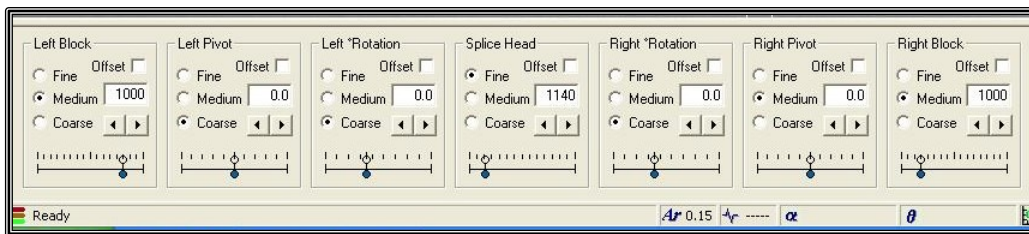
Standard Positions For Fiber Holding Blocks

3. Reset

Required once a day and after EACH splice. Make sure the FHBs and Transfer Jig are

engaged in the Splice Station, then press Reset button on the software process toolbar. A safe range for the left block is 900 – 1100.

4. Check V-Groove Size and FBG Tension

The Normalization procedure will use SMF28 fiber to set the filament power. So the FHBs must be set hold and cleave SMF28. The 250 μm v-groove must be used for both FHBs. The tension should be set to 205 - 210 grams.

Changing V-groove

> 1. Remove FBH from Transfer Jig and open fiber holder lid

> 2. Remove the two small screws that hold the V-groove. Securely store the screws.

> 3. Using a small screwdriver, pull the V-groove out by pulling on the screws thru hole. Put the old V-groove away

> 4. Insert the new V-groove using a screwdriver thru its scree thru hole.

> 5. Replace the screws but do not over tighten them

Check and Set FHB Tension

> 1. Remove FBG from Transfer Jig and put in stripper slot.

> 2. Place Mitiutoyo Force Gauge as shown, making sure that only about 1 mm of the gauge handle is in contact with the FHB. The height the gauge is to be applied should be parallel to a horizontal notch in the FHB.

173
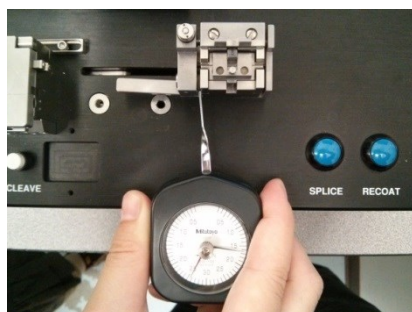
3. Apply pressure on the Force Gauge to approximately 220 grams

4. Apply rocking motion on top of FHB, with finger on fiber holder. If the Force Gauge

tension is too high, the number on the gauge will not move. Reduce tension on gauge till

the rocking causes the dial gauge to move. A correct Force Gauge measurement will

cause the needle to move only ±0.1 gram.

5. If tension is at 205 – 210 grams, this is good for SMF 28 fiber. To increase the tension,

turn the set screw on the FBH as shown. One complete clockwise turn increases the

tension by 40 grams.

6. Check tension once set with Force Gauge.

5. Normalization

- **Required once day in order to set the filament power.**

- Normalization maximizes the splice strength, it will add an offset to the splice power, within ±5W, and this offset-power will apply to all other splice files. The normalization procedure file is "F35-2520-C Normalisation_125 16Apr10.xml". Use SMF28 fiber. If working in the same power range (16 -22W) for different fibers, you do not need to re-run the normalization procedure.

- The normalization procedure applies heat to two cleaved SMF28 fibers. A splice is not made, but the two fiber ends become like round 'Q-tips'. The shape of the Q-tips is

measured and the power is changed accordingly.

- The normalization procedure is run using the Spice button (which performs an auto splice). **Please read the auto splice procedure before proceeding.** The details of cleaning, cleaving, and loading the fiber can be found in the next section. Place the Transfer Jig in the offset position and push the Spice button. The program will tell when to load fibers and the final Q-tip tolerances. If the auto align fails the normalization procedure can be run as a manual splice.

- Tolerance acceptance: ±2% (98~102%). It may take up to four attempts to reach the correct tolerance acceptance.

5. Perform Splice

Auto splice procedure

- The auto splice procedure is used for splicing SMF28 and Panda PM fiber:

  SMF-28: "F35-2520C SMF28-SMF28 27Mar09.xml" Panda PM: "F35-2520C 125um Panda 125umPanda 27Mar09.xml". Auto splice is also used for the Normalization procedure.

- Clean and strip fibers. Place fiber in FHB v-groove. Open stripper/cleaver lid, place FHB in stripping guide while laying fiber in stripping v –groove. Make sure the tip of the fiber is between the two blades on the opposite end of the stripper. CAREFULLY close lid, wait till heater light is completely red, and pull FHB away from stripper while in stripping guide. Open lid and clean with vacuum.

- Clean and cleave fibers. Move tension arm of fiber holder to 90 degrees. Open stripper/cleaver lid, lay fiber in cleaving v–groove making sure enough fiber is in the v-groove. Close lid, move tension arm to 180 degrees and press the cleave button on the splicer. Open lid and remove fiber shard.

FHB 180 Degrees (under tension)

FHB 90 Degrees (no tension)
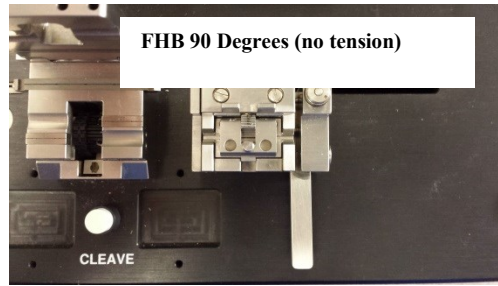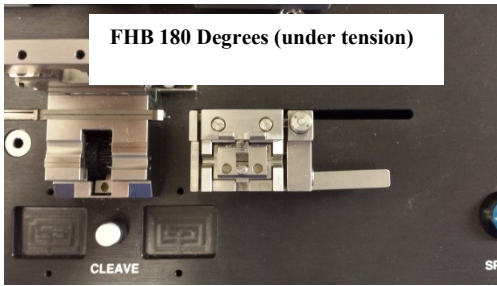
- Place Transfer Jig in offset position (not in holes) and place fiber holders in transfer jig. Ensure they are properly fit.

Transfer Jig Offset Position

Transfer Jig Load Position
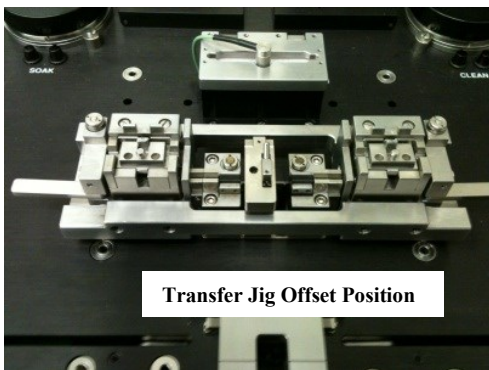
- Open Splice Properties (from the 'splice' pull-down menu) and ensure the values are correct (see below sample below).

- Open Splice Process and check the splice process.

- Check motor position and compare to numbers below. If not repeat Reset
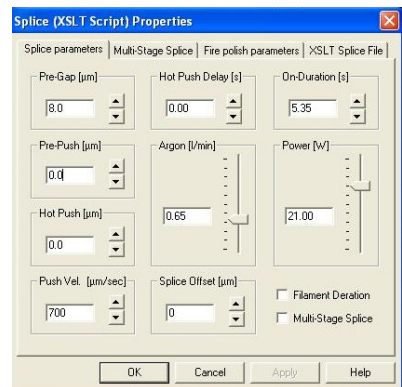
- Press the "Splice" button on the toolbar (NOT the "Splice Only") and follow the instruction provided by the software. DO NOT load the fibers (place Transfer Jig with FHB into jig holes) until the program tells you to.

- When you load the fiber, open the Splice Top, make sure the FHB and Transfer Jig are engaged, and the fiber is properly set in the graphite holder and metal v grooves. Close the

176

Splice Top and the Mirror Toggle is in Side View (away position)

Side View Position   **End View Position**

- Let splice procedure run. DO NOT hit Stop on process toolbar when the motors are moving.

- If the PM Panda routine is run, follow the instructions to set the Mirror Toggle when directed.

- If splice is final step, remove fiber from holder while the Transfer Jig is loaded.

6.   Manual splice

- Prepare fibers as done above (strip and cleave)

- Place Transfer Jig in offset position (not in holes) and place fiber holders in Transfer Jig.

- Load the fibers by the Load Fiber button on process toolbar.

- When loading, open the Splice Top, make sure the FHB and transfer jig are engaged, and the fiber is properly set in the graphite fiber holder and metal v grooves. Close the Splice Top and ensure the mirror toggle is in Side View (toward you)

Steps for non-PM fiber:

- Make sure fiber targets in back view: then click Exposure Level (auto illumination), Focus, Gap , Edge Align ;

- Switch to Front view. Set Exposure Level, Focus, Edge Align; Do not Gap in front view.

- Then switch to Back View again and then Edge Align;

- In Back View push Splice Only button on process toolbar (make sure fiber in the gap line).

Steps for PM splice:

- Pull back (or use Motor Engage once), go to Left View, Exposure, Focus, Rotate (remember the way you choose the orientation in the left view and mimic that on the right view, you could use the cleave marks and the stress rods).

- Repeat in the Right View, Exposure, Focus, Rotate;

- Switch to Back View, do Gap and Edge Align;

- Switch to Front View: Edge Align;

- Switch to Back View: do Edge Align again,

- Push Splice Only button on toolbar. Good splice: extinction ratio 34-35+ dB (auto PM splice, manual splice may be 5dB lower)

7. Turn-Off Procedure (end of day)

- Close FFS-2000 software

- Turn off FFS-2000 unit

- Turn off camera light

- Turn off both vacuum pumps

- Turn off computer

- Close both Argon gas valves.

D.5 Specific Splice Recipes

D.5.1 EDF (Er110) to SMF-28

- Put the critical fiber (less stable) on the left, the right fiber (normally SMF) will be pushed to the left fiber.

- Different methods are used depending on how the core of different fibers matches. If you are trying to splice the EDF (Erbium Doped Fiber) to SMF-28, since the EDF has a smaller core size than SMF-28, fire polish is used to scan the splice area (thermal expansion) back and forth to expand the EDF's core to match the SMF-28.
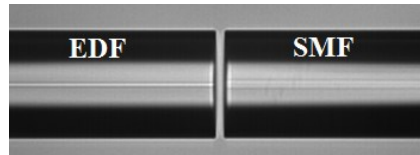
> If only EDF core is expanding, create a splice file and do fire polishing on the splice area; If both cores are expanding, fire polishing the fibers first, then create a splice only file to splice the core expanded EDF to another SMF-28.

Process to create a new splice file (Er110 to SMF-28):

1) Normalization.

2) Starting from a standard SMF file, splicing without fire polishing. (During the training, the cleave parameter is changed: left 2170, right 1490 - 1480 is too long, and 1500 didn't work).

Loss estimation and post splice tension processes from this splice routine.
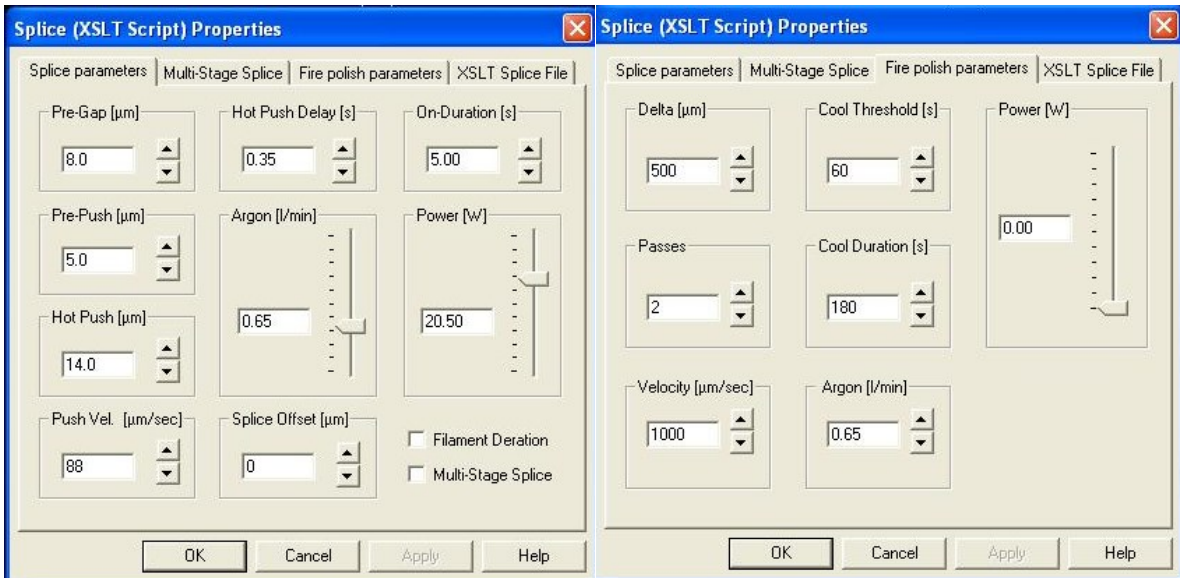
Splice image (after this splice 1): a small amount expansion on the EDF core, but no clear expansion was observed on SMF-28.

This tells us the EDF core expands fast in 5 sec, and we want to split the splice and fire polish process to tell when the expanding happens. After this splice, the EDF core is still smaller than the SMF, so you need to fire polish this splice area.
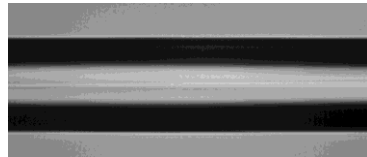
3) Fire polishing to expand the fiber core more:

- The power of fire polish (21W) > splice power (20.5 W) to apply the same amount of power of fiber since the splice head moving more distance and faster.

- Fire polishing always starts at max velocity: 1000μm/s, it's easier to increase the number of passes and decrease the delta to have more heats. If the heating is still not enough, then you could decrease the velocity.
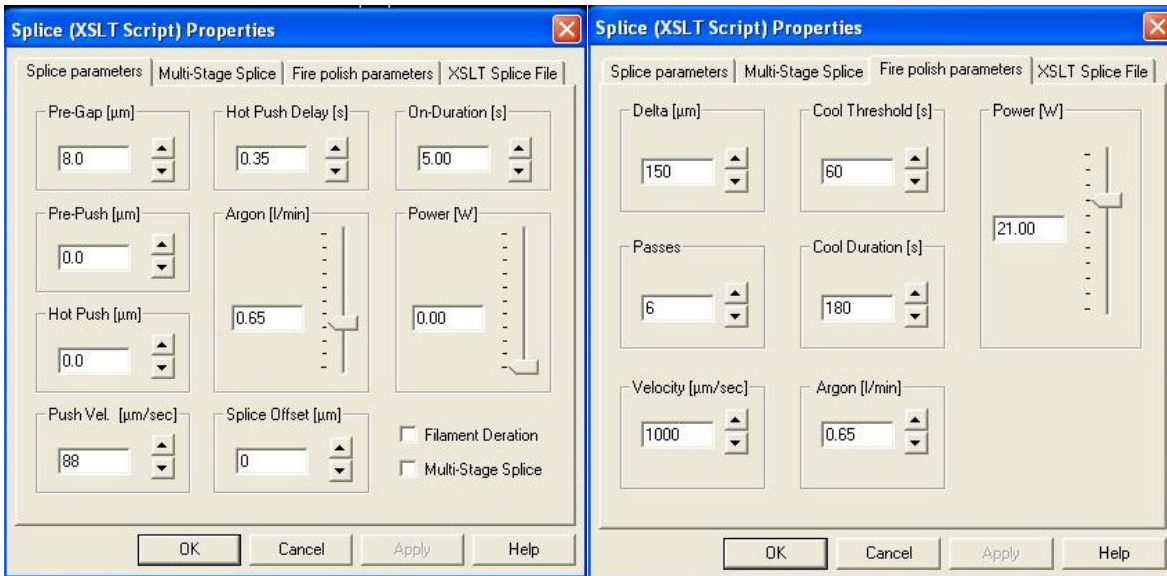
- Image: fire polishing x1; the core size of EDF keeps expanding, but it's still smaller than SMF.

This tells us we need a total fire polish distance (more passes, more expansion on the fiber core). To figure out how much total fire polish length, repeat this fire polishing process. Images: after 2nd and 3rd fire polishing.
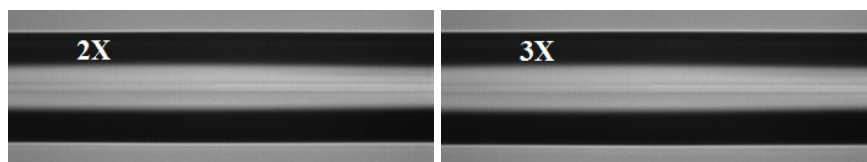
4) After the splicing process and three times fire polish process, the core of EDF almost matches the core of SMF-28. Creating a single file to splice EDF to SMF-28 based on the parameters on the splice and fire polish.

To determine the "fire polish parameters" (the same amount heat goes to the fiber):

A simple calculation: $\frac{3}{1}$ (times) $= \frac{9}{6}$ (passes) $\times \frac{1000}{500}$ (speed), delta $\times$ passes $= 900$

Times to run fire polish	3x	1x
Delta (µm)	150	100
Passes	6	9
Speed (µm/s)	1000	500

Final file:
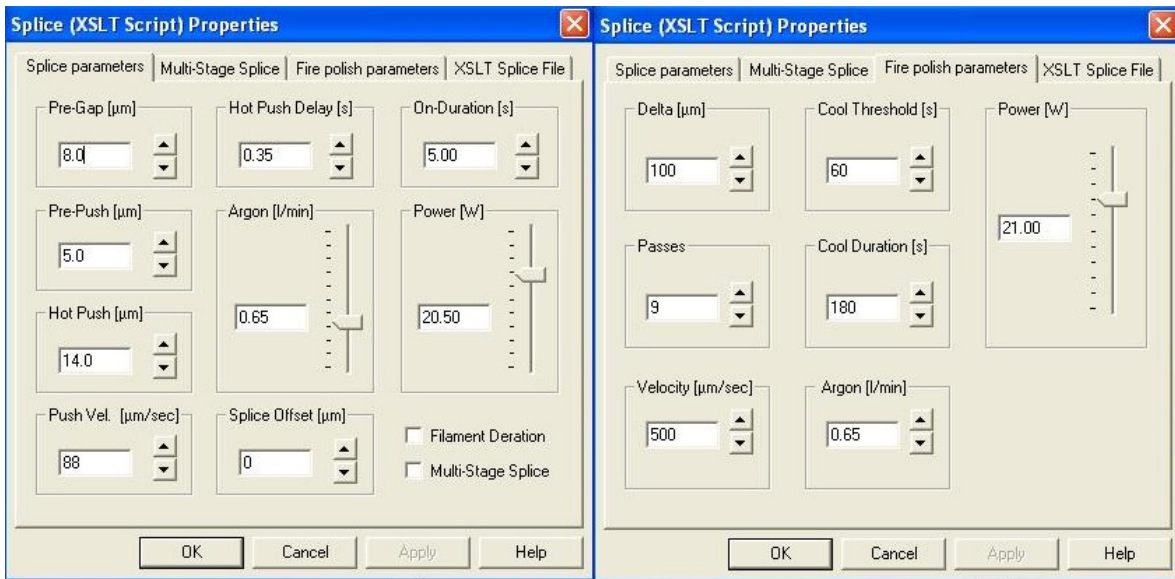
Splice (EDF-left to SMF-right) before and after using this created file:

(F35-2520C Er110-SMF28 - Splice 2 - with FP - 30May12)
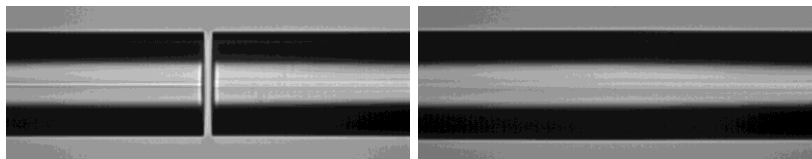
Estimate the loss by the software: 0.079 dB.

Please remember add post-splice tension to the splicing process, tension the splice to prevent

fiber from touching the tip.

D.5.2 PCF (PBG 10μm) to SMF-28

- To cleave the PCF, the tension on the FHB has to be reduced to 115 to 120 gram.

- To splice to PCF to SMF: tack and reheat, and offset on the SMF side 100μm. No fire polishing, because during the scan in the fire polish process, the holes of PCF may collapse.

- Before the splice, clean the PCF using file "F35-2520C PBGF Cleaning 30May12".

- Setting: pre-gap huge (30μm), so the heat will go to the middle. On-duration: 1s; power: 13.5W (14W will collapse the fiber core a little; 13W is enough to get rid of all particles).
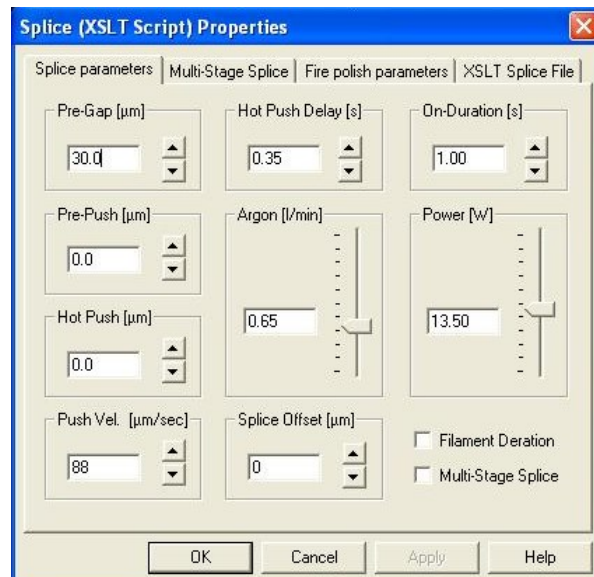
1) Starting the file (parameters in this file is from solid-core PCF recipe - PCF to PCF): Remove loss estimation and post-splice tension, add lens back.

"F35-2520C PBGF-10 SMF28 - Splice 1 - 30May12"

Critical: splice offset: 100μm.

Pre-gap: 8μm shows in the software, actually it is ~10μm (number could be found in notification viewer)

Push velocity: 88μm/s <100μm/s
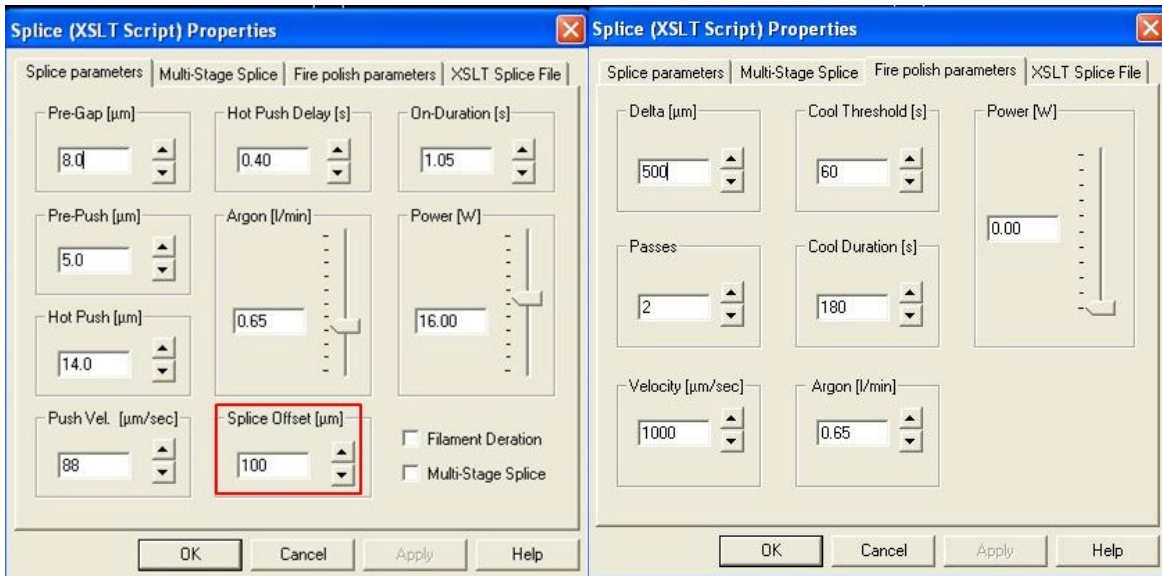
Images after splice (PCF to SMF-28):

Splice, pull back to break, left view (PCF side), right view (SMF side)
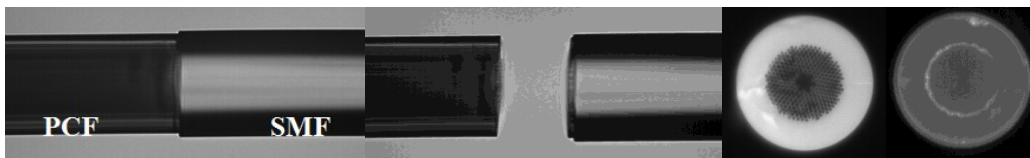
From the figures, the out layer collapse, and the center core seems bigger, may the surrounding comes apart (heat or the tension and torsion), this is too much for the first tack, so we need to reduce the splice strength:

- Reduce the splice power;

- Reduce the hot-push delay time (or increase the velocity);

- Put the fibers closer (pre-push), push them less (hot-push).

2) Splice 2: "F35-2520C PBGF-10 SMF28 - Splice 2 - 30May12"

To reduce the tack strength, back of power for 1W.

Increase the pre-push by 3μm, hot-push should be 11μm, but during the test we have seen it jumping 4μm, so the hot-push back to 6μm here.

Pre-push + Hot-push ~ 14μm, and hot push delay (s) is always the last thing to change.

184
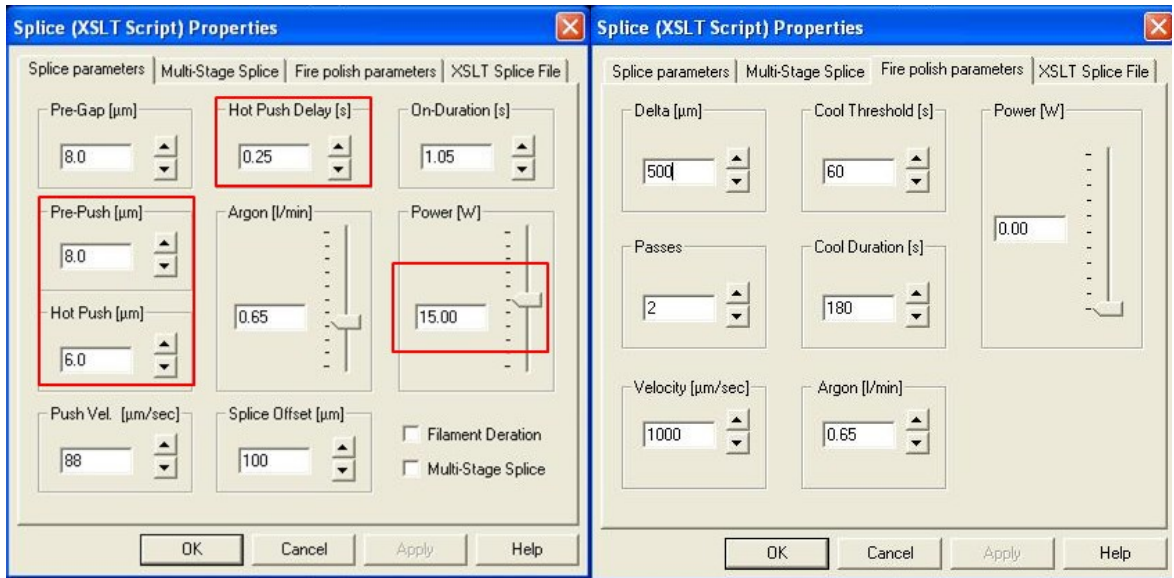
Loss estimation: 0.5dB.

Image after splice:
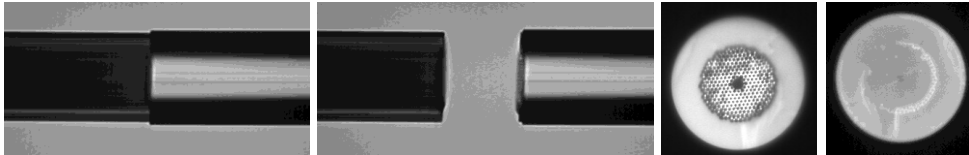
The best way to analyze is to do the splice, and cleave 10-20μm away from the splice position to say if the core still collapse.

Cleave mode#: LDC-400 (LDC-200 in training)

3) You can also create a multi-stage splice for splicing PCF to SMF, please refer to the section: "Multi-stage splice" in this manual.

Final recipe: splice 2 & reheat 1.

D.5.3 PCF (PBG 20μm) to SMF-28

1) Splice 3: "F35-2520C PBGF-10 SMF28 - Splice 3 - 30May12"

"Hot-push delay" is increased to 0.35s. Tension on FHB is 120 gram (4.5 turns counter – clockwise from 210 gram)
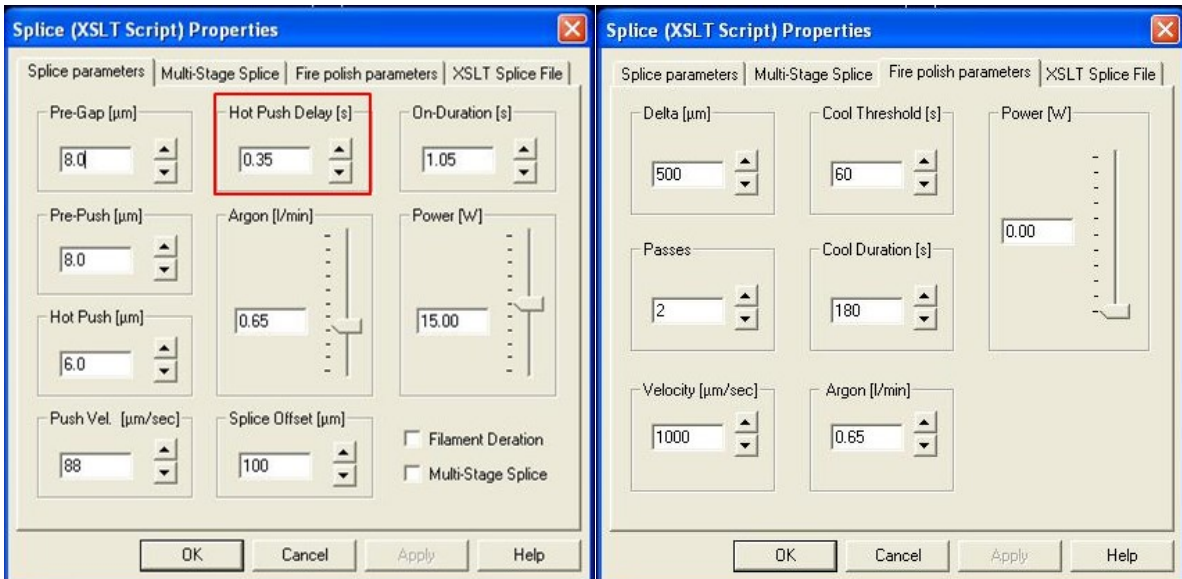
Image after splice:
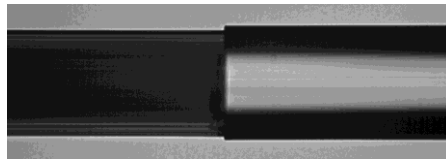
Create a reheat file to increase the splice strength.

2) Reheat 1: "F35-2520C PBGF-10 SMF28 - Reheat 1 - 30May12".

Use the same power as splice3 file, and no pre-push and no hot-push.
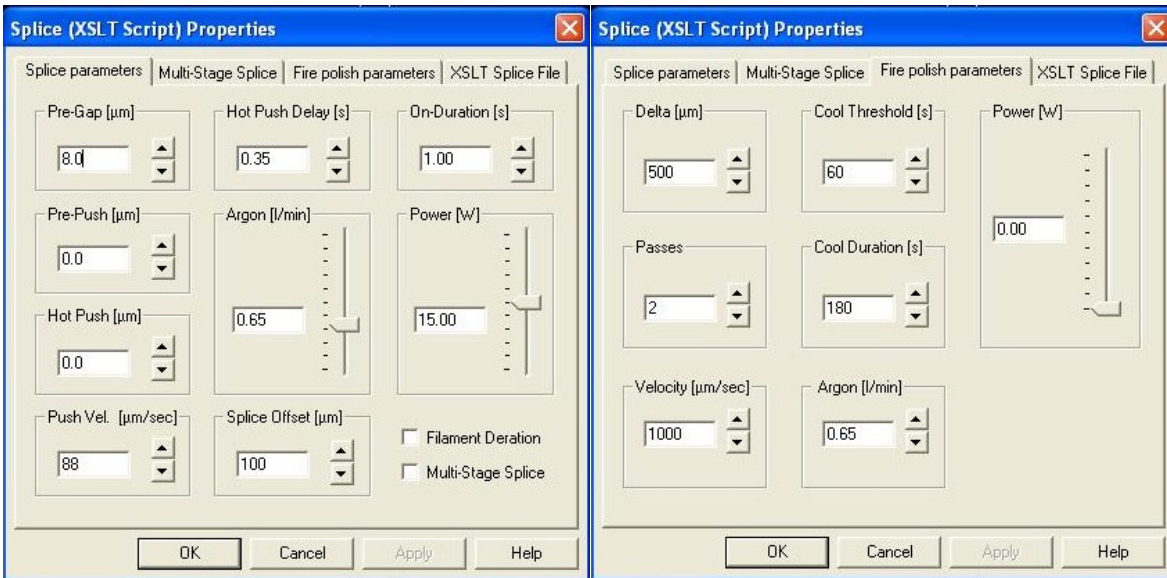
Image after reheat1:
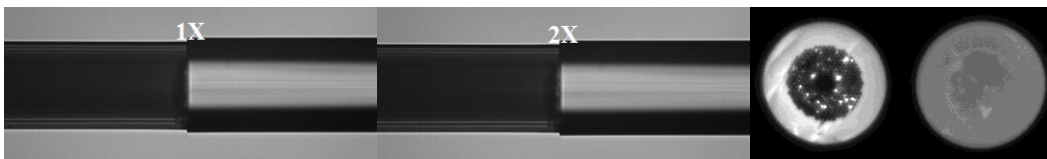
Then break the splice by pull back the fiber. After the reheat1 process, you could increase the power to 17 W to make the splice stronger - recipe "Reheat 2."

3) Reheat 2: "F35-2520C PBGF-10 SMF28 - Reheat 2 - 30May12"
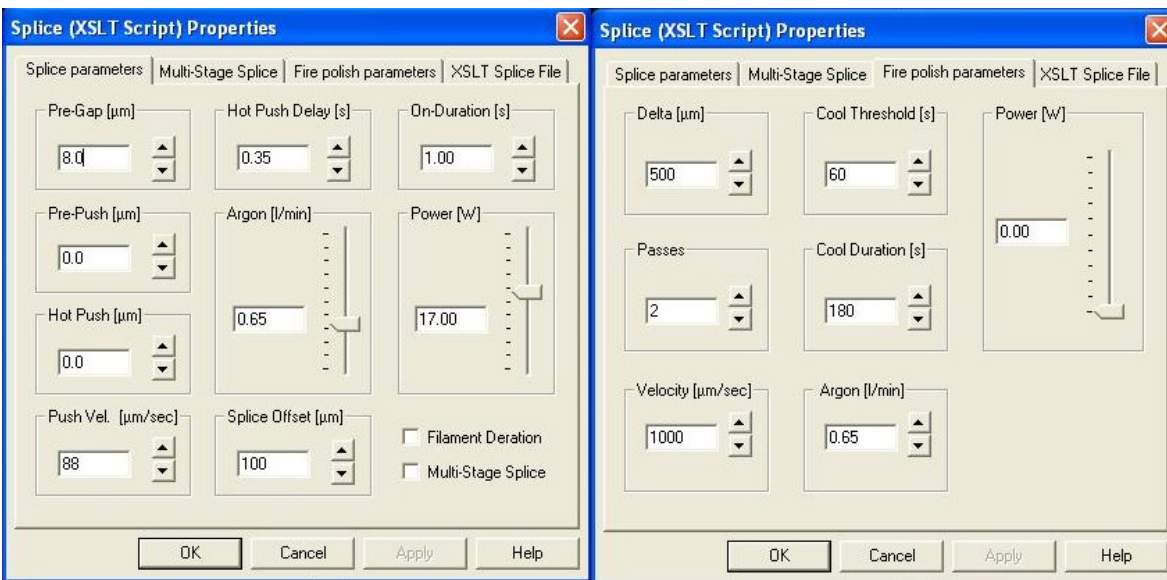
Image after reheat 2:
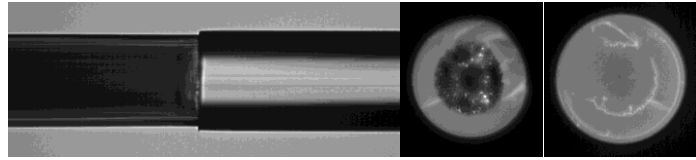
Final recipe: splice 3 & reheat 1. (Reheat 2 may collapse some outer layer holes)

Cleave with FFS, splice and reheat, it requires to pull 150µm back to break the splice.

D.5.4 HNLF to SMF-28

During the training, the inserts on the left FHB is changed to 135µm to hold HNLF.

Need overlap for HNLF to SMF-28. Otherwise if you only tack it, you will end with solid to solid.

1)   Splice 1: "F35-2520C HNLF-SMF28 - Splice 1 - 30May12"

High Power & short time; Overlap is reduced by 2µm (14µm→12µm)
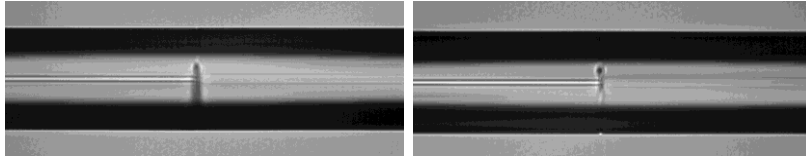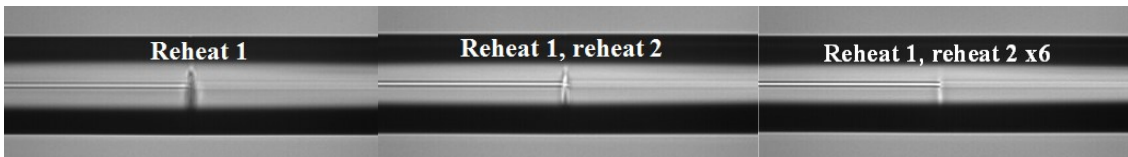
No fire polish, 21.5W just a starting point.
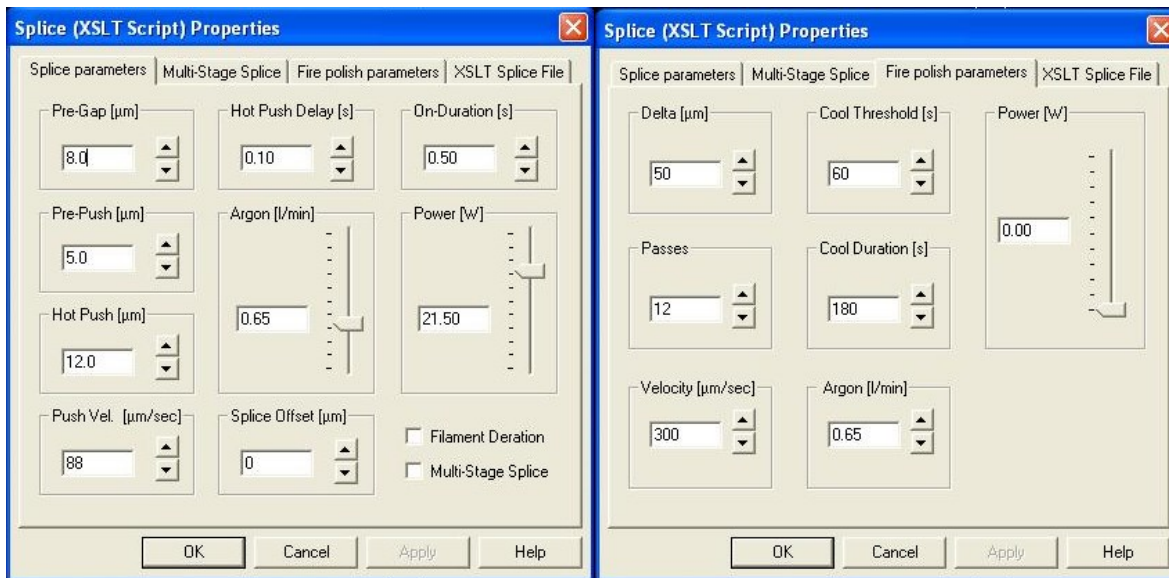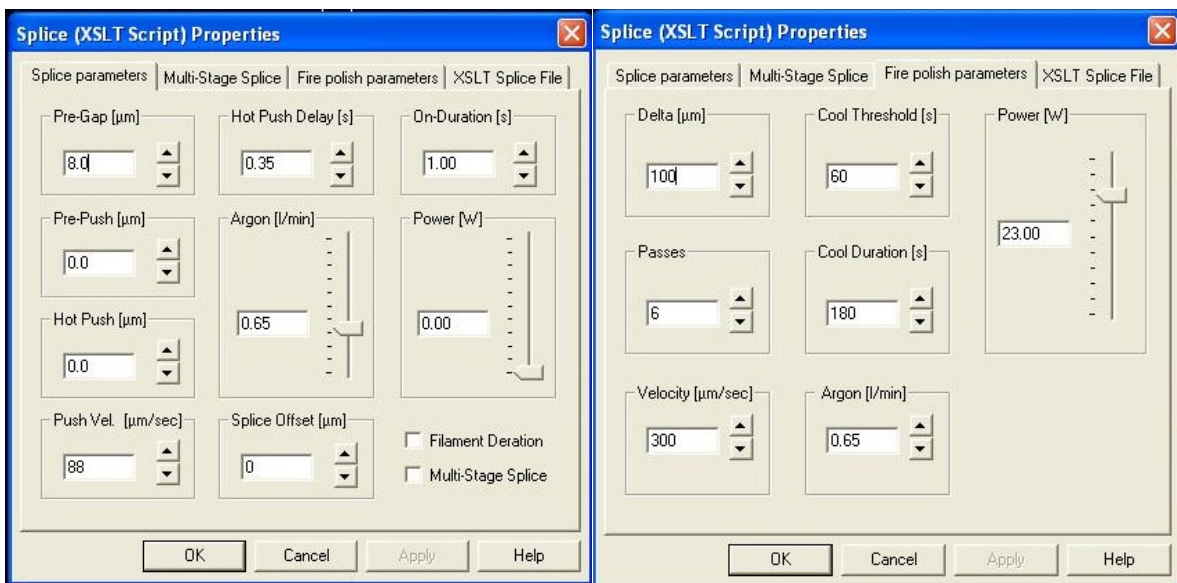

Image after splice: (back view and front view)

The defect is around the fiber, something outside. Create reheat recipe to expand the core.

2) Reheat 1: duration 1s, power 19.5W; reheat 2: duration 1s, power 20.5W.

   Image after reheat:

3) Based on the reheating process, create a fire polish recipe.

Fire polishing time: (100+**200**+300+400+500+600)/300= 7 sec (total reheat duration)

Power increased to 23W.

Use the same splice and use the fire polish. Cleave position is ~60μm from the center.

4) Combine the splice and fire polish recipe -"Splice 2", splice power and On-duration is increased. Fire polish delta is half, and passes are doubled to have more heat near the splice point.
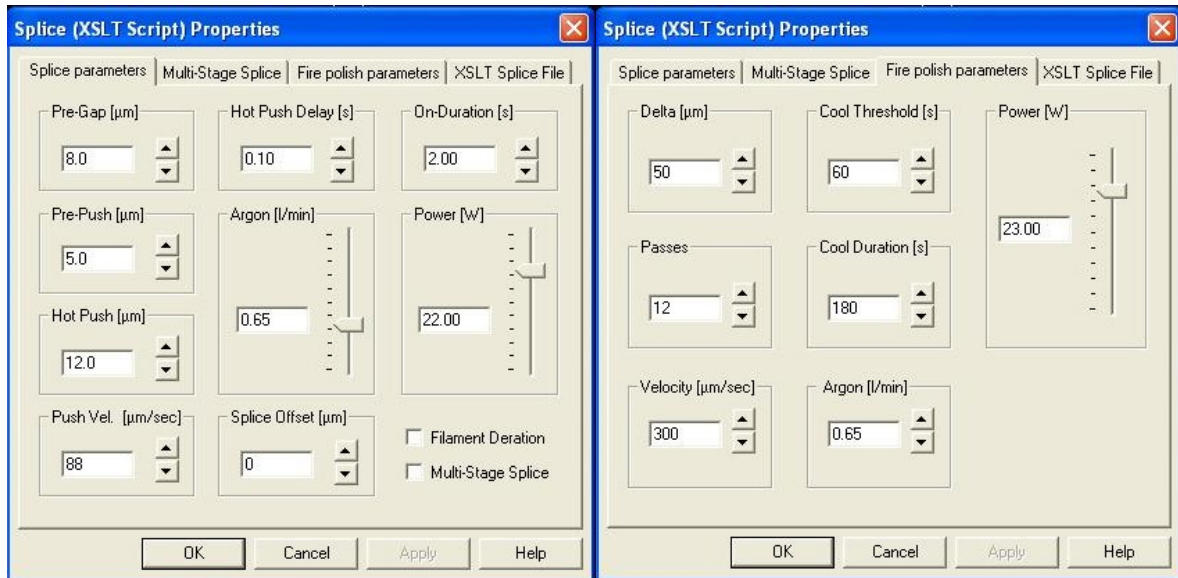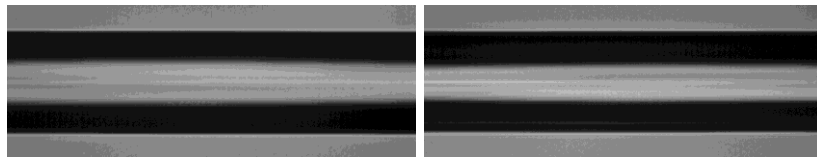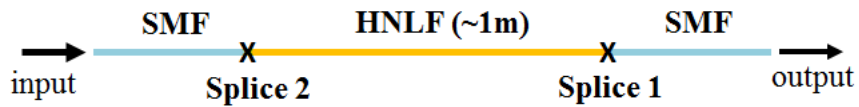
189

Image (back view and front view):

5) Final recipe: Splice 2 (with fire polish) or splice 3 (without fire polish).
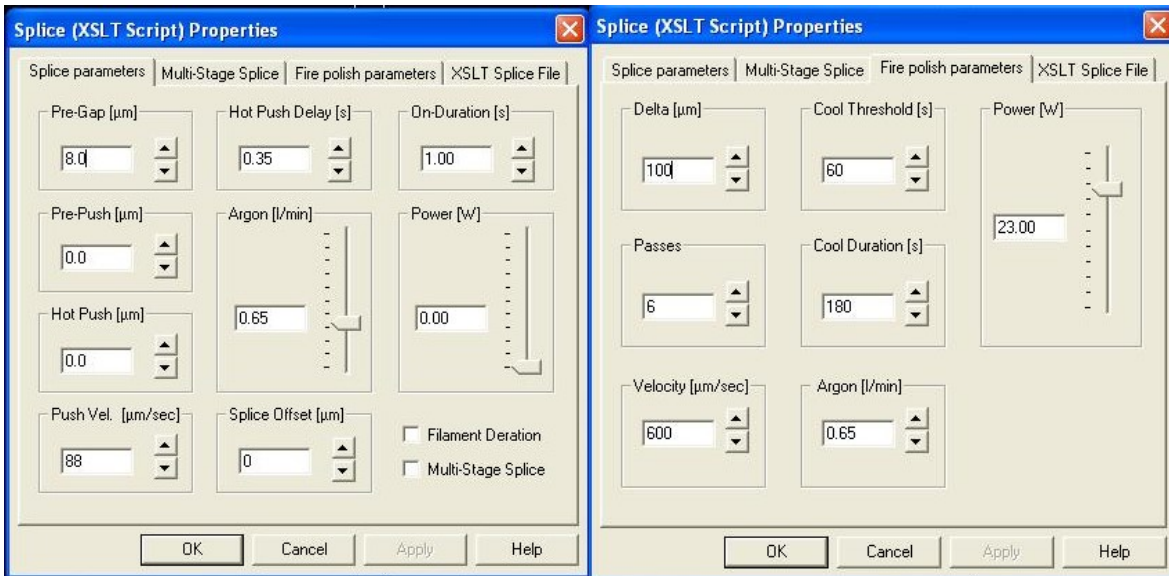
6) Testing the splice HNLF to SMF-28.

Splice 1: splice recipe 3 (without fire polish, 2s, 22 W)
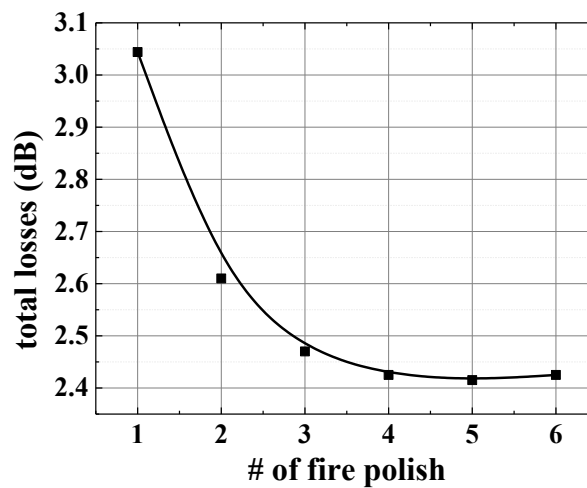
Splice 2: pre-loos (butt coupled) 5.7dB, after splice (splice3) 4.7dB.

Fire polishing ("Firepolish2") step by step:

Parameters: 100μm×6, 600μm/s, 23W.
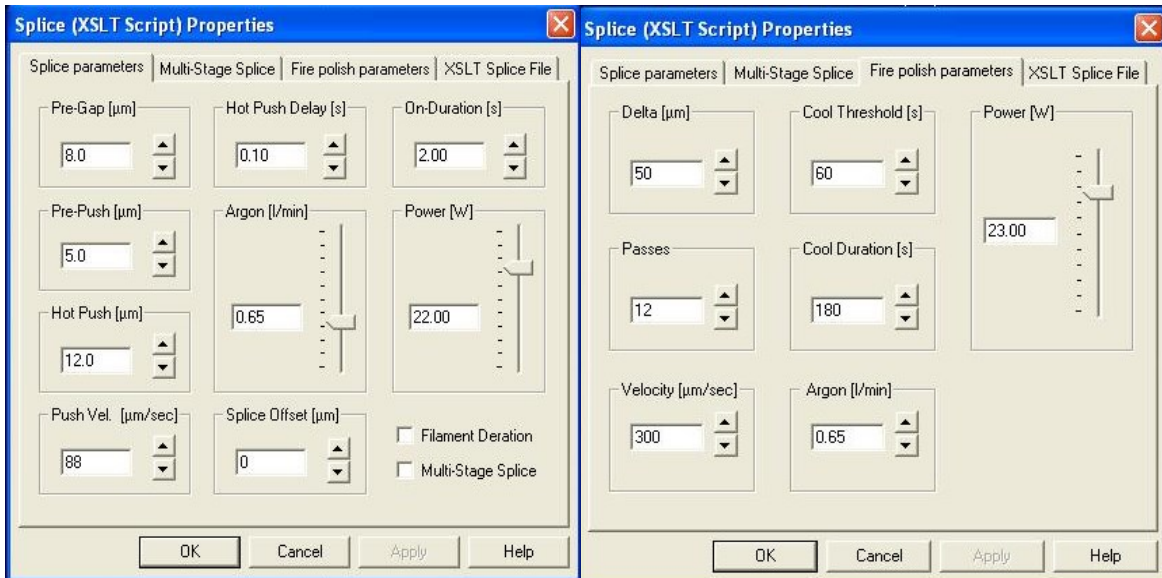
Loss vs. # of splice:

4 steps to get the minimum loss, so we create a new splice recipe with fire polishing (splice 4)

7) Splice 4:

$$4 \times [(100 + 600) \times 6/2]/600 = 4 \times 3.5$$

$$[(50 + 600) \times 12/2]/300 = 17$$

Redo "splice 1" pre-loss 3.76dB, after splice 0.137dB.

Redo "splice 2" pre-loss 3.7dB, after splice 0.142dB.

The single splice from HNLF to SMF-28 is 0.07dB.

8) Final recipe: "Splice 4" (with fire polishing)

B.7 Troubleshooting

1) Problem: Fibers are not in the center of view or not along guidelines when loaded

   Action: Check that fibers are properly in the v-grooves. Make sure the proper length of the buffer is removed from the fiber. May need put Transfer Jig into offset position, replace FHB, and then repeat splice procedure.

2) Problem: Accidentally move motors when fiber holder is not in place

   Action: See manual for the reset procedure

3) Problem: Fiber does not cleave

Action: Check FHB proper v-groove size. Look for fiber shards in cleaver. Check FHB tension. If fiber breaks than the tension is too high. If large cleave angle is present or does cleave occur, increase the tension.

4) Problem: Fiber does not strip

Action: Make sure cleaver is clean. Check proper v-groove size. If this does not work, see the manual for cleaver/stripper lid adjustment.

5) Problem: Motor positions not in the ordinary place or close to end of motion

Action: Do reset. If does not fix the problem see manual

6) Problem: Anything else?

Action: See manual

B.8 Do Not's

1) Do not use the splicer when argon is not flowing;

2) Do not overwrite any splice recipes;

3) Do not touch any mechanical screws unless recovery is required;

4) Do not push "Stop" button when any motor is moving;

5) Do not "Reset" when FHBs and transfer Jig are not engaged;

6) Never open "File - Database Options";

7) Never change "Configuration - Image - CCD camera - Camera Properties"

    "Configuration - Image - Imaging Processing Set-Up"

    "Configuration - Mechanical";

8) Never touch "Splice - Splice parameters - XSLT Splice File" and "Splice - Process Libraries"

Appendix E Permission

E.1.   Permission for Vytran training material

Christopher Gaeta [cgaeta@vytran.com]

Hello Chenchen,

We would be more than happy for you to use our material in your PHD dissertation! All that we ask is that you promote the use of Vytran products in your professional career. We wish you the best of luck in all your future endeavors.

Best Regards,

Christopher Gaeta

Service Engineer
Vytran LLC.
1400 Campus Drive West
Morganville, NJ 07751
1-732-972-2880 x 161

Wang, Chenchen

To:
 Christopher Gaeta [cgaeta@vytran.com]
Cc:
 John Hanigofsky [jHanigofsky@vytran.com]
Attachments:
Vytran manual.pdf (4 MB)[Open as Web Page]
Sent Items

Dear Christopher,

This is a letter asking for permission to use figures and materials on Vytran-2000 manual in my PhD dissertation. One appendix of my dissertation is a manual wrote based on Vytran Training June 2012 with your previous employee Usman B. Nasir and also some figures and materials from the official Vytran-2000 manual. The file is enclosed in this email. Could you please check if the Vytran corporation is fine with this?

The requested permission extends to any future revisions and editions of my dissertation, including the prospective publication of my dissertation by a future publisher. The publisher may produce small quantities of my dissertation on demand and may make my dissertation available for free internet download. These rights will in no way restrict republication of the material in any other form by you or by others authorized by you.

Thanks a lot! I am looking forward to your reply!

Best,
Chenchen

Chenchen Wang
Graduate Research Assistant
Dept. of Physics, Kansas State University

E.2. Permission for Figure 1-1

F.	**Subject**
Elsevier Customer Service Science Direct	

Discussion	

Response Via Email (Kathy Fernandez)	13/01/2015 05.40 PM

Hello Chenchen,

Thank you for contacting the E-Helpdesk for ScienceDirect. I understand that you are inquiring about permissions to reuse this article. This article is open access. Because of that status, the license is here :
http://www.elsevier.com/open-access/userlicense/1.0/ ;

This link appears on the article page. You might need to click on the "Show More" option to view the link. It appears right above the 'Choose an option to locate/access this article:" box.

If you have any questions, please contact our Permissions team at:

Tel: (+1) 800-523-4069 x 3808 (US)
E-mail: permissions@elsevier.com

Please let me know if you have any questions.

Regards,
Kathy Fernandez
Elsevier Customer Service
usinfo@elsevier.com
1 888 615 4500
Americas

Customer By Email (ScienceDirect Message Center)	12/01/2015 11.00 PM

This comment has been sent from the following URL -
http://www.sciencedirect.com/science/article/pii/S003040180500595X

The browser type is - Mozilla/5.0 (Windows NT 6.1; WOW64) AppleWebKit/537.36 (KHTML, like Gecko) Chrome/39.0.2171.95 Safari/537.36
Primary Account Structure for the Current session:
- Account: Kansas State University [C000025157]
- Group: IP_Univ Kansas State
IP address: 129.130.18.97
Sent by: Chenchen Wang
Country: United States
Location: My institution/company
Subject: Information requests (prices, marketing, reports, reproduction of articles, etc)
Details:
To whom it may concern:

I am completing a doctoral dissertation at Kansas State University entitled "Optical Frequeny references in acetylene-filled hollow-core optical fiber and photonic mircocells". I would like your permission to reprint in my dissertation excerpts Figure 2 from the following paper, along with a complete citation of the original material in my dissertation:

Tuominen, J., et al., Gas filled photonic bandgap fibers as wavelength references. Optics Communications, 2005. 255(4–6): p. 272-277

The requested permission extends to any future revisions and editions of my dissertation, including the prospective publication of my dissertation by a future publisher. The publisher may produce small quantities of my dissertation on demand and may make my dissertation available for free internet download. These rights will in no way restrict republication of the material in any other form by you or by others authorized by you.

Thanks a lot! I am looking forward to your reply!

Best,
Chenchen

[---001:003074:46667---]